DOT/FAA/TC-22/17

Federal Aviation Administration
William J. Hughes Technical Center
Aviation Research Division
Atlantic City International Airport
New Jersey 08405

Bonded Repairs of Composite Wing Panel Structure: Phase 3, Bonded Repair Size Limits Study for Solid Laminates with Double-Sided Scarf Panels

June 2022

Final report

U.S. Department of Transportation
Federal Aviation Administration

NOTICE

This report is available at the Federal Aviation Administration William J. Hughes Technical Center's Full-Text Technical Reports page: actlibrary.tc.faa.gov in Adobe Acrobat portable document format (PDF).

Form DOT F 1700.7 (8-72) Reproduction of completed page authorized

1. Report No.	2. Government Accession No.	3. Recipient's Catalog No.
DOT/FAA/TC-22/17		

4. Title and Subtitle	5. Report Date
Bonded Repairs to Composite Wing Panel Structure: Phase 3, Bonded Repair Size Limits Study for Solid Laminates with Double-Sided Scarf Configurations	

7. Author(s)	8. Performing Organization Report No.
Reewanshu Chadha[1], Tim M. Labik[2], John G. Bakuckas, Jr.[3], John Z. Lin[4], Michael Fleming[4], Erick Espinar-Mick[5] [1]Federal Aviation Administration (Diakon Solutions, LLC) [2]Federal Aviation Administration (FAA-Drexel Fellow) [3]Federal Aviation Administration [4]Boeing Research & Technology [5]Boeing Commercial Airplane	

9. Performing Organization Name and Address	10. Work Unit No. (TRAIS)
William J. Hughes Technical Center Aviation Research Division Structures and Materials Section Atlantic City International Airport, NJ 08405	11. Contract or Grant No.

12. Sponsoring Agency Name and Address	13. Type of Report and Period Covered
U.S. Department of Transportation Federal Aviation Administration Transport Standards Branch Airframe & Cabin Safety Section, AIR-675 2200 South 216th Street Des Moines, Washington 98198	Final Report
	14. Sponsoring Agency Code AIR-675

15. Supplementary Notes

The FAA William J. Hughes Technical Center Aviation Research Division COR was John G. Bakuckas, Jr.

16. Abstract

In a collaborative effort, the Federal Aviation Administration (FAA) and The Boeing Company are assessing bonded repair technologies of composite panels representative of transport airplane wing-structures through test and analysis using the FAA's Aircraft Beam Structural Test (ABST) fixture. Emphasis has been placed on investigating methods and tools used to conduct analysis and predict structural performance of bonded repairs and those used to monitor and evaluate repair quality and durability over the life of the part. This project was carried out in a phased approach. Current phase 3 efforts support bonded repair size limit (BRSL) studies and methods used to predict the limit-load residual strength for failed repair scarf configurations. Full-depth, half-depth, and double sided scarfs were inserted in carbon-fiber-reinforced polymer (CFRP) panels having an 18-ply quasi-isotropic layup. The panels were attached as top-side components (e.g., skins) of a cantilevered, 24-inch-wide by 40-inch-long wingbox structure. These panels were subjected to constant-moment loads either tested quasi-statically to failure or subjected to fatigue before loading them to failure. The applied fatigue loading conditions simulated normal operational strain levels for transport-category wing panels for 165,000 cycles, which is approximately equal to three design service goals (DSGs). Results for full-depth scarf and half-depth scarf configurations is documented in a companion technical report (DOT/FAA/TC-21-27). This report focuses on panels with double-sided scarf configurations, where two panels had no repair patches and three panels had single-sided repair patches representing a half-depth scarf. In general, methods under development for BRSL residual strength predictions correlated well with test results. At low strain survey load, the strains in the panel with double-sided scarf and single-sided patch were comparable to the half-depth scarf panels. However, the single-sided repair patch was not effective in restoring strength. During residual strength tests, the repair patch experienced early bondline failure from high peel stresses caused by bending eccentricity. While these results provide valuable insights to the residual strength behavior of CFRP panels with various scarf configurations, caution must be exercised in their direct application to real structure having reinforcing substructure.

17. Key Words	18. Distribution Statement
Bonded repair size limits, Double-sided scarf, Scarf repairs, Carbon fiber reinforced polymer, Nondestructive inspection, Test, Analysis, Digital image correlation, Thermography	This document is available to the U.S. public through the National Technical Information Service (NTIS), Springfield, Virginia 22161. This document is also available from the Federal Aviation Administration William J. Hughes Technical Center at actlibrary.tc.faa.gov.

19. Security Classif. (of this report)	20. Security Classif. (of this page)	21. No. of Pages	22. Price
Unclassified	Unclassified	195	

Contents

Figures

Tables

Acronyms

Acronym	Definition
ABST	Aircraft Beam Structural Test
BRSL	Bonded repair size limit
CFRP	Carbon-fiber-reinforced polymer
DIC	Digital image correlation
DSG	Design service goal
DSO	Design service objective (used interchangeably with DSG)
FAA	Federal Aviation Administration
FEA	Finite element analysis
FEM	Finite element model
NDI	Nondestructive inspection
NFOV	Narrow field of view
PFA	Progressive failure analysis
SHM	Structural health monitoring
SL	Service load (used interchangeably with normal operational load)
WFOV	Wide field of view

Executive summary

In a collaborative effort, the Federal Aviation Administration (FAA) and The Boeing Company are assessing bonded repair technologies of composite panels representative of transport airplane wing structures through test and analysis using the FAA's Aircraft Beam Structural Test (ABST) fixture. Emphasis has been placed on investigating methods and tools used to conduct analysis and predict structural performance of bonded repairs and those used to monitor and evaluate repair quality and durability over the life of the part. This project was carried out in a phased approach. Current phase 3 efforts support bonded repair size limit (BRSL) studies and methods used to predict the limit-load residual strength for failed repair scarf configurations. Full-depth, half-depth, and double sided scarfs were inserted in carbon-fiber-reinforced polymer (CFRP) panels having an 18-ply quasi-isotropic layup. The panels were attached as top-side components (e.g., skins) of a cantilevered, 24-inch-wide by 40-inch-long wingbox structure. These panels were subjected to constant-moment loads either tested quasi-statically to failure or subjected to fatigue before loading them to failure. The applied fatigue loading conditions simulated normal operational strain levels for transport-category wing panels for 165,000 cycles, which is approximately equal to three design service goals (DSGs). Results for full-depth scarf and half-depth scarf configurations is documented in a companion technical report (DOT/FAA/TC-21-27). This report focuses on panels with double-sided scarf configurations, where two panels had no repair patches and three panels had single-sided repair patches representing a half-depth scarf. In general, methods under development for BRSL residual strength predictions correlated well with test results. At low strain survey loads, the strains in the panel with double-sided scarf and single-sided patch were comparable to the half-depth scarf panels. However, the single-sided repair patch was not effective in restoring strength. During residual strength tests, the repair patch experienced early bondline failure from high peel stresses caused by bending eccentricity. While these results provide valuable insights to the residual strength behavior of CFRP panels with various scarf configurations, caution must be exercised in their direct application to real structure having reinforcing substructure.

1 Introduction

In a multiyear, multiphase research program, the FAA and The Boeing Company are working in partnership to gain better insight into the fatigue and damage tolerance performance of adhesive-bonded repairs and to help address issues cited in the FAA Bonded Repair Size Limits (BRSL) policy statement (Federal Aviation Administration, 2014). Focus is on testing and analysing bonded repairs to representative composite wing panels using the Aircraft Beam Structural Test (ABST) fixture (Chadha, Bakuckas Jr., Fleming, Lin, & Korkosz, 2019), a new structural test capability at the FAA William J. Hughes Technical Center. The program objectives are to characterize the fatigue and damage tolerance performance of bonded repairs subjected to simulated normal operational or service load (SL) conditions and to evaluate the limit-load capability of a typical composite wing panel of transport category aircraft with a failed repair. In addition, methods and tools used for the performance analysis and for evaluating and monitoring repair integrity are being assessed.

Current phase 3 of this program directly supports the FAA BRSL policy issued to address concerns of not being able to detect weak bonds that result in failure. BRSL analysis methods for sizing bonded repairs to critical solid laminates and honeycomb panels are needed. Tests validated such analysis methods to determine allowable repair sizes within the requirements of BRSL policy. Test information will be useful because of the ABST fixture's ability to produce effects of boundary conditions and load redistribution that can be understood and incorporated into analysis models and tools used to develop design curves. Initial phase 3 efforts focused on limit-load characterization for half- and full-depth scarf configurations (Figure 1a and b) for solid laminates under tension produced by constant moment. A total of four panels (panels 3–6) were tested in phase 3, and the results are reported in (Neel R. C.-M., 2021). The benefit gained in the residual-strength limit-load capability of a half-depth scarf was revealed in these tests. In addition, analytical models currently under development to accurately predict the strain levels associated with scarfs with failed repair were demonstrated.

In this current phase 3 effort, focus was on limit-load characterization for double-sided scarf configurations for solid laminates (Figure 1c and d) under tension produced by constant moment. Double-sided scarf configuration is being investigated to study if the backside repair patch is sufficient to carry limit load if the top side repair fails due to complete disbonding. This technical report addresses the challenges with the double-sided scarf configurations (panels 7 to 11), where panels 7 and 8 had no repair patches and panels 9, 10, and 11 had single-sided repair patches representing half-depth scarf configuration. Panels 7 and 8 were tested to study the effect of fatigue on the residual strength of the panels with double-sided scarf configurations with no

repair patches and panels 9, 10 and 11 were tested to characterize the limit-load capacity of the double-sided scarf configuration with a single-sided repair patch to compare to the half-depth scarf configuration.

Future phase 3 efforts will study fatigue and residual strength aspects for more configurations and loading for both solid laminates and honeycomb panels. In addition, compression loading tests and analysis are considered in the longer-term planning of this program.

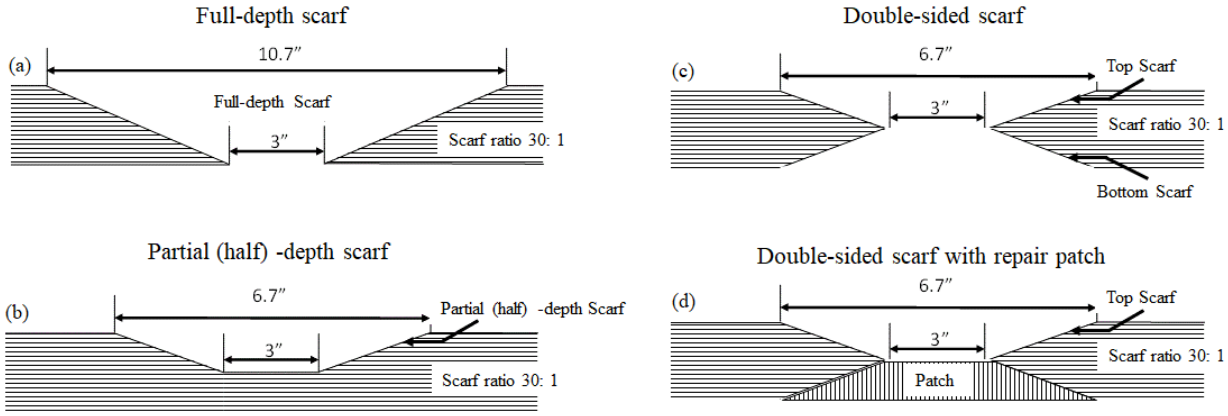

Figure 1. Scarf configurations tested in phase 3

2 Experimental procedures

A description of the experimental procedures used in this program, including the test fixture, panels, applied loads, and the inspection and monitoring methods, are outlined in this section.

2.1 Test fixture description

Testing was conducted by the FAA using the ABST fixture located at the FAA William J. Hughes Technical Center. The ABST fixture, shown in Figure 2 was developed in collaboration with the Boeing Company as phase 1 of this program and is capable of applying major modes of loading to panels representative of a typical wing or stabilizer components.

A detailed, component-by-component description of the ABST fixture and supporting systems (MTS systems) within the Structures and Materials Laboratory is provided by (Chadha, Bakuckas Jr., Fleming, Lin, & Korkosz, 2019).

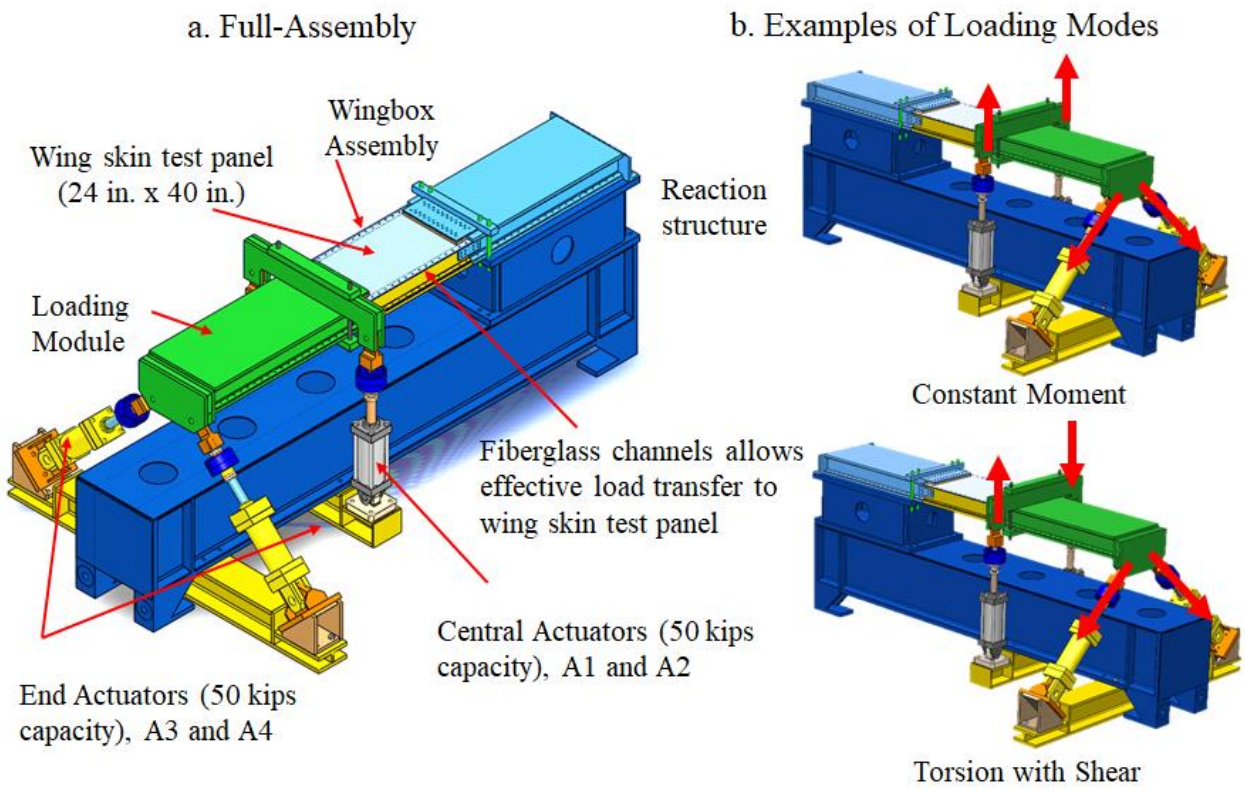

Figure 2. (a) ABST fixture and sub-components; (b) examples of fixture loading modes

2.2 Test specimen descriptions

The test articles fabricated by Boeing were flat composite solid laminate panels (24-in wide, 40-in long, and 0.135-in-thick) representing typical carbon-fiber reinforced polymer (CFRP) skin panels of wing or empennage components. An 18-ply panel was considered having a quasi-isotropic lay-up, $[\pm 45°_{fabric}/-45°/90°/45°/0°/-45°/90°/45°/0°]_s$. Panels were fabricated with a high modulus carbon/epoxy prepreg material, a typical material used by Boeing for the composite primary structure of commercial applications. These panels had holes machined to match the fixture attachment points. The 24-in long ends of the panel were reinforced with doublers (end tabs) for load introduction into the test article. These end tabs were made from the same material and lay-up as the test panel and included a taper region with ratios of around 30:1.

In this current study, five 18-ply solid laminate panels having a double-sided scarf configuration were tested; panels 7 and 8 with no repair patches and panels 9, 10 and 11 with single-sided repair patches. Figure 3 shows images of the top and bottom sides of panels 7 and 8, the schematic of the section cut A-A, and the ply layup.

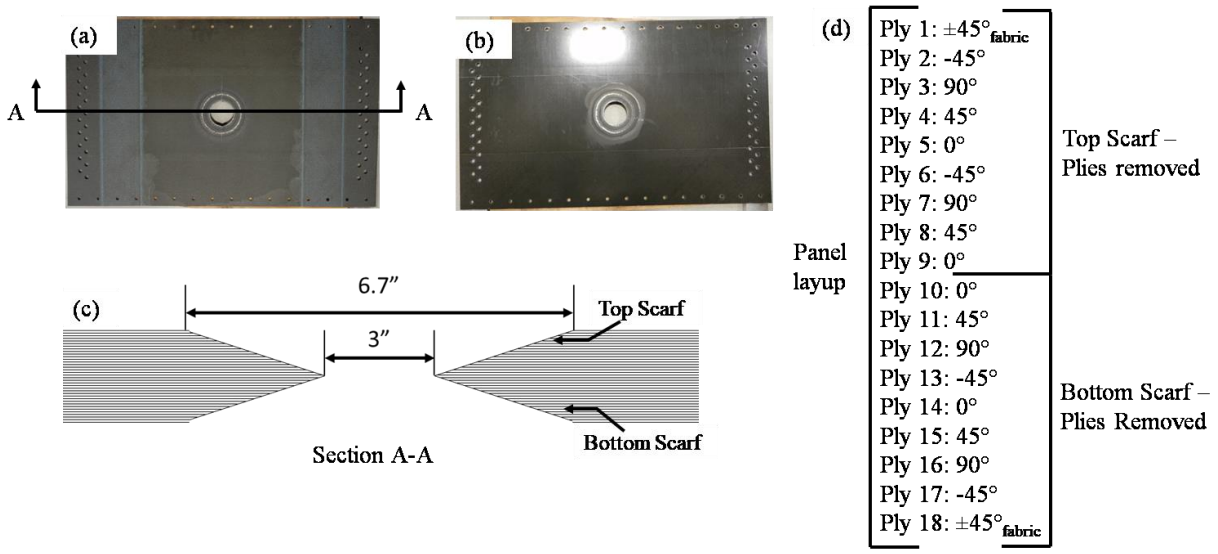

Figure 3. Panels 7 & 8 (a) top view, (b) bottom view (c) section A-A, (d) panel and scarf layups

Images of the top side and the bottom sides of panels 9, 10 and 11 are shown in Figure 4a, and b. As seen in the figure, the image of the top side of the panel shows the scarf and the bottom side shows the patch. In addition, Figure 4c shows the section view of the panel and Figure 4d provides the ply layup of the panel and the patch, as well as the plies removed to fabricate the scarfs. These three panels with single-sided repair patch were fabricated by two separate organizations within Boeing to account for potential variations in production processes. Panels 9 and 10 were fabricated at Boeing Research and Technology-South Carolina Center and panel 11 was fabricated at Boeing Research and Technology Structural Repair Lab in Seattle, Washington. The scarfs in all five panels had 3-inch inner dimeter and 6.7-inch outer diameter. The detailed drawing of the panels are provided in appendix A.

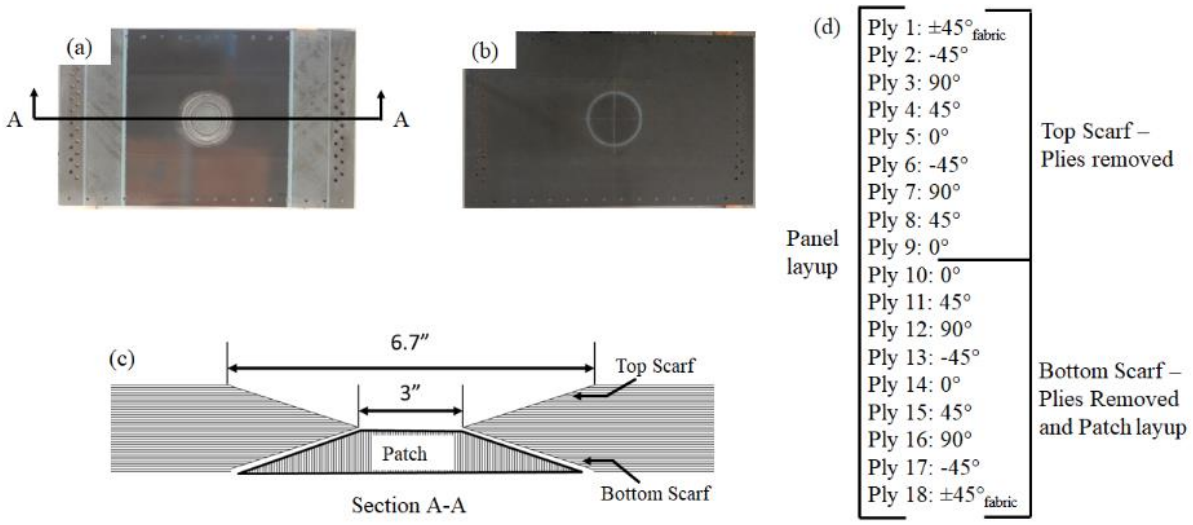

Figure 4. Panels 9, 10 & 11 (a) top view, (b) bottom view (c) section A-A, (d) panel and patch layups

2.3 Applied loads and test matrix

The applied test loads used in this study represent the strains experienced by a composite wing panel of a typical transport-category aircraft, which usually includes compression, tension, and shear. Three loading types were considered:

1. Strain survey loads applied quasi-statically to a percentage of the SL conditions (typically 75%–100% of the SL conditions) to ensure proper load introduction into the panel.
2. Fatigue loads simulating normal operational or SL conditions during a flight cycle, the peak of which is estimated to be 37% of the ultimate load conditions. If required, elevated fatigue loads were used to induce damage growth (40%–60% of the ultimate load conditions). Fatigue loading conditions did not consider scatter.
3. Ultimate loads applied quasi-statically based on notched allowable coupons or barely visible impact damage load-conditions.

A summary of these load configurations and the corresponding strain values is provided in Table 1. The tests covered in this report were for tensile loading conditions only.

Table 1. Strain levels used in program

Test Description	**Load Type**	**Strains (με)**
		Tension
Strain survey—75%–100% of the simulated service loads (SL) strain conditions	Static	1,660 – 2,200

Test Description	Load Type	Strains (με)
		Tension
Fatigue—simulated SL conditions (37% of ultimate strains)	Cyclic (R = 0.1)	2,200
Fatigue—elevated loads to induce damage growth (40 - 60% of ultimate strain)	Cyclic (R = 0.1)	2,400 – 3,600
Residual strength (ultimate strains)— typical design ultimate loads of notched allowables	Static	6,000

The sequence of applied loads used for panels tested are shown in Table 2. Panel 3 and 4 were tested previously (Neel R. C.-M., 2021) and had partial (half)-depth and full-depth scarf configurations, respectively. They are listed here for comparison purposes. Panel 7 was first subjected to strain surveys and then loaded quasi-statically up to failure to determine the baseline residual strength of the double-sided scarf configurations. Panel 8 was also subjected to strain surveys and then to 3 DSG i.e., 165,000 cycle fatigue-loading intervals to determine the effect of fatigue on post-fatigue residual strength. Panels 9, 10 and 11 were first subjected to strain surveys and then loaded quasi-statically up to failure to determine the residual strength of the double-sided scarf configurations with single-sided patch. All testing was conducted under laboratory environment.

For panels 7 and 8, the failure loads were expected to be close to the failure loads of panels with failed (cavity) full depth scarf (e.g. panel 4 in Table 2) due to similar material removal in both configurations. For panels 9, 10 and 11 the goal was to see how well the double-sided scarf with single-sided repair patch can restore the strength as compared to the panels with failed (cavity) half-depth scarf (i.e. panel 3 in Table 2). The load path in half-depth scarf panel and double-sided scarf with single-sided repair patch is similar, with a difference that in the latter scenario due to the disrupted load path across the bondline from the parent material to the patch (Figure 5).

Table 2. Summary of applied loads

Test Panel	Panel	Test Description	Moment (lb_f-ft)	Actuator 1 & 2 (lbf)	Actuator 3 & 4 (lbf)	Far-field Strain (με)
Partial (half)	3	Predicted critical loads	169,318	-20,117	28,445	9,000

Test Panel	Panel	Test Description	Moment (lb_f-ft)	Actuator 1 & 2 (lbf)	Actuator 3 & 4 (lbf)	Far-field Strain (με)
depth scarf panel		Measured failure loads	168,611	-20,033	28,123	8,619
Full depth scarf panel	4	Predicted critical loads	95,698	-11,370	16,078	3,653
		Measured failure loads	81,068	-9,632	13,620	3,125
Double-sided scarf panels	7	Measured failure loads	94,418	-11,218	15,862	4,958
	8	Maximum fatigue Loads (R=0.1)	36,798	-4,372	6,183	2,200
		Measured failure loads	95,024	-11,290	15,965	5,153
Double-sided scarf panels with single-sided repair patch	9	Measured failure loads (test stopped before final failure)	92,954	-11,044	15,616	N/A
	10	Measured failure loads	98,374	-11,688	16,527	4,815
	11	Measured failure loads	97,454	-11,578	16,374	4,580

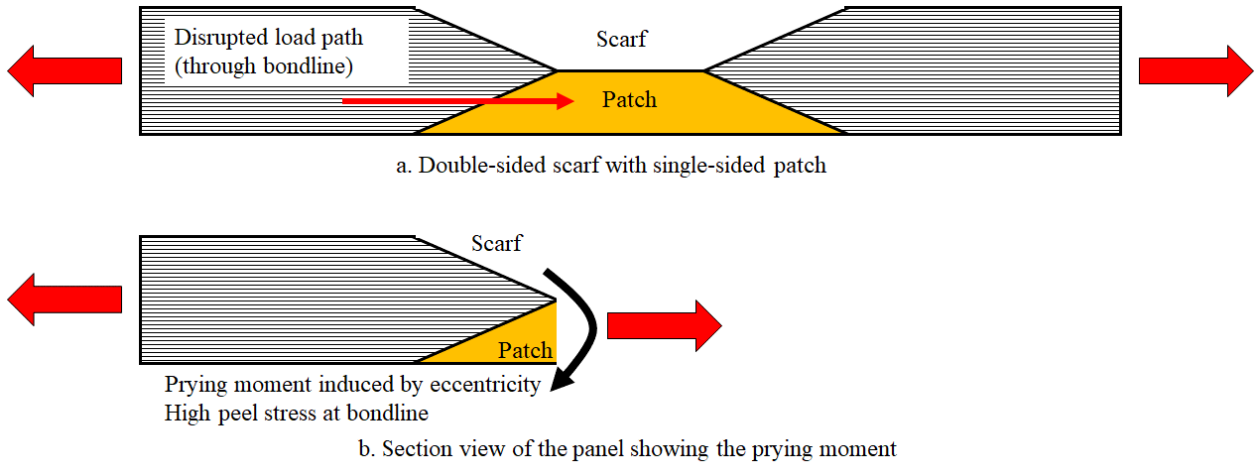

Figure 5. Load path comparison for two types of configurations

2.4 Inspection and deformation monitoring methods

Several methods were used to monitor the deformation of the specimens throughout the duration of the tests. Displacement sensors installed at the ends of the load application assemblies were used to monitor the horizontal and vertical deflections of the cantilevered wing box. Strain gages installed in the internal and external surfaces of the panel, and DIC systems situated above the wing box were used to monitor strains in the axial, transverse, and 45-degree directions. The strain gage map and the DIC field of view for all four panels are shown in Figure 6 and Figure 7 respectively. Detailed descriptions of these instruments are provided in (Neel, et al., 2020).

Throughout the duration of the test, several methods were utilized to monitor the initiation and growth of damage within the CFRP specimens. For visual detection, several camera systems, with varying specifications, were used to monitor the specimen from a multitude of magnifications and angles. For detection of non-visual damage, flash thermography, phased array ultrasonic, and pulse-echo ultrasonic methods were used. Additionally, a structural health monitoring system was used intermittently. Detailed descriptions of these instruments are provided in (Neel, et al., 2020).

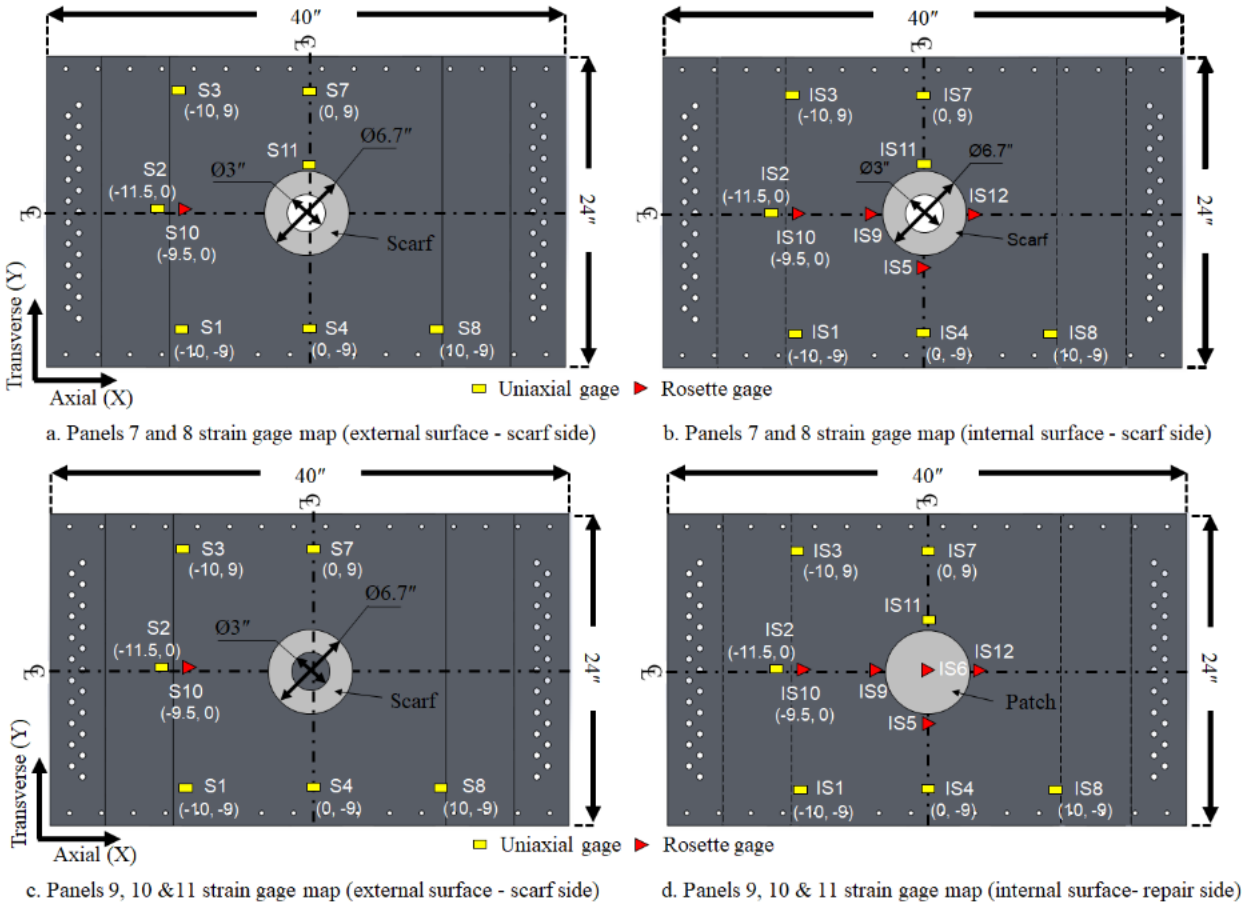

Figure 6. Strain gage layout for panels 7 & 8 (a,b); panels 9,10 & 11 (c, d)

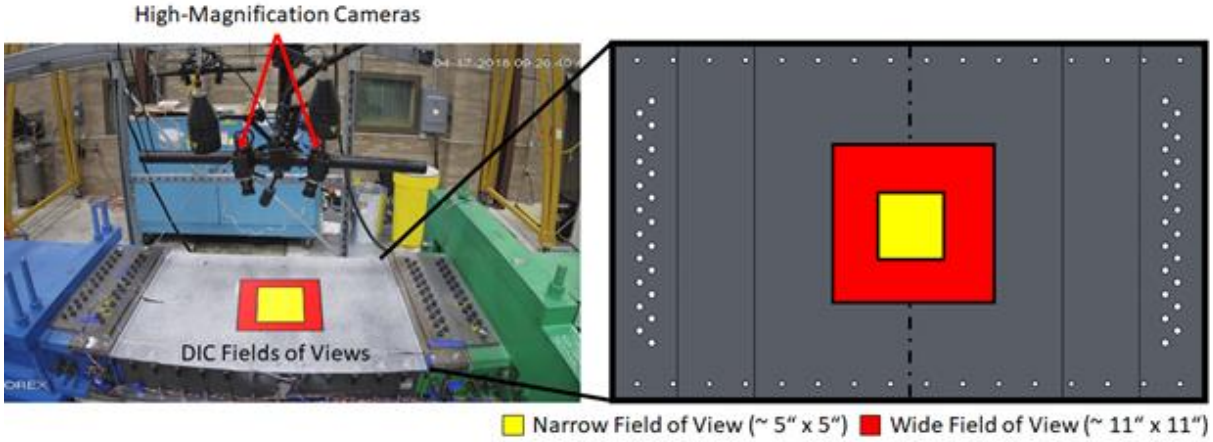

Figure 7. Images displaying typical setup of a DIC system during the tests

3 Analytical procedures

Boeing conducted the analysis in support of this program, as outlined in sections 3.1 and 3.2. Finite element models (FEM) of the test fixture and test panels were created to simulate the loading of the panel prior to actual testing and provided predictions of: (1) actuator loads that the ABST fixture should apply to provide appropriate target strains; (2) stress and strain fields; (3) damage initiation and growth in the composite panel, and; (4) ultimate load and residual strength.

3.1 Finite element analysis (FEA) for double-sided scarf panels

For panels 7 & 8, no repair patch was bonded to parent panels. This is a worst-case situation that under single cure condition bondline quality is assumed to be inadequate. An advanced progressive failure analysis (PFA) approach was used to predict the ultimate load levels for various damaged panels in this test program. The current approach implements the Hashin in-plane failure criteria (Hashin, 1980) and the PFA input properties were derived from analysis and tests for the specific materials, processes and design practices. An example of a double-sided scarf panel model at final failure point is shown in Figure 8.

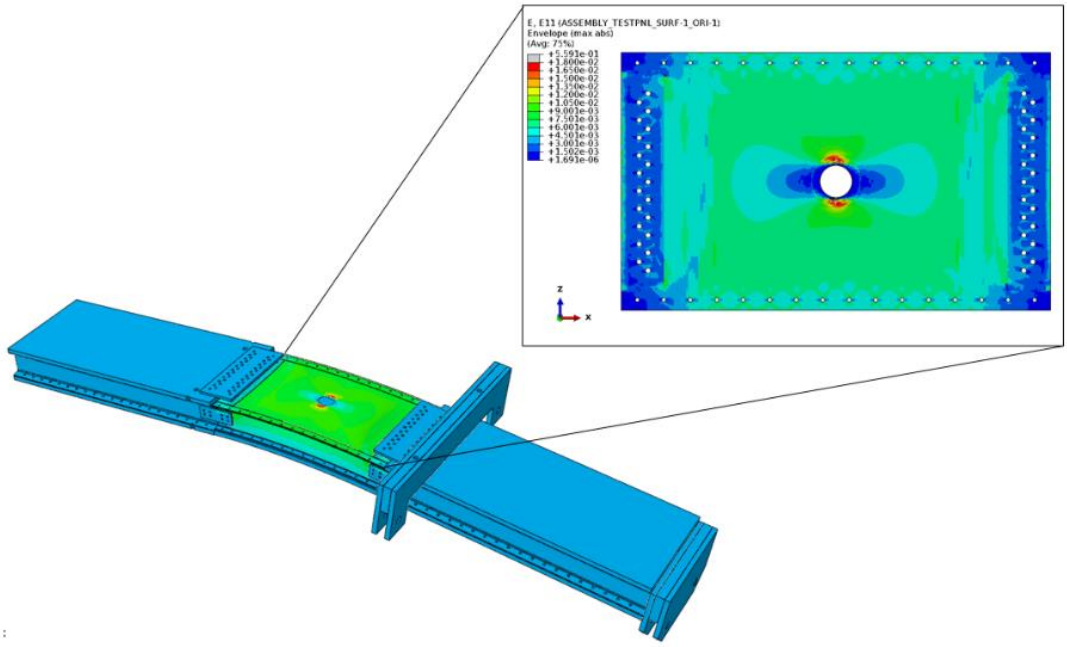

Figure 8. FEM axial strain contour of a double-sided scarf panel at failure

Figure 9 shows the matrix and fiber tensile failure index contours at ultimate load for the double-sided 30:1 scarf panel (only the damaged regions were shown). The predicted failure onset load was 11,400 lbs for vertical actuators, correlating well with the test results shown in Table 2.

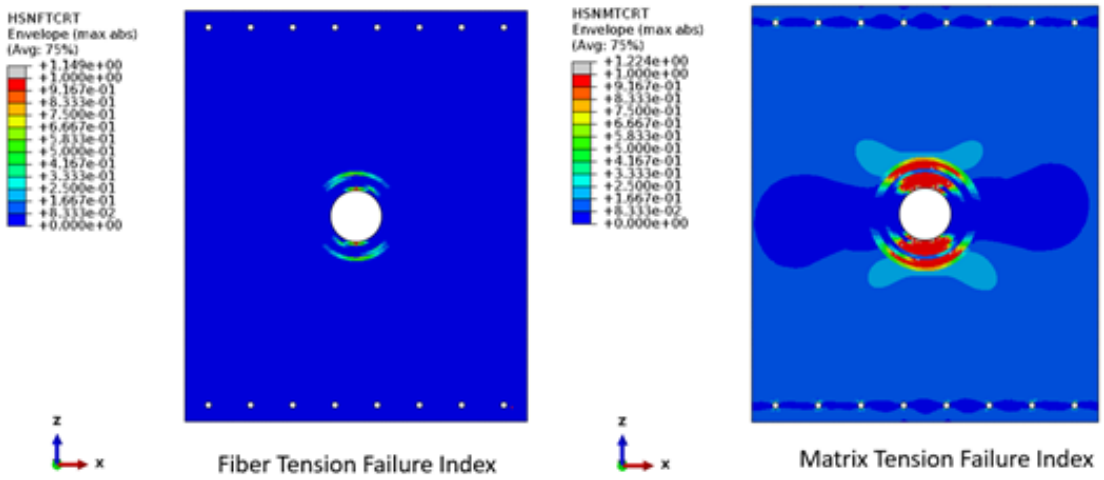

Figure 9. The PFA approach to predict residual strength for panels 7 & 8 at the onset of final failure

3.2 FEA for double-sided scarf panels with single-sided repair patch

One of the most significant findings during this phase of testing was that one remaining perfectly bonded patch did not improve the residual strength at all (see results from Table 2). From a free-body analysis under tensile loading, one can hypothesize that due to the prying moment induced by the eccentricity from the pristine region to the scarfed region, the peel stress in the bondline would be high and caused premature failure of the bondline and hence deemed the patch entirely ineffective. This hypothesis was confirmed by PFA analysis of the double-sided scarf with single-sided repair patch, panels 9 thru 11. In this model, adhesive bondline was modeled with 3-D cohesive elements with damage initiation and progression properties derived from fundamental tests (static tension, shear, Mode-I & II fracture energy measurements using double cantilever beam (DCB) and end notch flexure (ENF) tests). Table 3 lists such properties for the adhesive used. Figure 10 shows the adhesive failure index contour at 5300 με and on the right are simulated axial strain histories as a function of applied load fraction. Both the initiation of bondline failure and final two-part failure strains at gage IS6 (at the center of patch on the interior side) correlate with test results very well. So is the final failure mode (Figure 11).

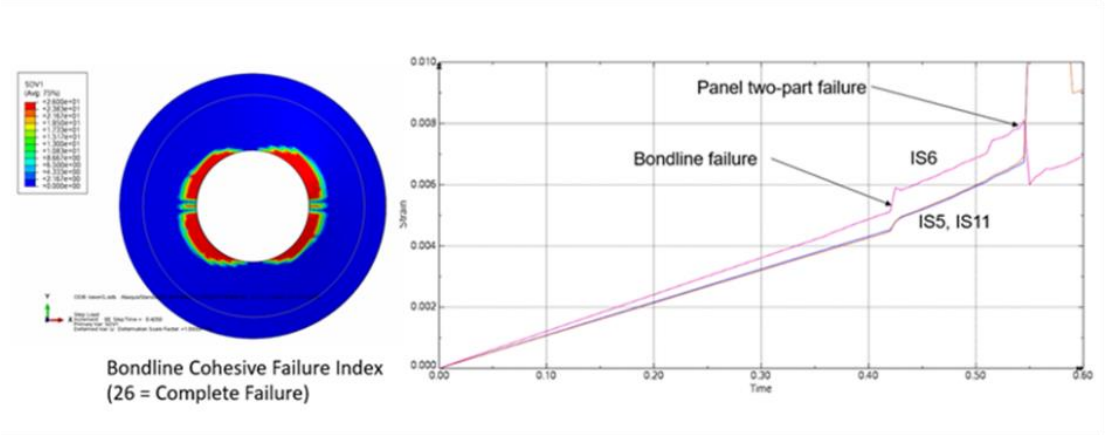

Figure 10. Adhesive failure index contour at 5300 με and the simulated SG results (IS6, IS5 & IS11)

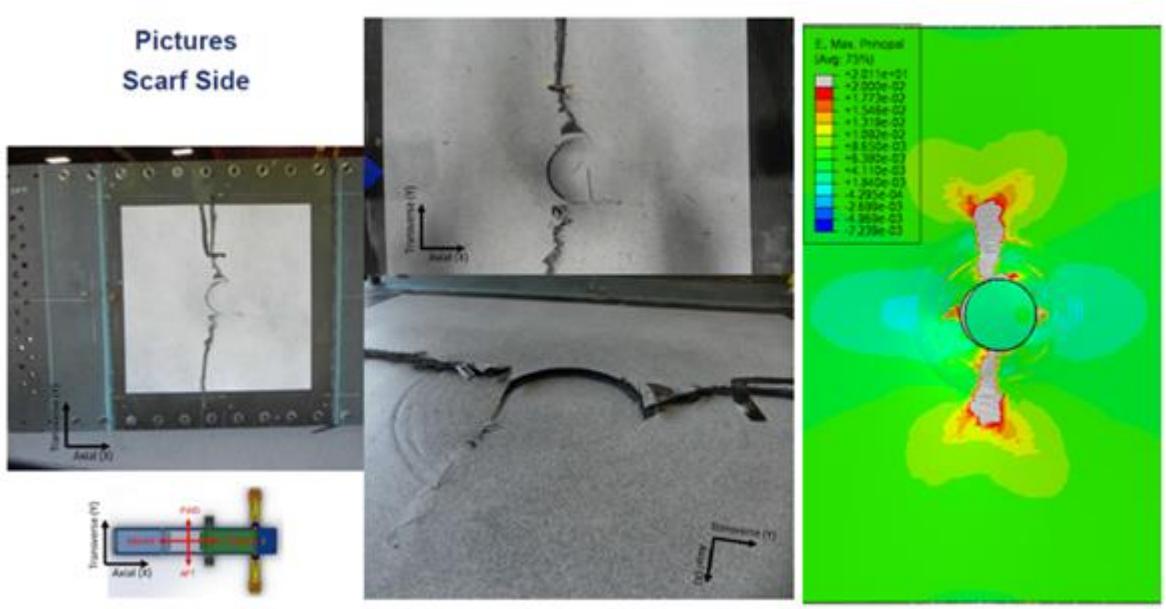

Figure 11. Final failure mode correlation between test and PFA

Table 3. Adhesive properties for PFA analysis

Adhesive Spec	Elastic Modulus (psi)			Strength (psi)			Fracture Toughness (in-lb/in^2)		
	Mode I	Mode II	Mode III	Mode I	Mode II	Mode III	Mode I	Mode II	Mode III
BMS5-154	500000	178571.4	178571.4	7400	7500	7500	2.95	17.6	17.6

4 Results and discussion

During strain survey, fatigue, and residual strength testing of each panel, several strain measurement techniques and NDI methods were used to monitor and assess distributions of strain, as well as detect damage. Representative results are provided in the subsequent sections.

4.1 Double-sided scarf panels (panels 7 and 8)

Panel 7 was quasi-statically loaded to failure and panel 8 was subjected to three design service goals (DSG) i.e. 165,000 fatigue cycles (with a load ratio of R=0.1) before quasi-statically loading the panel to failure. The goal of these tests was to study the effect of fatigue on the residual strength of the panels with double-sided scarfs and no patches and to study the effectiveness of single-sided patch by comparing the residual strength of panel 7 with that of panels 9, 10 and 11.

4.1.1 Baseline inspection and strain survey results

Both panels 7 and 8 were inspected visually and with NDI to detect any anomalies prior to loading. Apart from a few porosity indications, nothing else was found. The panels were subjected to initial strain surveys where they were quasi-statically loaded to yield far-field target strains of 1800 με. The comparison of axial strain distribution away from the scarf region and in the vicinity of the scarf are shown in Figure 12c and d respectively. As shown in Figure 12, the initial strain surveys revealed similar strains throughout the panel for both panels 7 and 8. During the strain surveys it was also observed that for both the panels, matrix cracking initiated in the middle 0° ply at very low load levels. In the absence of any material in the center of the scarf, the first ply acted as a sharp knife edge, which caused the initial cracking. However, these cracks did not extend beyond the first ply in the subsequent strain surveys. Figure 13 shows the matrix cracking in the first ply of the scarf and von-Mises strains in the scarf region showing the stress concentration due to the cracked first ply. Detailed strain gage and DIC results are provided in appendices B and D.

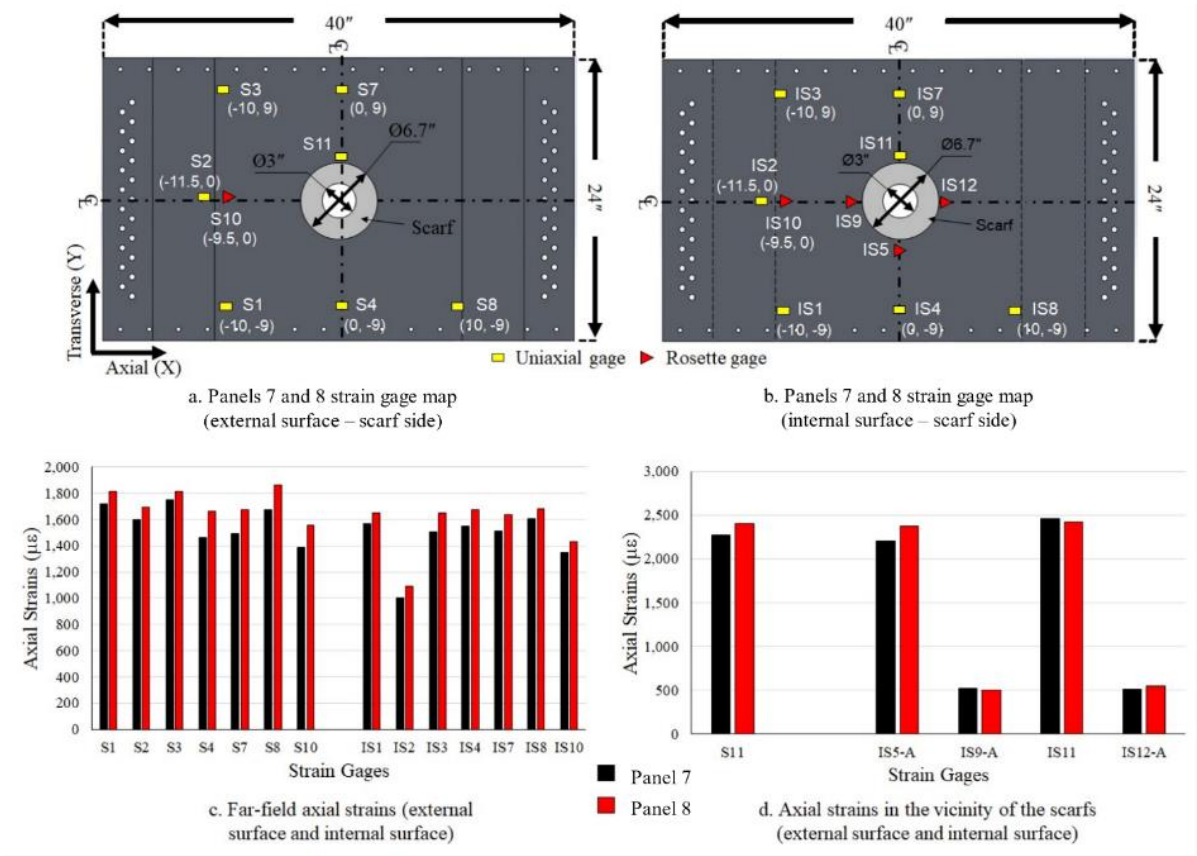

a. Panels 7 and 8 strain gage map (external surface – scarf side)

b. Panels 7 and 8 strain gage map (internal surface – scarf side)

c. Far-field axial strains (external surface and internal surface)

d. Axial strains in the vicinity of the scarfs (external surface and internal surface)

Figure 12. Initial strain survey far-field and near-scarf axial strains, panels 7 and 8

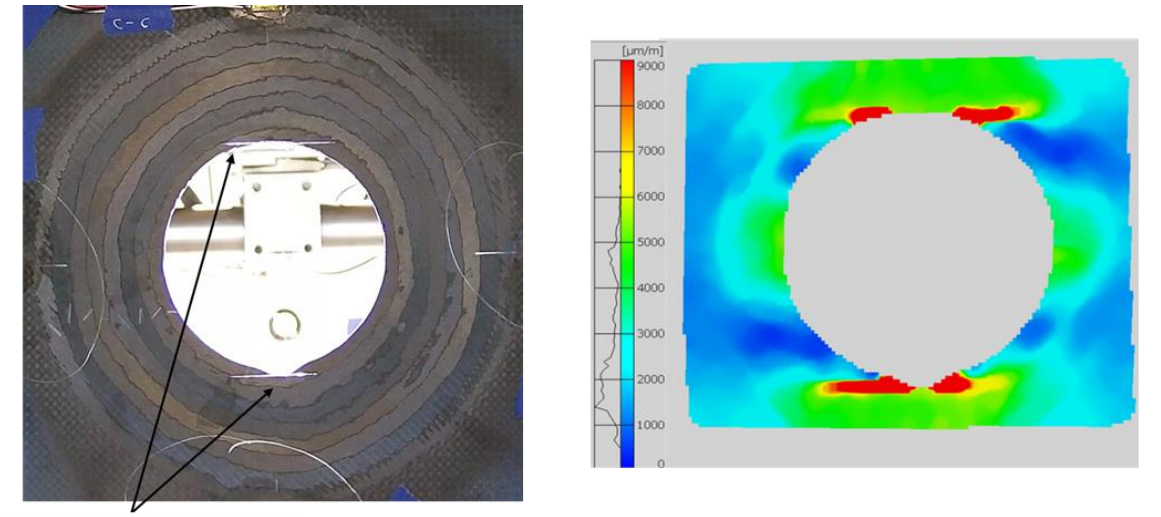

a. Image of scarf indicating matrix cracking in the first ply

b. Von-mises strains in the scarf region showing stress concentration in the first ply

Figure 13. Panel 7 a) visual image and b) von-Mises strains, during initial strain survey

4.1.2 Panel 7 residual strength test results

After the initial strain survey, panel 7 was subjected to residual strength test. The panel was loaded quasi-statically in a saw-tooth profile, increasing the load level up to the predicted critical loads of panel 4 with failed (cavity) full depth scarf (95,698 ft-lb_f), which was considered as 100%. The load profile is shown in Figure 14a. During loading, damage formation was monitored visually using high-magnification cameras and DIC. After each loading, the scarf region was inspected using the flash thermography system. Detailed strain gage results for all the panels collected during residual strength tests are provided in appendix C.

The cracks at the 6 o' clock and 12 o' clock locations, which developed during initial strains surveys, barely progressed till the final failure. Post-test DIC data analysis was able to detect the slight crack progression as shown in Figure 14c. Neither thermography inspections nor visual inspections were able to detect progression of these cracks. In addition to the 6 o' clock and 12 o' clock cracks, the delaminations initiated at 2 o' clock and 8 o' clock locations in the 5^{th} ply (first 0^o ply from the top). This occurred at increment 7 (90 % load level; 86,128 lb_f-ft) and is shown in Figure 14c and d. Apart from slight progression in the above mentioned cracks and delaminations, the scarf region remained intact all the way up to the final failure of the panel. The panel failed catastrophically along the net section, at the applied moment of 94,418 lb_f-ft (Figure 14b). The images of the failed panel are shown in Figure 15. The final failure initiated from the cracked first plies at 6 o' clock and 12 o' clock locations. As the load was increased, the crack extended to the 8^{th} ply (45^o ply), and then further turning along the 45^o direction going past the 7^{th} (90^o ply) and 6^{th} (-45^o ply), all the way to the 5^{th} ply (first 0^o ply from the top). Once the 0^o ply fibers failed, damage progressed through the net section causing sudden catastrophic failure of the panel. All these events happened in the last load step and very rapidly. Neither DIC system nor visual cameras were able to capture the final stages of damage progression. Images of the failed panels and flash thermography results are provided in appendices E and F.

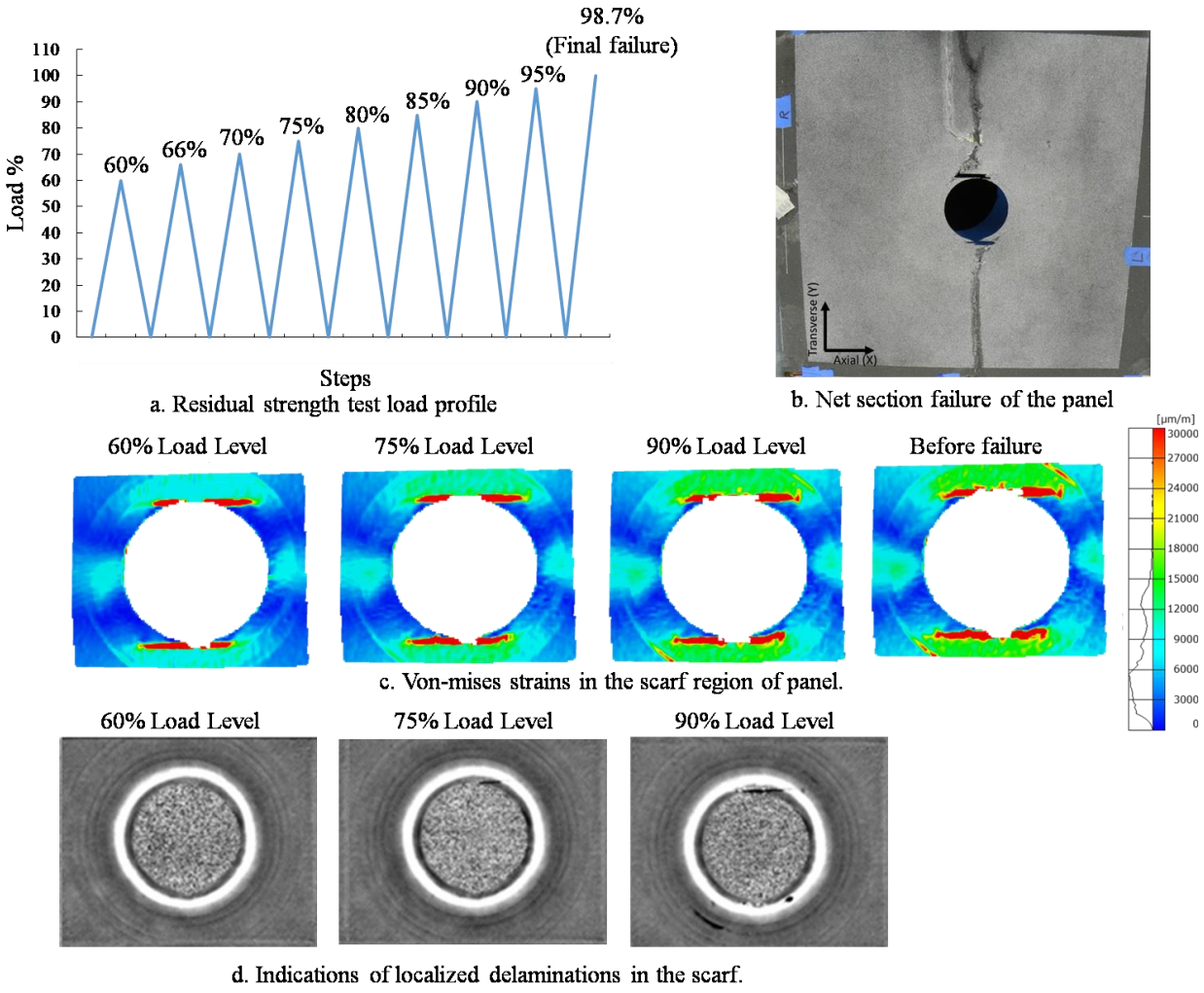

Figure 14. Panel 7 residual strength test; a) load spectrum, b) DIC, c) thermography results

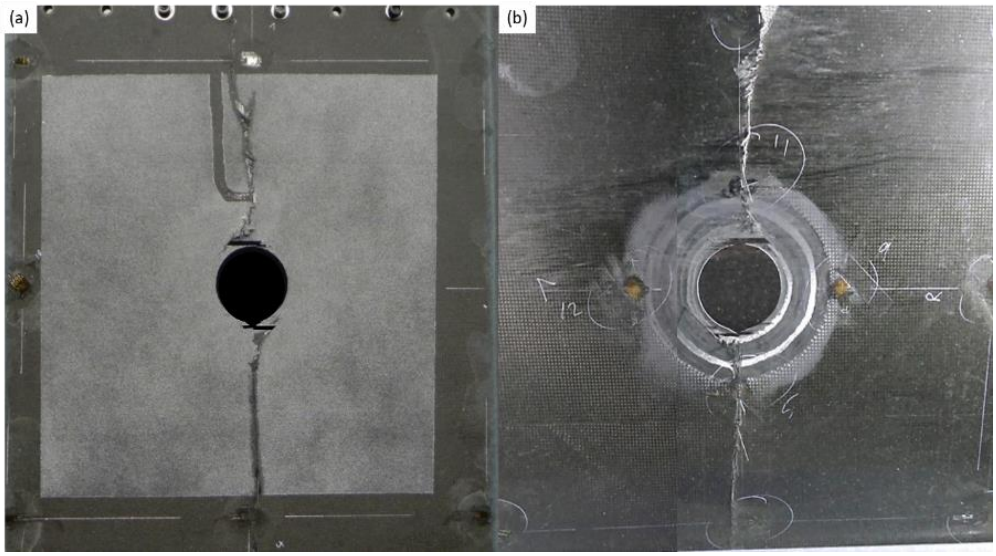

Figure 15. Images of failed panel 7, a) the top side and b) bottom side, showing the scarf

4.1.3 Panel 8 fatigue at service load (SL) strain level

After the initial strain surveys, panel 8 was subjected to three DSGs, i.e. 165,000 fatigue cycles at target maximum far-field strain of 2,200 με (average of strain gage S1 and S3) and R=0.1. No strain redistribution was observed during the fatigue cycles as shown by DIC and strain gage results in Figure 16, where the strains remained relatively similar throughout fatigue. During the tests, the panel was also inspected using a flash thermography system and the inspection results indicted a few small delaminations at 5 o' clock and 11 o' clock locations (Figure 17b). These delaminations were too small to have any effect on the durability of the scarf. In addition, the crack in the middle ply (0^o ply) along the inner edges of the scarf did not grew due to fatigue, as shown in Figure 17. Overall, the double-sided scarf panel was able to sustain 3 DSGs without any new damage formation or growth.

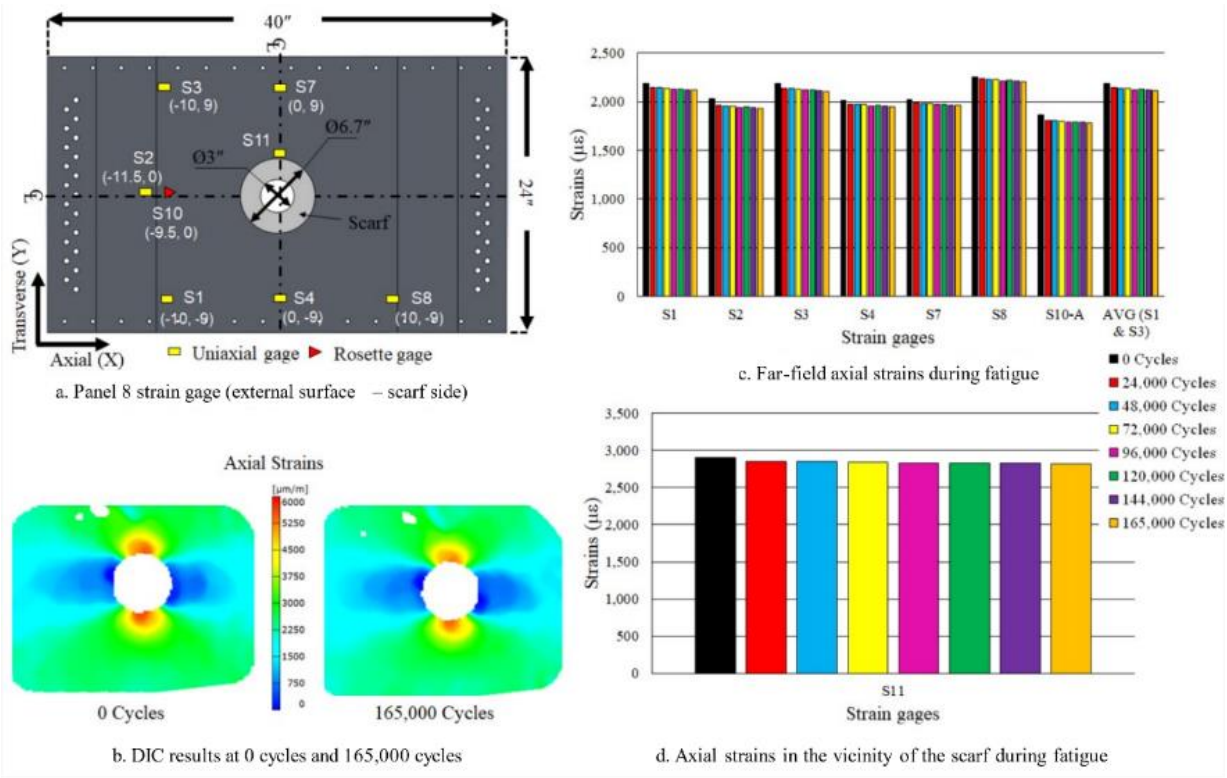

Figure 16. Panel 8 axial strain distribution during fatigue, from strain gages and DIC data

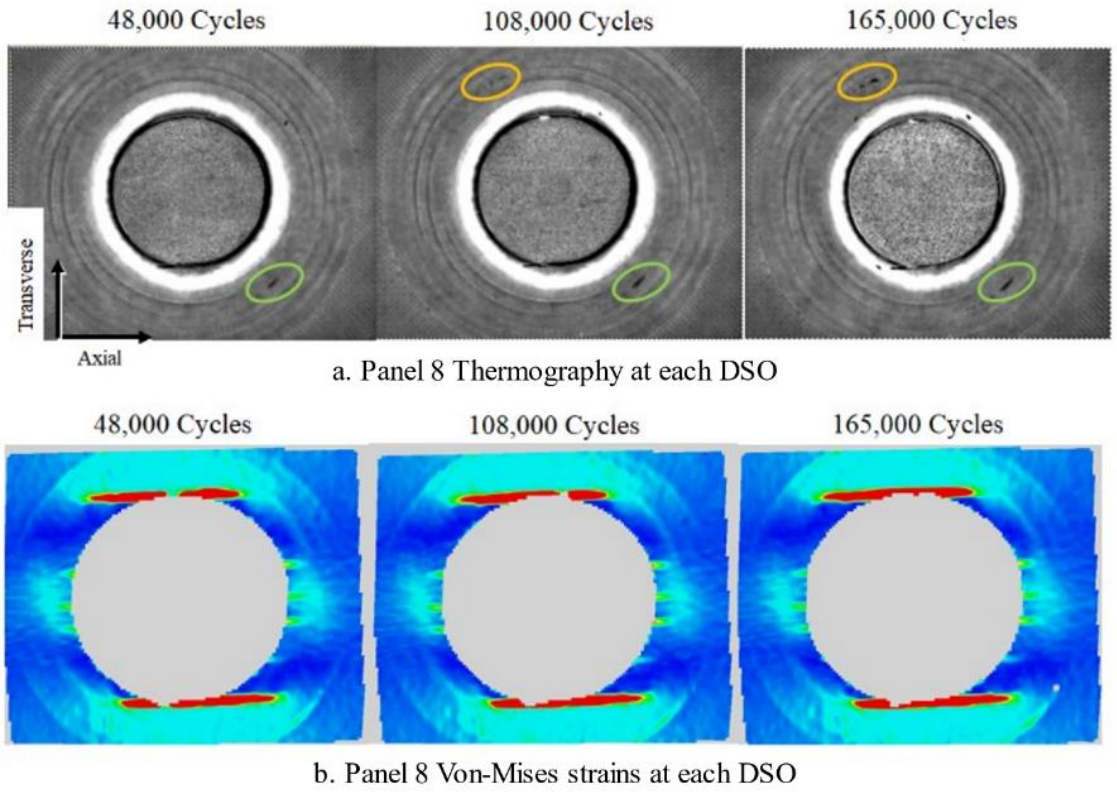

Figure 17. Panel 8 a) thermography images and b) von-Mises strains at each DSG

4.1.4 Panel 8 residual strength test results

After subjecting panel 8 to 3 DSGs, a residual strength test was performed. The load increments of the residual strength test were identical to panel 7 (Figure 14a), where the panel was loaded quasi-statically in a saw-tooth profile, increasing the load level up to the predicted critical loads of panel 4 with failed (cavity) full depth scarf (95,698 ft-lb_f), which was considered as 100%.

Both DIC system and thermography inspections showed that at each load increment, the results of panels 7 and 8 were very similar. The comparison of thermography and von-Mises strain images for both the panels are shown in Figure 18 and Figure 19, respectively. Both the panels showed minimal crack growth at the 6 o' clock and 12 o' clock locations, as shown in Figure 18. The delaminations in the 5^{th} ply (first 0^o ply from the top) were at the 11 o' clock and 5 o' clock locations in panel 8, as compared to the 1 o' clock and 7 o' clock locations in Panel 7, shown by thermography images in Figure 18 and DIC results in Figure 19.

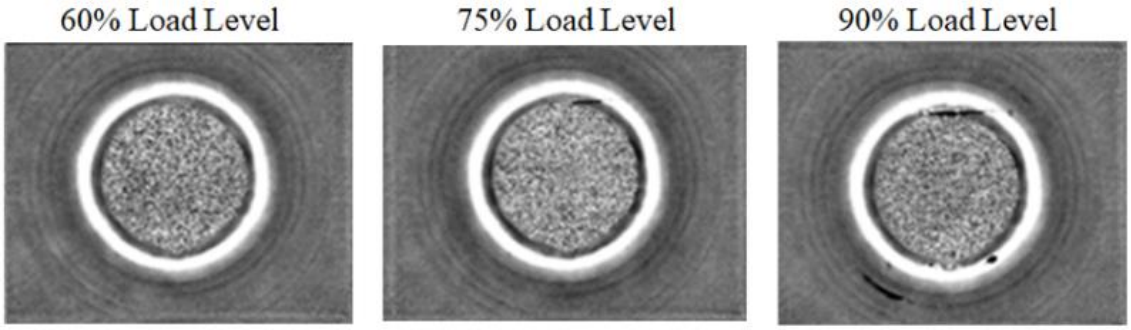

a. Thermography images of the scarf region of Panel 7

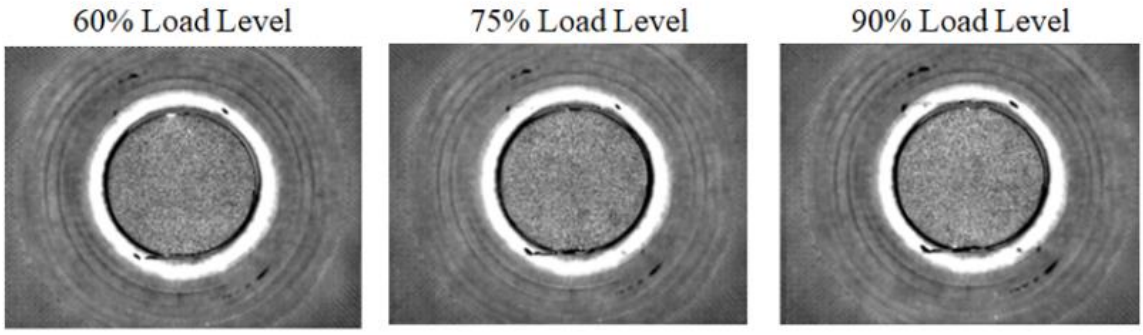

b. Thermography images of the scarf region of Panel 8

Figure 18. Thermography results in the scarf region for a) panel 7 and b) panel 8

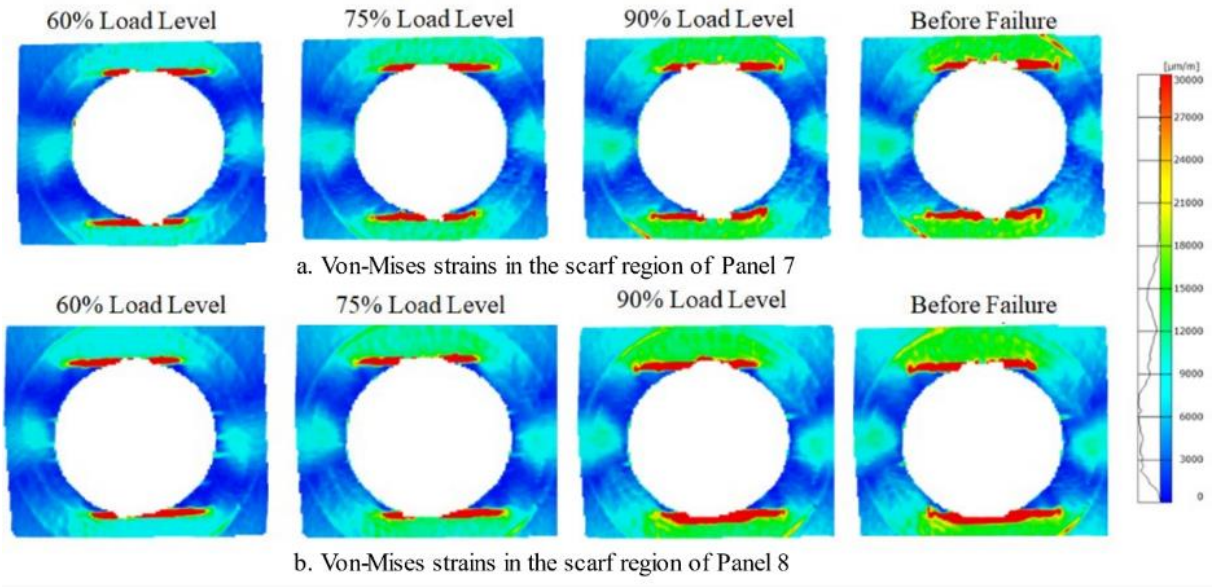

Figure 19. Von-Mises strain in the scarf region for a) panel 7 and b) panel 8

In the last load increment, the panel failed catastrophically through the net section at the applied moment of 95,024 lb_f-ft. This is within 1% of the failure load of panel 7 (94,418 lb_f-ft), indicating that there is no debit in strength of panel 8 after 165,000 fatigue cycles. The damage progression to the final failure of the panel 8 was a diagonal mirror image of panel 7. Since both the panels were subjected to constant moment loading, the similarity in damage progression was expected. The difference in the direction of damage progression could be due to practical differences in the panels' manufacturing.

4.2 Double-sided scarf panels with single-sided patch (panels 9, 10 and 11)

Three additional double-sided scarf panels with single-sided repair patch were tested. The goal of these tests was to evaluate that how well the double-sided scarf panels with single-sided repair patch are able to restore the strength as compared to the half-depth scarf panel 3. As mentioned above, these three panels were fabricated by two separate organizations within Boeing to account for potential variations in production processes. Panels 9 and 10 were fabricated at Boeing Research and Technology-South Carolina Center and panel 11 was fabricated at Boeing Research and Technology Structural Repair Lab in Seattle, Washington.

4.2.1 Baseline inspection and strain survey results

All three panels were quasi-statically loaded to failure to measure the residual strength of these panels. Prior to the residual strength tests, these panels were inspected both visually and with NDIs to detect any anomalies. Both visual inspection and phased array inspection showed that, as compared to panel 10 and 11, there was a slight offset in the patch and the scarf in panel 9. The images of the offset in panel 9 are shown in Figure 20. The effect of the offset in panel 9 was noticed during the initial strain surveys where the panel was quasi-statically loaded to yield far-field target strains of $1800\mu\varepsilon$. As shown in Figure 21b and c, the axial strain distribution in the vicinity of the scarf in panel 9 is asymmetric, with high stress concentration on the right inner edge of the scarf. This is the same section of scarf-patch offset as explained above. Unlike panel 9, the axial strains in the vicinity of the scarf in panel 10 and 11 were very symmetric as shown in Figure 21d-f.

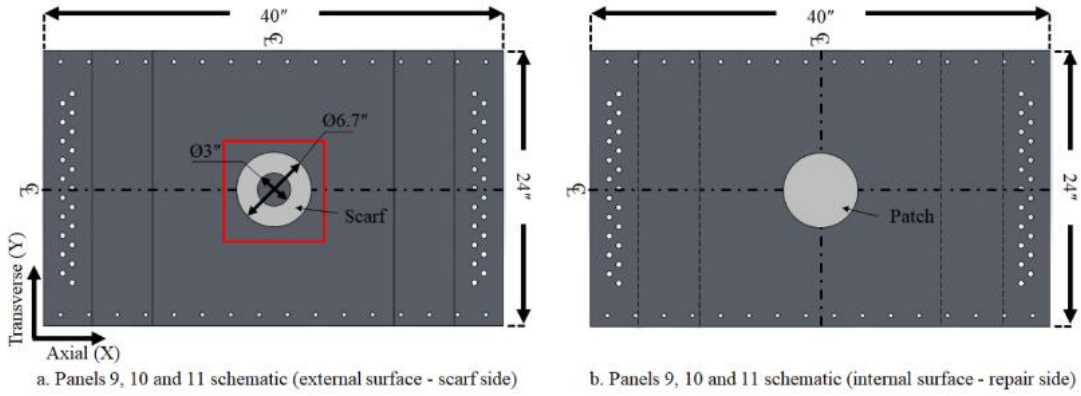

a. Panels 9, 10 and 11 schematic (external surface - scarf side)

b. Panels 9, 10 and 11 schematic (internal surface - repair side)

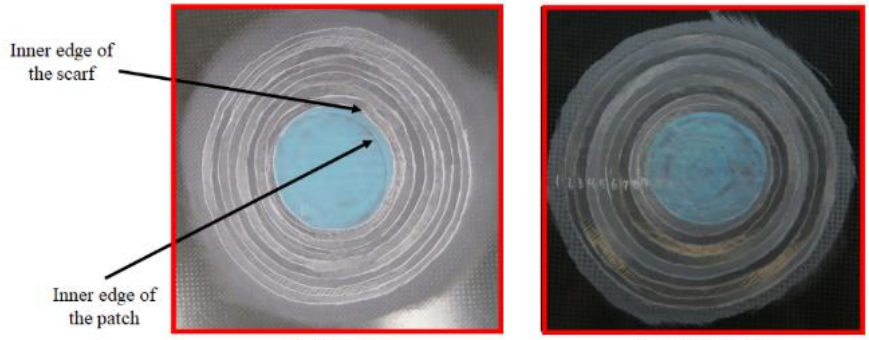

c. Panel 9 scarf

d. Panel 10 scarf

Figure 20. Images of Panels 9 and 10 showing the offset between patch and scarf in panel 9

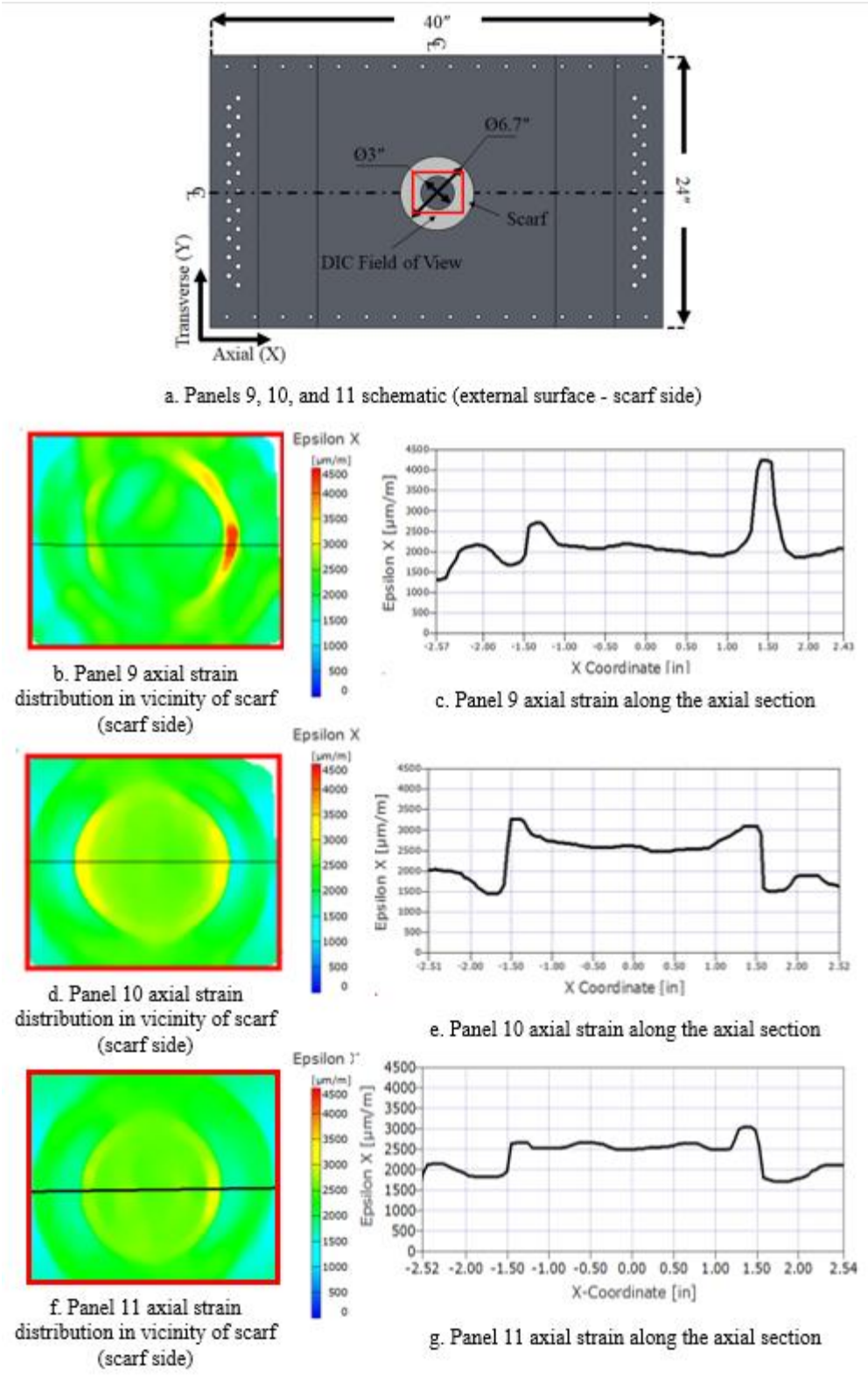

a. Panels 9, 10, and 11 schematic (external surface - scarf side)

b. Panel 9 axial strain distribution in vicinity of scarf (scarf side)

c. Panel 9 axial strain along the axial section

d. Panel 10 axial strain distribution in vicinity of scarf (scarf side)

e. Panel 10 axial strain along the axial section

f. Panel 11 axial strain distribution in vicinity of scarf (scarf side)

g. Panel 11 axial strain along the axial section

Figure 21. Axial strain distribution of panels 9, 10, and 11 measured using DIC system

The offset between the scarf and the patch in panel 9 did introduce local stress concentration in the inner edge of the scarf, but the effect of this offset was very local and did not affect the far-field strains in the panel, as shown in Figure 22 As shown in the figure, the axial strains measured using strain gages for panels 9, 10 and 11 were very similar for the same strain survey load-levels. Also shown is an excellent comparison of strains between the in double-sided scarf panel with single-sided repair patch (panels 9, 10 and 11) and half-depth scarf panel 5 during strain survey loading. Although for panels 9, 10 and 11 the load transfer from the parent material to the patch will not be as smooth and continuous as panel 5 due to the bondline (Figure 5), a good bond is able to transfer the load perfectly. Thus at strain survey loads, the double-sided scarf with single sided patch configuration works as the half-depth scarf configuration and shows similar strain distribution.

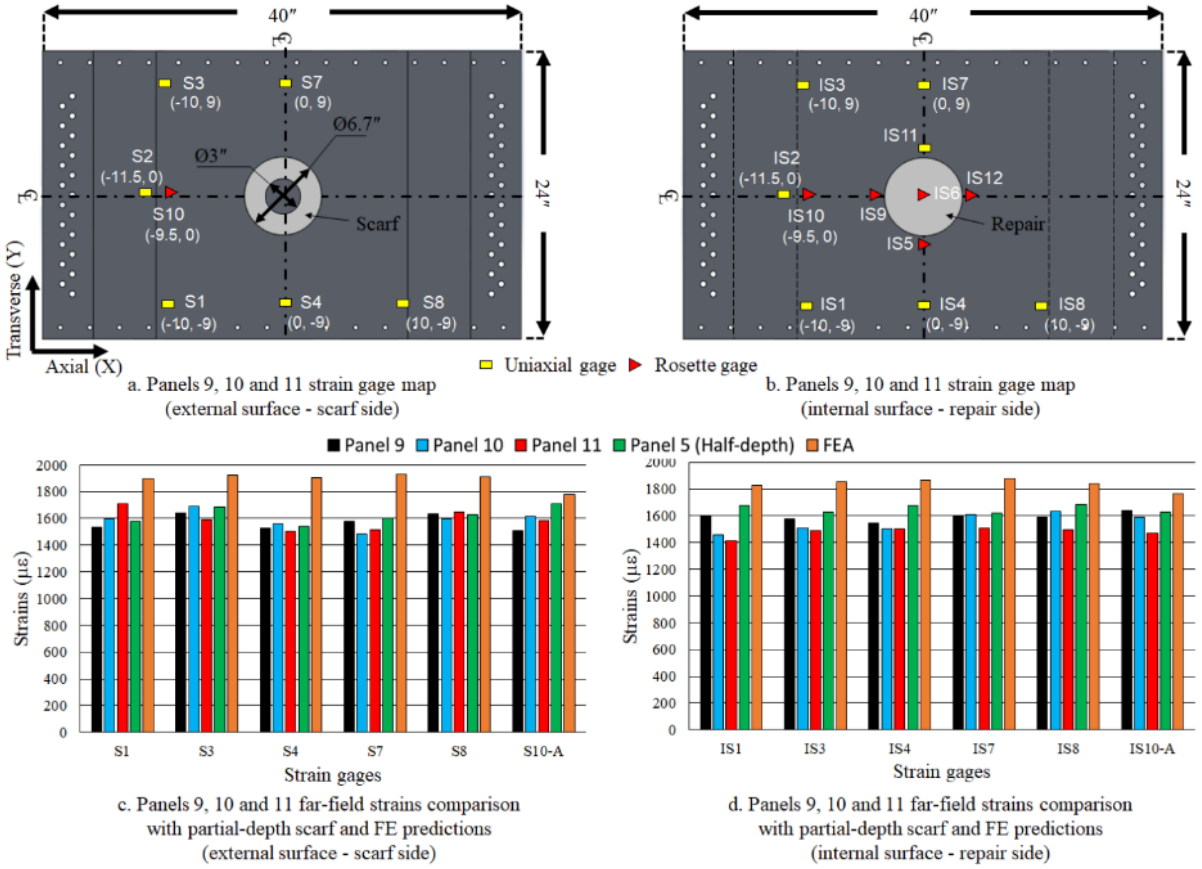

a. Panels 9, 10 and 11 strain gage map (external surface - scarf side)

b. Panels 9, 10 and 11 strain gage map (internal surface - repair side)

c. Panels 9, 10 and 11 far-field strains comparison with partial-depth scarf and FE predictions (external surface - scarf side)

d. Panels 9, 10 and 11 far-field strains comparison with partial-depth scarf and FE predictions (internal surface - repair side)

Figure 22. Far-field axial strains in panels 9 and 10 measured during initial strain surveys

4.2.2 Residual strength tests

After the initial strain surveys, residual strength tests were performed to panels 9, 10 and 11. The panels were loaded quasi-statically in a saw-tooth profile, increasing the load level up to the predicted critical loads of panel 3 with failed (cavity) half-depth scarf (168,611 ft-lb_f), which was considered as 100%. During loading, damage formation was monitored visually using high-magnification cameras and DIC. After each loading, the scarf and its vicinity were inspected using thermography. For panel 9, the target of the first load increment was 60% of the half-depth scarf panel 3 predicted critical load, but the damage was first detected visually at 35% load level in the form of edge delamination (first 0^o ply) along the scarf inner-edge, at the 3 o'clock position. As the delamination was detected, the test was unloaded, and thermography inspection was conducted to document the delamination. The panel was then reloaded to higher load level and at 42% load level (72,983 ft-lb_f), the patch unexpectedly failed. The test was subsequently stopped at 55% load level (92,954 ft-lb_f) to save the panel for future inspections. Since the patch had failed, further loading the panel would have caused catastrophic failure of the panel. Figure 23 shows the schematic of loading profile, DIC results at the peak loads and thermography results after each unloading.

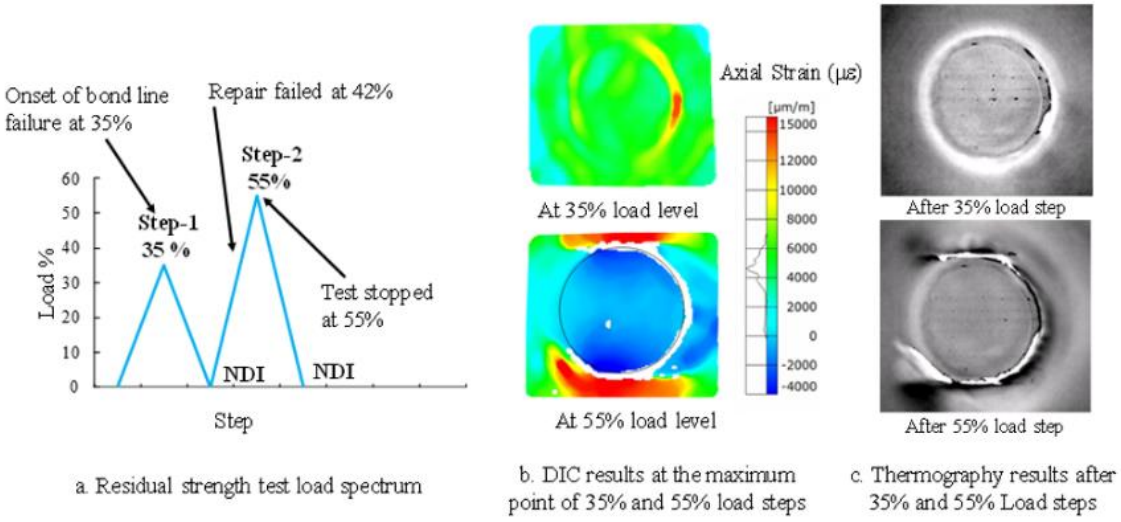

Figure 23. Panel 9 residual strength test; a) load spectrum, b) DIC, c) thermography results

Panels 10 and 11 were subjected to similar residual strength test. The loading profile, axial strain distribution in the vicinity of the scarf and within the scarf just prior to panel failure measured using the DIC system for panels 9, 10 and 11 are shown in Figure 24. As shown in the figure, the axial strain distribution in panel 10 scarf just prior to failure was symmetric at 3'o clock and 9' o clock locations, thus providing negligible indication of the path of load transfer. The panel failed

catastrophically along the net section at 59% load level. In panel 11, the axial strains in the scarf shows a slightly higher stress concentration at the 3'o clock location, which indicated that the patch is separating from the parent material at the 9' o clock location causing the strain to rise at the 3'o clock location. Further, the panel failed at 58% load level. The failure was so sudden that neither DIC nor the video cameras were able to capture the progression of failure.

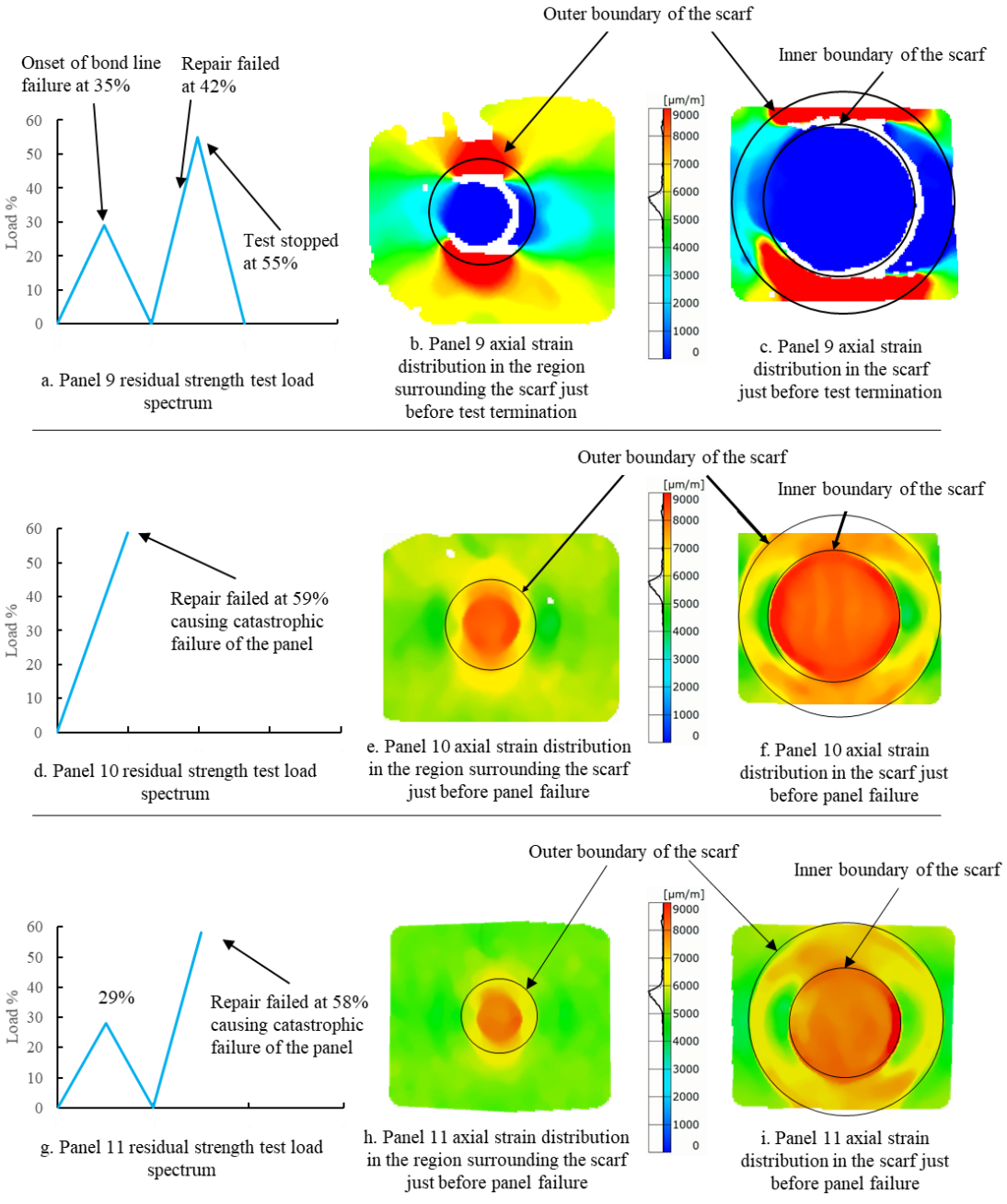

Figure 24. Ultimate load DIC strain fields for (a-c) panel 9, (d-f) panel 10, and (g-i) panel 11

The images of failed panels 9, 10, and 11 are shown in Figure 25. In general, bondline failure of the repair patch occurred first followed by rapid catastrophic net-section fracture of the panels.

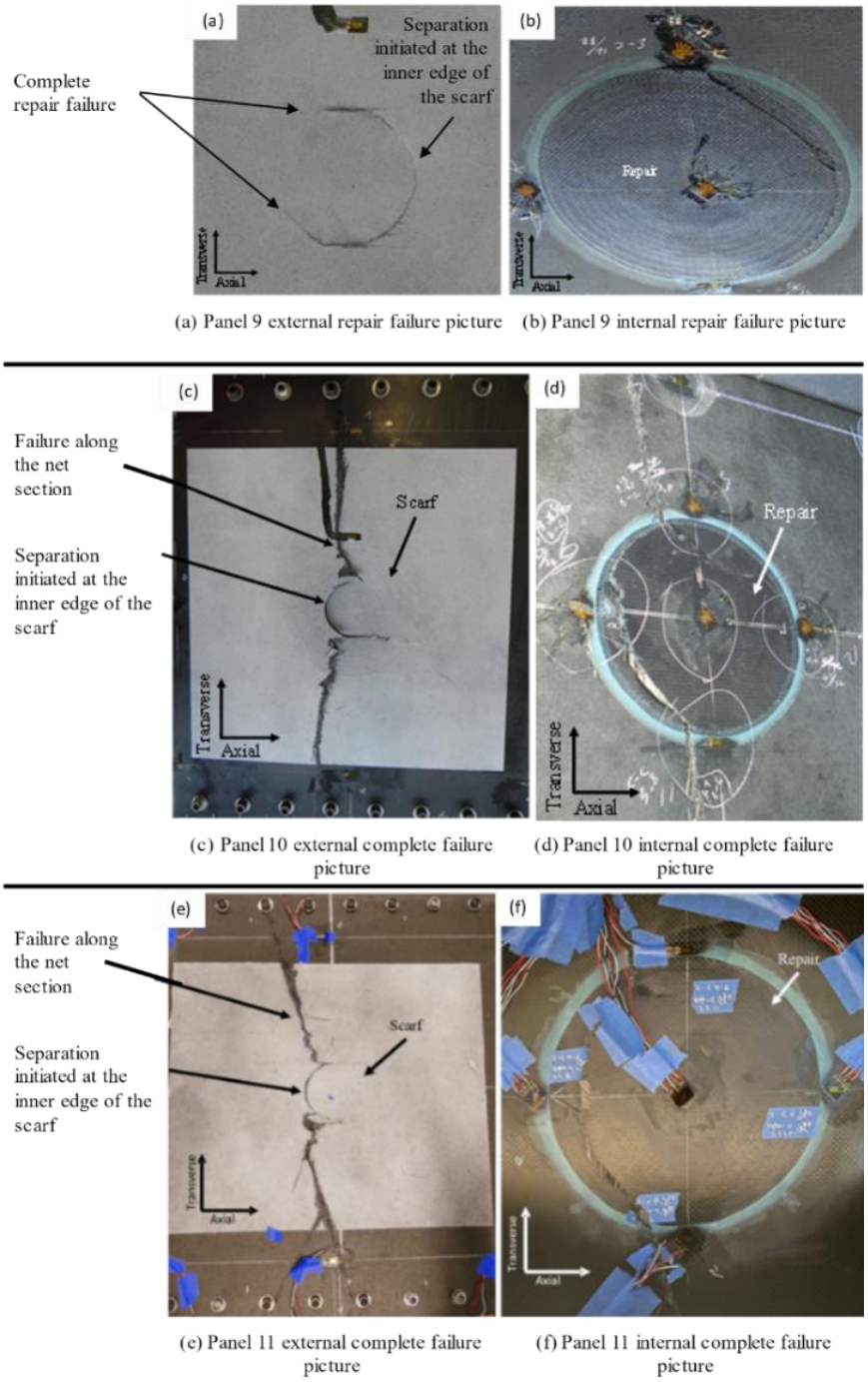

Figure 25. Post-failure pictures of (a,b) panel 9, (c,d) panel 10, and (e,f) panel 11

As mentioned above, panels 10 and 11 failed catastrophically and for panel 9, the test was stopped before complete failure to inspect the fractured surfaces. The images of the fractured panel 9 bondline is shown in Figure 26.

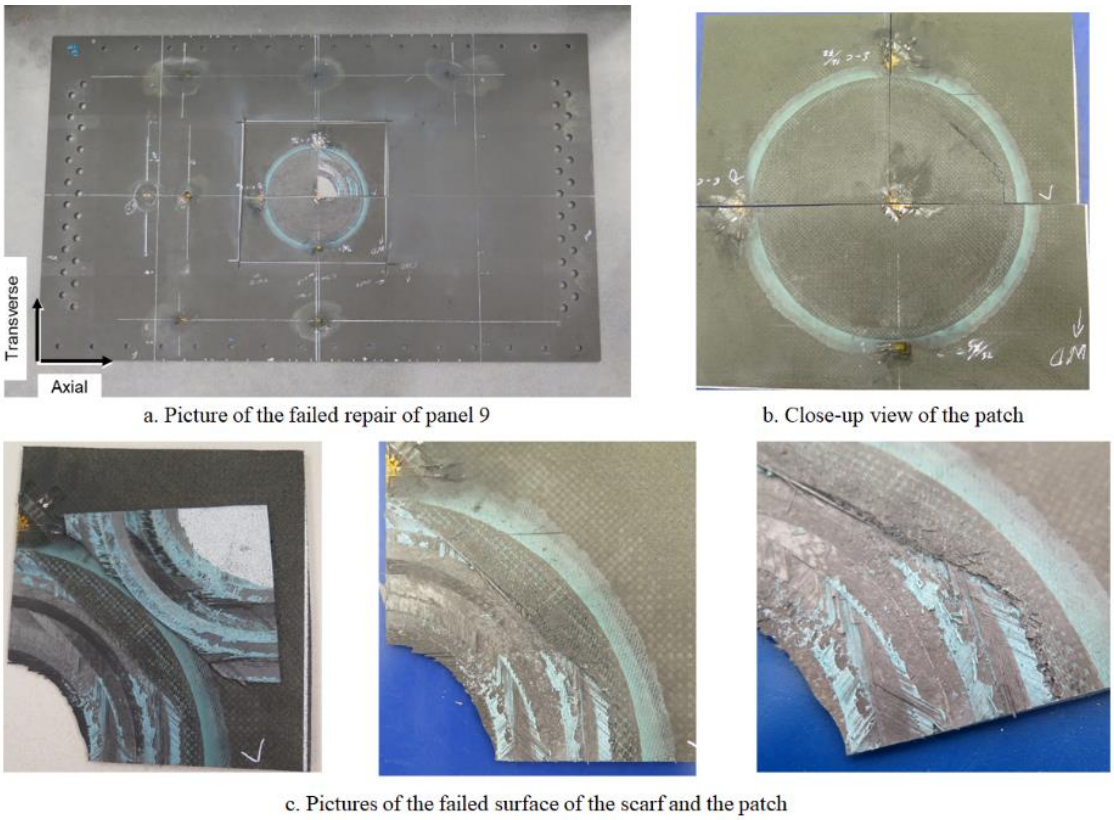

a. Picture of the failed repair of panel 9

b. Close-up view of the patch

c. Pictures of the failed surface of the scarf and the patch

Figure 26. Post-test visual inspection of failed panel 9 (repair patch side)

The pictures of the interface between the patch and scarf shows the bondline failure and separation between the patch from the parent material and thus transferring the load to the net section leading to the catastrophic failure of the panel.

The bondline failure can be explained via Figure 27. As shown in the figure, a single-sided repair patch resulted in an eccentrically loaded moment and higher peel stresses causing the bondline failure. It should be mentioned that there was no substructure in these panels. The presence of stringers would have reduced the eccentricity and peel stresses on the bond by transferring more load on the stringer and reducing the prying moment.

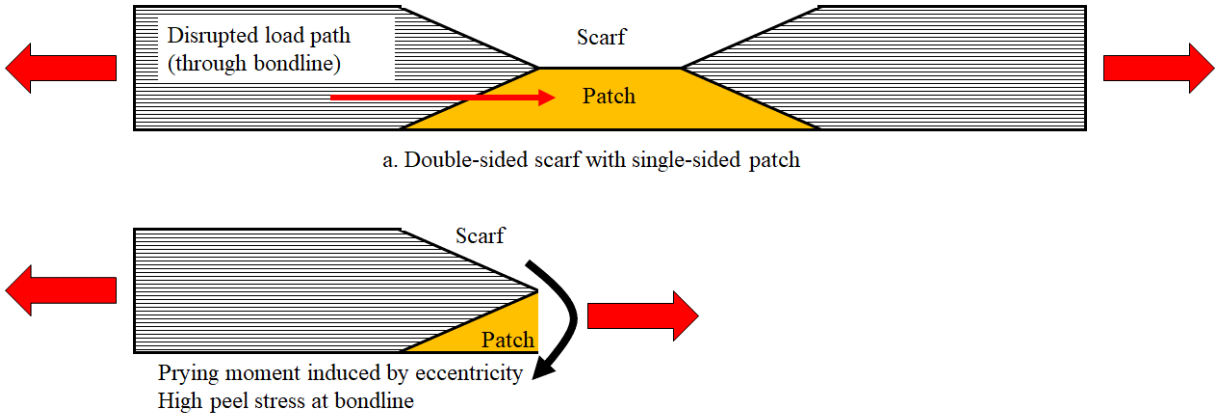

Figure 27. Schematics showing the prying moment induced by the eccentricity

The load transfer leading up to the failure of the panel can be studied by the strain gage results. As an example axial strains measured prior to and during repair failure for panel 10 are shown in Figure 28. As shown in Figure 28c, during the repair failure the strains at the ends of the panel reduced (strain gages S1, S3, S8 and IS1, IS3, IS8) but the strains in the net section increased significantly (strain gages S4, S7 and IS4, IS7) indicating the load transfer to the net section of the panel. The strains in the vicinity of the patch (strain gages IS5, IS9, IS11 and IS12) shown in Figure 28d also rise significantly due to the load transfer. Figure 28d also shows the strains at the patch edge at 9 o' clock position (IS9) were slightly higher than at 3 o' clock position (IS12) indicating the failure initiated from the 9 o' clock position, which was confirmed by visual inspection of the panel after failure. Overall, the strain gages were able to capture the load transfer prior to the panel failure.

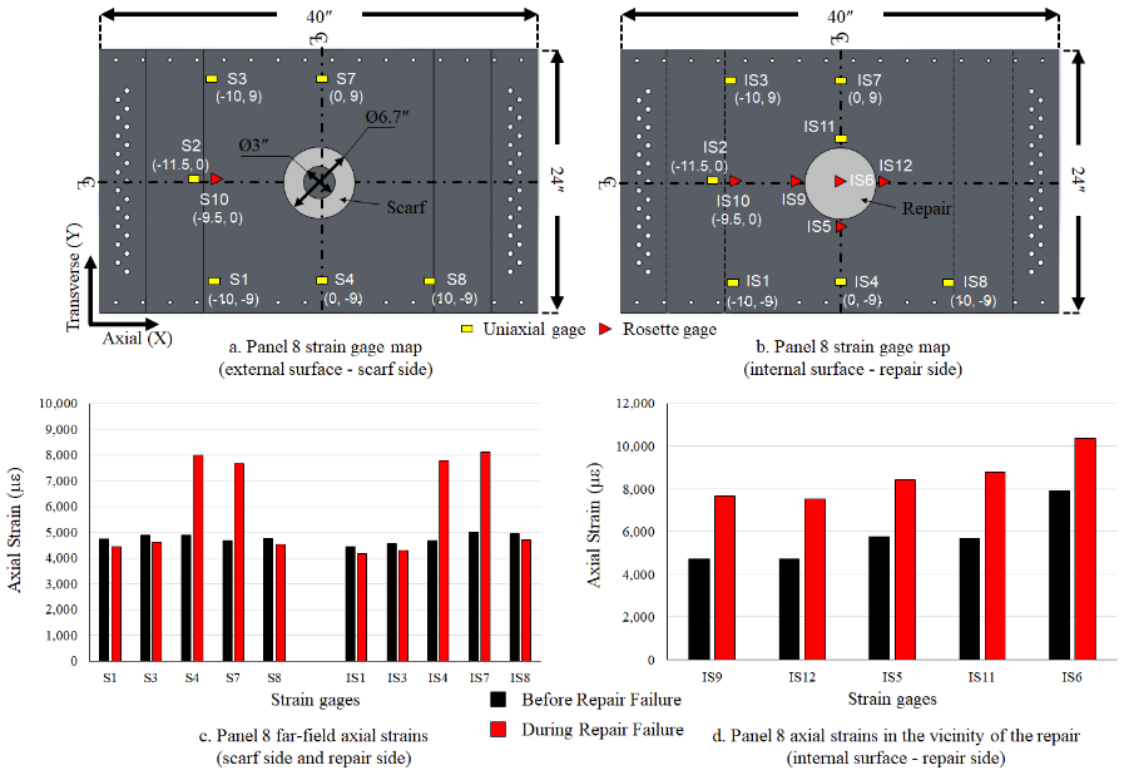

Figure 28. Panel 10 axial strains captured just before and during the repair failure

4.3 Comparison of the residual strength of all the panels (panels 7 - 11)

The goal of panels 7 and 8 tests was to study the effect of fatigue on the residual strength of the panels with double-sided scarfs without any patches. For panels 9, 10 and 11 test, the target was to measure the effectiveness of panels with double-sided scarfs that are partially repaired (single-sided patch) in restoring the strength when compared to the panels with half-depth scarfs. In order to compare the effectiveness, the strengths of panels 7 -11 are plotted in Figure 29. These strengths are normalized by the strength of an open-hole panel tested in phase 2 (Neel, et al., 2020). In addition, the figure also shows the normalized strength of panels with half-depth scarf (panels 3 and 5) and full-depth scarf (panels 4 and 6) tested in phase 3 (Neel R. C.-M., 2021). As seen in the figure, the strength of panels 9, 10, and 11 was similar to that measured in panels 7 and 8, indicating that within the scope of this research, the single-sided patch was not effective at all in restoring strength. Bondline failure of the repair patch occurred in panels 9 – 11 at the same load level as net section failure observed for the double-sided scarf panels 7 and 8. In addition, the comparison of strengths of panels 9, 10, and 11 with half-depth scarf panels 3 and 5 shows the inability of the single-sided repair patch to be as effective as panel with half-depth scarf. The strength of panel 8 as compared to panel 7 shows that subjecting the panel with double-sided scarf to 3 DSGs had no effect on its residual strength.

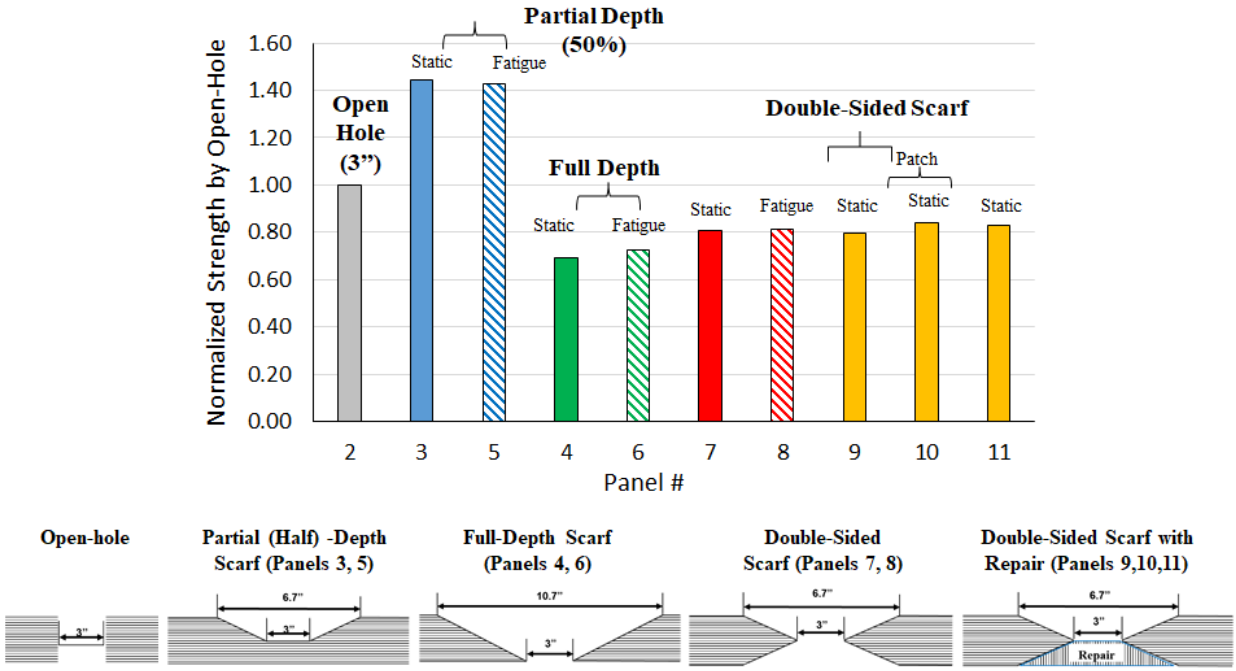

Figure 29. Comparison of strength of all the panels

4.4 Summary

In a joint effort, The Federal Aviation Administration and The Boeing Company are addressing safety and structural integrity issues of bonded repair technology. Recent efforts have focused on bonded repairs to composite panels representative of typical transport aircraft wing structure. The program objectives are to characterize the fatigue and damage tolerance performance of bonded repairs subjected to simulated service load and to evaluate the limit-load capability of typical composite wing panels with a failed repair. Emphasis has been placed on investigating the methods and tools used for predicting structural performance of repairs and as those used to evaluate and monitor repair integrity over the life of the part.

A phased approach is being undertaken in the multiyear effort. The initial baseline testing (phase 2) of this program characterized the material response of composite panels in the unnotched pristine and open-hole configurations under constant moment loading. This verified the test-fixture loading, validated analysis models, and provided an initial reference point for NDI and SHM systems.

The third phase of this program characterized the limit-load capability for partial (half)-depth, full-depth and both side half-depth scarf configurations for solid laminates under tension produced by constant moment. The benefit gained in the residual-strength limit-load capability of a failed half-depth scarf was revealed and documented in the first technical report of this

phase (Neel R. C.-M., 2021). For both half-depth scarf and full-depth scarf configurations, there was no debit in strength due to 3 DSGs. In addition, analytical models currently under development to accurately predict the strain levels associated with failed repair depth were demonstrated.

This report documents additional work in phase 3 considering double-sided scarfs with and without single-sided patch configurations for solid laminates under tension produced by constant moment. Benefits realized by double-sided scarfing include less material removal, a smaller repair footprint and consequently a slightly higher residual strength compared to a full-depth scarf configuration. As with the full-depth and half-depth scarfs, there was no debit in strength after fatigue load application of 3 DSGs. At low load levels, the single-sided repair patch in a double-sided scarf was effective in restoring load transfer similar to that observed in the half-depth scarf panel. However, results show that a single-sided repair patch in a double-sided scarf tested in this program cannot be credited for restoring the strength of the panel. Bondline failure of the repair patch occurred at the same load level as net section failure for the double-sided scarf configurations due to high peel stresses induced by bending eccentricity. It should be noted that these experiments were limited to 18-ply CFRP panels without any stiffening sub-structure, which does not represent an actual configured wing panel. For such structure, the stiffening elements (stringers, ribs, etc.) would in many cases react most of the bending moment, thus mitigating the effect of any eccentricity within the panel. While these results provide valuable insights to the residual strength behavior of CFRP panels with various scarf configurations, caution must be exercised in their direct application to real structure.

5 References

Baker, A. A., Rose, L., & Jones, R. (Eds.). (2003). *Advances in the bonded composite repair of metallic aircraft structure* (Vol. 1). Elsevier.

Chadha, R., Bakuckas Jr., J. G., Fleming, M., Lin, J., & Korkosz, G. (2019). *Airframe beam structural test (ABST) fixture—capabilities description and user manual.* DOT/FAA/TC-TN19/7.

Federal Aviation Administration. (2011, January 13). *Damage tolerance and fatigue evaluation of structure.* Advisory Circular AC 25.571-1D. Retrieved from https://www.faa.gov/documentLibrary/media/Advisory_Circular/AC_25_571-1D_.pdf

Federal Aviation Administration. (2014). *Bonded repair size limits.* FAA Policy Statement No. PS-AIR-20-130-01, U.S. Department of Transportation.

Hashin, Z. (1980). Failure Criteria for Unidirectional Fiber Composites. *Journal of Applied Mechanics, vol. 47*, 329–334.

Neel, R. C.-M. (2021). *Bonded Repairs to Composite Wing Panel Structure: Phase 3, Bonded Repair Size Limits Study for Solid Laminates with Full-Depth and Partial-Depth Scarf Configurations.* DOT/FAA/TC-21/27.

Neel, R. J., Chadha, R., Bakuckas Jr., J. G., Fleming, M., Lin, J., & Espinar-Mick, E. (2020). *Bonded Repairs to Composite Wing Panel Structure: Phase 2, Baseline Study.* DOT/FAA/TC-21/17.

A Specimen Engineering Drawings

INTRODUCTION

Provided in this appendix are detailed drawings of the pristine and open-hole panels.

SPECIMEN ENGINEERING DRAWINGS

Detailed drawings of the double-sided scarf without repair (Panel 7 and Panel 8) is provided in Figure A-1, a drawing of the repair patch is provided in Figure A-2, and an assembly drawing of the double sided scarf with a repair patch (Panels 9-11) is provided in Figure A-3.

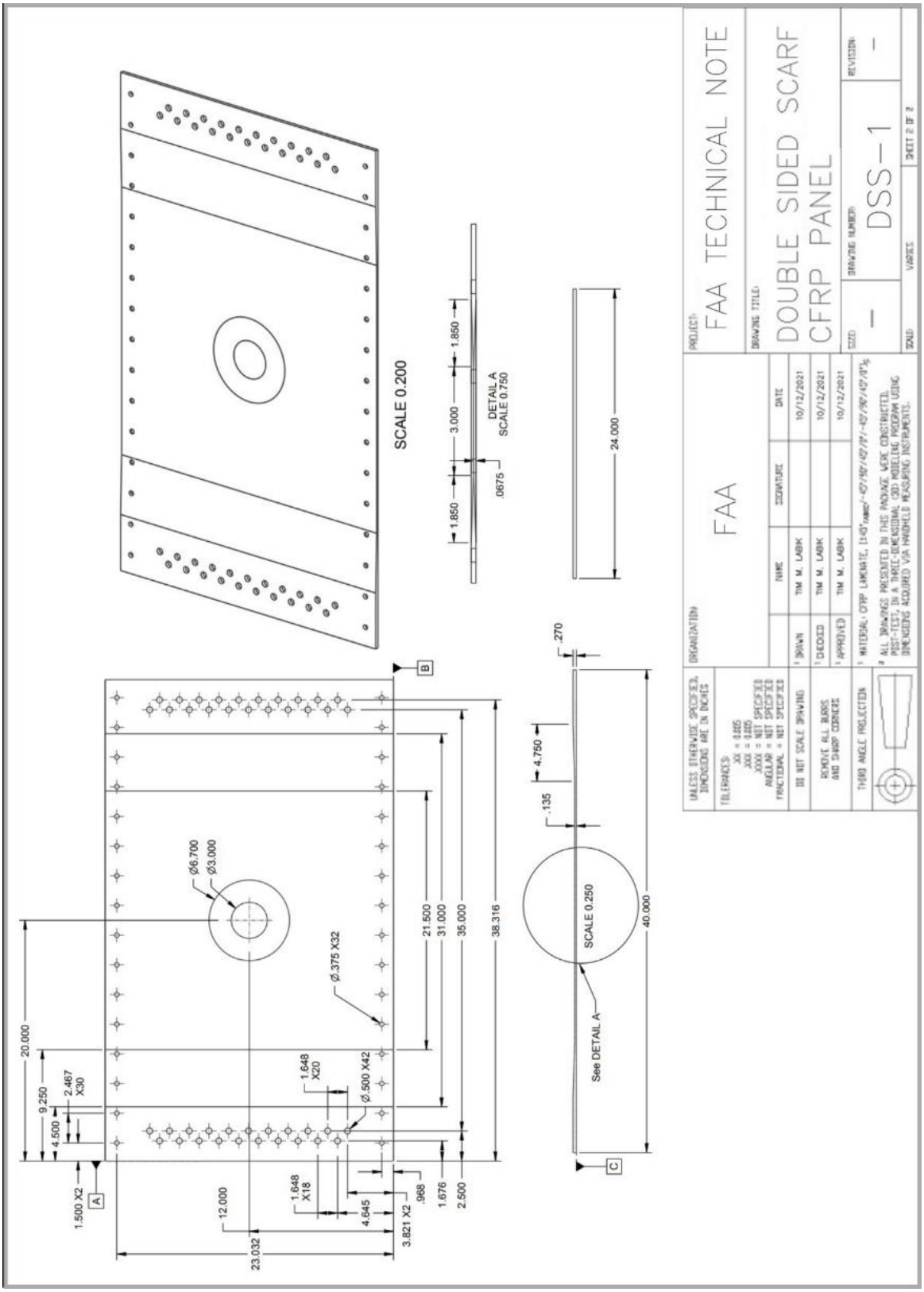

Figure A-1 Drawing of the double-sided scarf specimen without repair

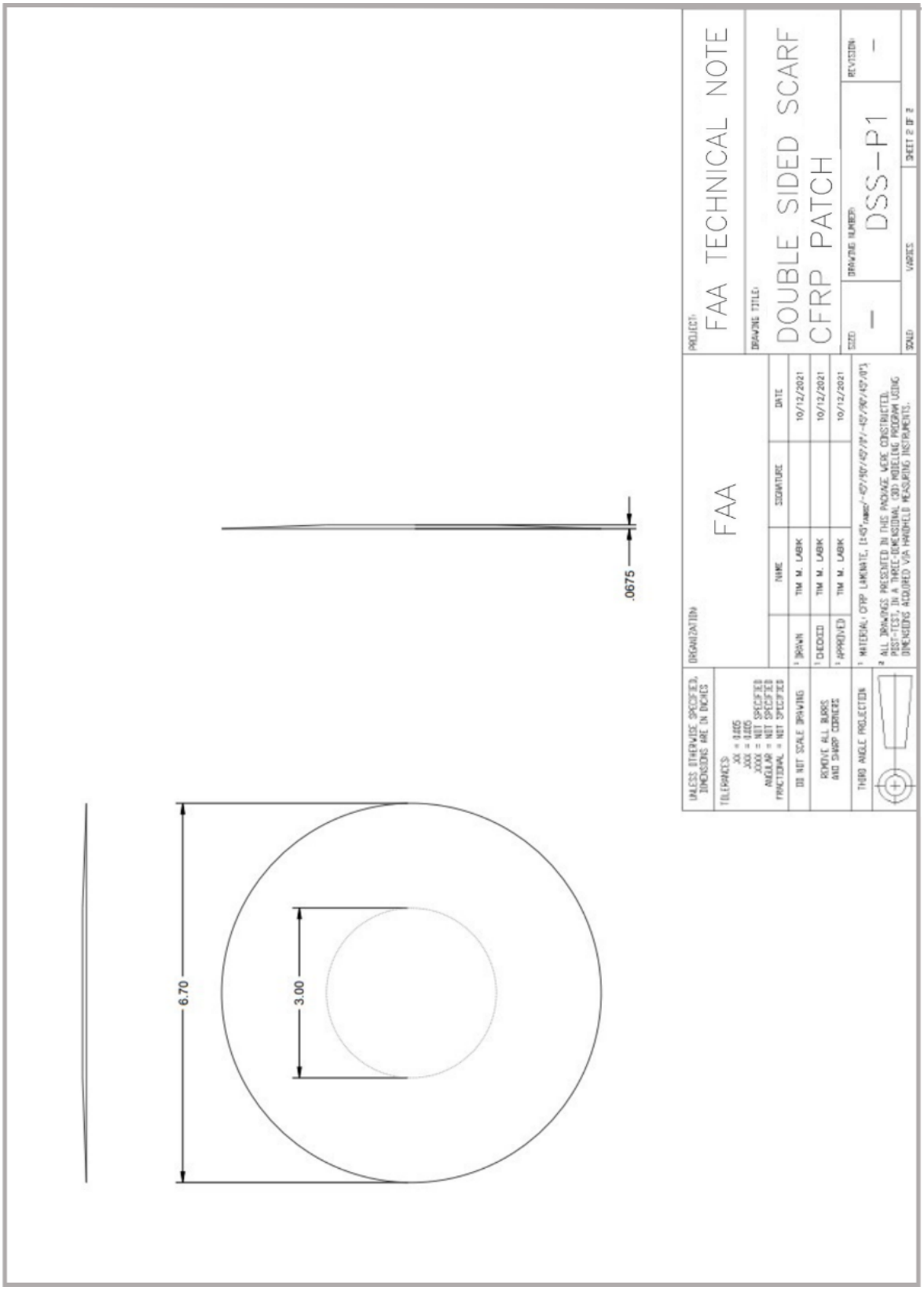

Figure A-2. Drawing of the single sided repair patch

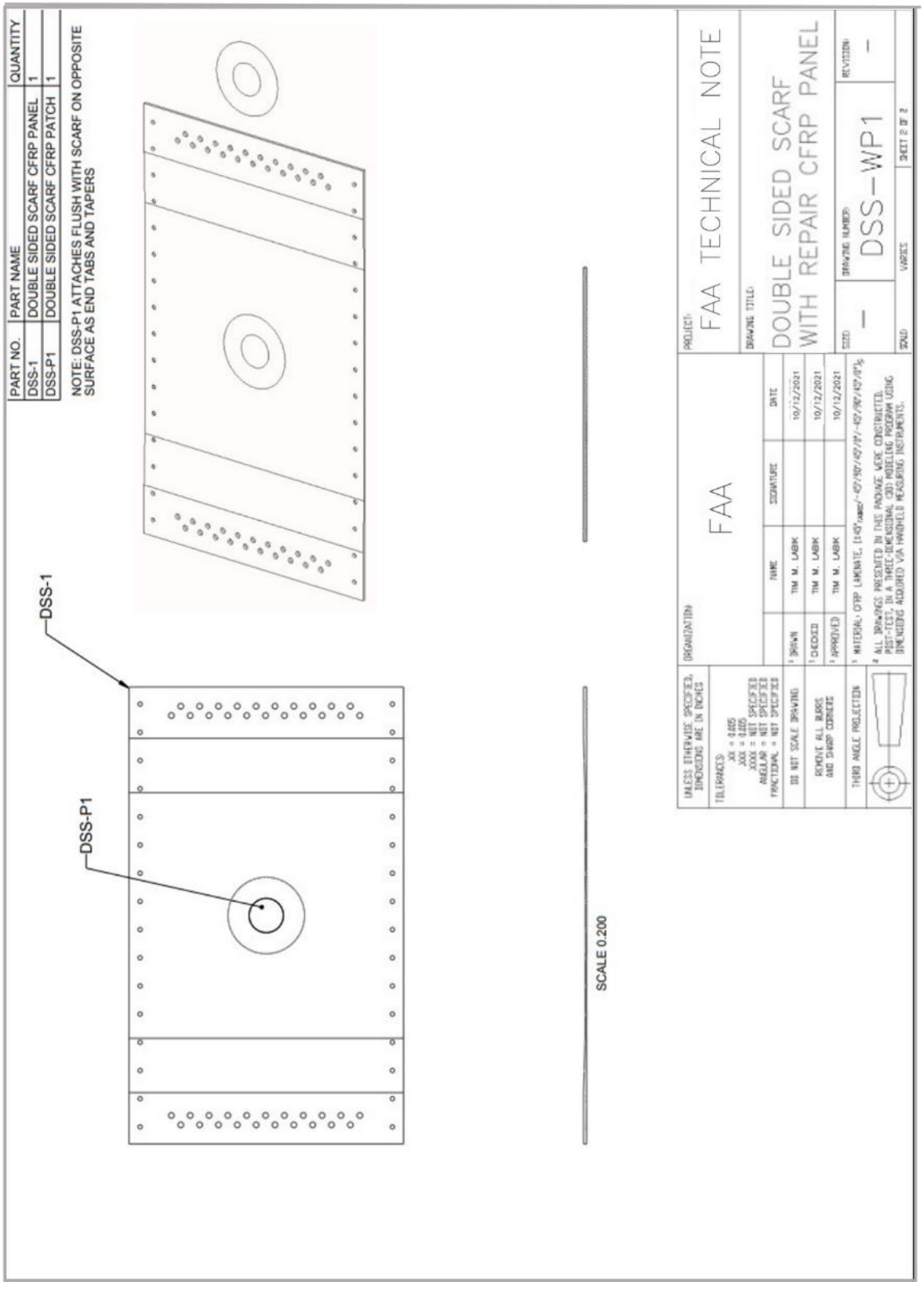

Figure A-3. Assembly drawing of the double-sided scarf panel with repair

B Strain and Displacement During Strain Surveys

INTRODUCTION

Provided in this appendix are strain gages results captured during quasi-static loading of the double-sided scarf panel specimens.

STRAIN SURVEY RESULTS

The location and nomenclature for displacement sensors and strain gages for the panels are shown in Figure B-1 and Figure B-2, respectively. For Panel 7, all the strain and displacement measurements collected at 0 cycles are shown in Figures B-3 – B-4. For Panel 8, the strain survey results for from 0 – 165,000 cycles are shown in Figures B-5 – B-34. For Panel 9, Figures B-35 – B-36. For Panel 10, Figures B-37 – B-38. For Panel 11, Figures B-39 – B-40.

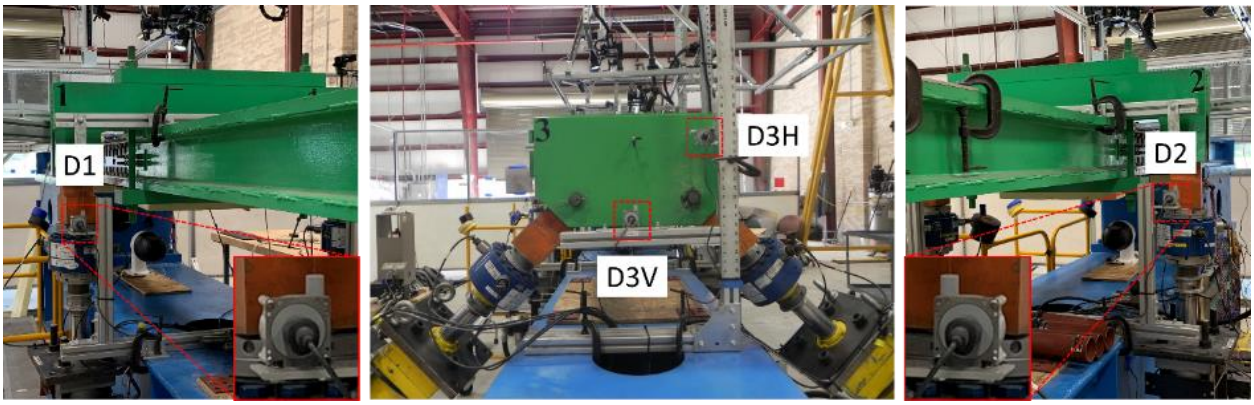

Figure B-1. Images displaying the (Elsevier) displacement transducer positions

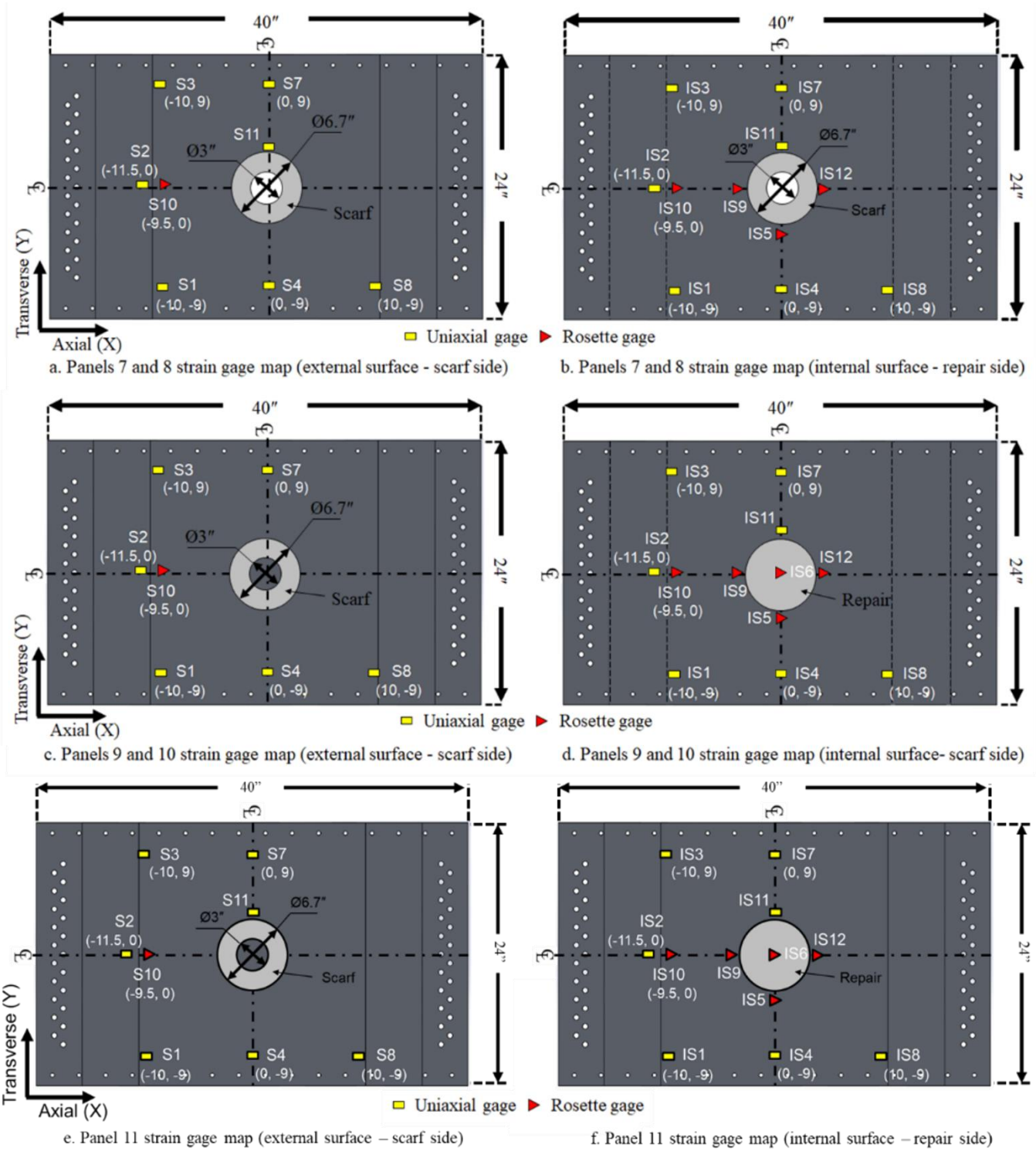

Figure B-2. Images displaying layout of strain gages for panels 7-11 during testing.

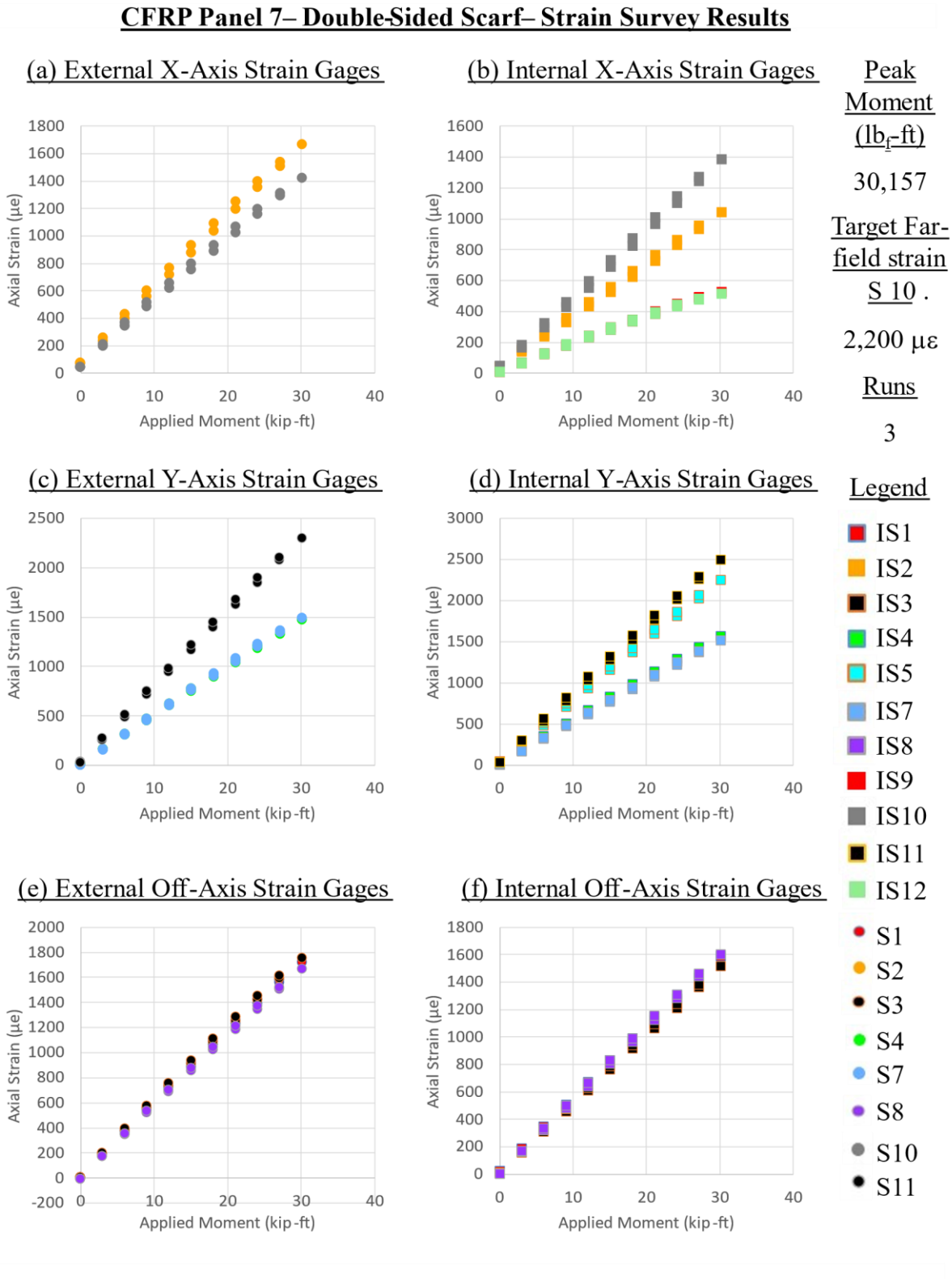

Figure B-3. Panel 7: baseline strain survey (axial strain)

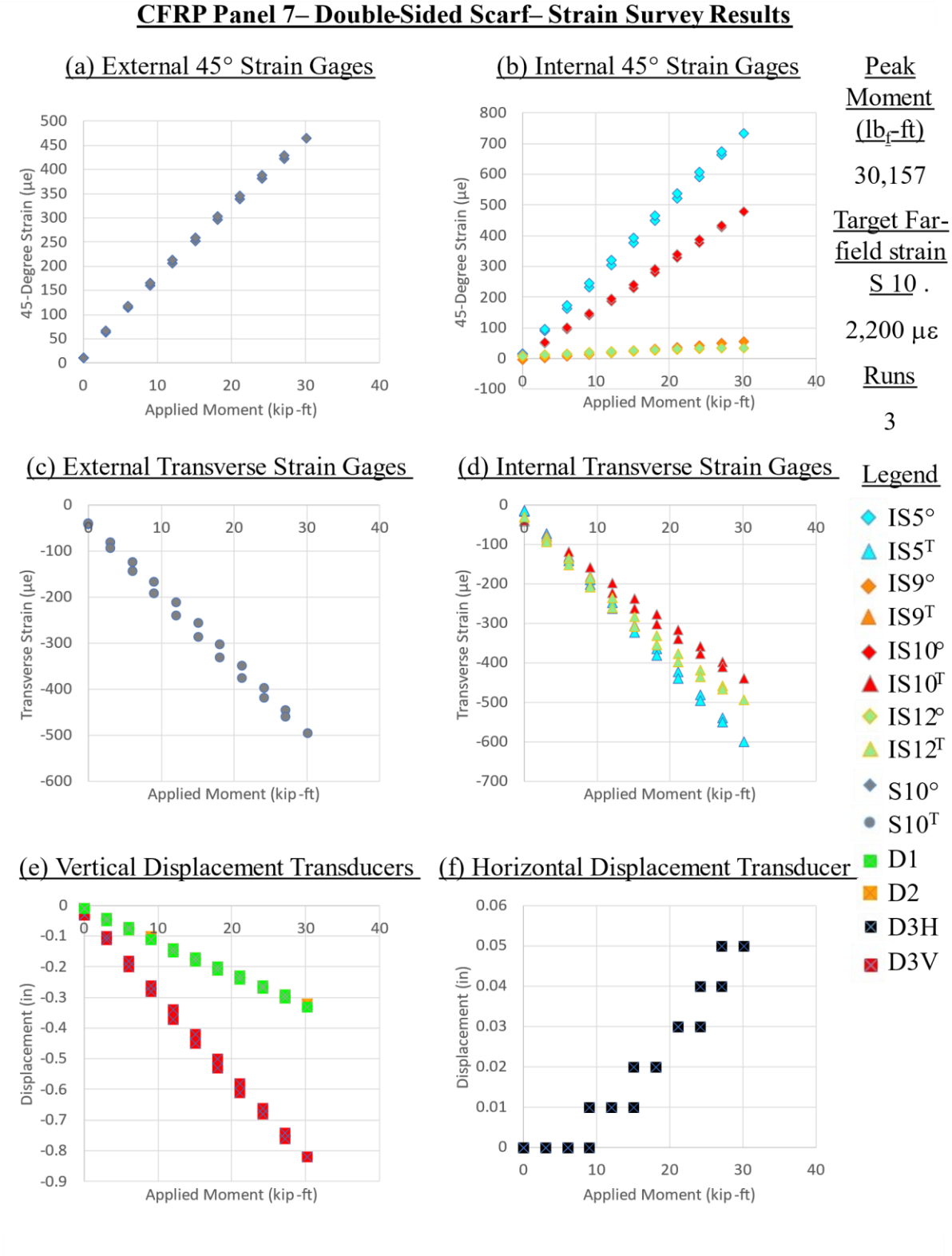

Figure B-4. Panel 7: baseline strain survey (non-axial strain and displacement)

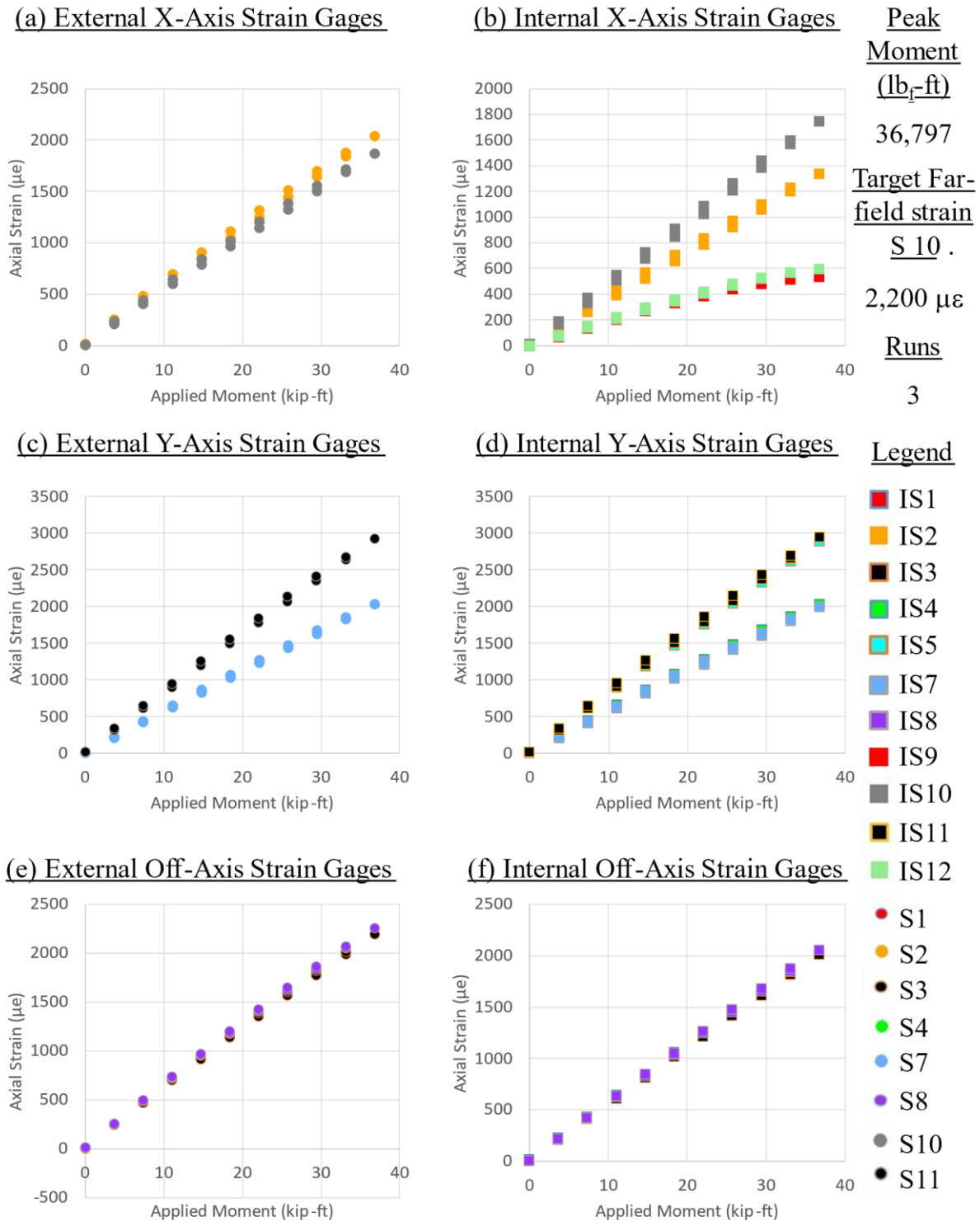

Figure B-5. Panel 8 (fatigue at SL strain level): strain survey at 0 cycles (axial strain)

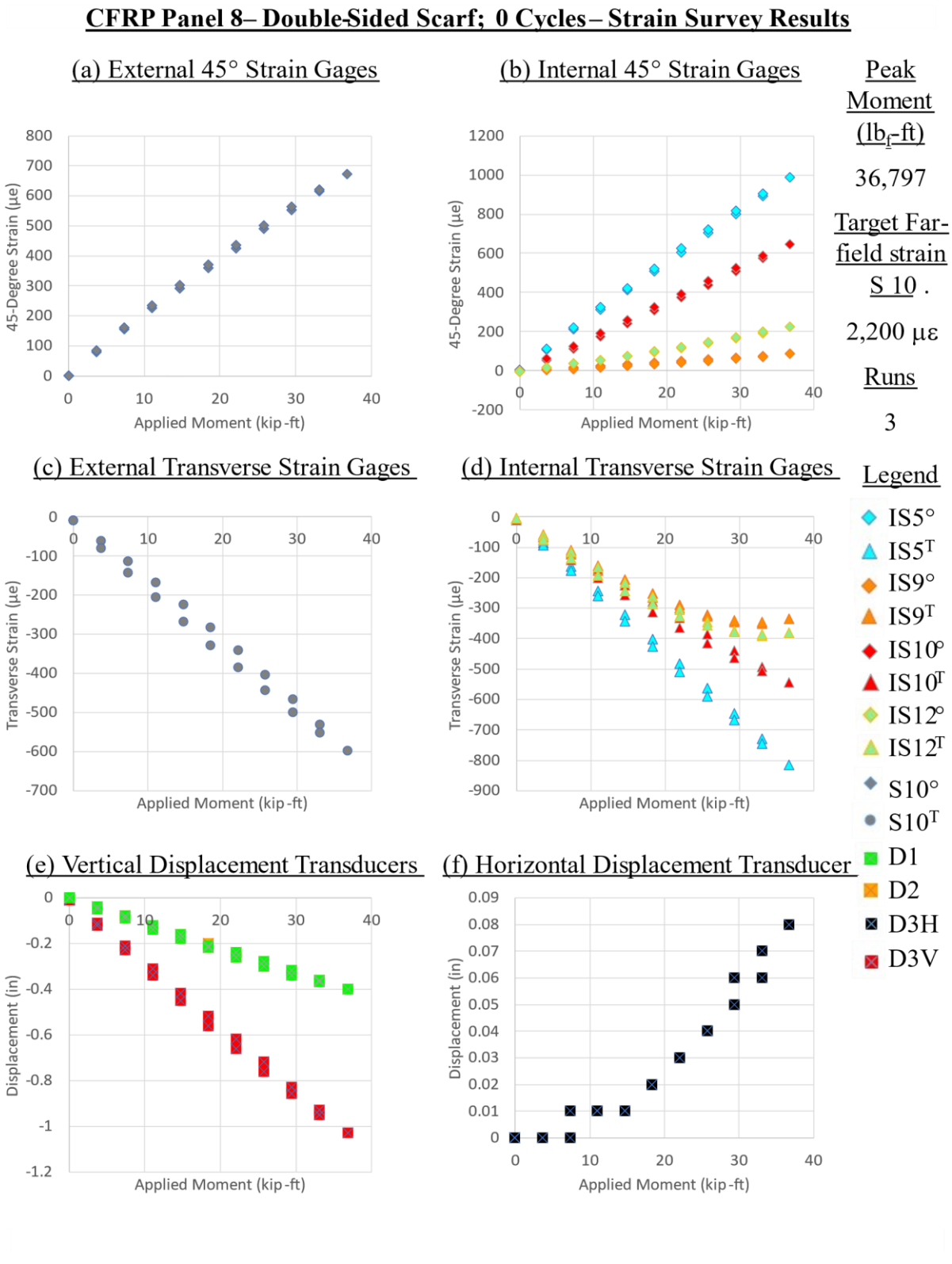

Figure B-6. Panel 8 (fatigue at SL strain level): strain survey at 0 cycles (non-axial strain and displacement)

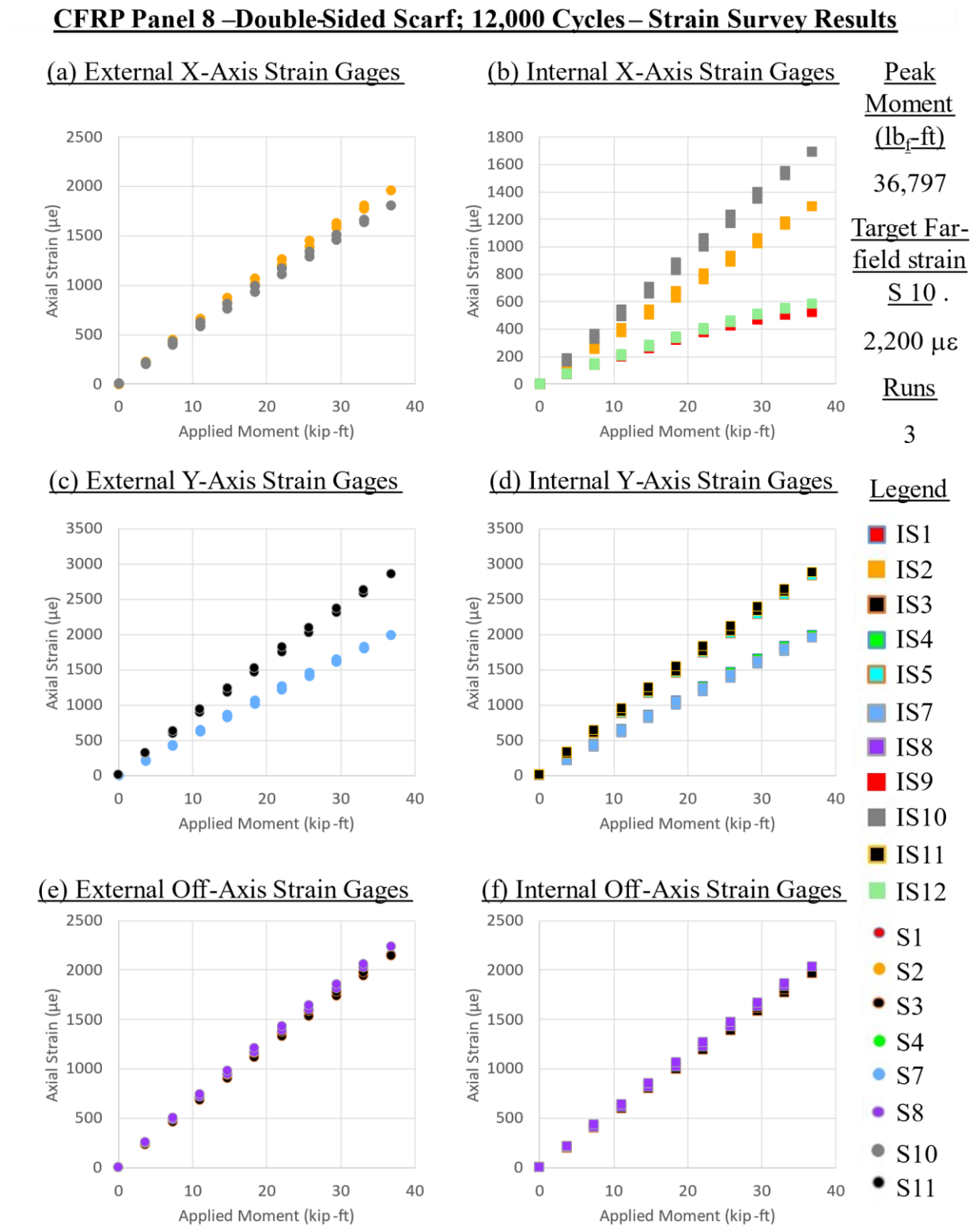

Figure B-7. Panel 8 (fatigue at SL strain level): strain survey at 12,000 cycles (axial strain)

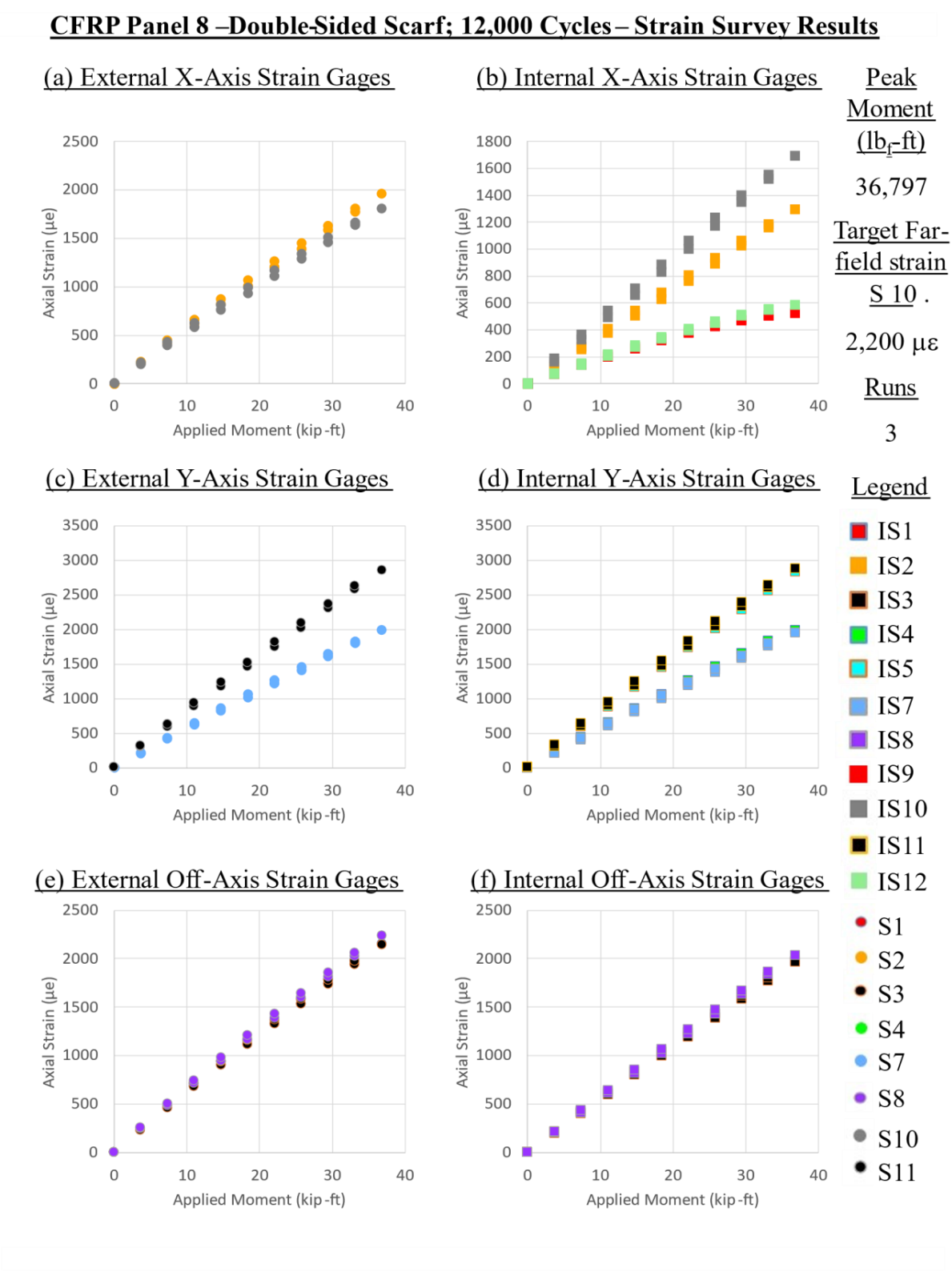

Figure B-8. Panel 8 (fatigue at SL strain level): strain survey at 12,000 cycles (non-axial strain and displacement)

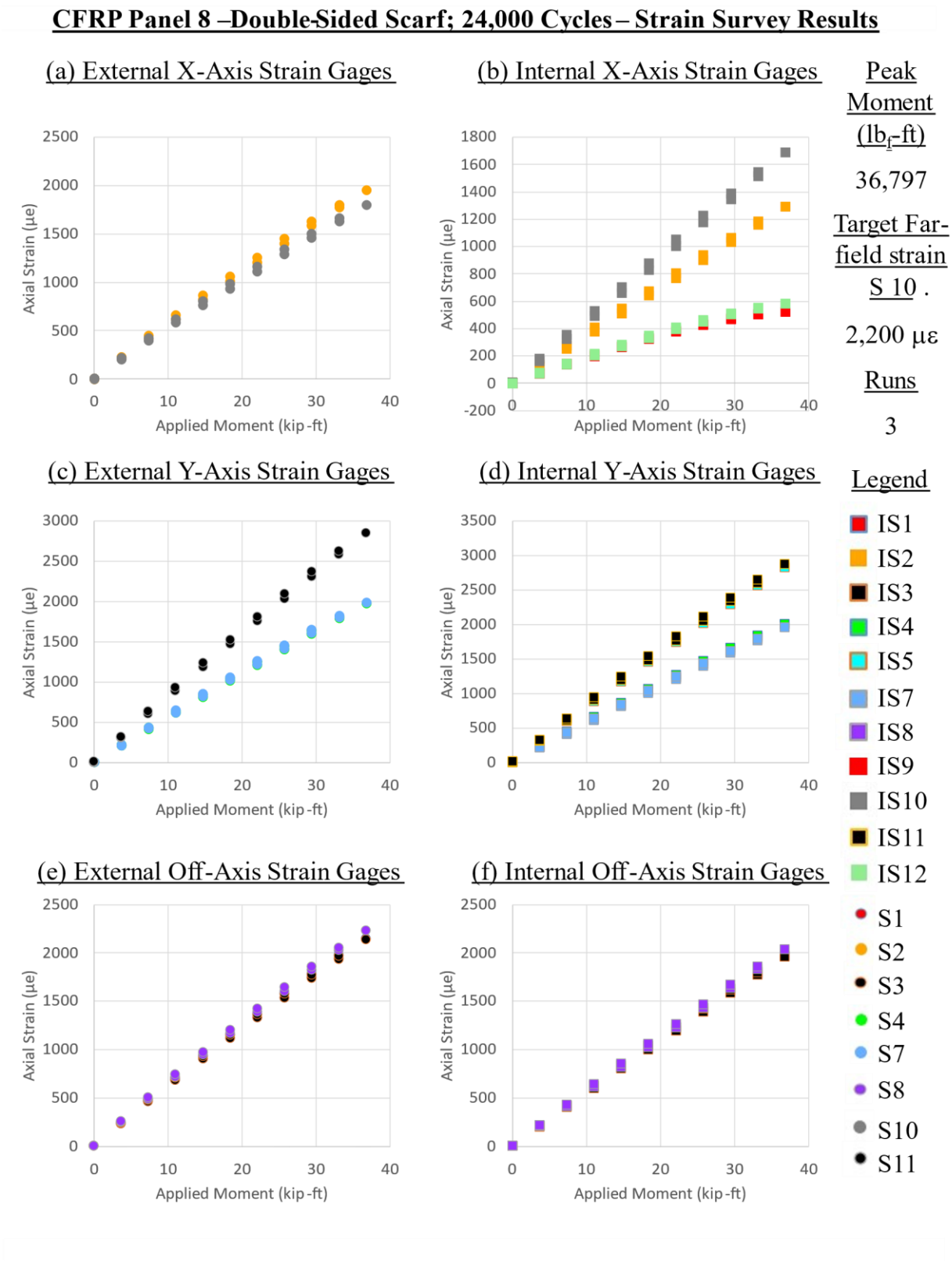

Figure B-9. Panel 8 (fatigue at SL strain level): strain survey at 24,000 cycles (axial strain)

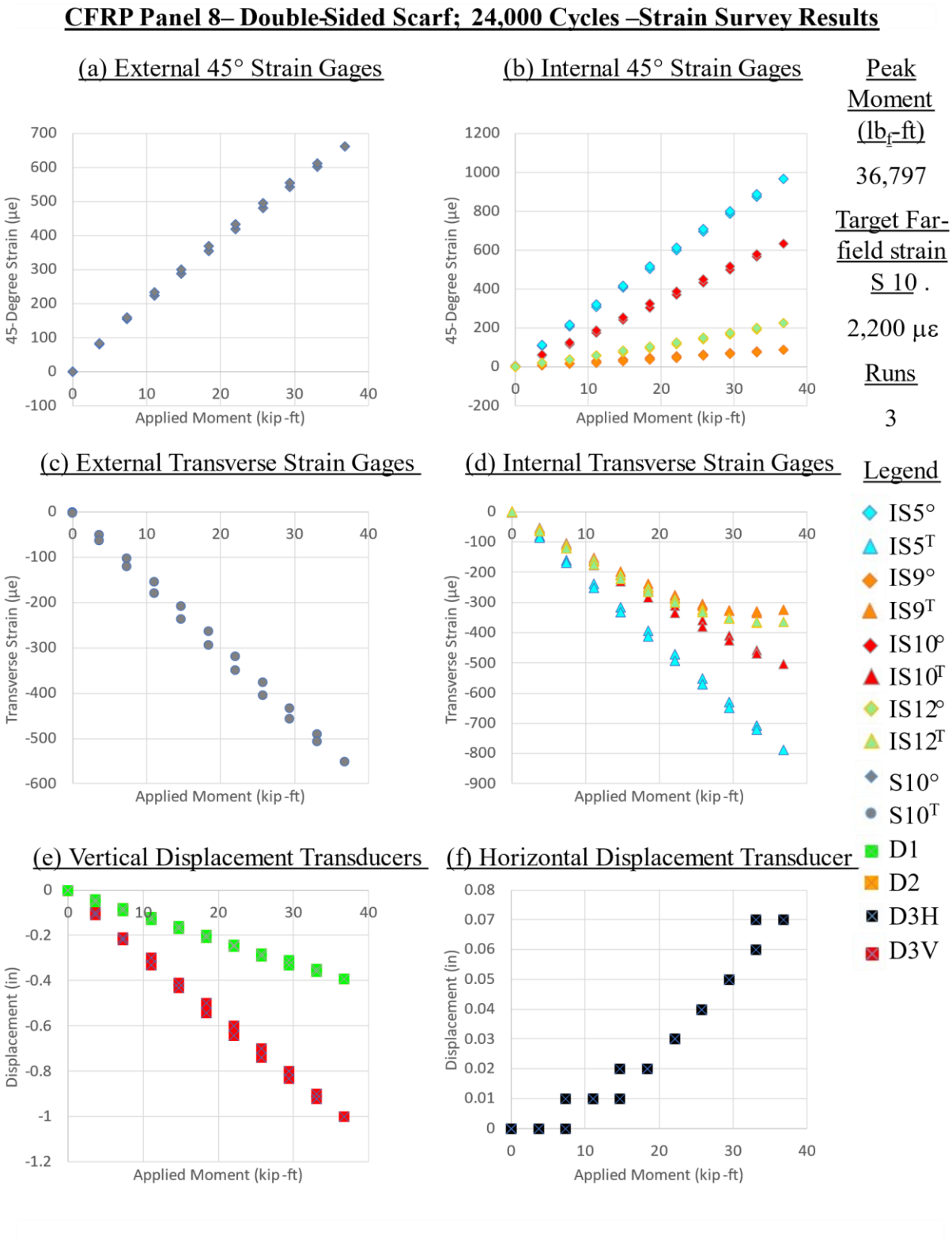

Figure B-10. Panel 8 (fatigue at SL strain level): strain survey at 24,000 cycles (non-axial strain and displacement)

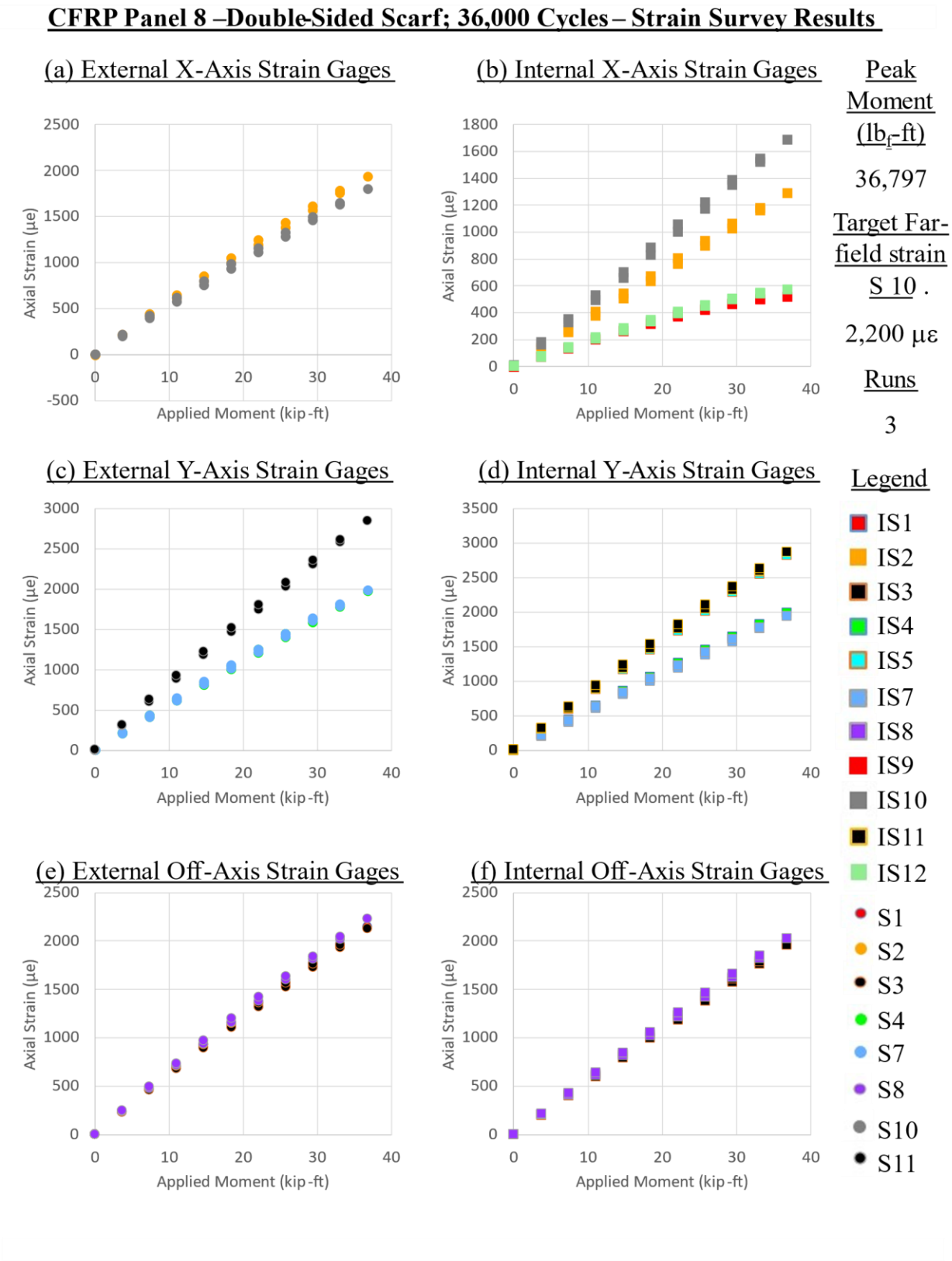

Figure B-11. Panel 8 (fatigue at SL strain level): strain survey at 36,000 cycles (axial strain)

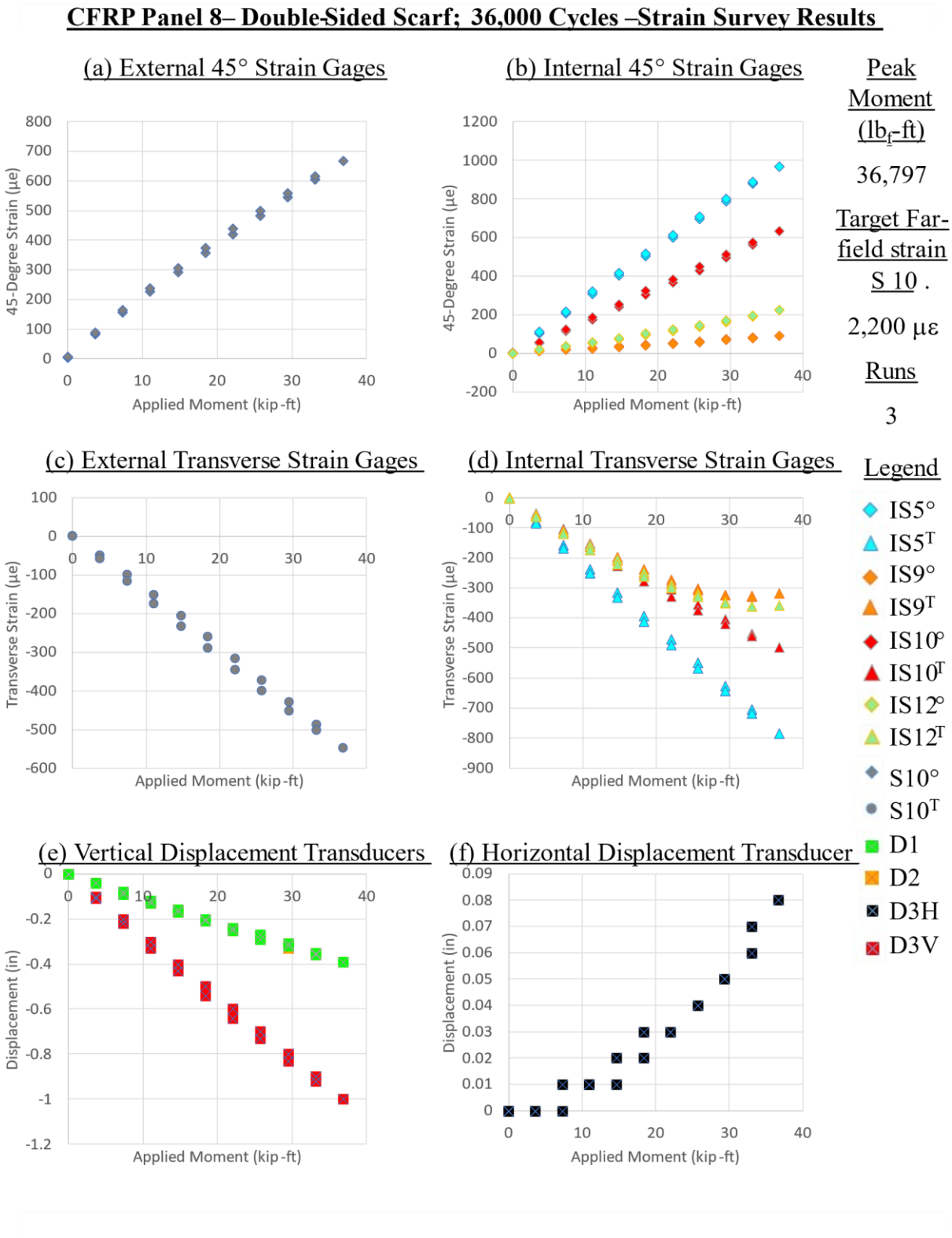

Figure B-12. Panel 8 (fatigue at SL strain level): strain survey at 36,000 cycles (non-axial strain and displacement)

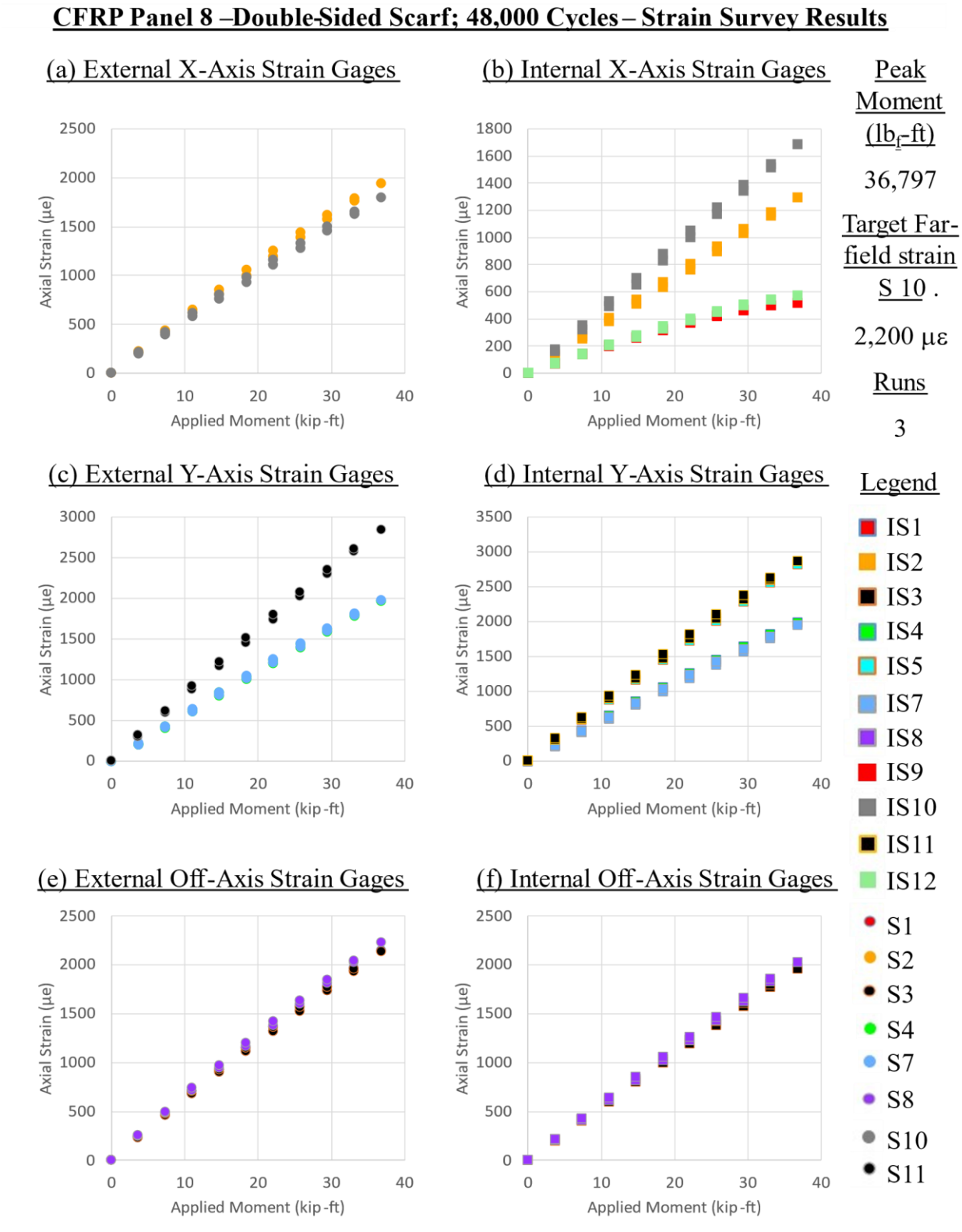

Figure B-13. Panel 8 (fatigue at SL strain level): strain survey at 48,000 cycles (axial strain)

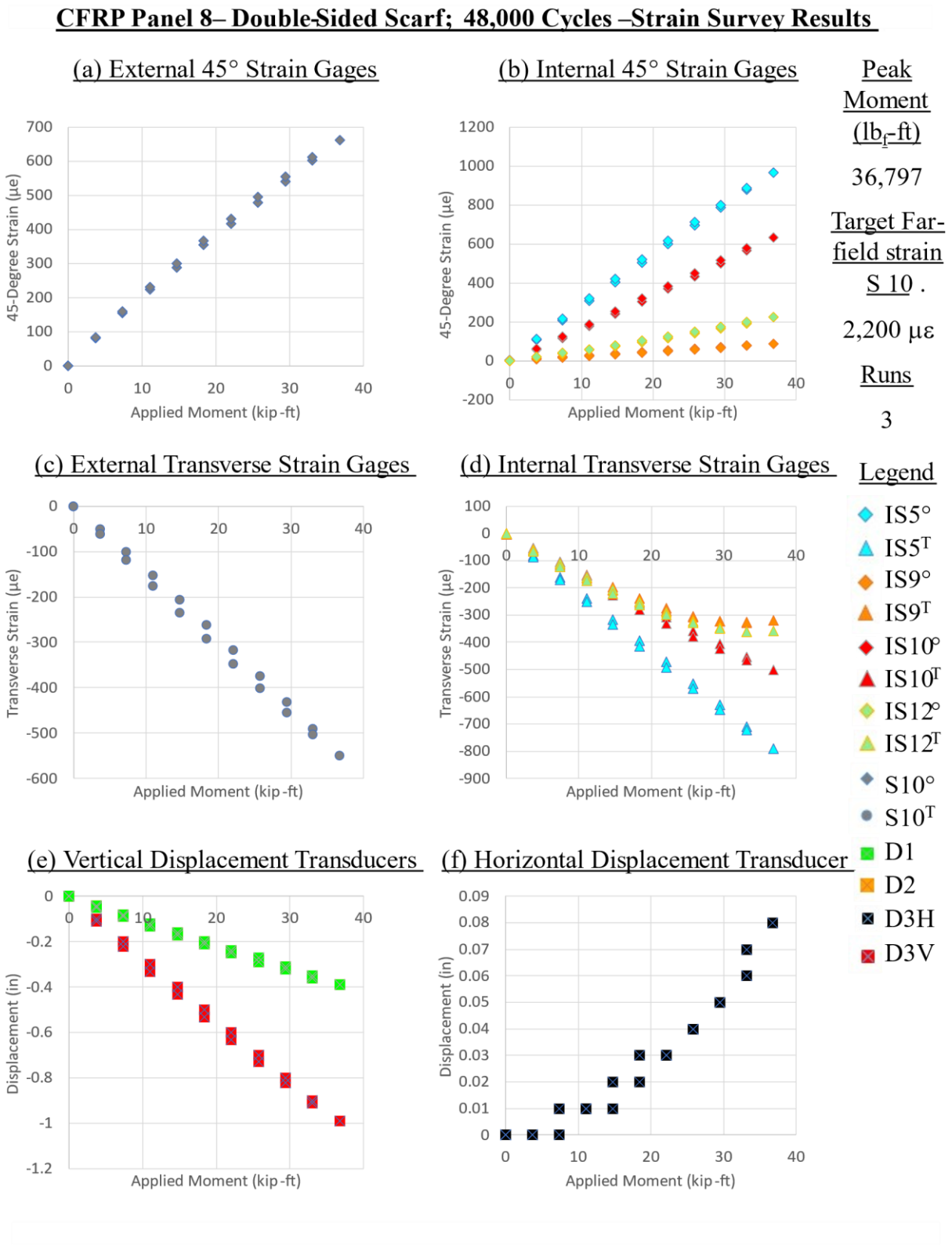

Figure B-14. Panel 8 (fatigue at SL strain level): strain survey at 48,000 cycles (non-axial strain and displacement)

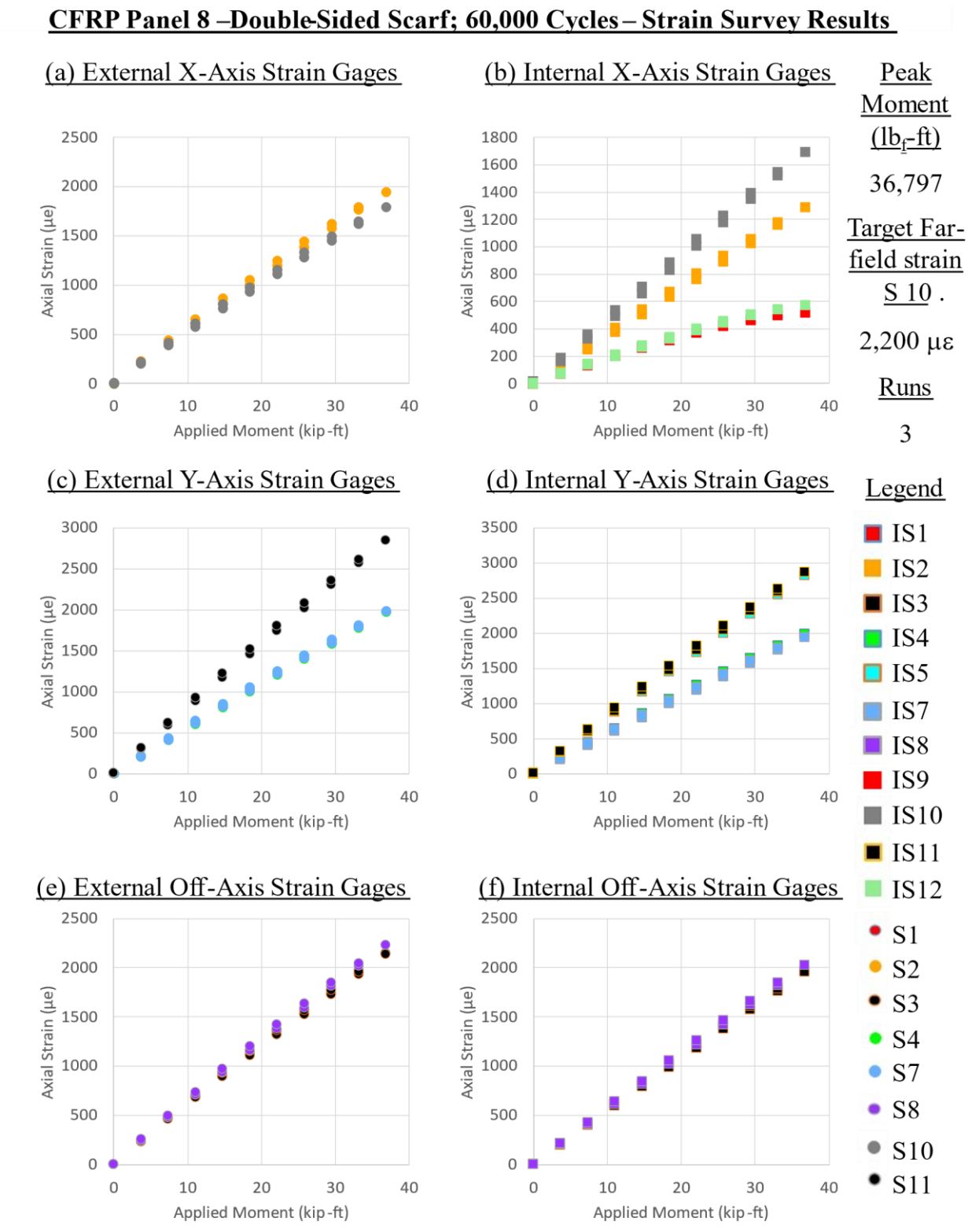

Figure B-15. Panel 8 (fatigue at SL strain level): strain survey at 60,000 cycles (axial strain)

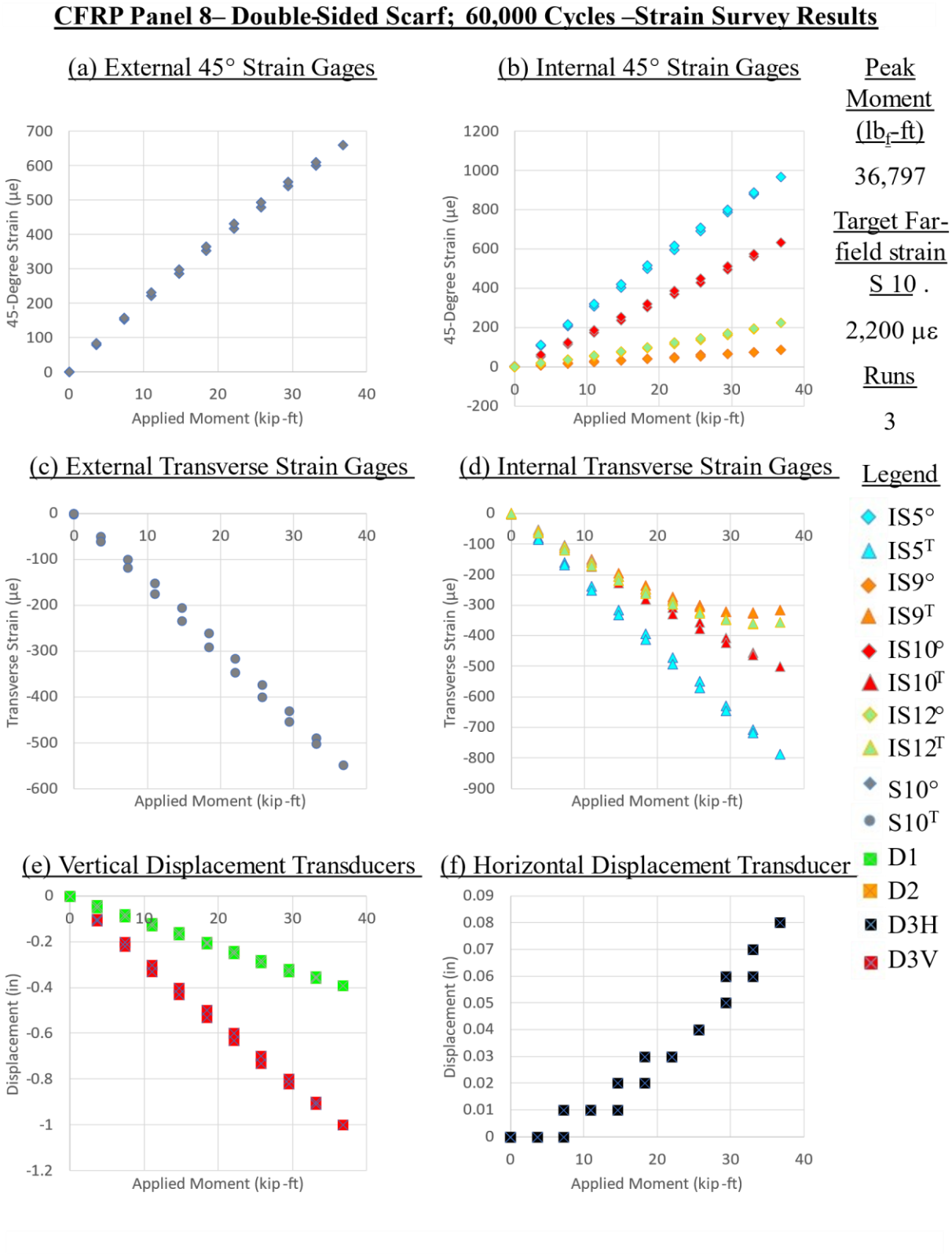

Figure B-16. Panel 8 (fatigue at SL strain level): strain survey at 60,000 cycles (non-axial strain and displacement)

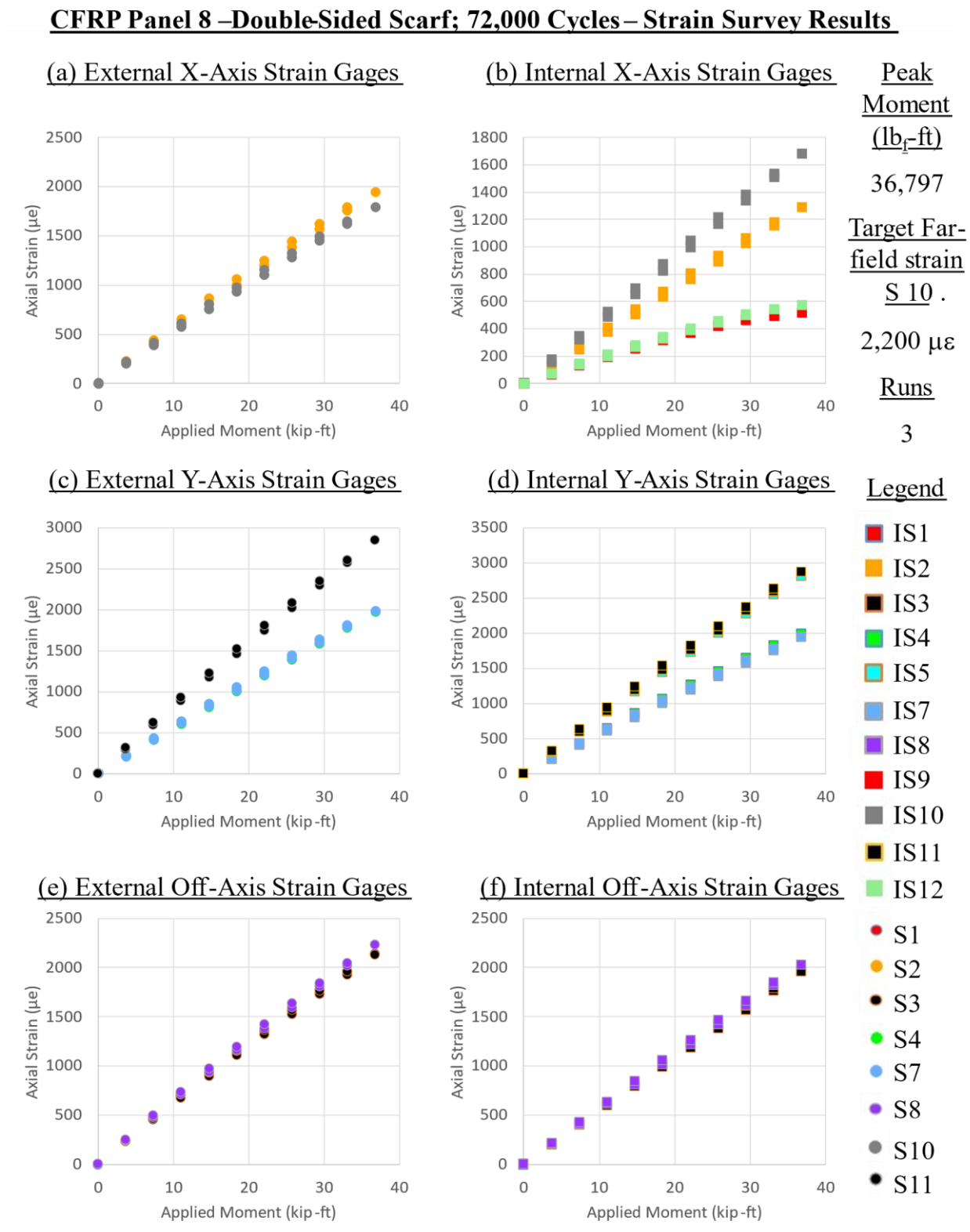

Figure B-17. Panel 8 (fatigue at SL strain level): strain survey at 72,000 cycles (axial strain)

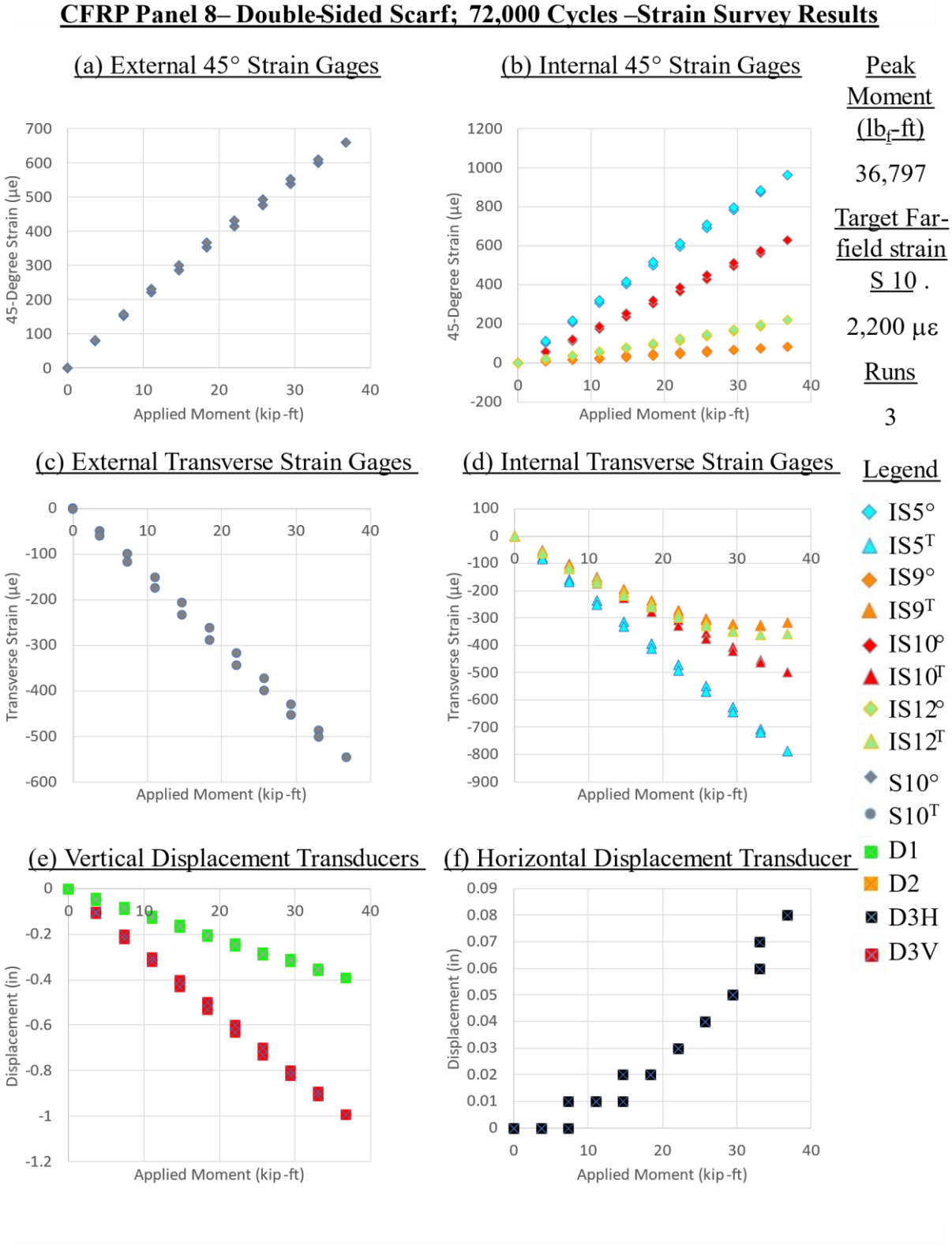

Figure B-18. Panel 8 (fatigue at SL strain level): strain survey at 72,000 cycles (non-axial strain and displacement)

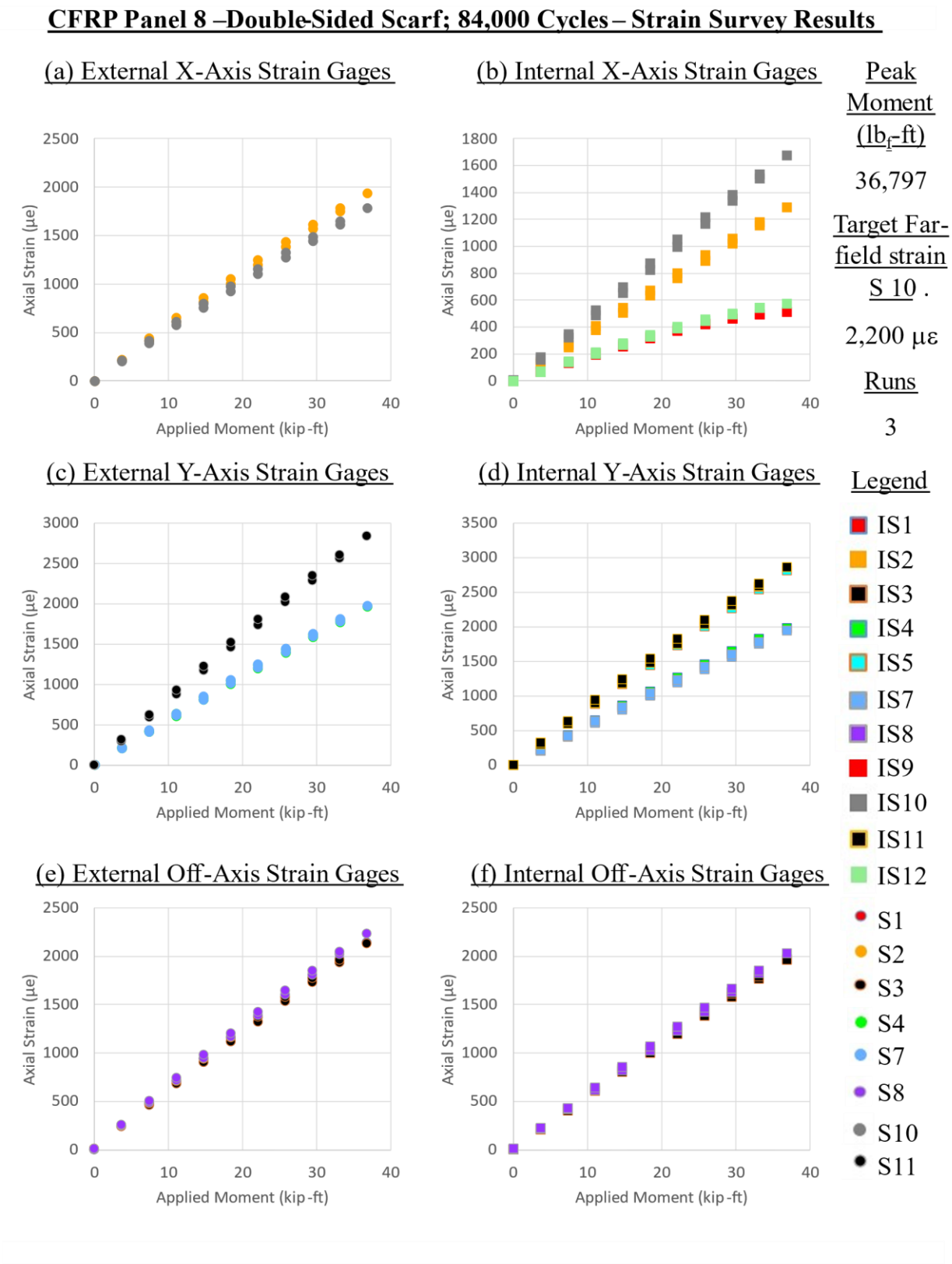

Figure B-19. Panel 8 (fatigue at SL strain level): strain survey at 84,000 cycles (axial strain)

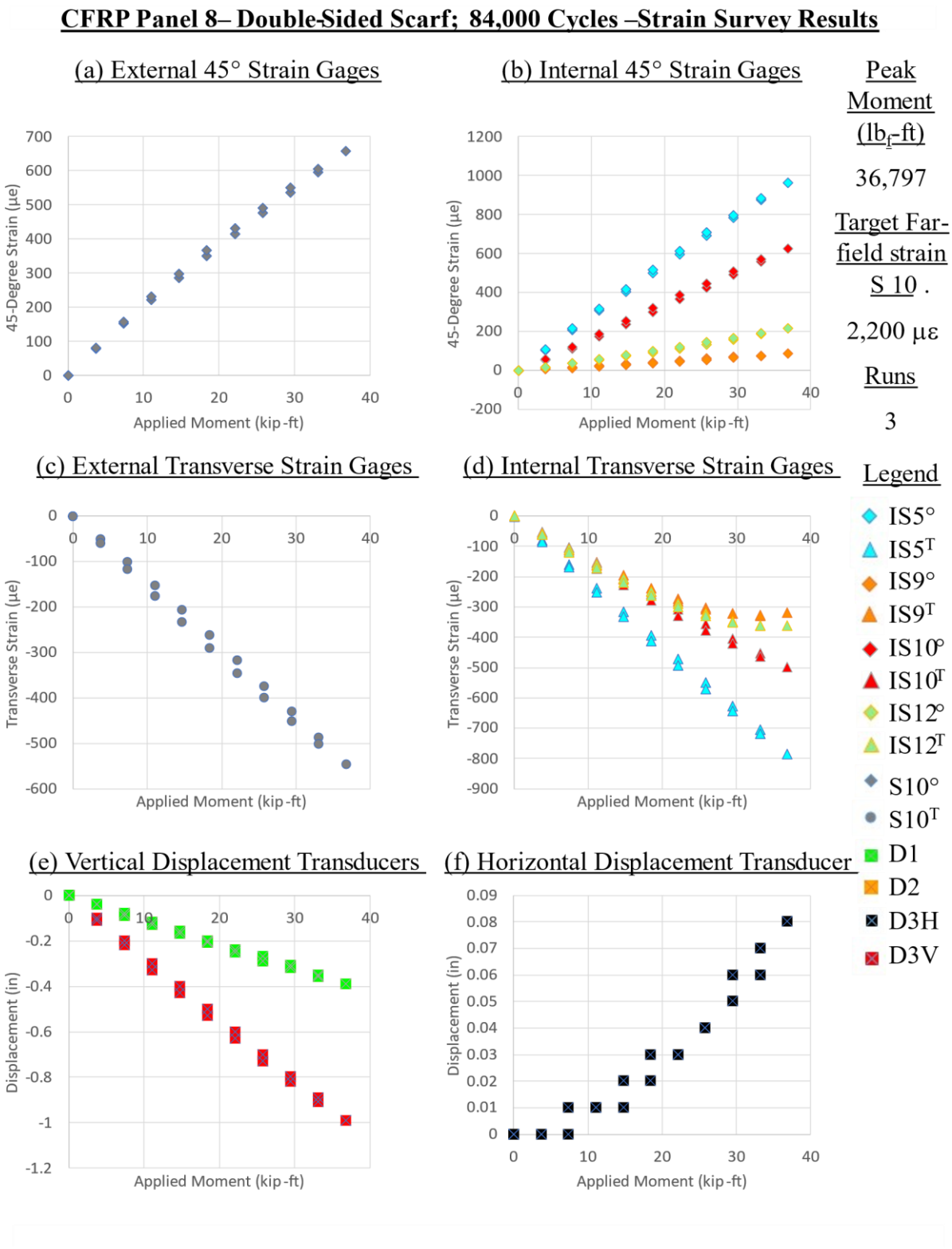

Figure B-20. Panel 8 (fatigue at SL strain level): strain survey at 84,000 cycles (non-axial strain and displacement)

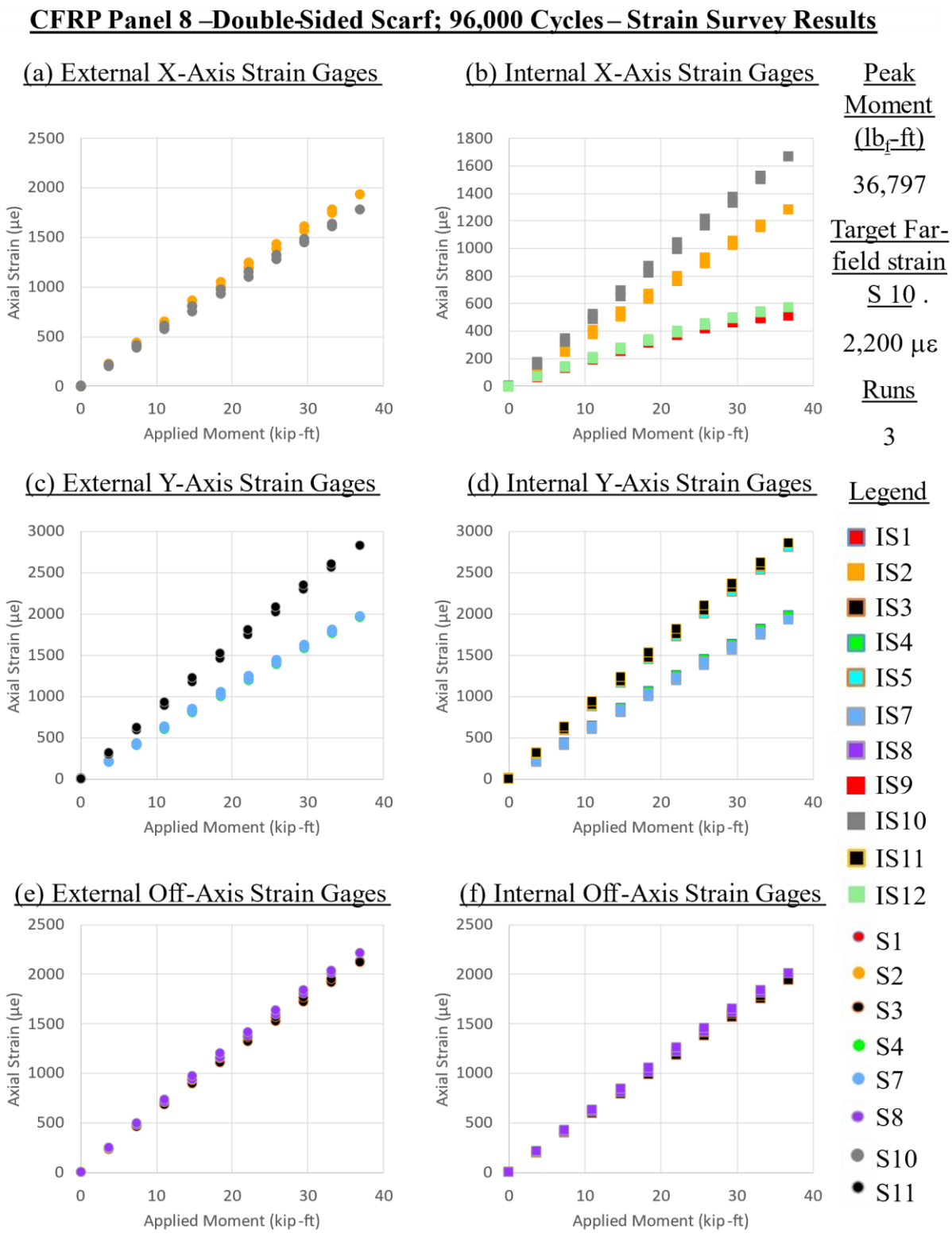

Figure B-21. Panel 8 (fatigue at SL strain level): strain survey at 96,000 cycles (axial strain)

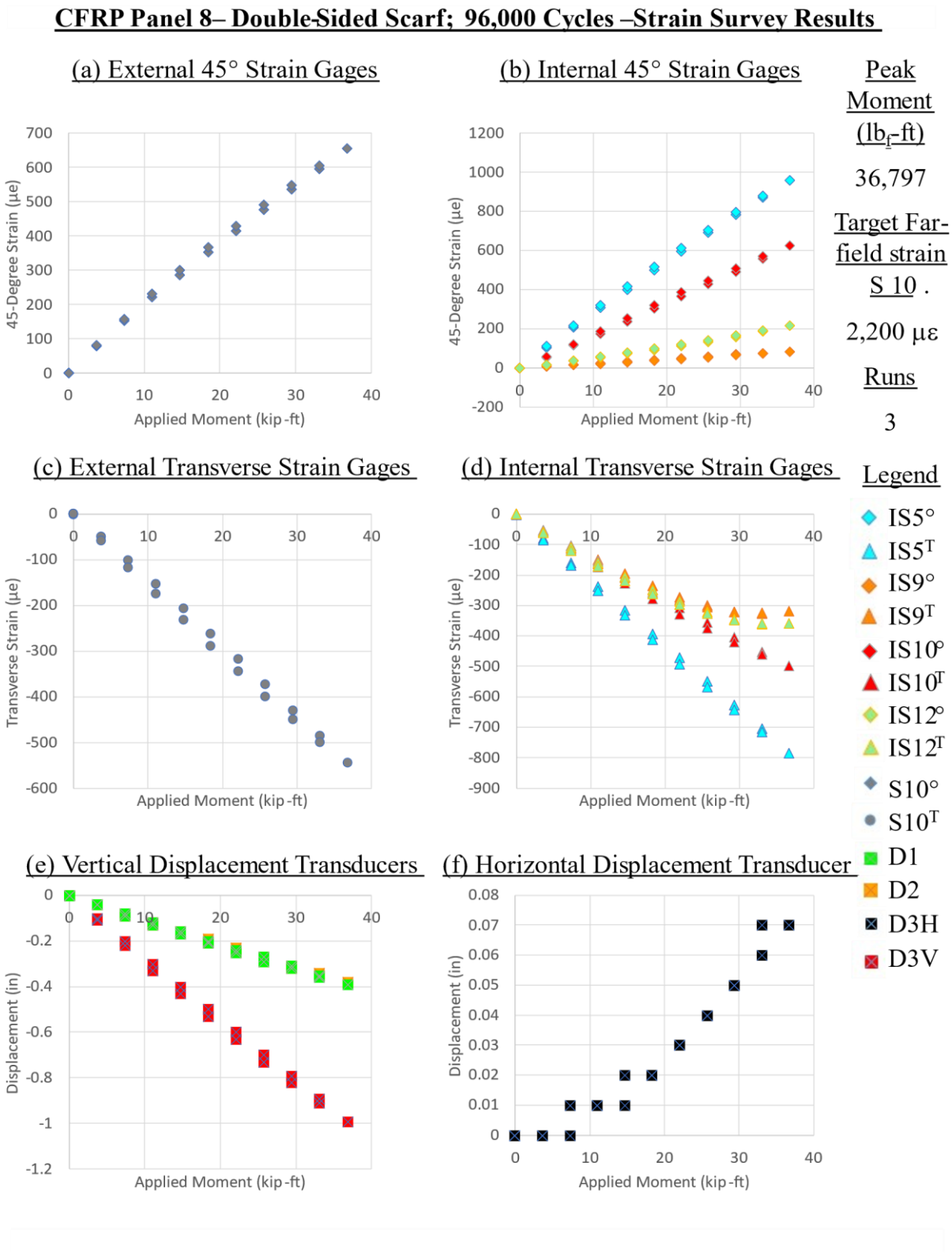

Figure B-22. Panel 8 (fatigue at SL strain level): strain survey at 96,000 cycles (non-axial strain and displacement)

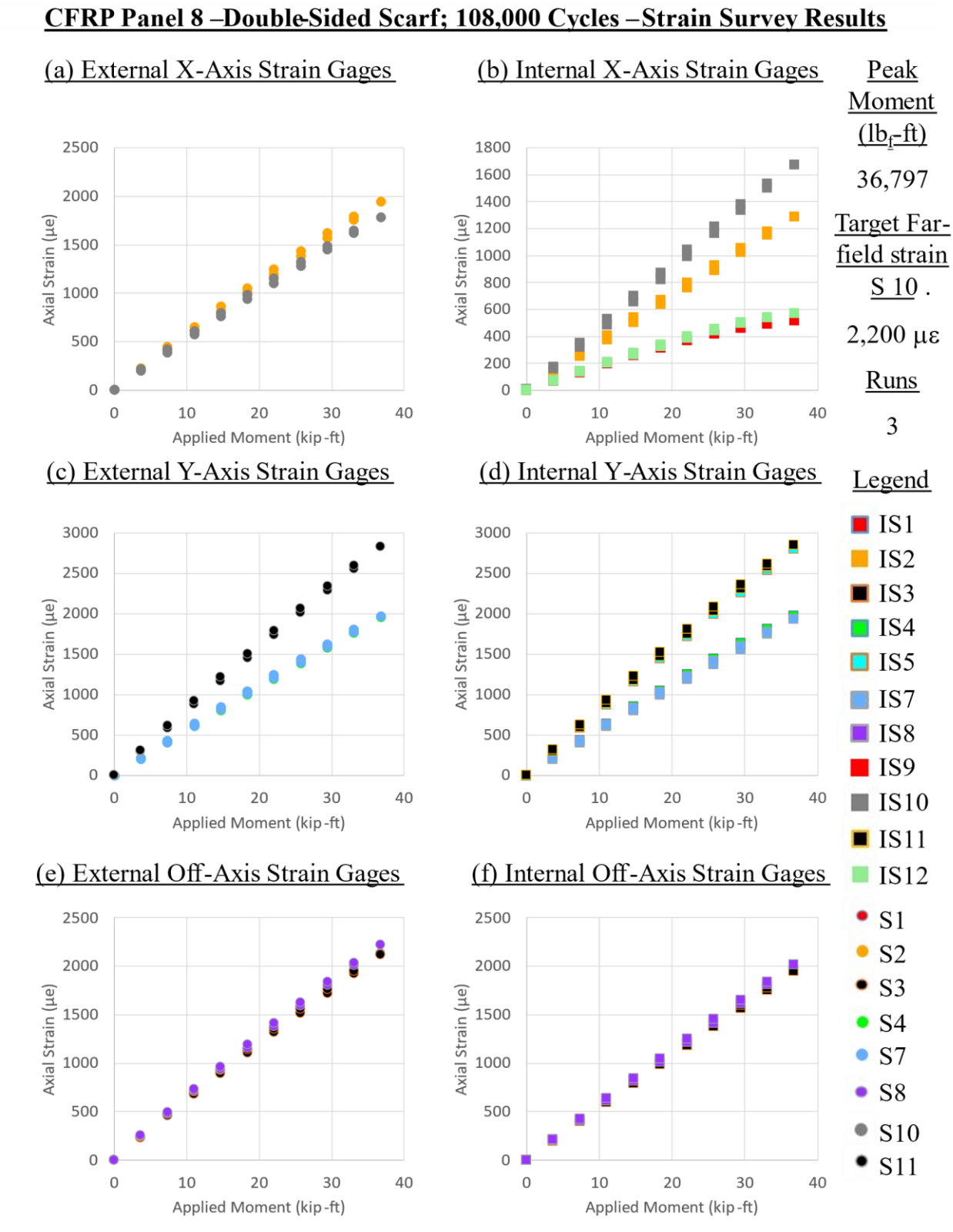

Figure B-23. Panel 8 (fatigue at SL strain level): strain survey at 108,000 cycles (axial strain)

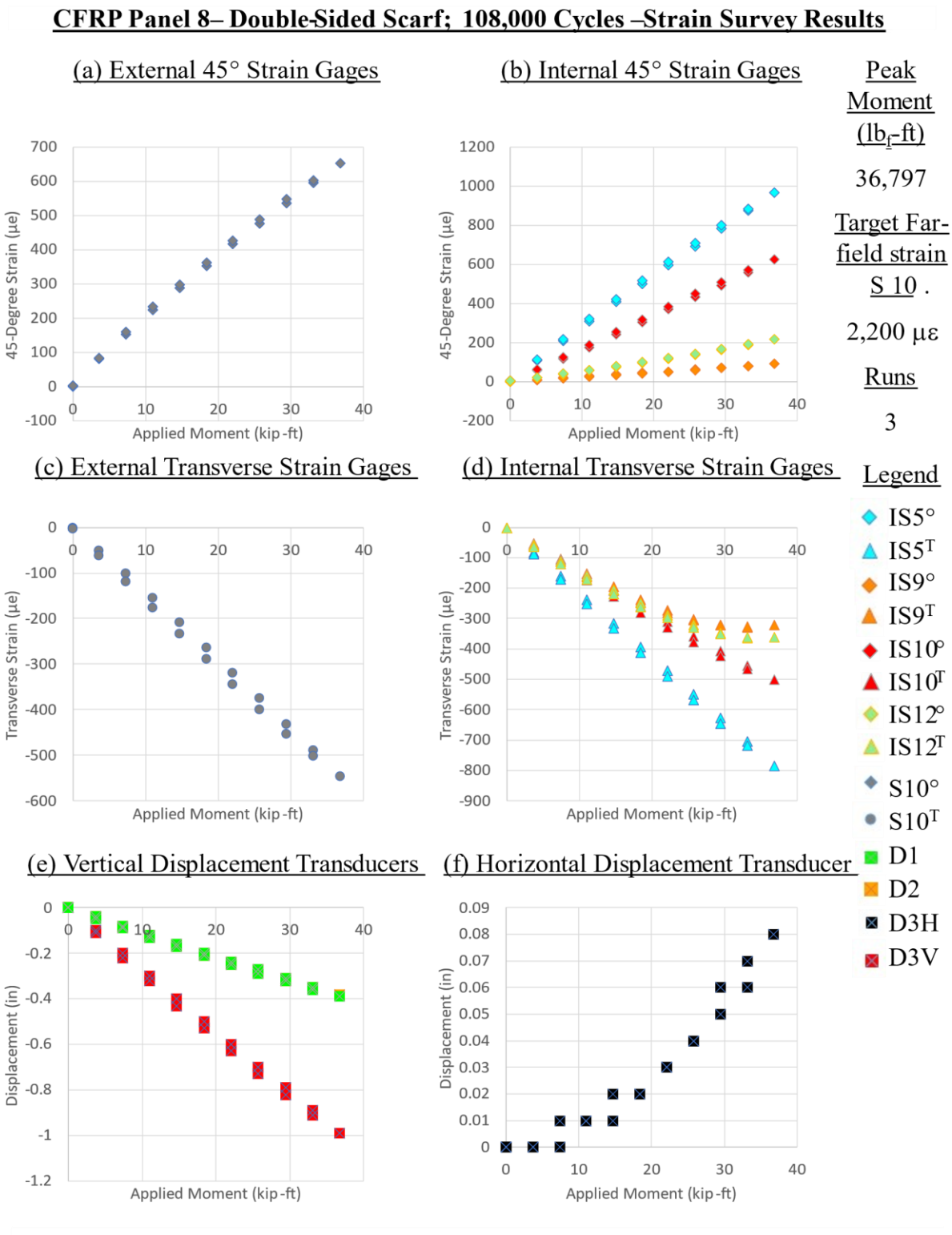

Figure B-24. Panel 8 (fatigue at SL strain level): strain survey at 108,000 cycles (non-axial strain and displacement)

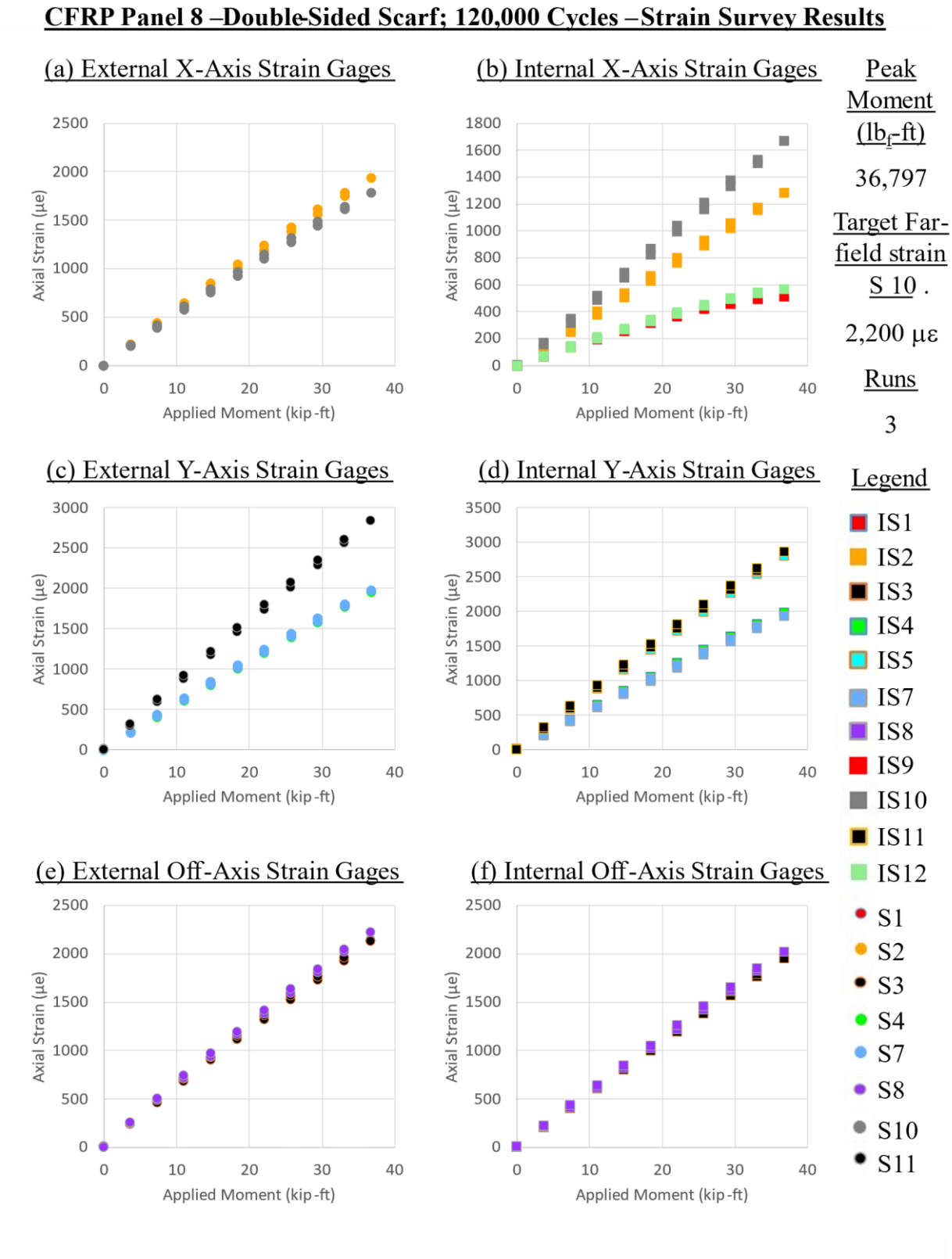

Figure B-25. Panel 8 (fatigue at SL strain level): strain survey at 120,000 cycles (axial strain)

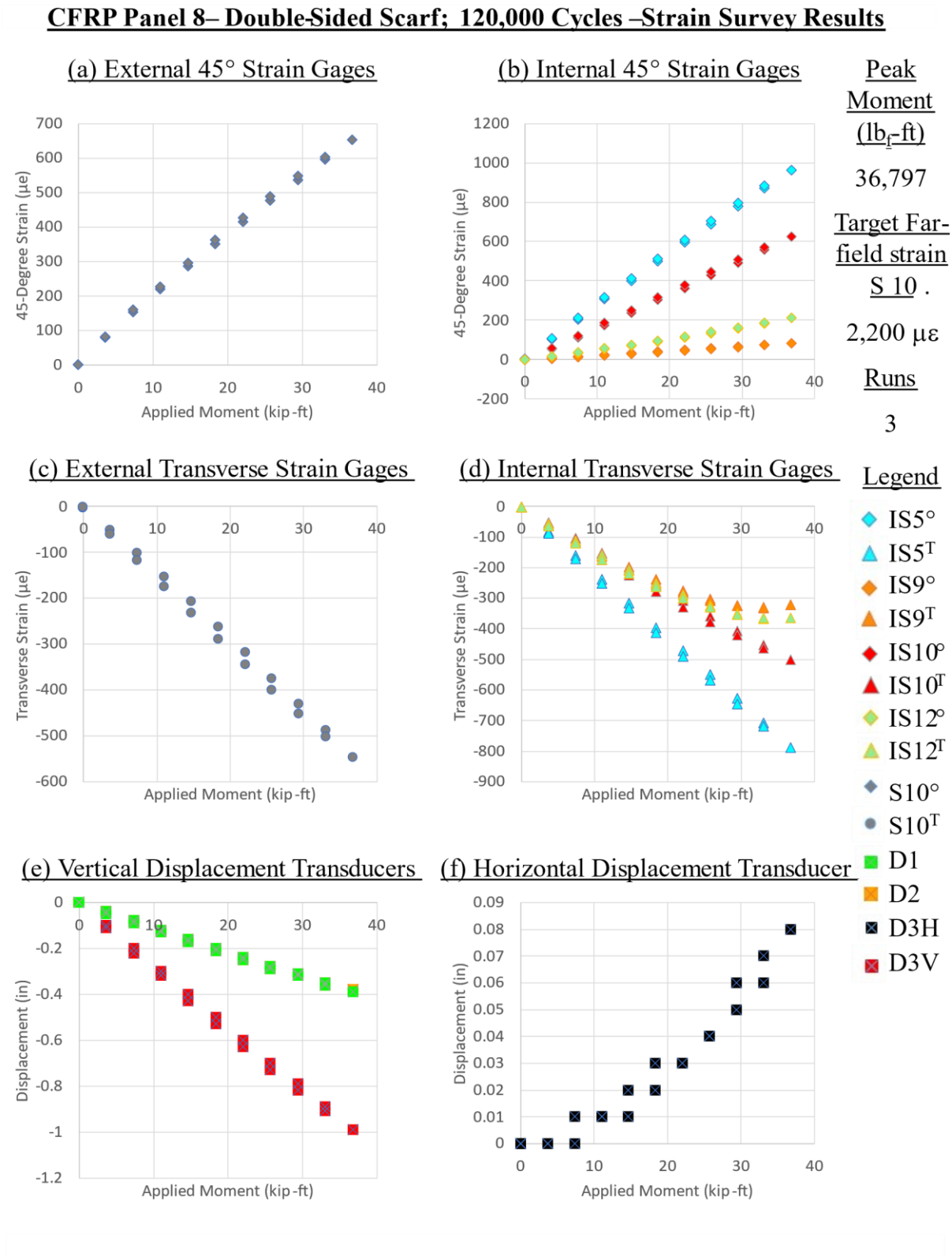

Figure B-26. Panel 8 (fatigue at SL strain level): strain survey at 120,000 cycles (non-axial strain and displacement)

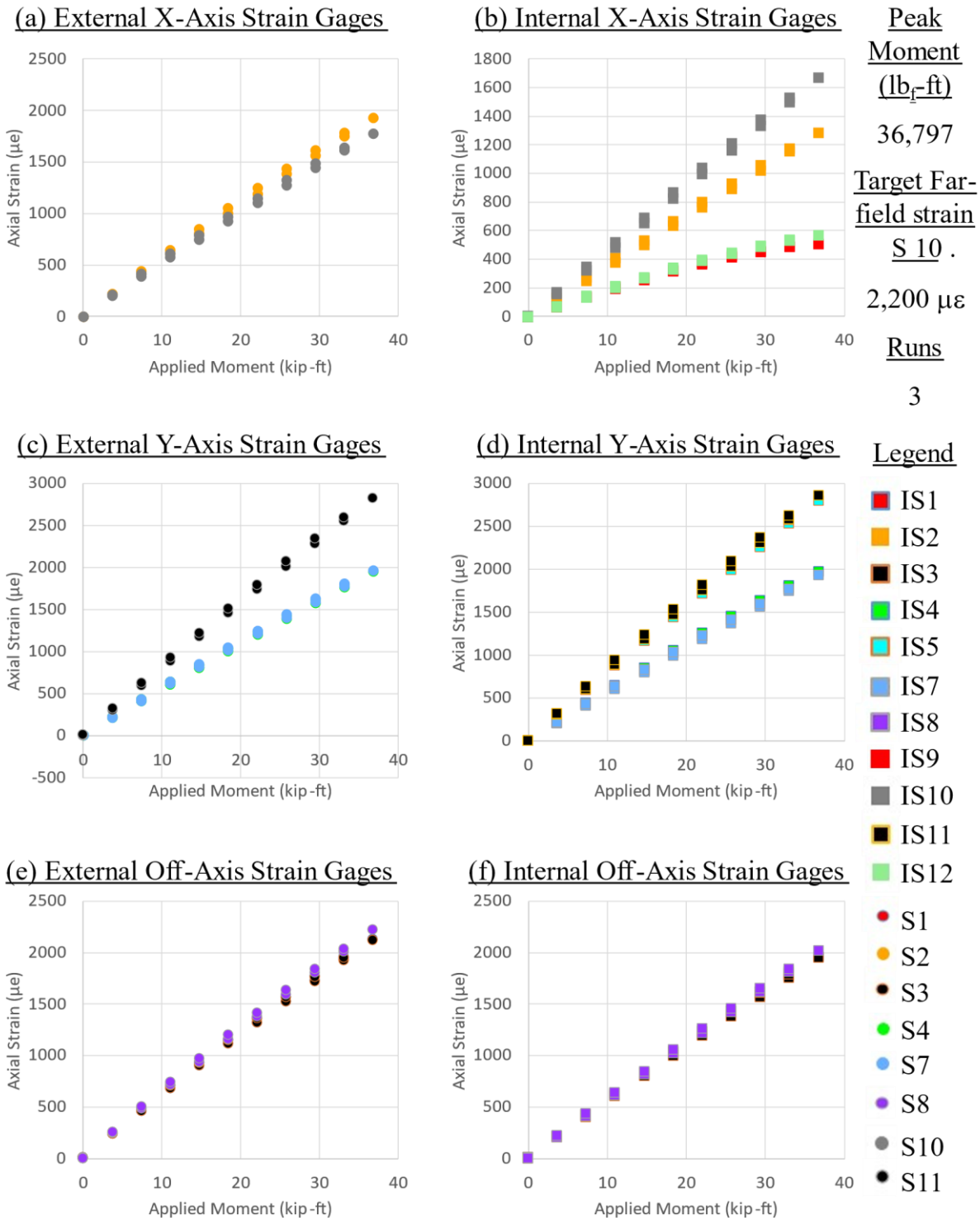

Figure B-27. Panel 8 (fatigue at SL strain level): strain survey at 132,000 cycles (axial strain)

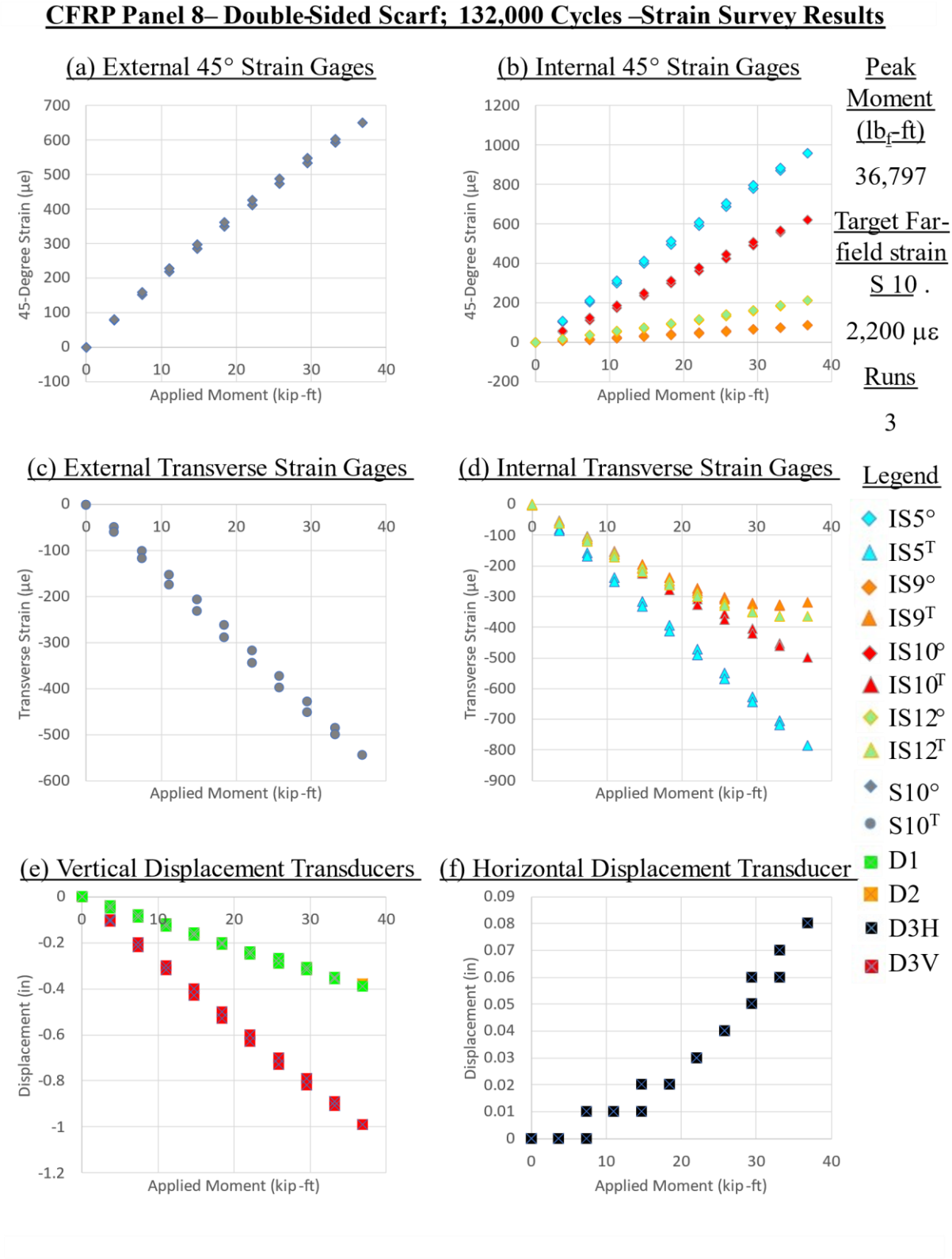

Figure B-28. Panel 8 (fatigue at SL strain level): strain survey at 132,000 cycles (non-axial strain and displacement)

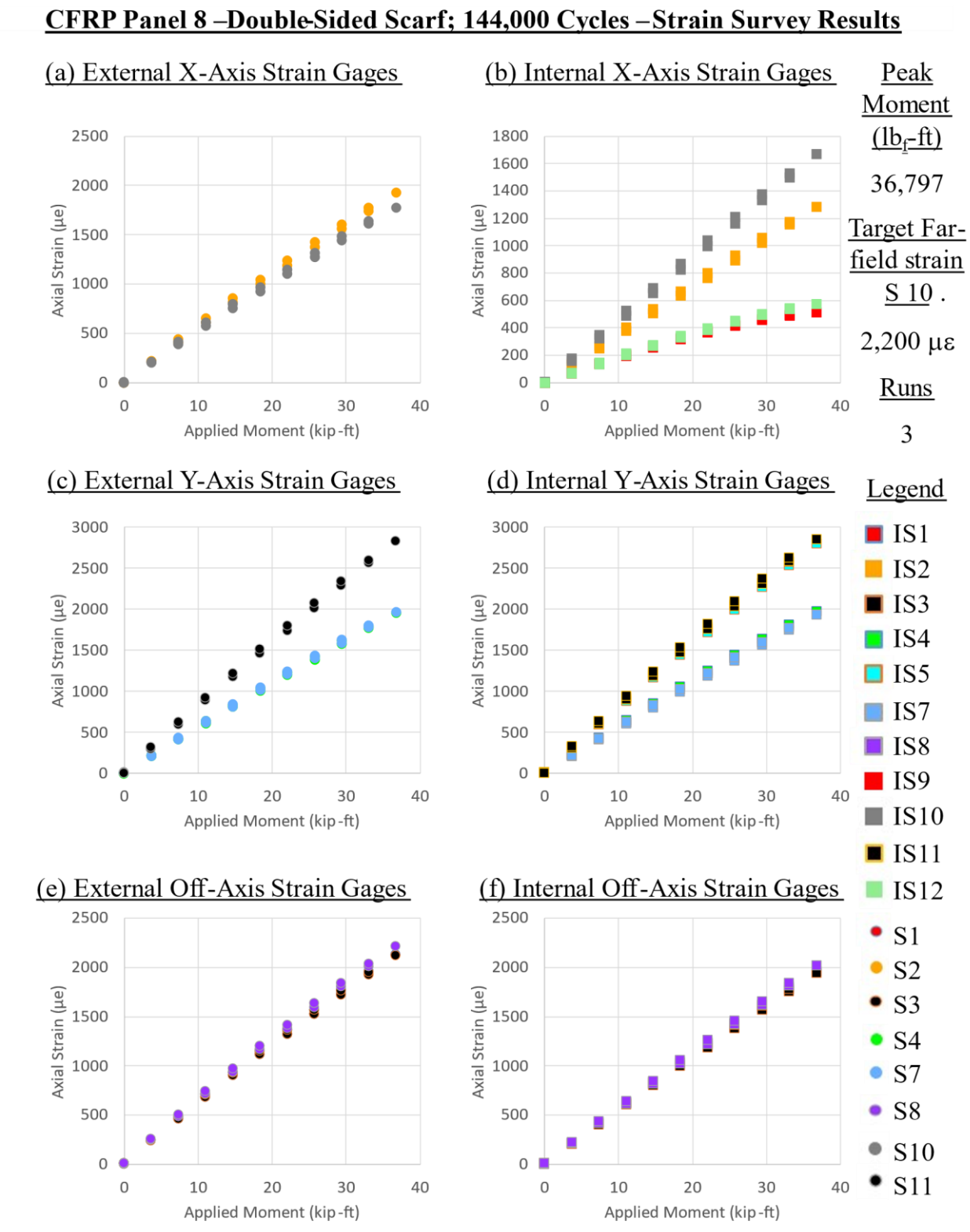

Figure B-29. Panel 8 (fatigue at SL strain level): strain survey at 144,000 cycles (axial strain)

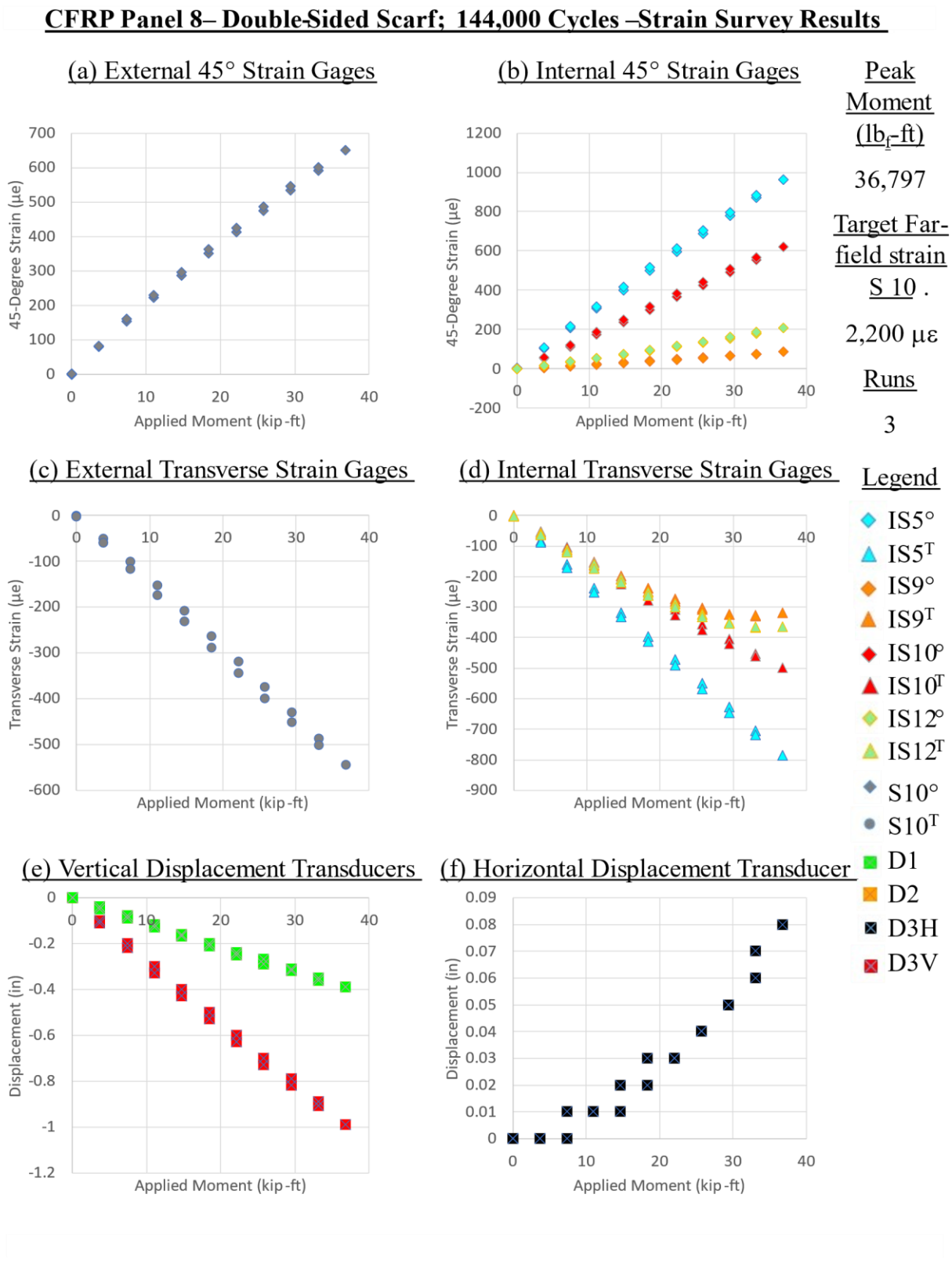

Figure B-30. Panel 8 (fatigue at SL strain level): strain survey at 144,000 cycles (non-axial strain and displacement)

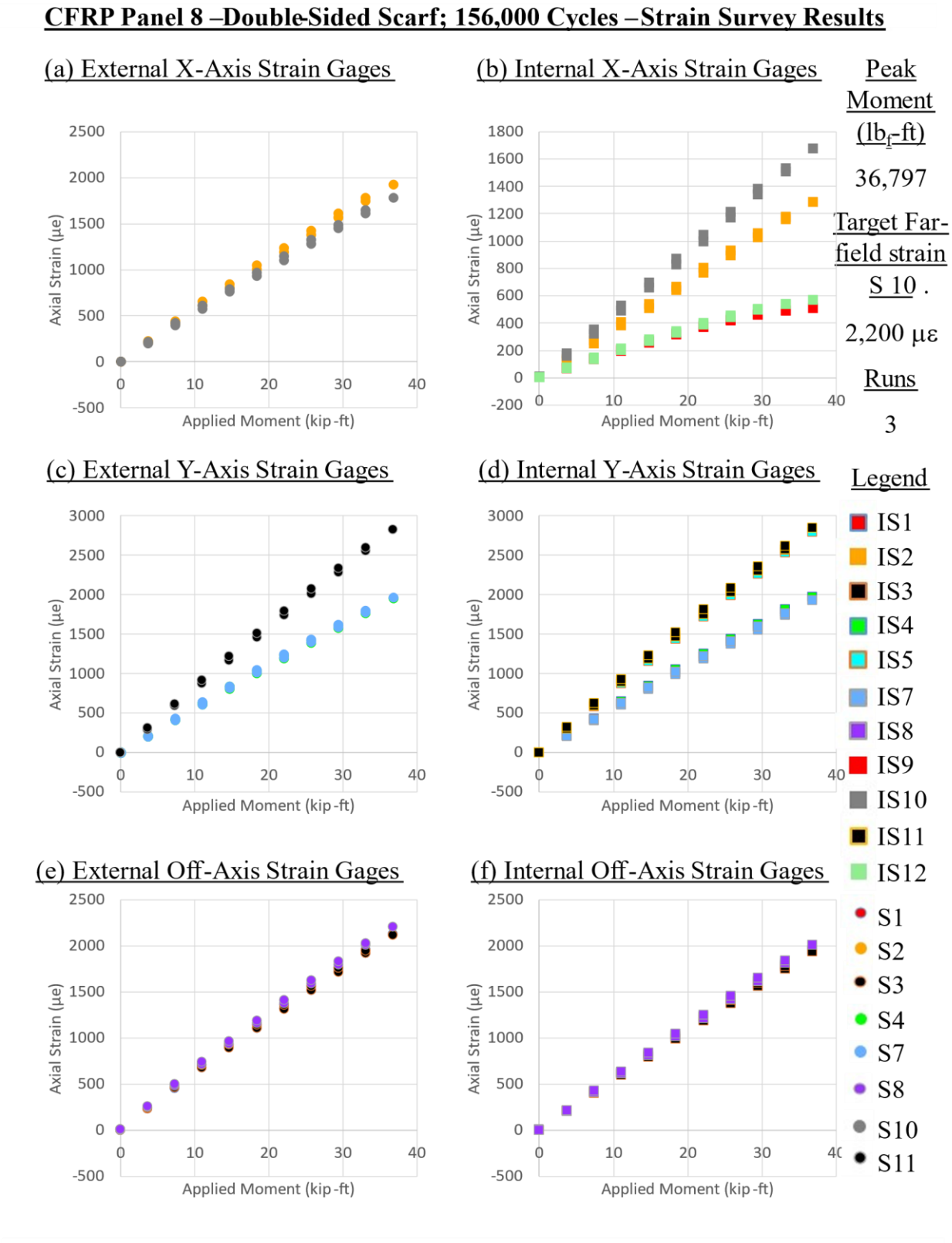

Figure B-31. Panel 8 (fatigue at SL strain level): strain survey at 156,000 cycles (axial strain)

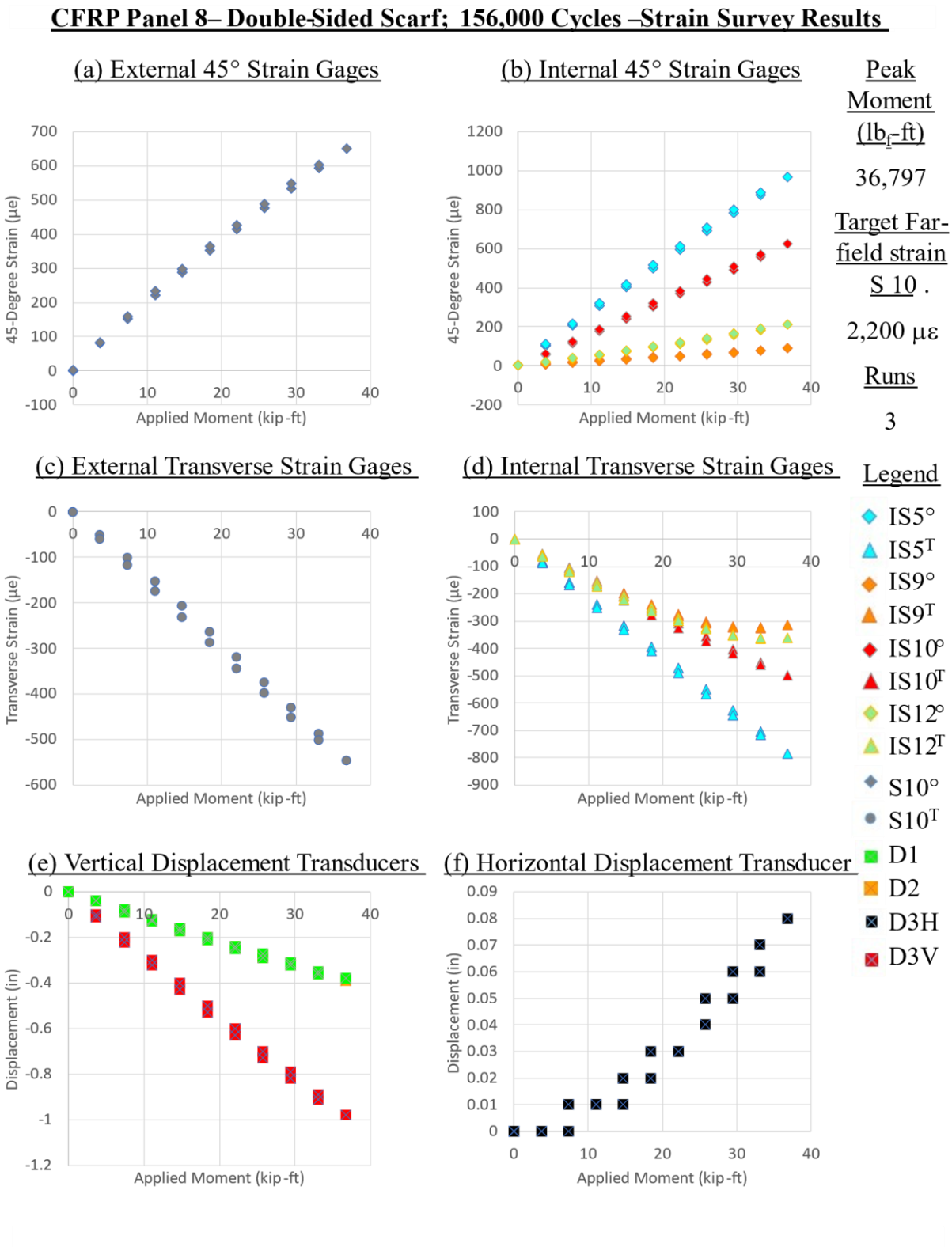

Figure B-32. Panel 8 (fatigue at SL strain level): strain survey at 156,000 cycles (non-axial strain and displacement)

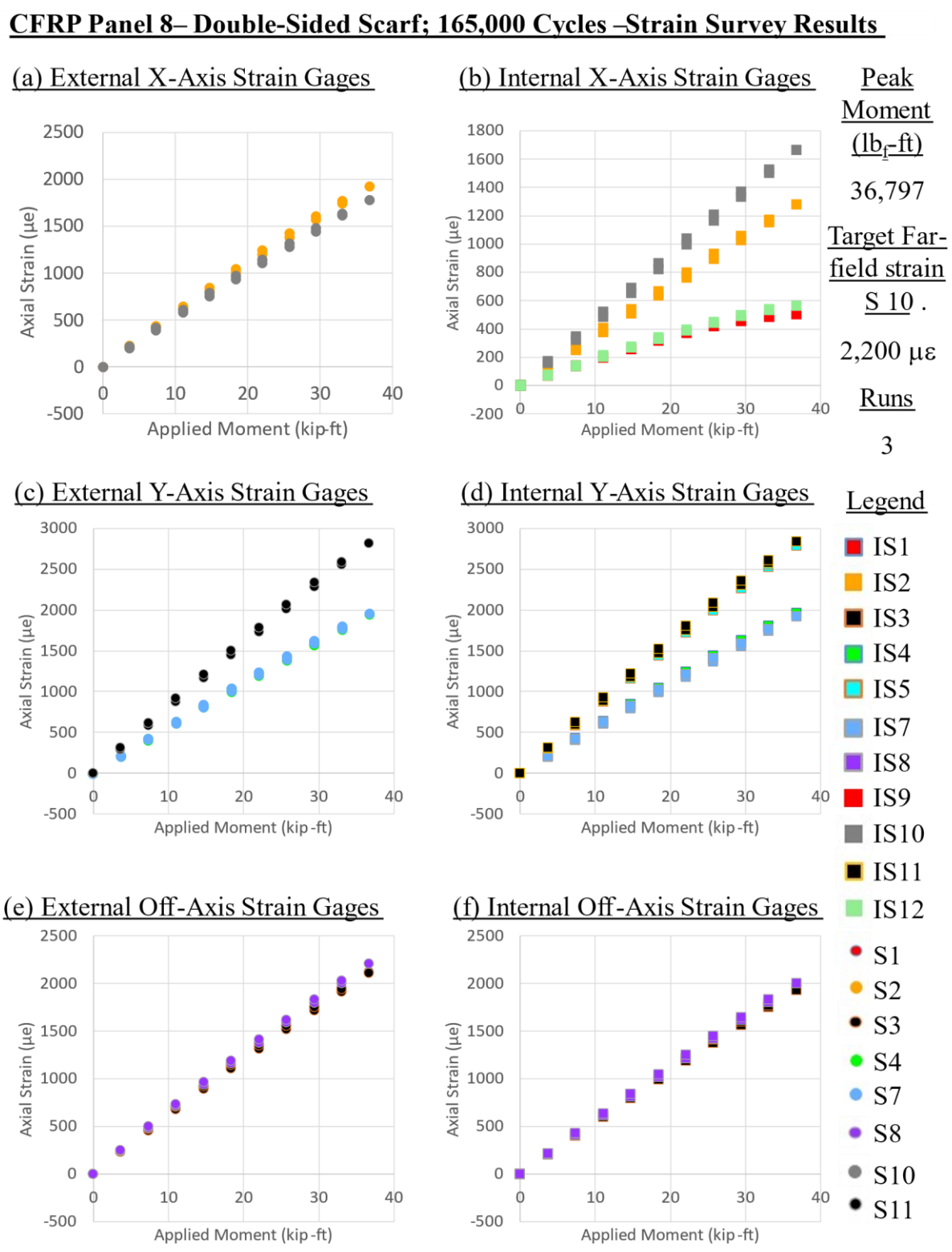

Figure B-33. Panel 8 (fatigue at SL strain level): strain survey at 165,000 cycles (axial strain)

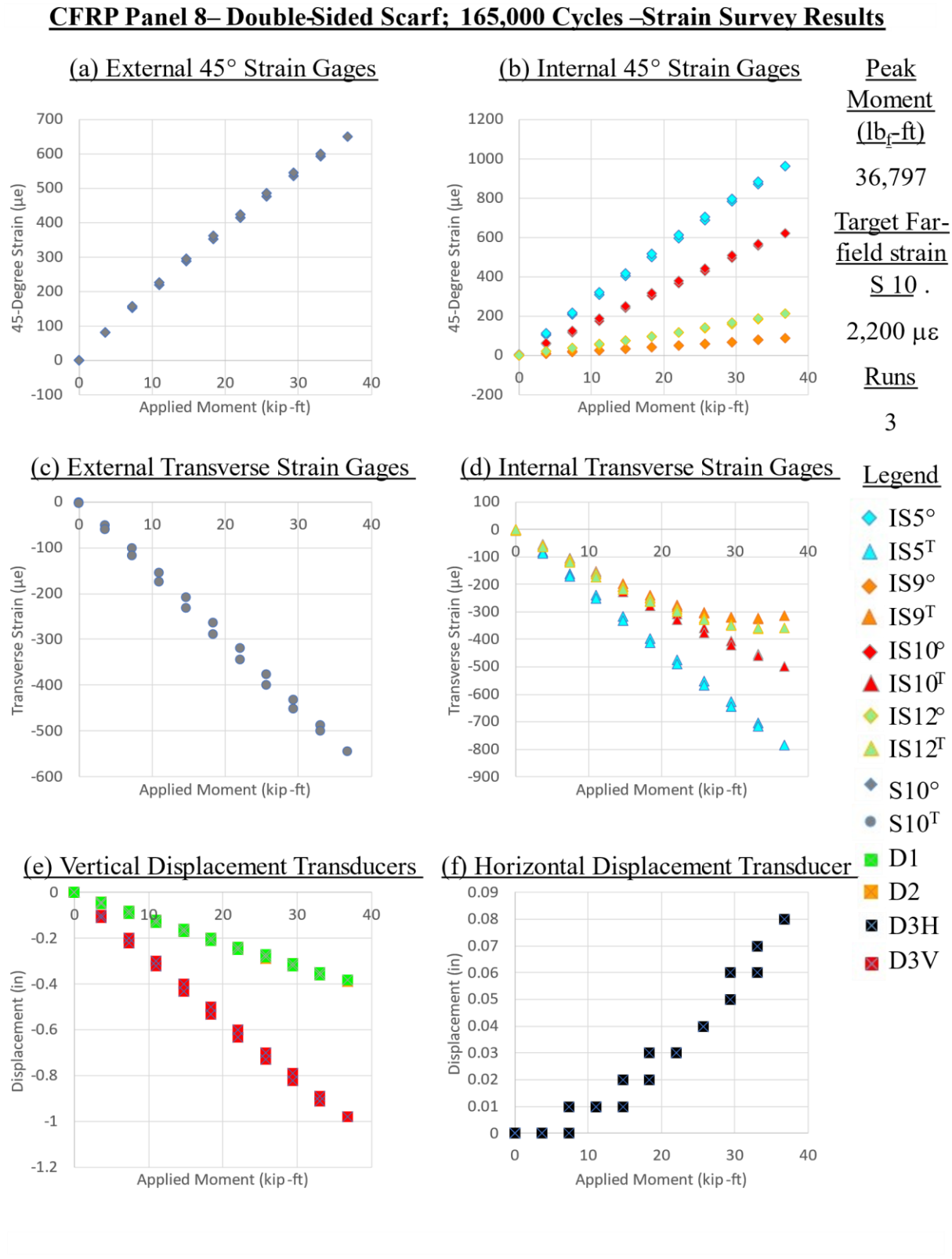

Figure B-34. Panel 8 (fatigue at SL strain level): strain survey at 165,000 cycles (non-axial strain and displacement)

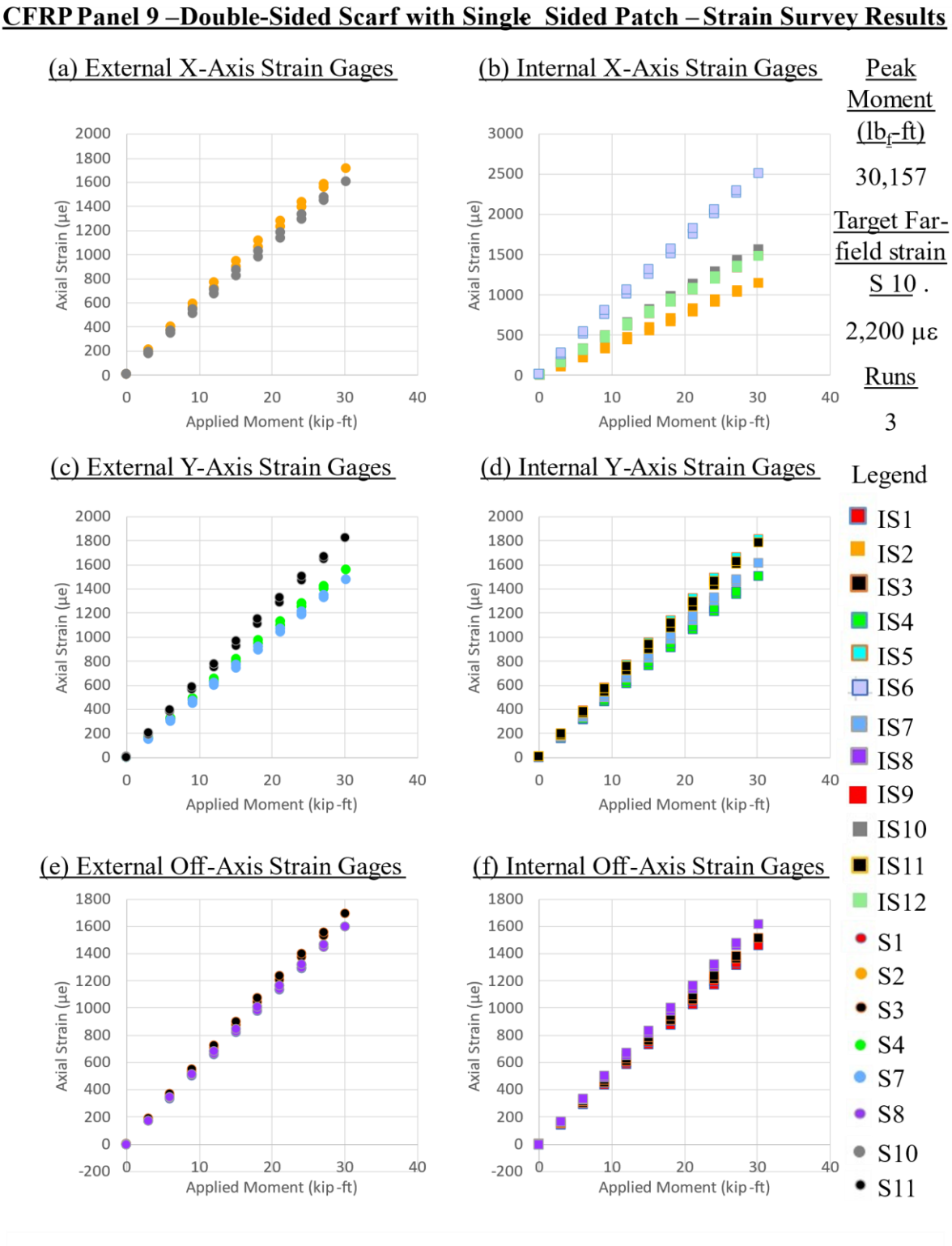

Figure B-35. Panel 9: baseline strain survey (axial strain)

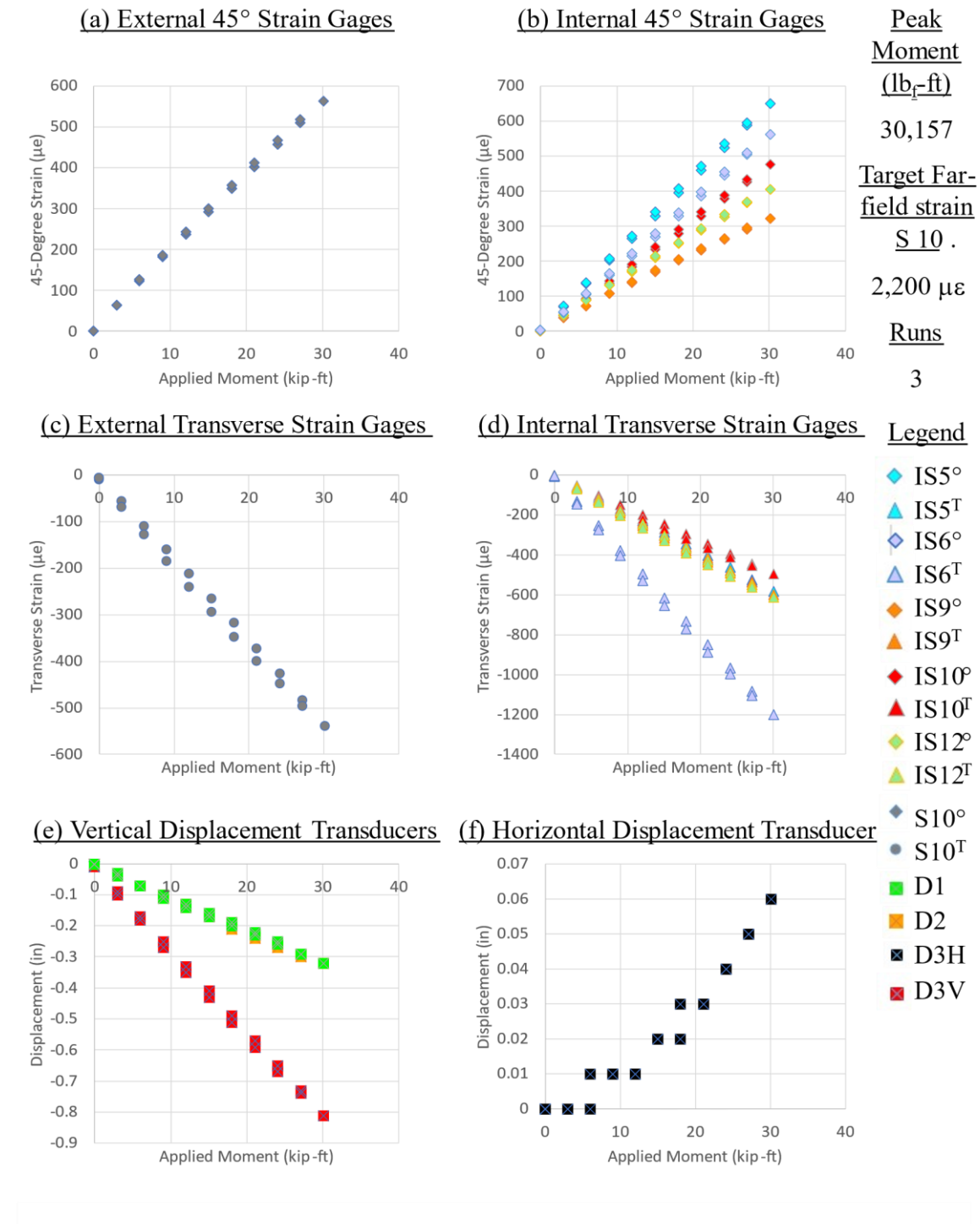

Figure B-36. Panel 9: baseline strain survey (non-axial strain and displacement)

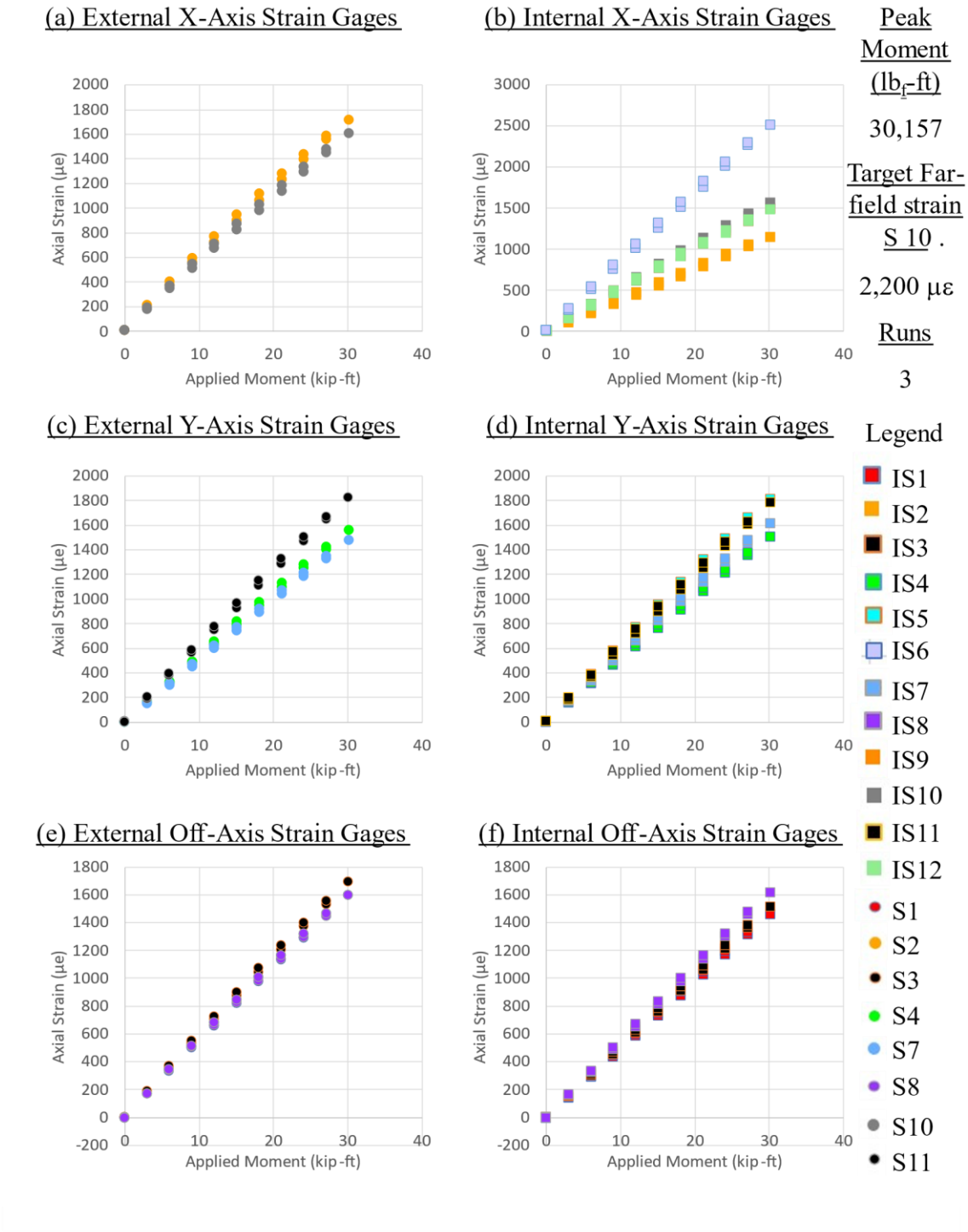

Figure B-37. Panel 10: baseline strain survey (axial strain)

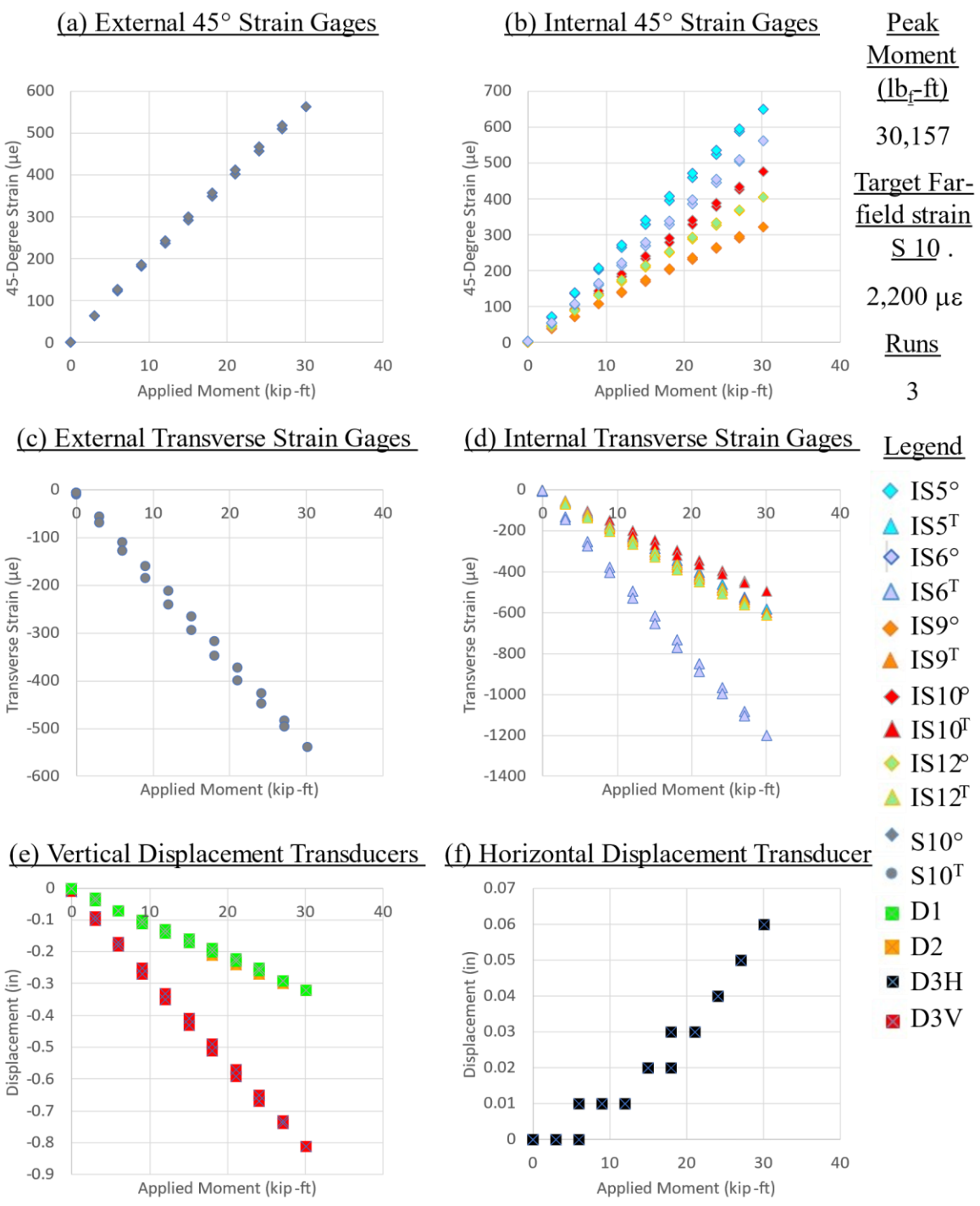

Figure B-38. Panel 10: baseline strain survey (non-axial strain and displacement)

CFRP Panel 11 –Double-Sided Scarf with Single -Sided Patch – Strain Survey Results

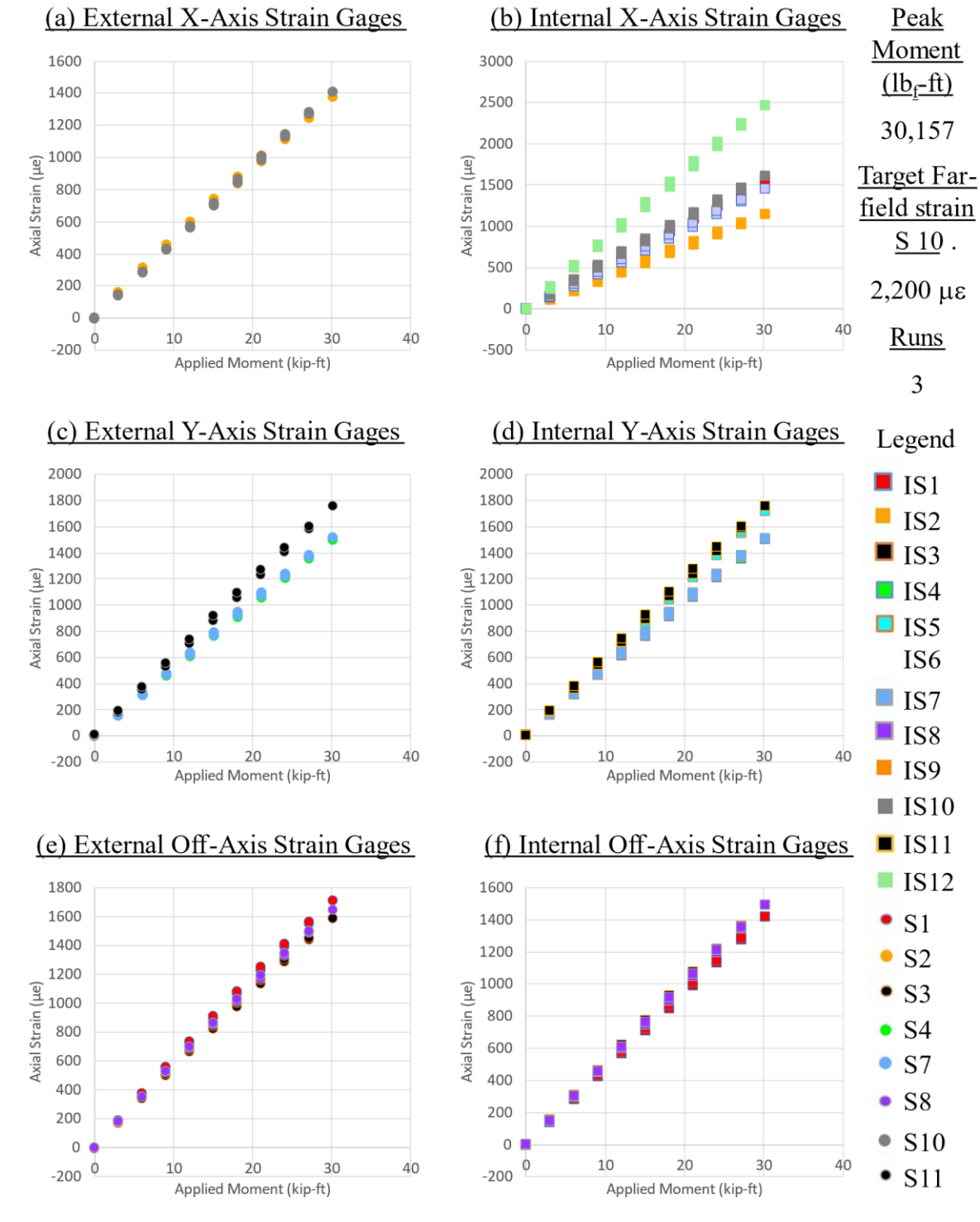

Figure B-39. Panel 11: baseline strain survey (axial strain)

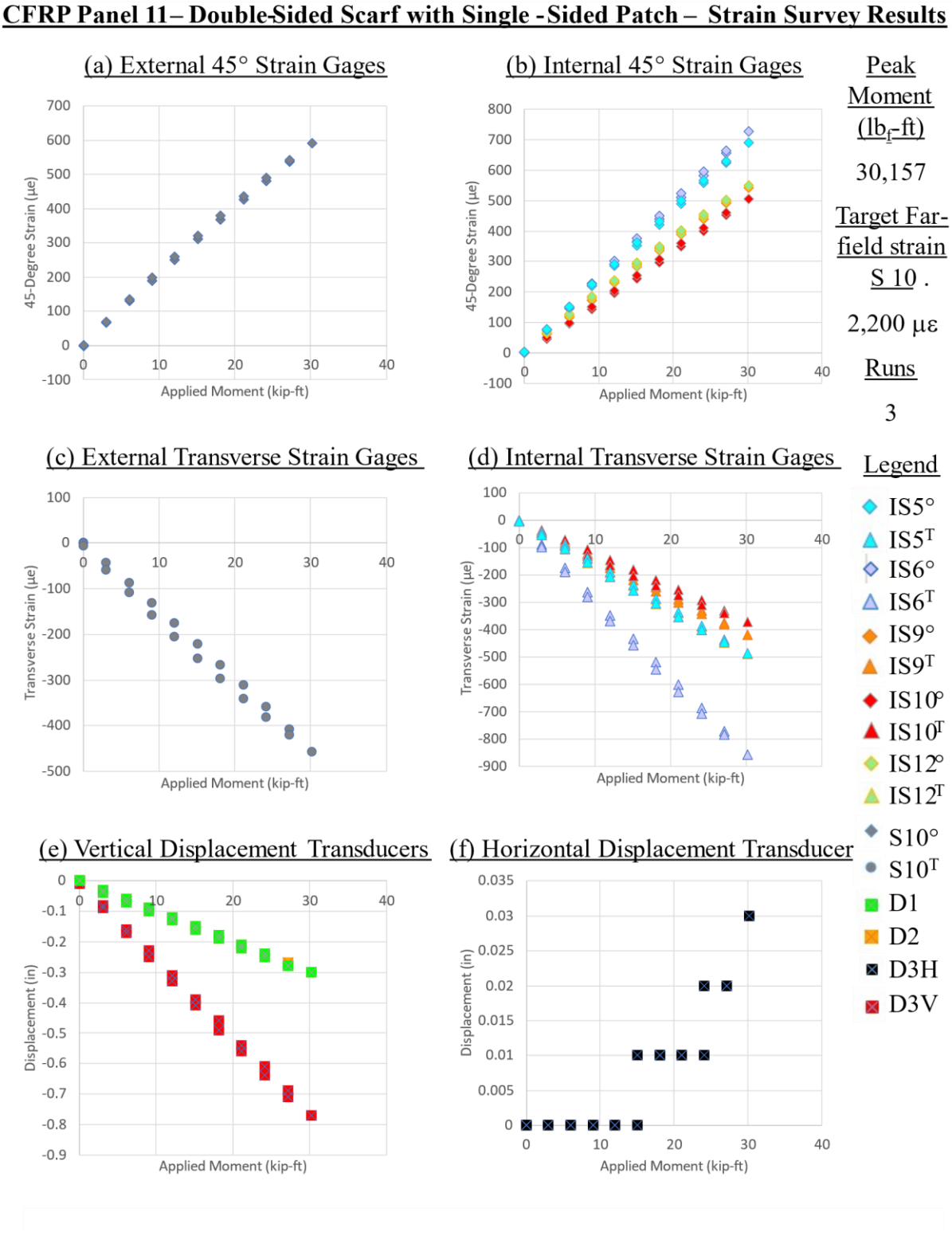

Figure B-40. Panel 11: baseline strain survey (non-axial strain and displacement)

C Strain and Displacement During Residual Strength Test

INTRODUCTION

Provided in this appendix are strain gages results captured during residual strength loading of the open-hole panel specimen.

RESIDUAL STRENGTH RESULTS

Figures C-1 – C36, C-37 – C-72, C-73 – C-80, C-81 – C-84, C-85 – C-92 show the applied loads, displacement, and axial, transverse, and 45-degree strain results at each load increment of the residual strength test of Panels 7, 8, 9, 10 and 11 respectively. These load increments were based on the percentage of predicted critical load (PCL) and include 60%, 66%, 70%, 75%, 80%, 85%, 90%, 95% of PCL and final failure loads for Panels 7 and 8, 35% and 55% for Panel 9, final failure (59%) for Panel 10, and 39% and final failure (57%) of Panel 11.

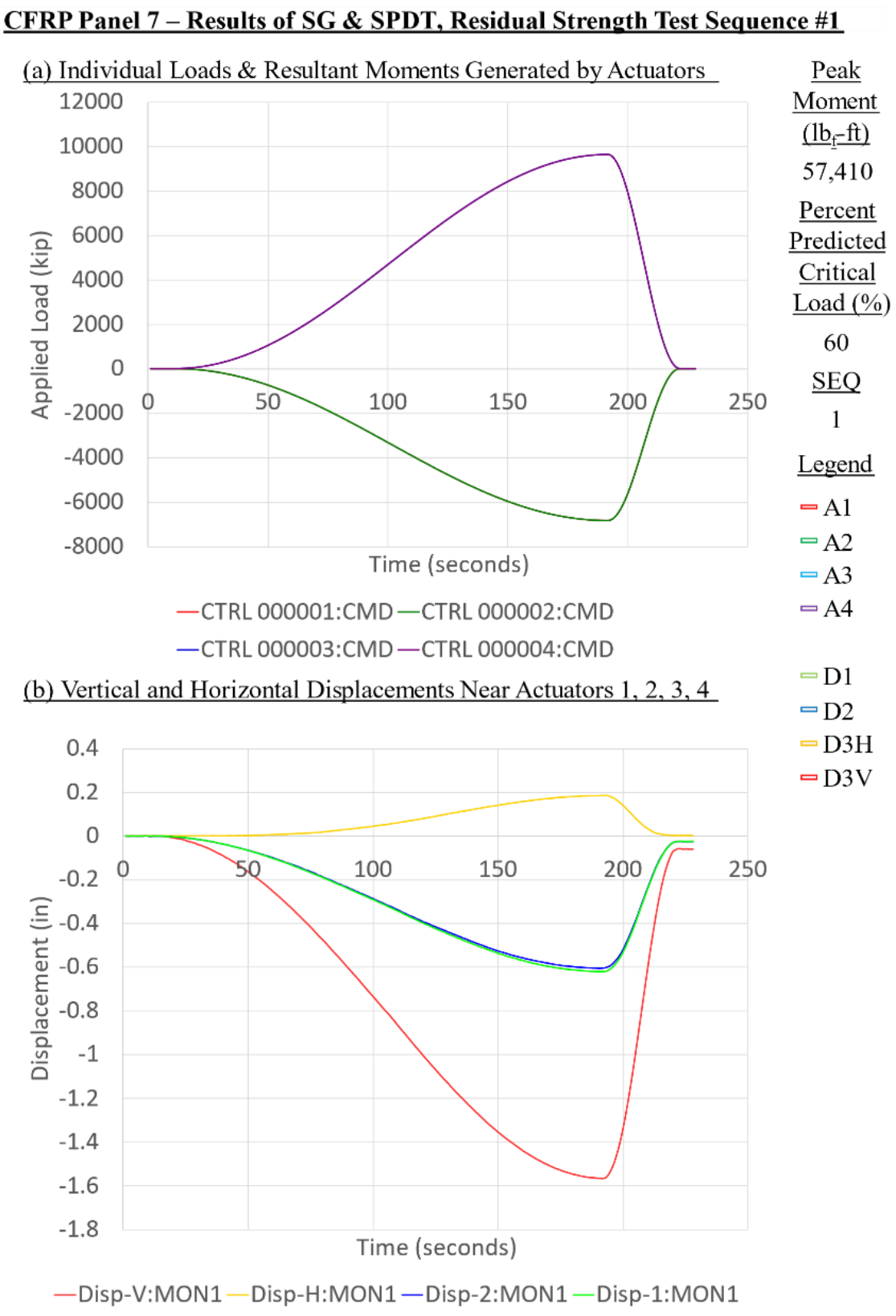

Figure C-1. Panel 7 load increment 1 (60% load level), load and displacement

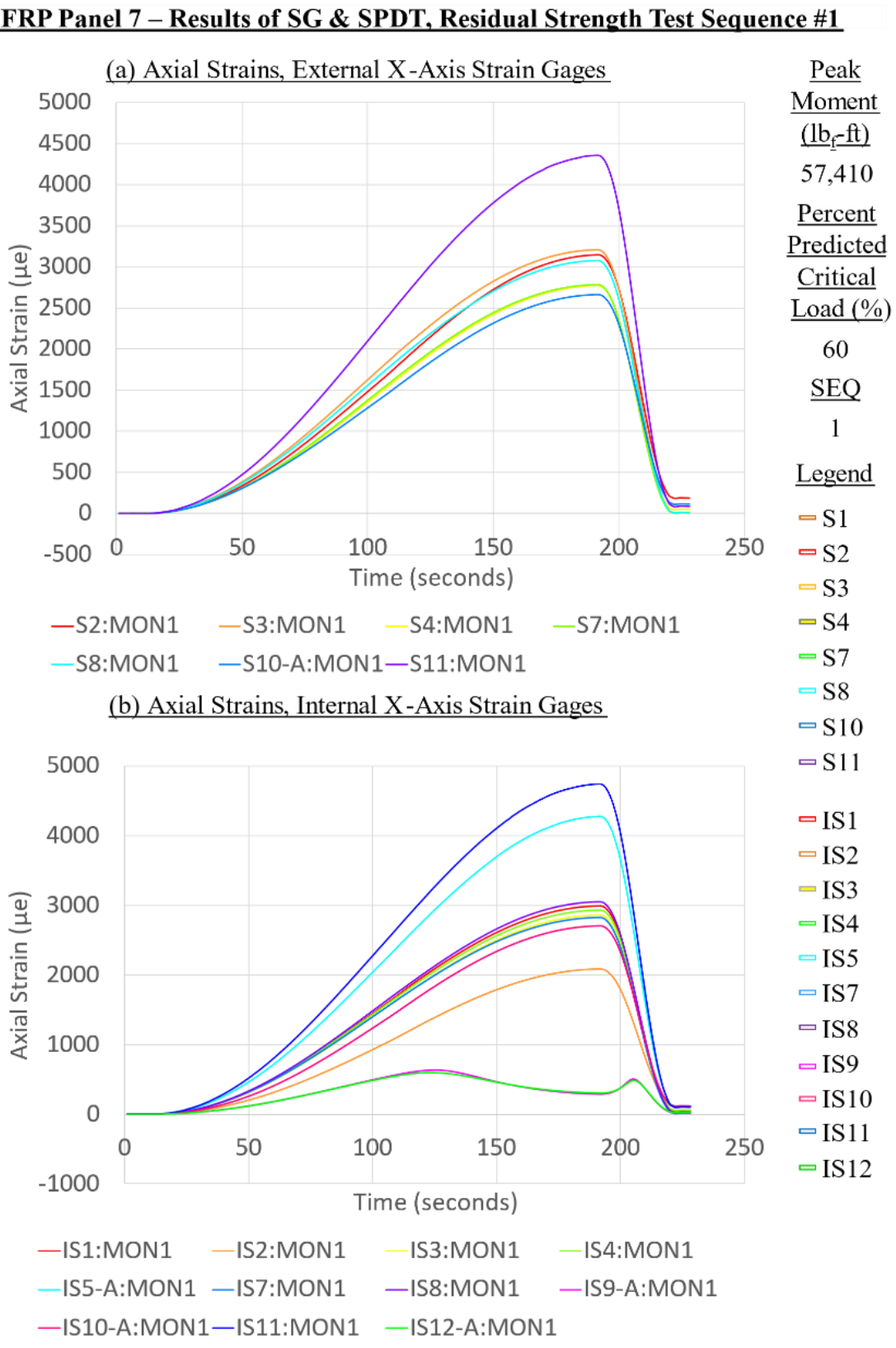

Figure C-2. Panel 7 load increment 1 (60% load level), axial strain

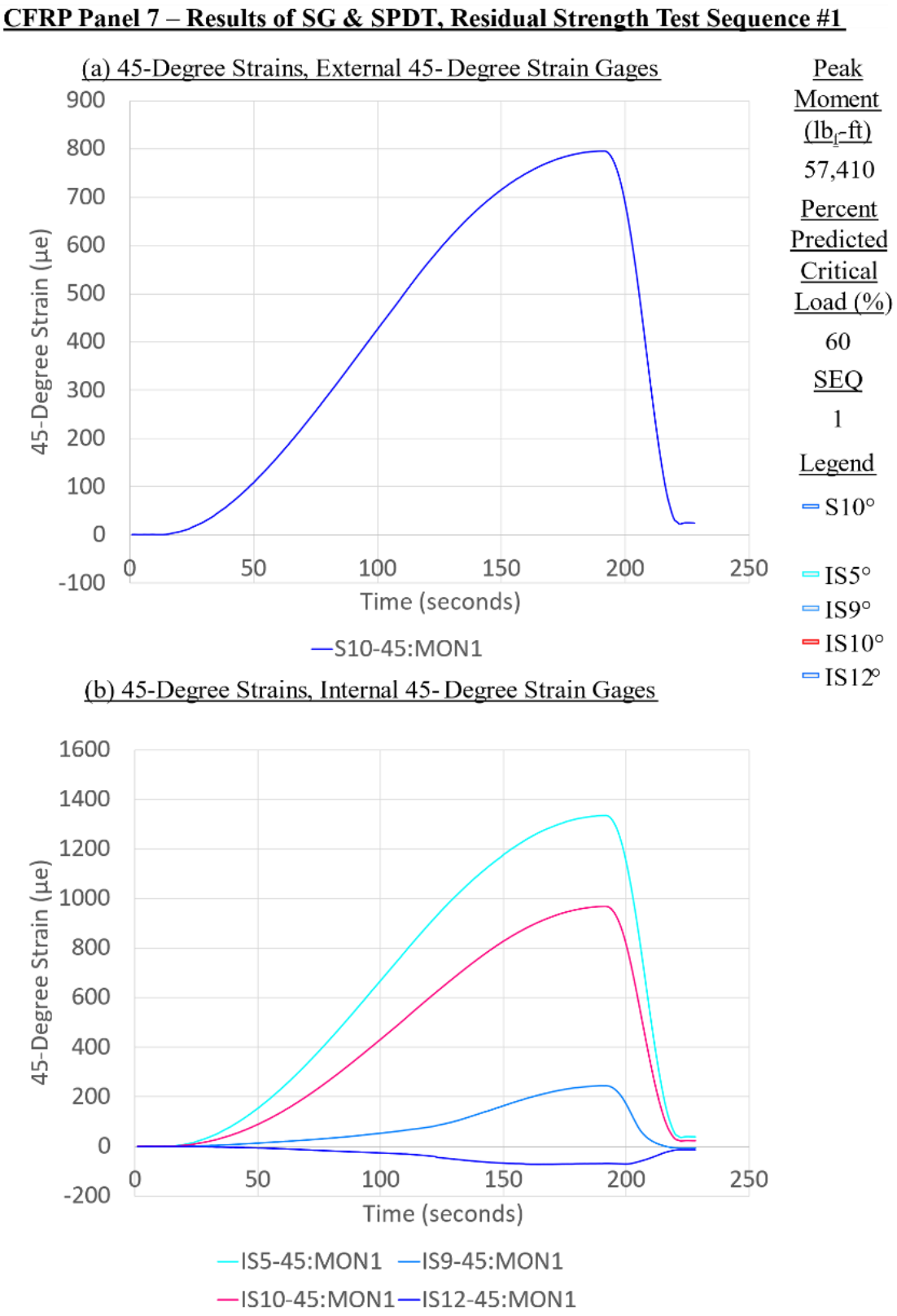

Figure C-3. Panel 7 load increment 1 (60% load level), 45-degree strain

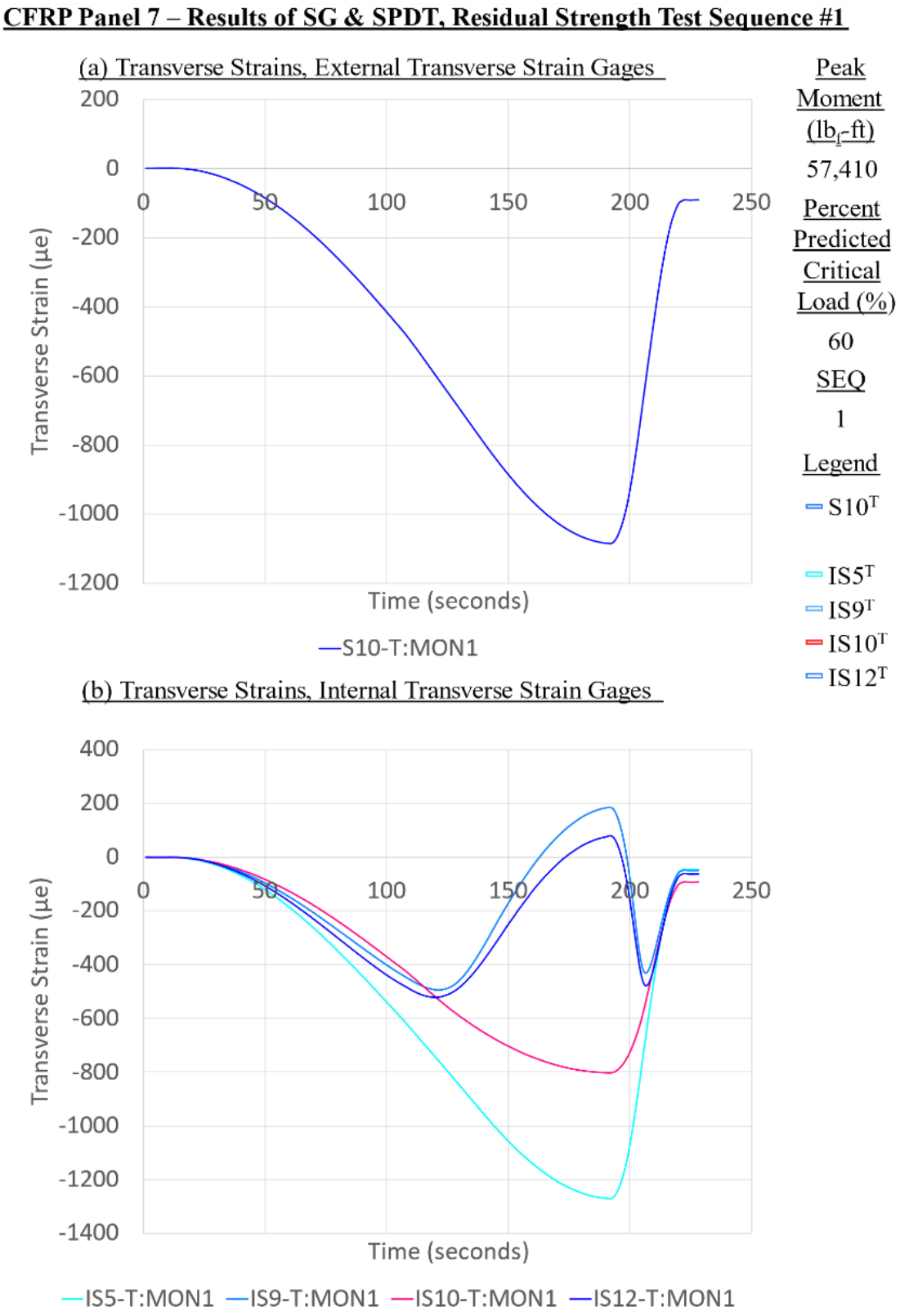

Figure C-4. Panel 7 load increment 1 (60% load level), transverse strain

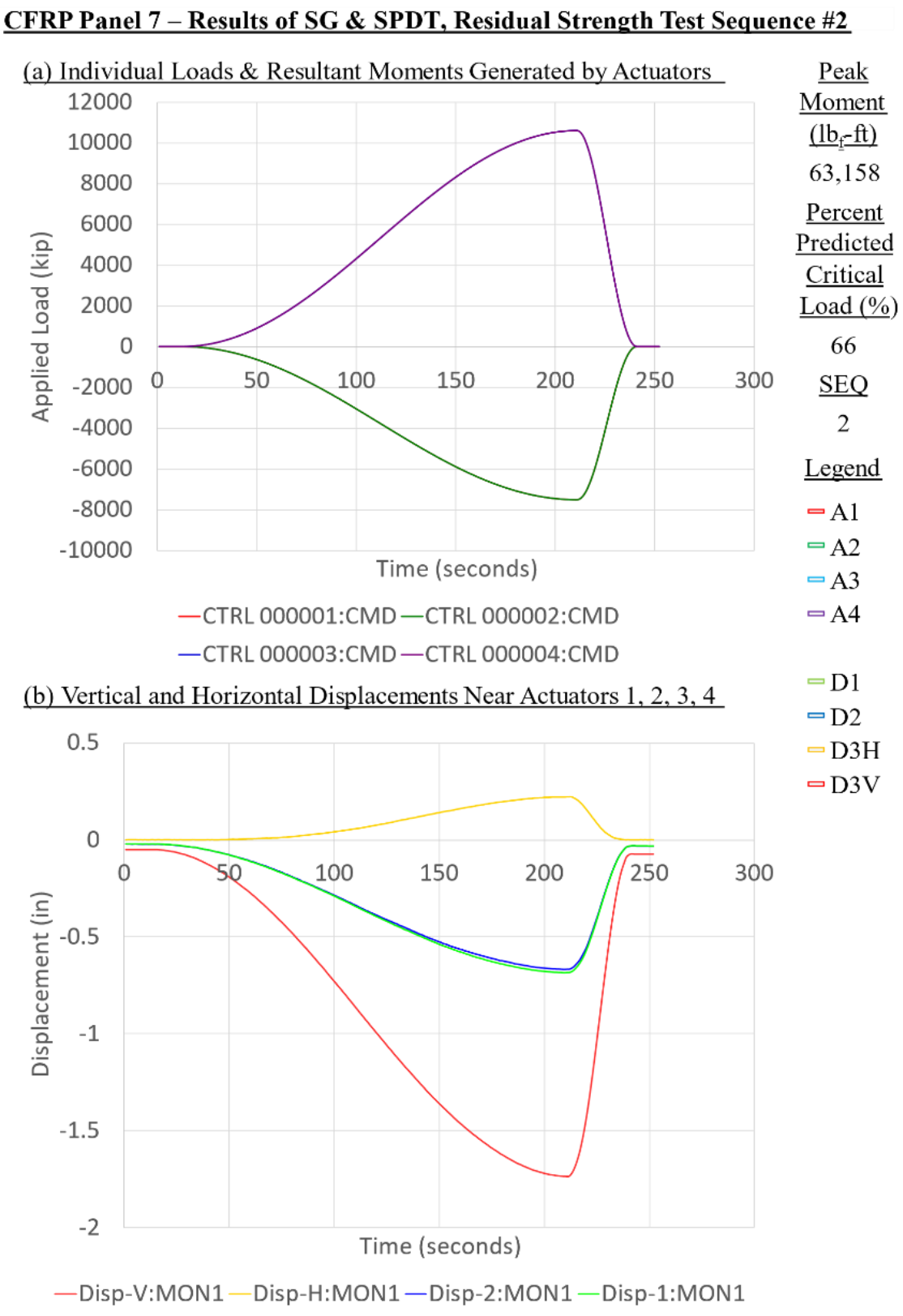

Figure C-5. Panel 7 load increment 2 (66% load level), load and displacement

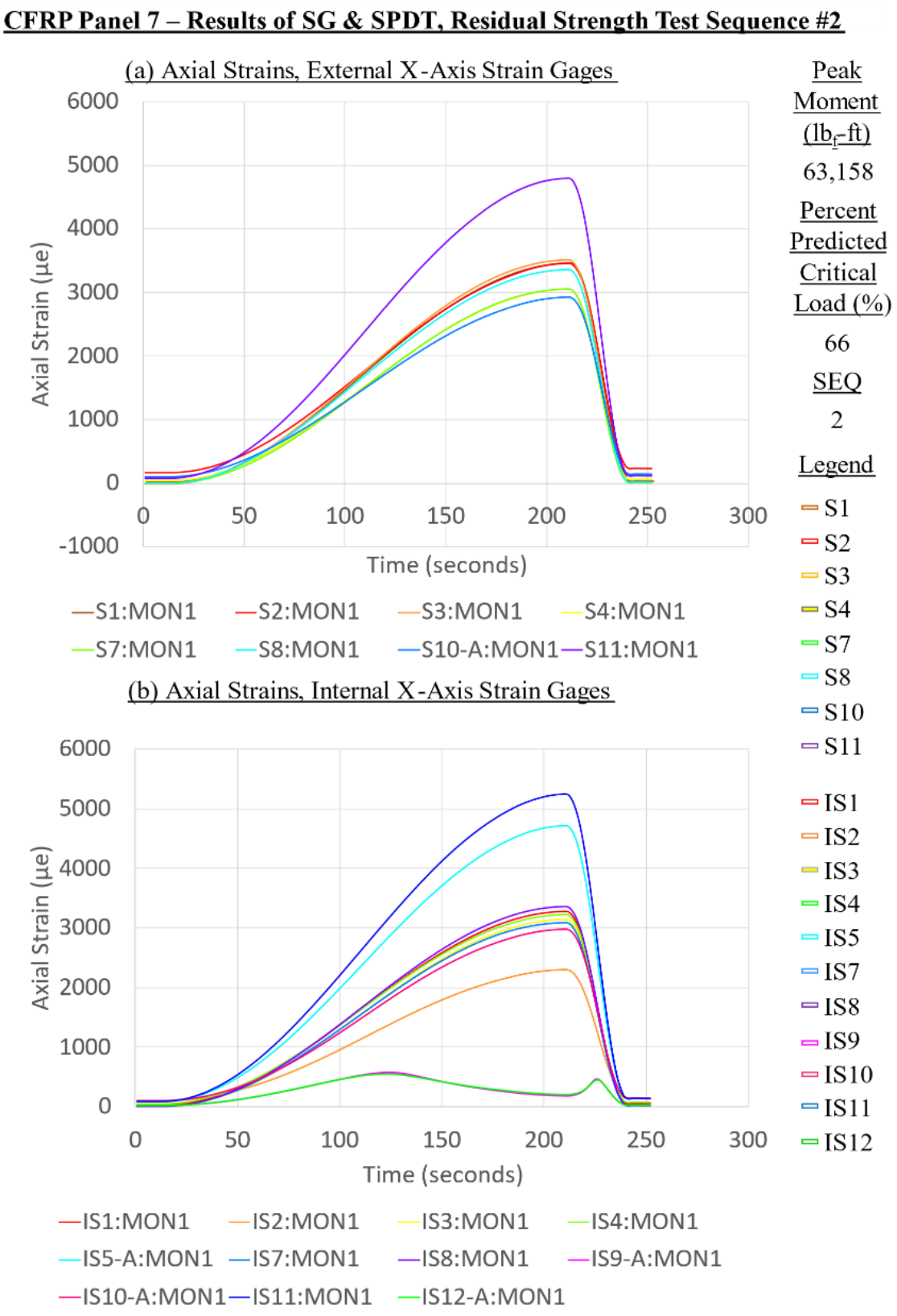

Figure C-6. Panel 7 load increment 2 (66% load level), axial strain

CFRP Panel 7 – Results of SG & SPDT, Residual Strength Test Sequence #2

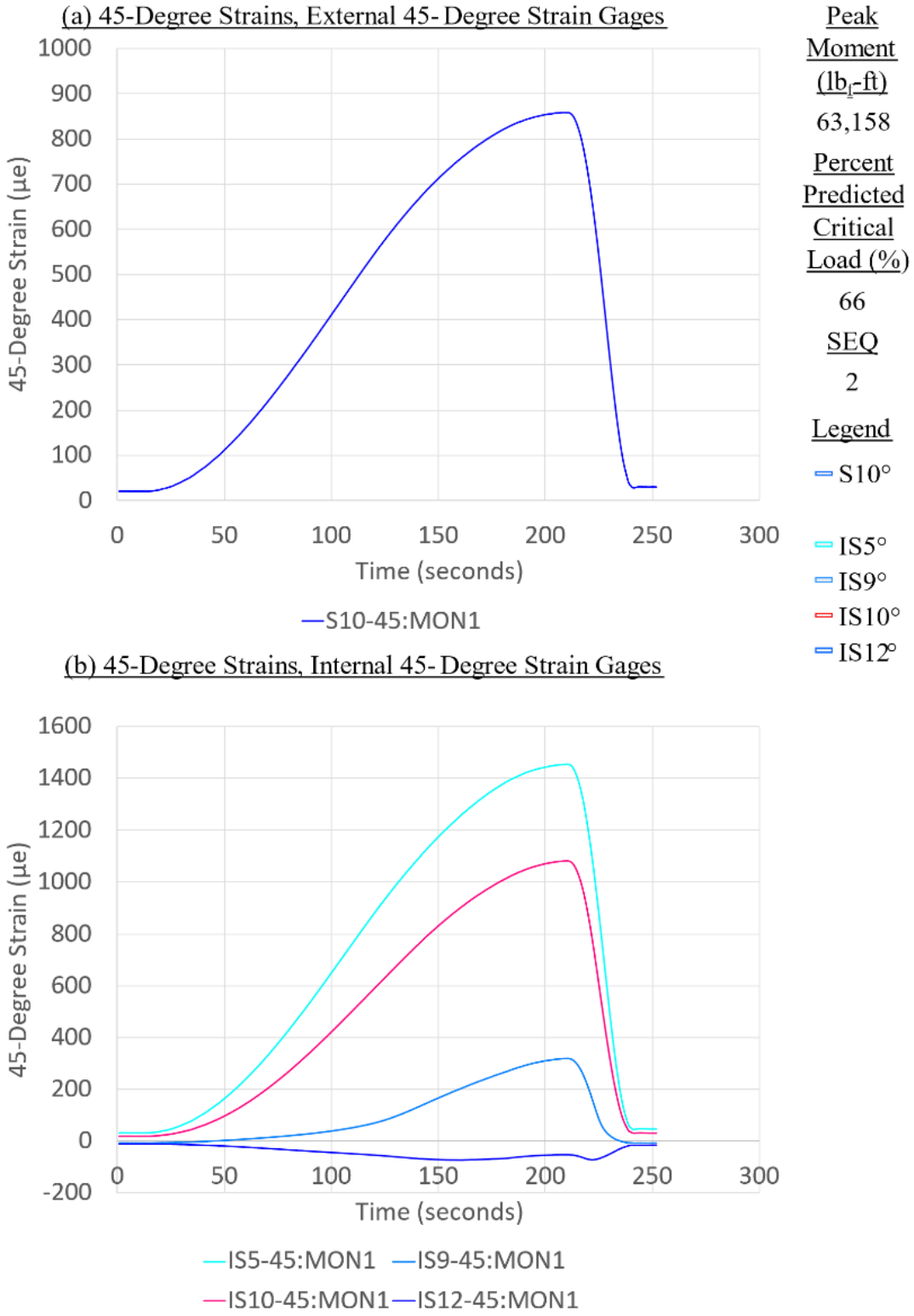

Figure C-7. Panel 7 load increment 2 (66% load level), 45-degree strain

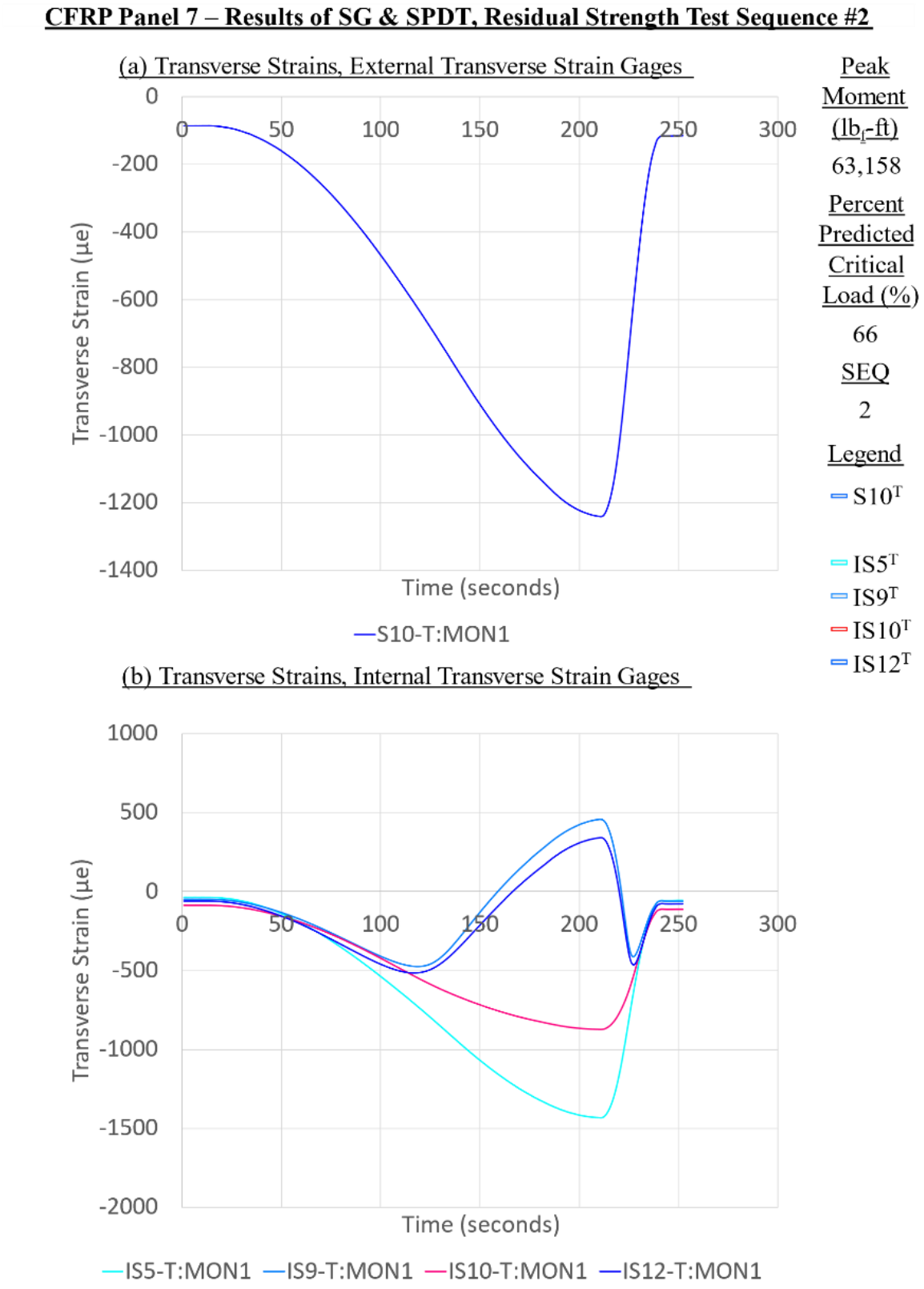

Figure C-8. Panel 7 load increment 2 (66% load level), transverse strain

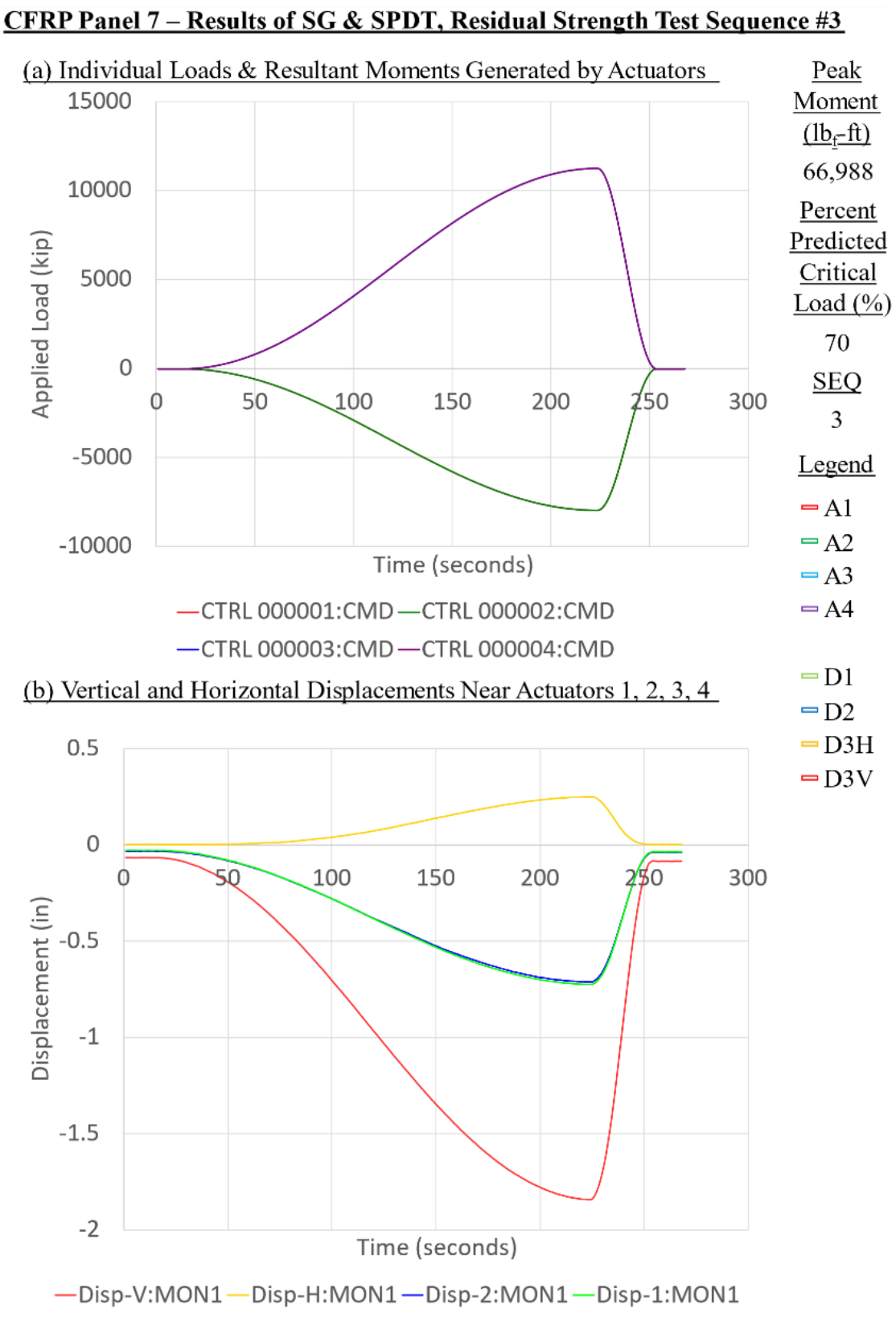

Figure C-9. Panel 7 load increment 3 (70% load level), load and displacement

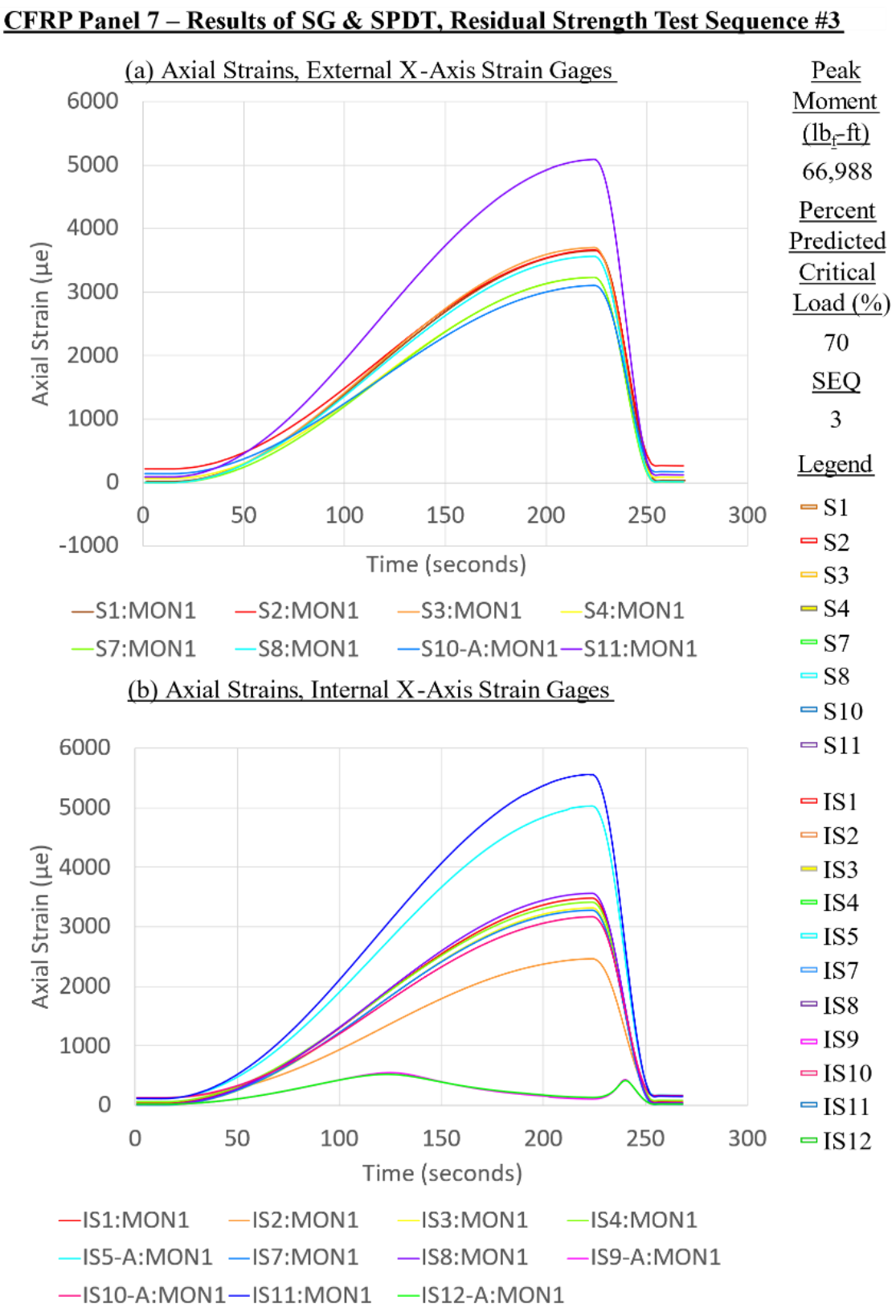

Figure C-10. Panel 7 load increment 3 (70% load level), axial strain

CFRP Panel 7 – Results of SG & SPDT, Residual Strength Test Sequence #3

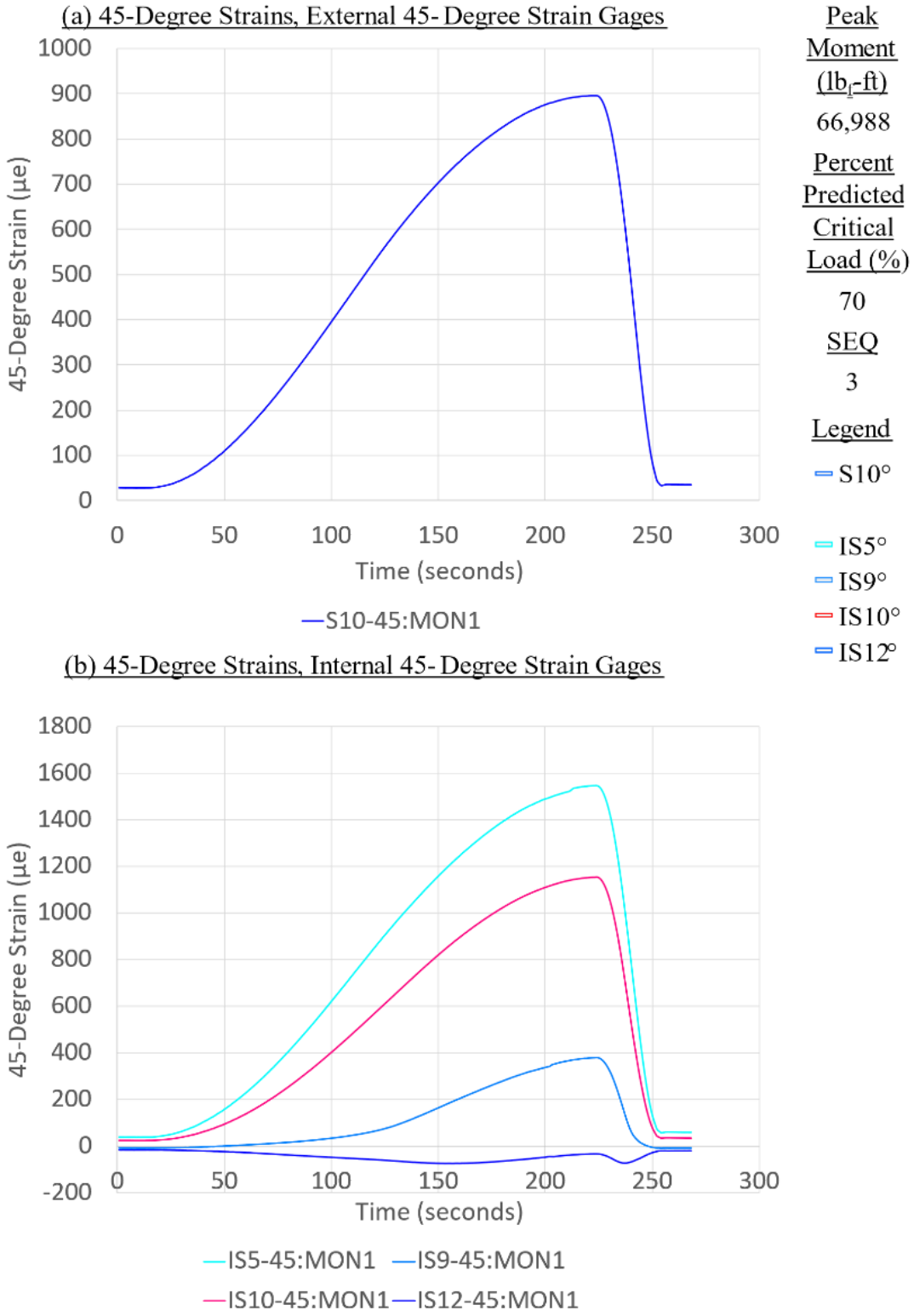

Figure C-11. Panel 7 load increment 3 (70% load level), 45-degree strain

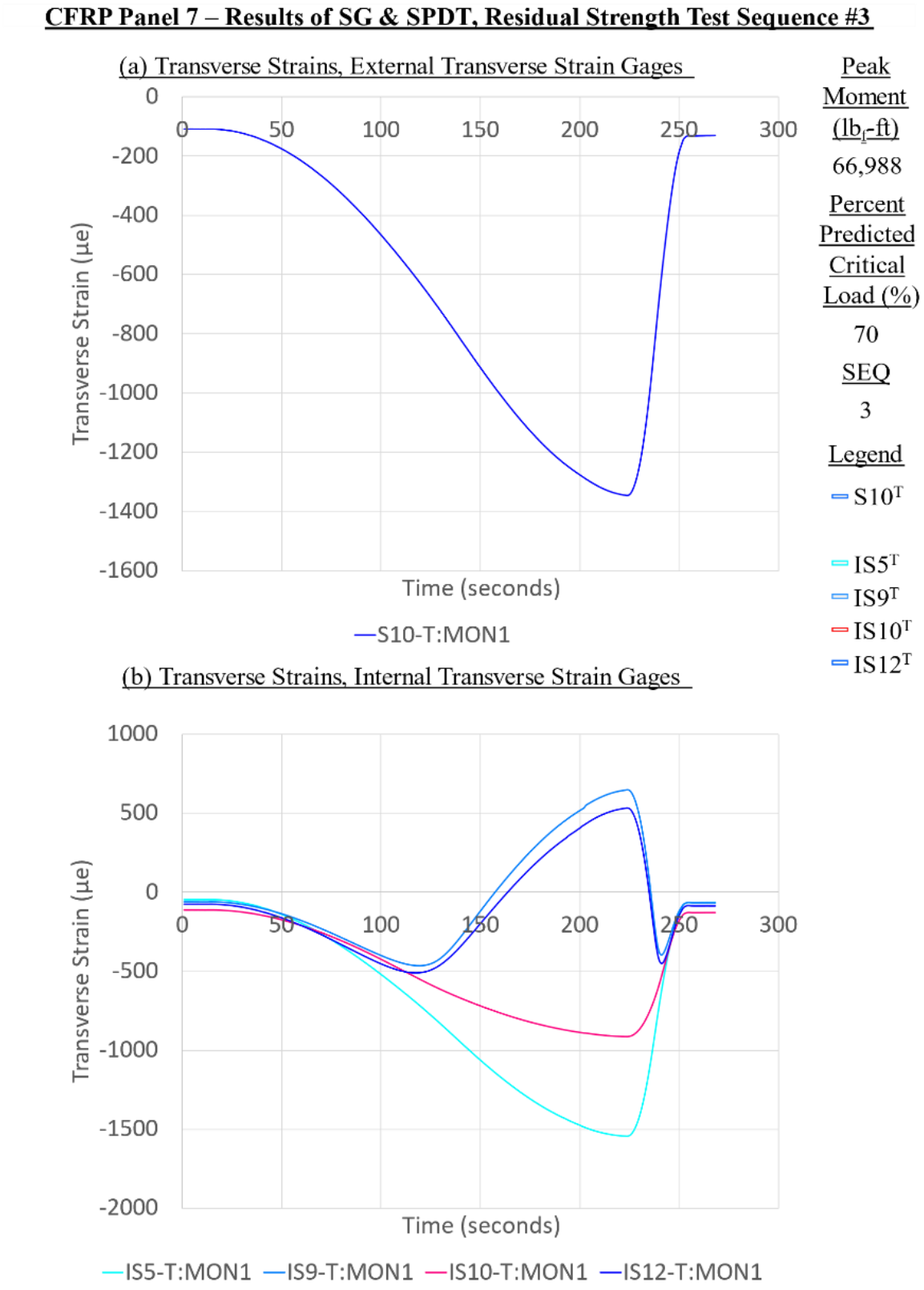

Figure C-12. Panel 7 load increment 3 (70% load level), transverse strain

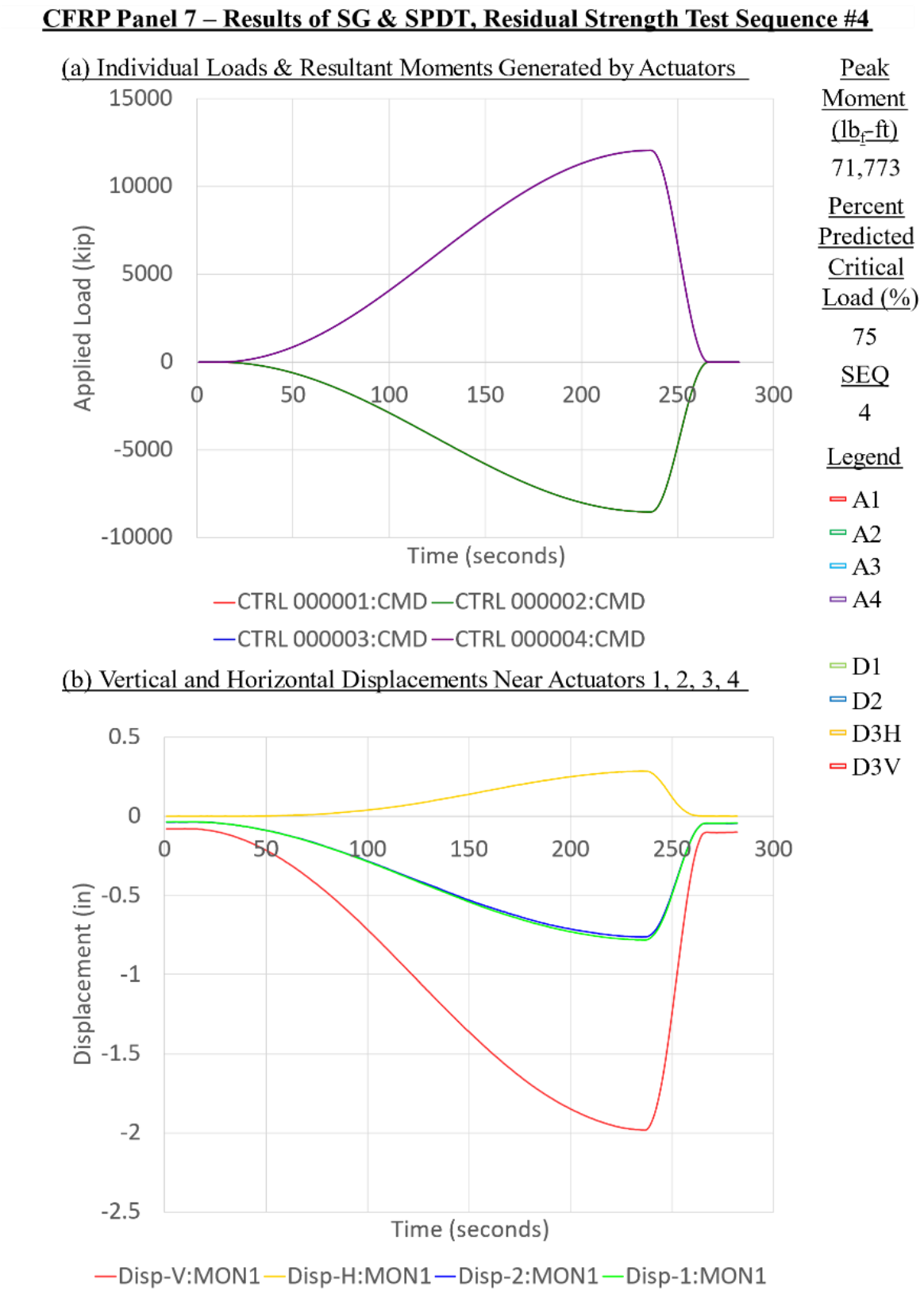

Figure C-13. Panel 7 load increment 4 (75% load level), load and displacement

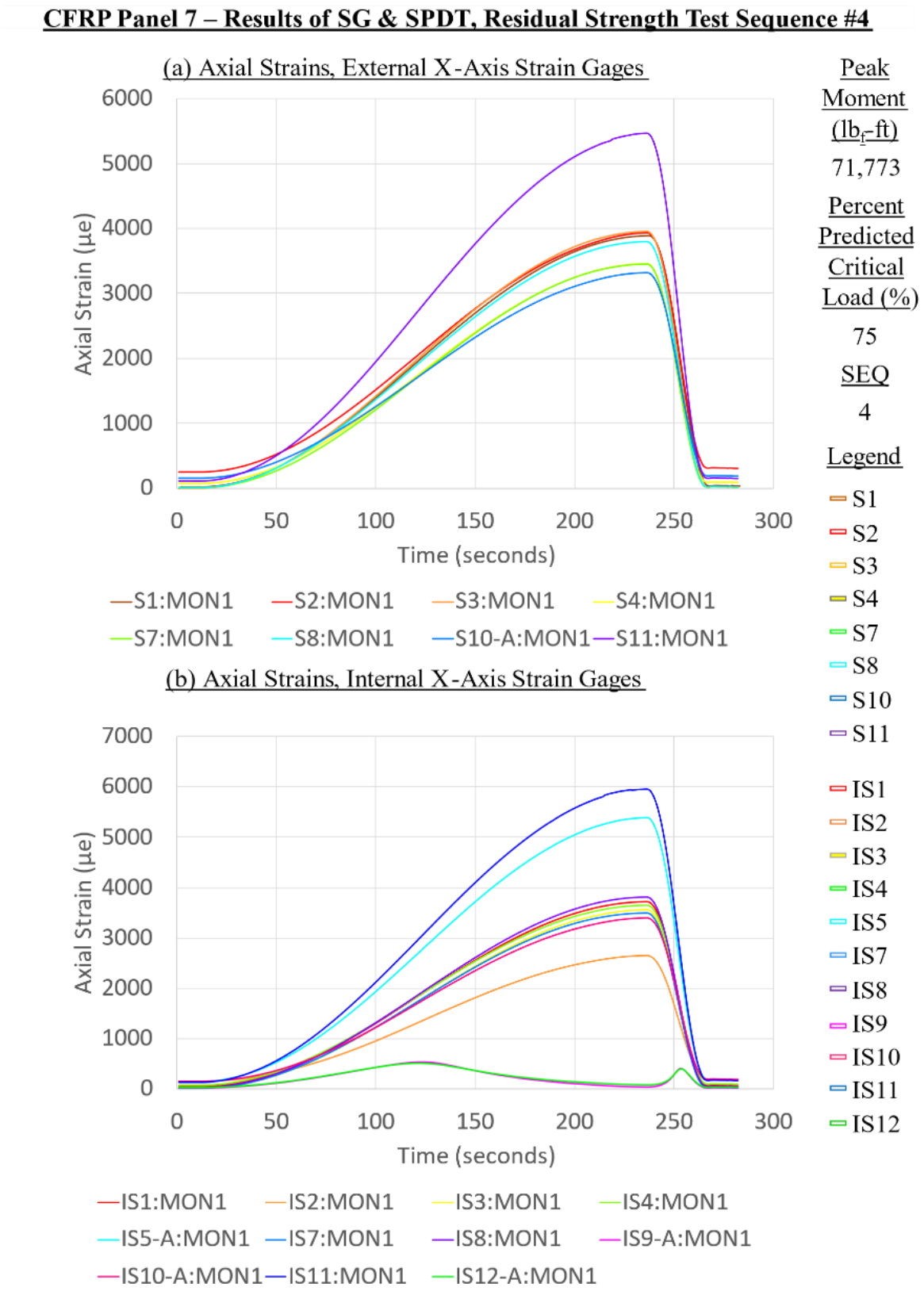

Figure C-14. Panel 7 load increment 4 (75% load level), axial strain

CFRP Panel 7 – Results of SG & SPDT, Residual Strength Test Sequence #4

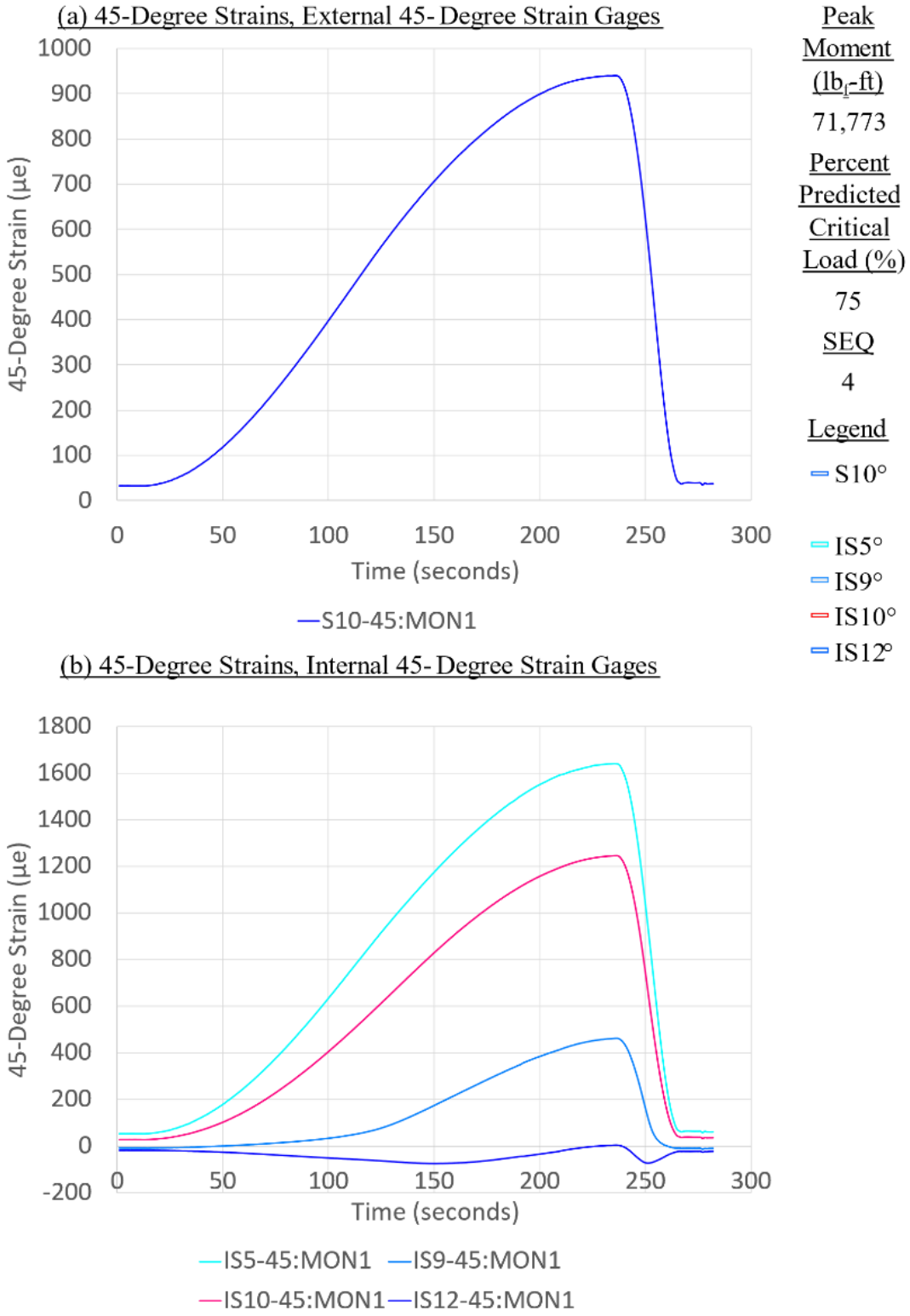

Figure C-15. Panel 7 load increment 4 (75% load level), 45-degree strain

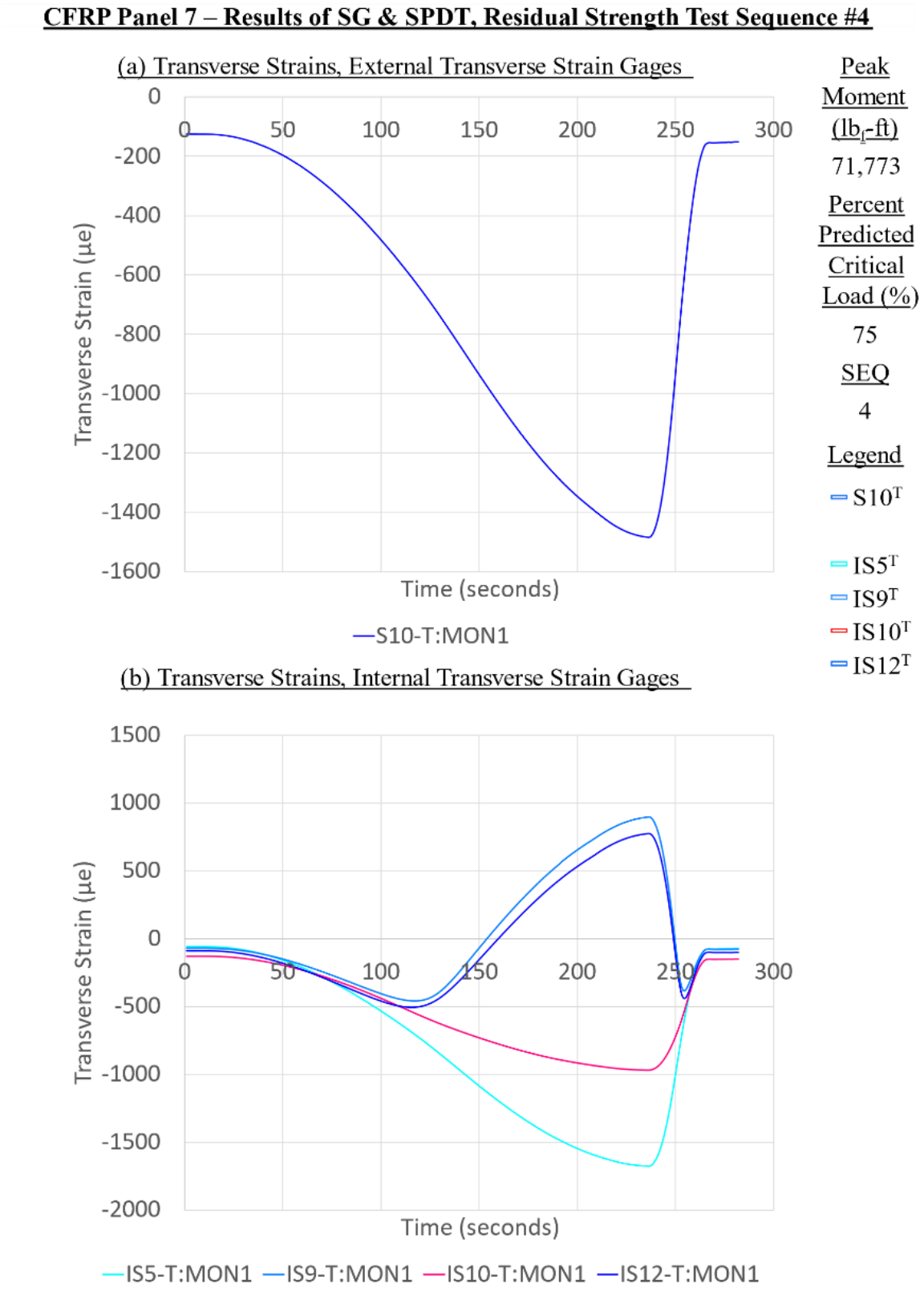

Figure C-16. Panel 7 load increment 4 (75% load level), transverse strain

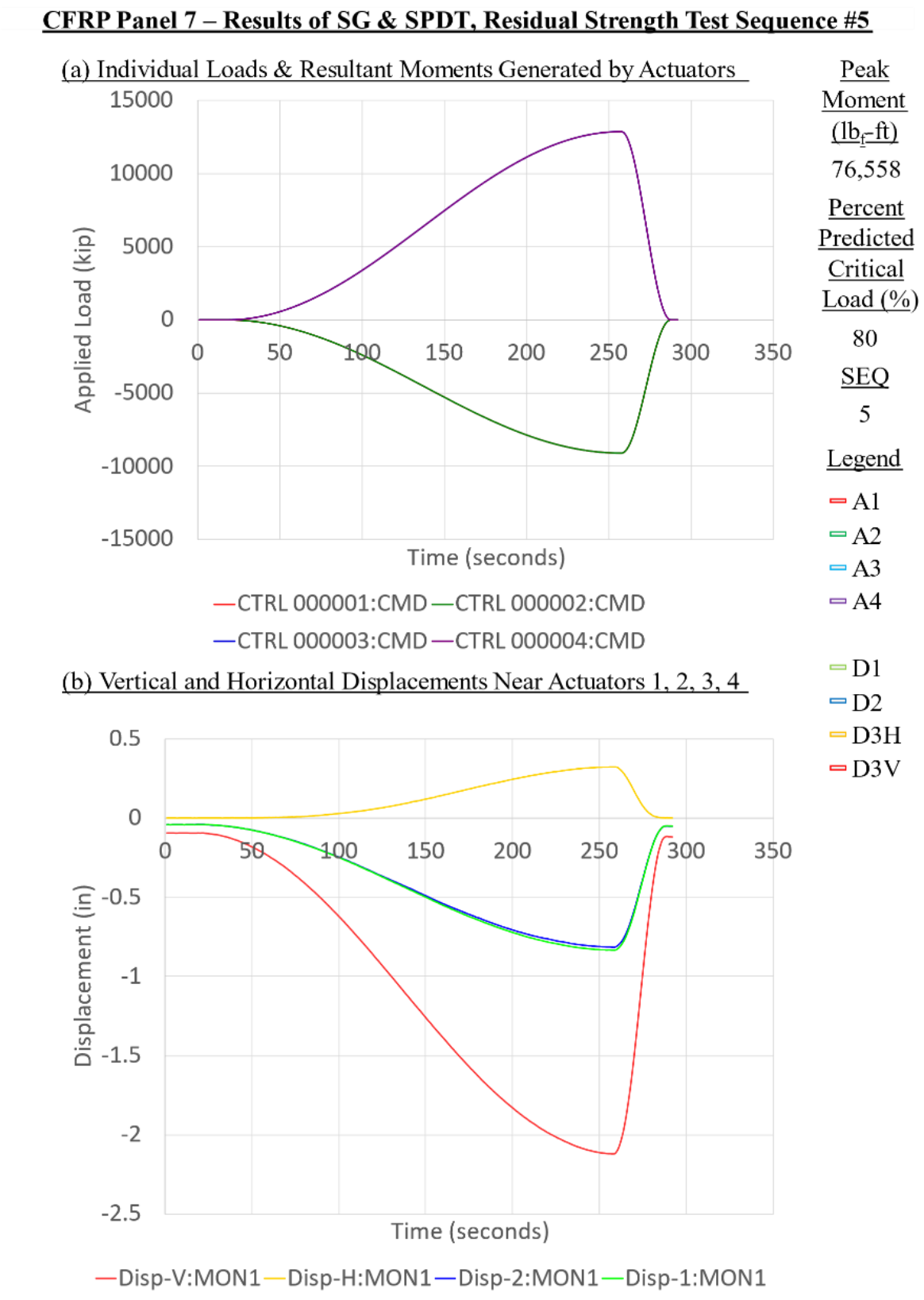

Figure C-17. Panel 7 load increment 5 (80% load level), load and displacement

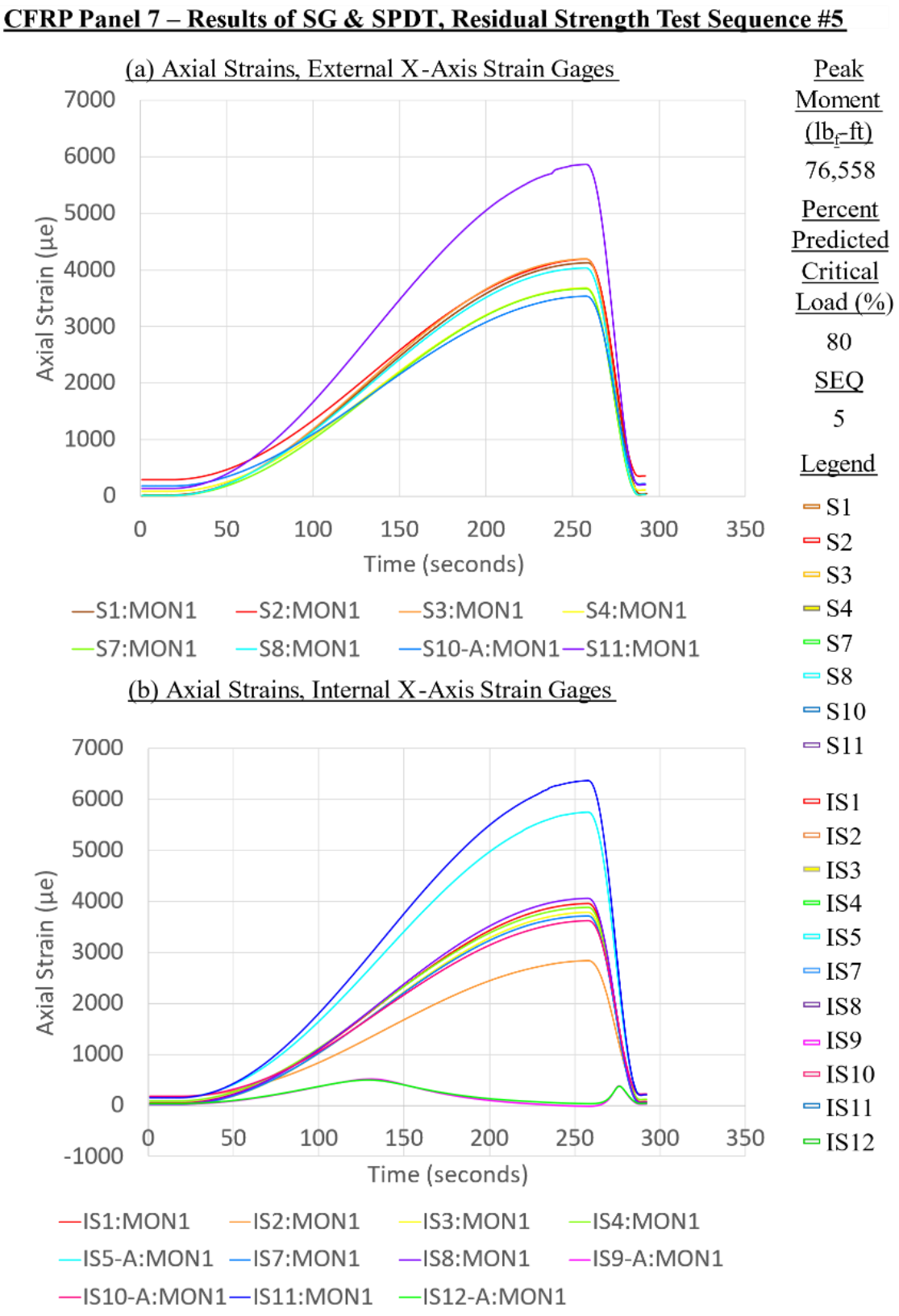

Figure C-18. Panel 7 load increment 5 (80% load level), axial strain

CFRP Panel 7 – Results of SG & SPDT, Residual Strength Test Sequence #5

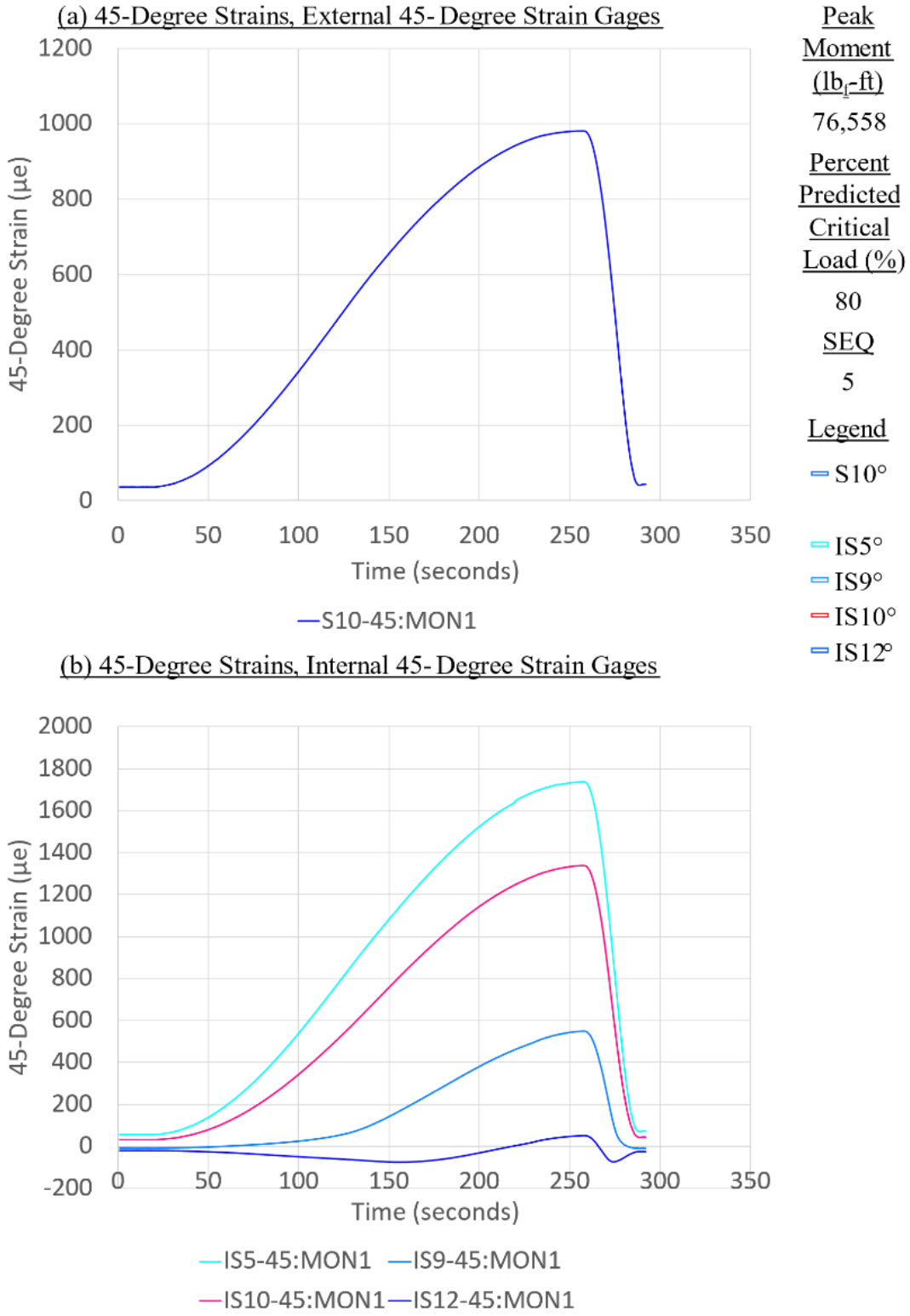

Figure C-19. Panel 7 load increment 5 (80% load level), 45-degree strain

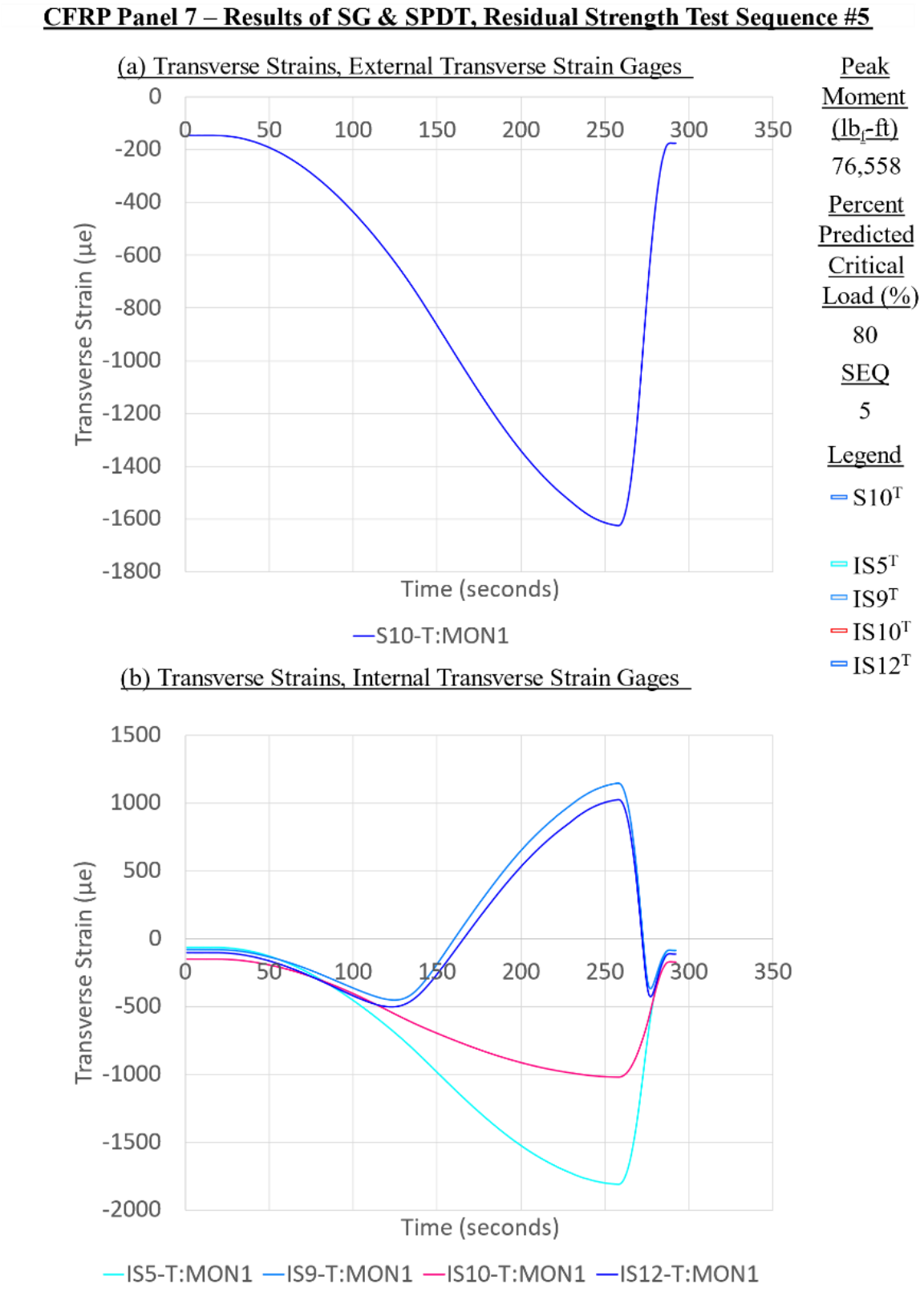

Figure C-20. Panel 7 load increment 5 (80% load level), transverse strain

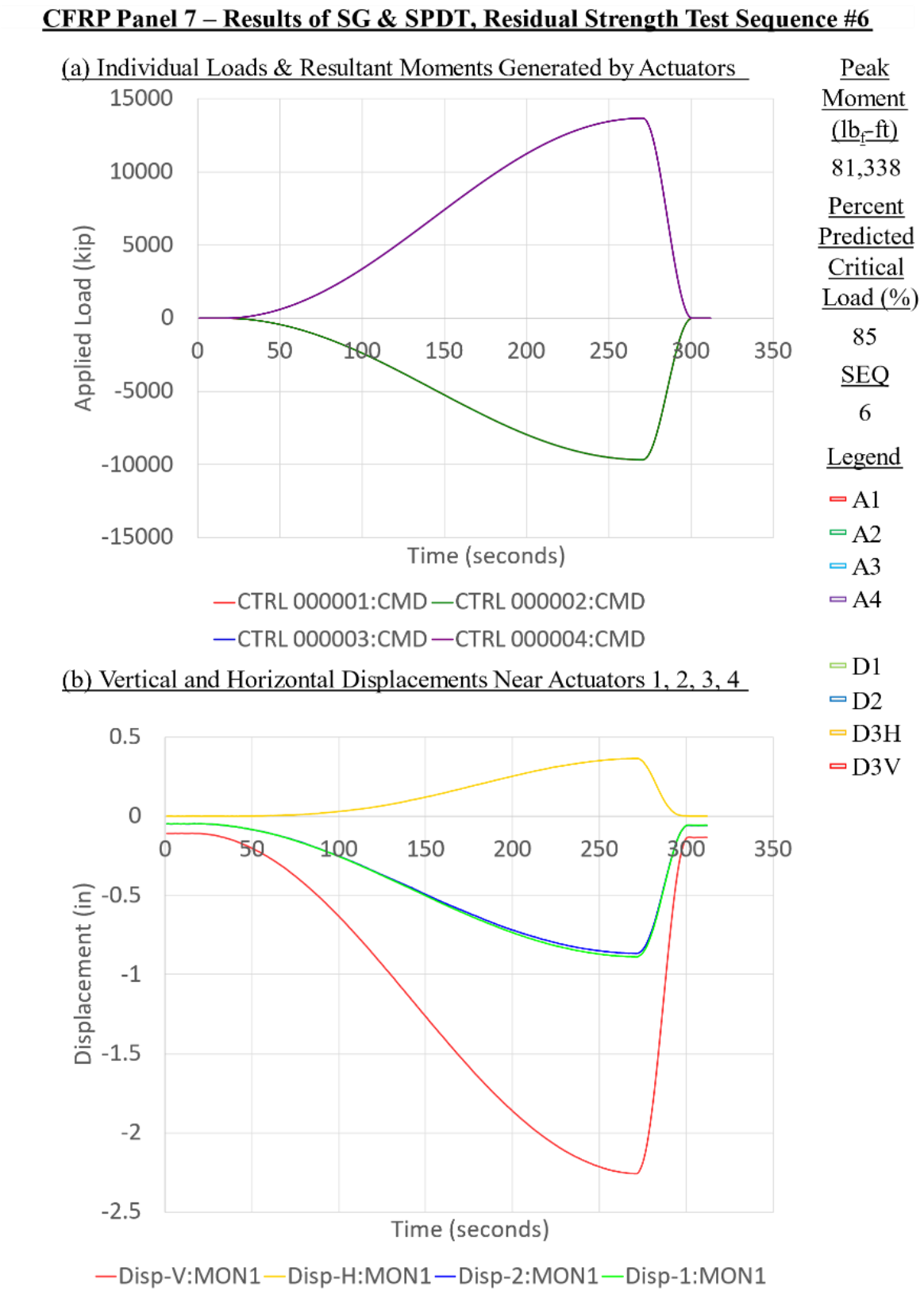

Figure C-21. Panel 7 load increment 6 (85% load level), load and displacement

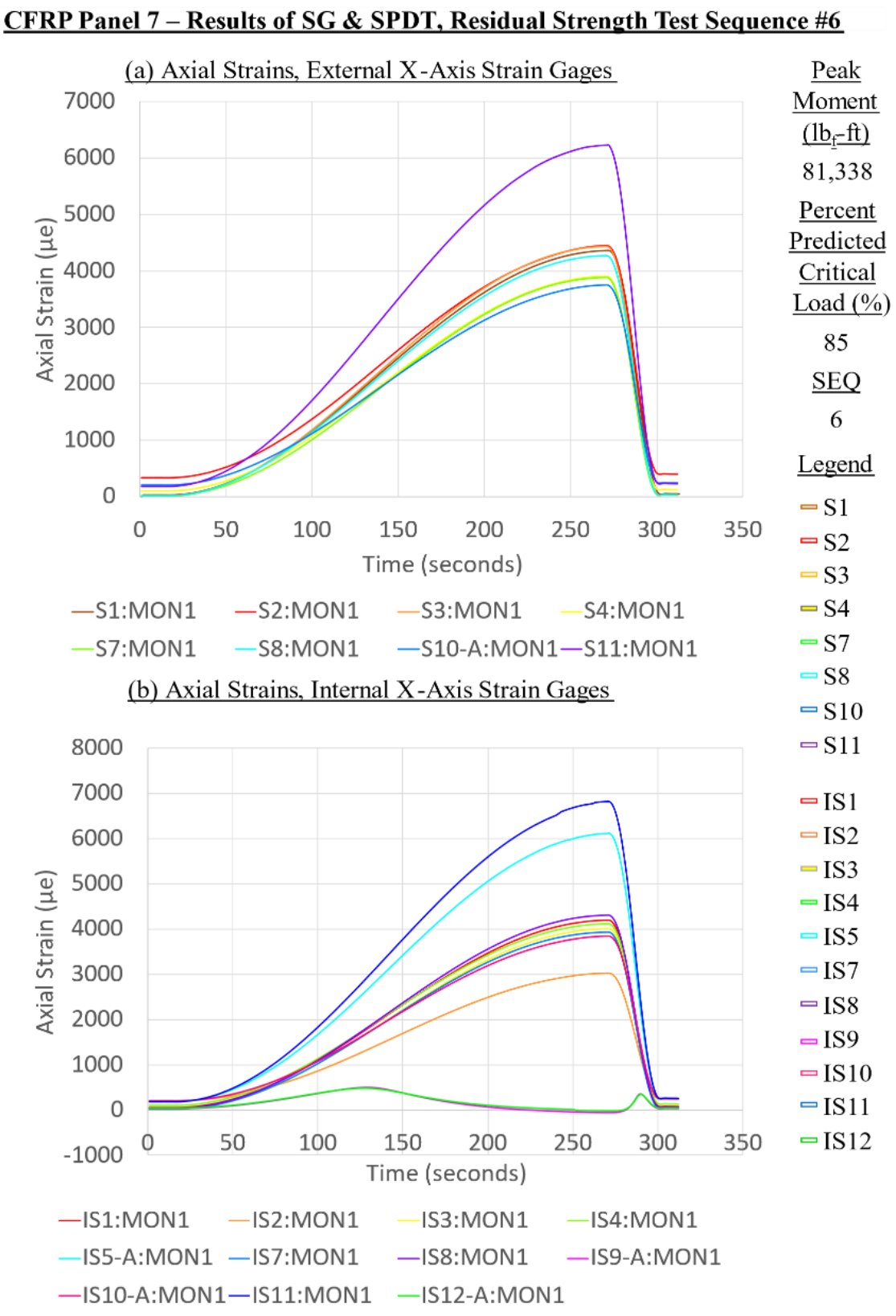

Figure C-22. Panel 7 load increment 6 (85% load level), axial strain

CFRP Panel 7 – Results of SG & SPDT, Residual Strength Test Sequence #6

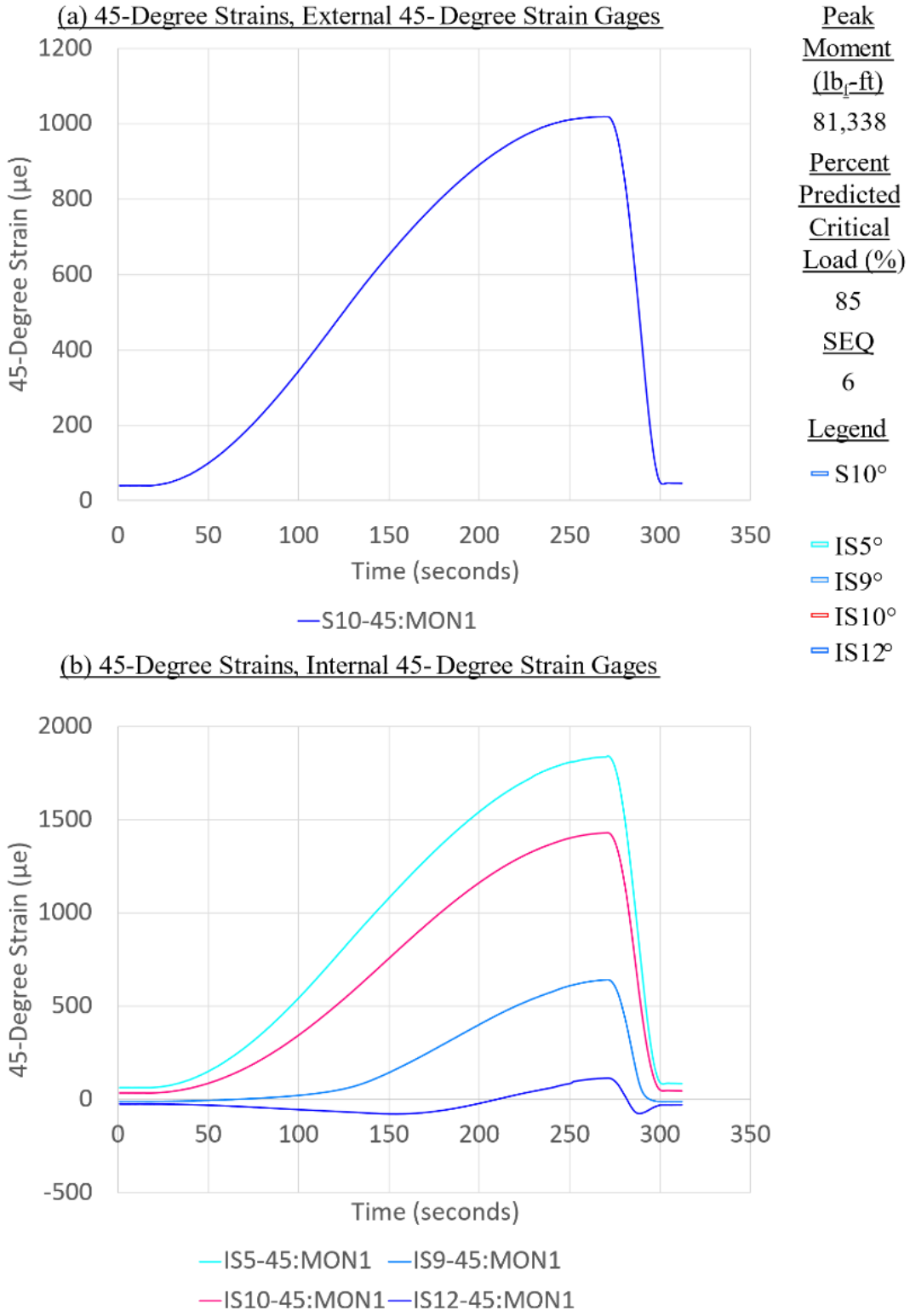

Figure C-23. Panel 7 load increment 6 (85% load level), 45-degree strain

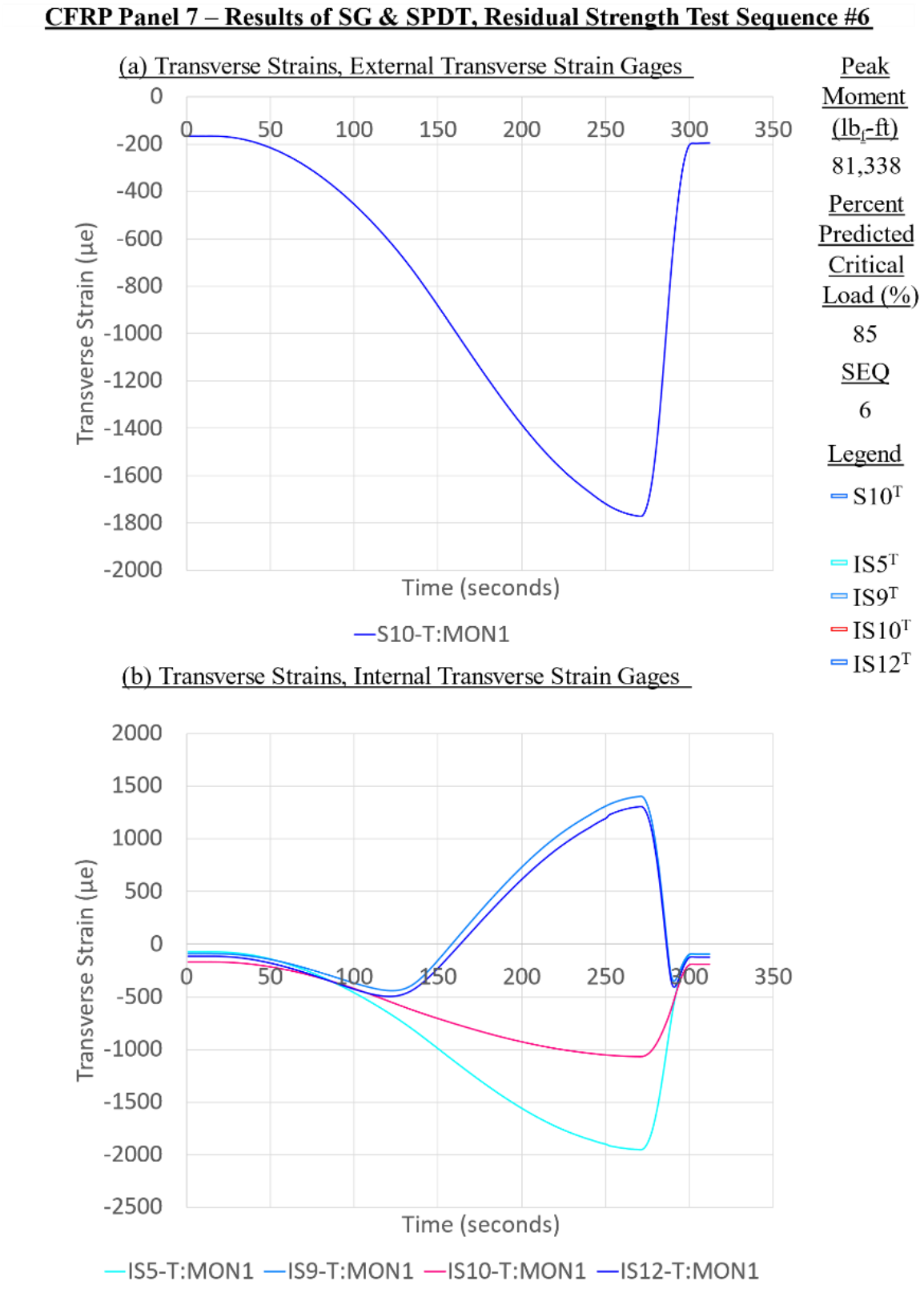

Figure C-24. Panel 7 load increment 6 (85% load level), transverse strain

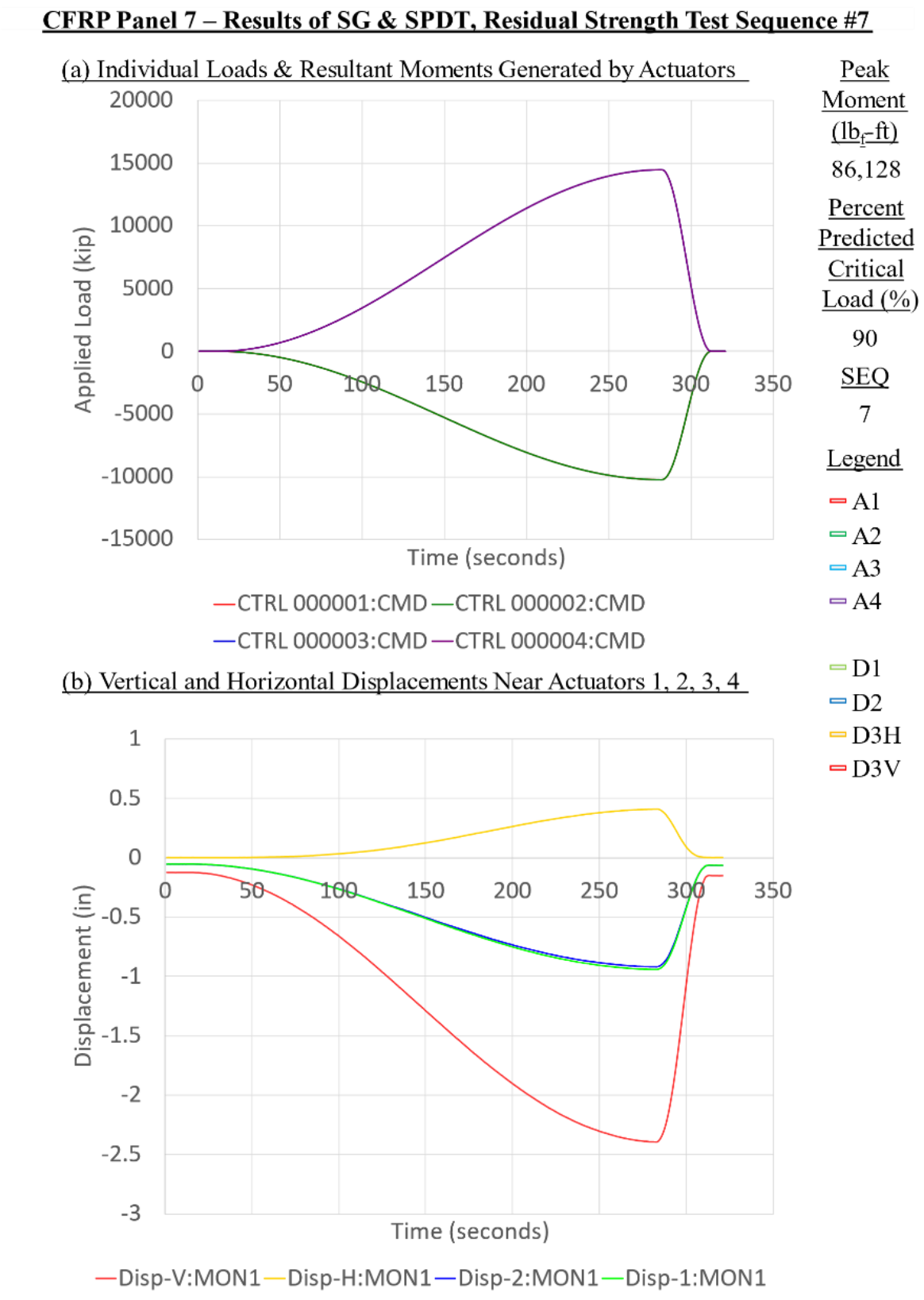

Figure C-25. Panel 7 load increment 7 (90% load level), load and displacement

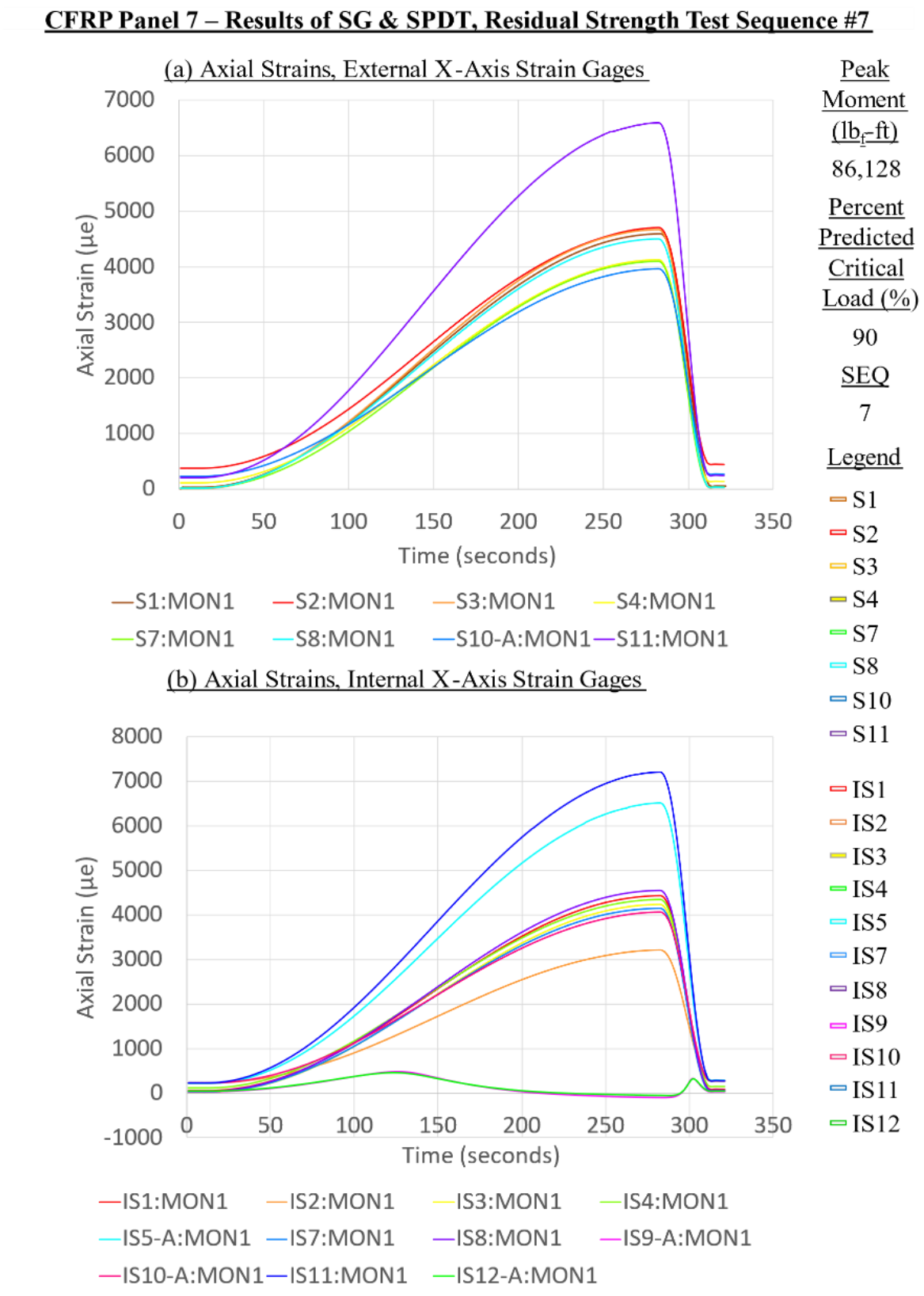

Figure C-26. Panel 7 load increment 7 (90% load level), axial strain

CFRP Panel 7 – Results of SG & SPDT, Residual Strength Test Sequence #7

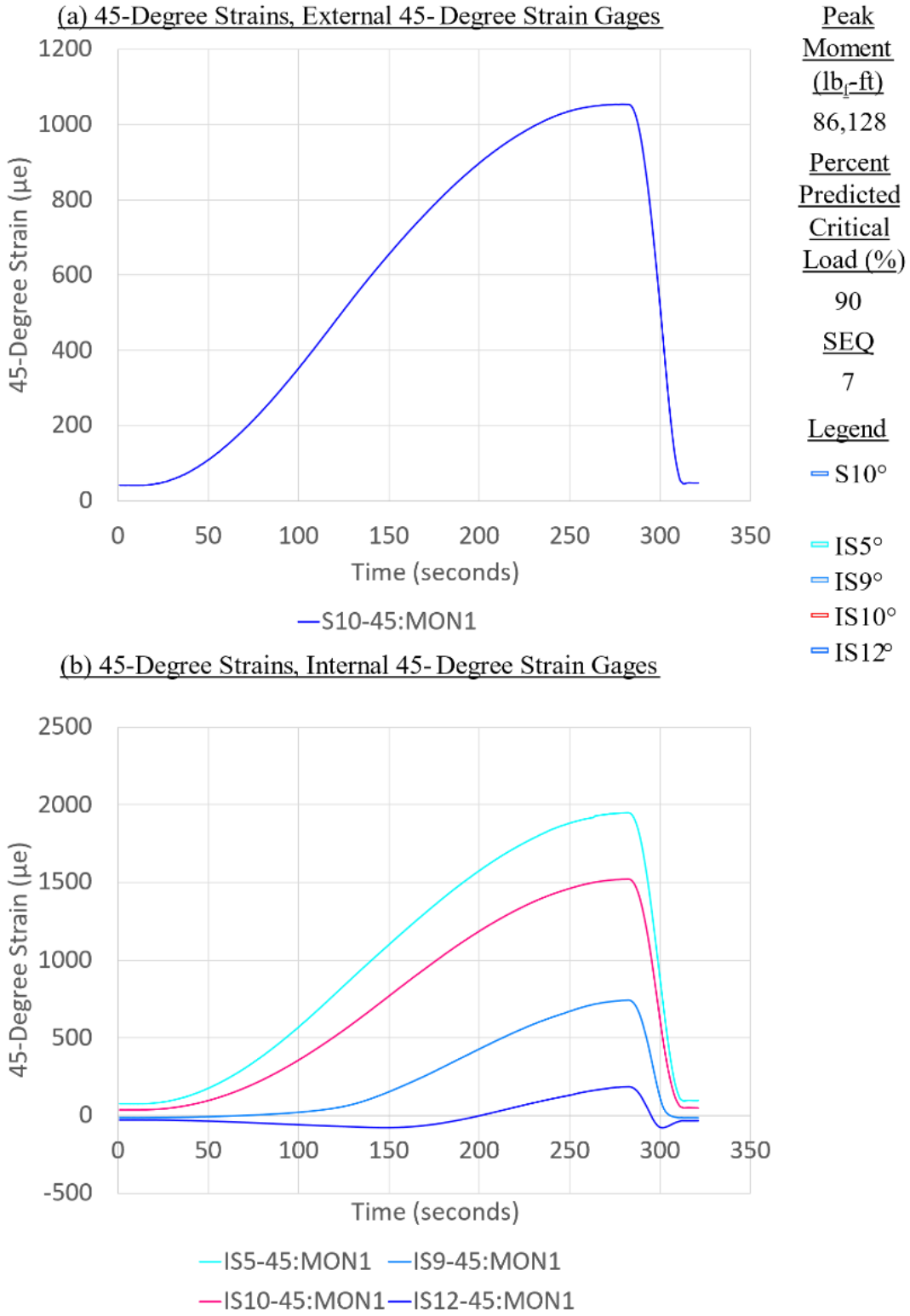

Figure C-27. Panel 7 load increment 7 (90% load level), 45-degree strain

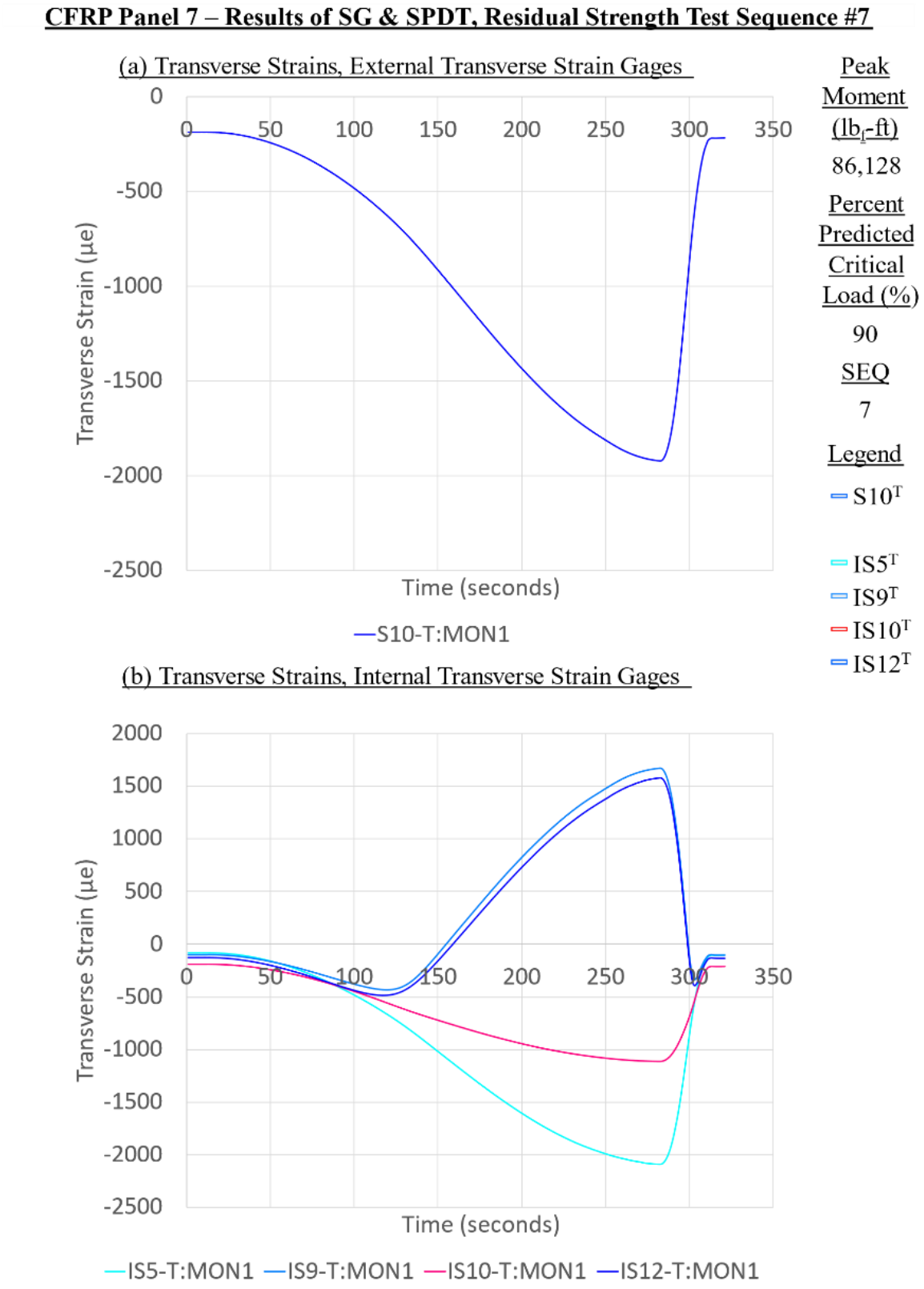

Figure C-28. Panel 7 load increment 7 (90% load level), transverse strain

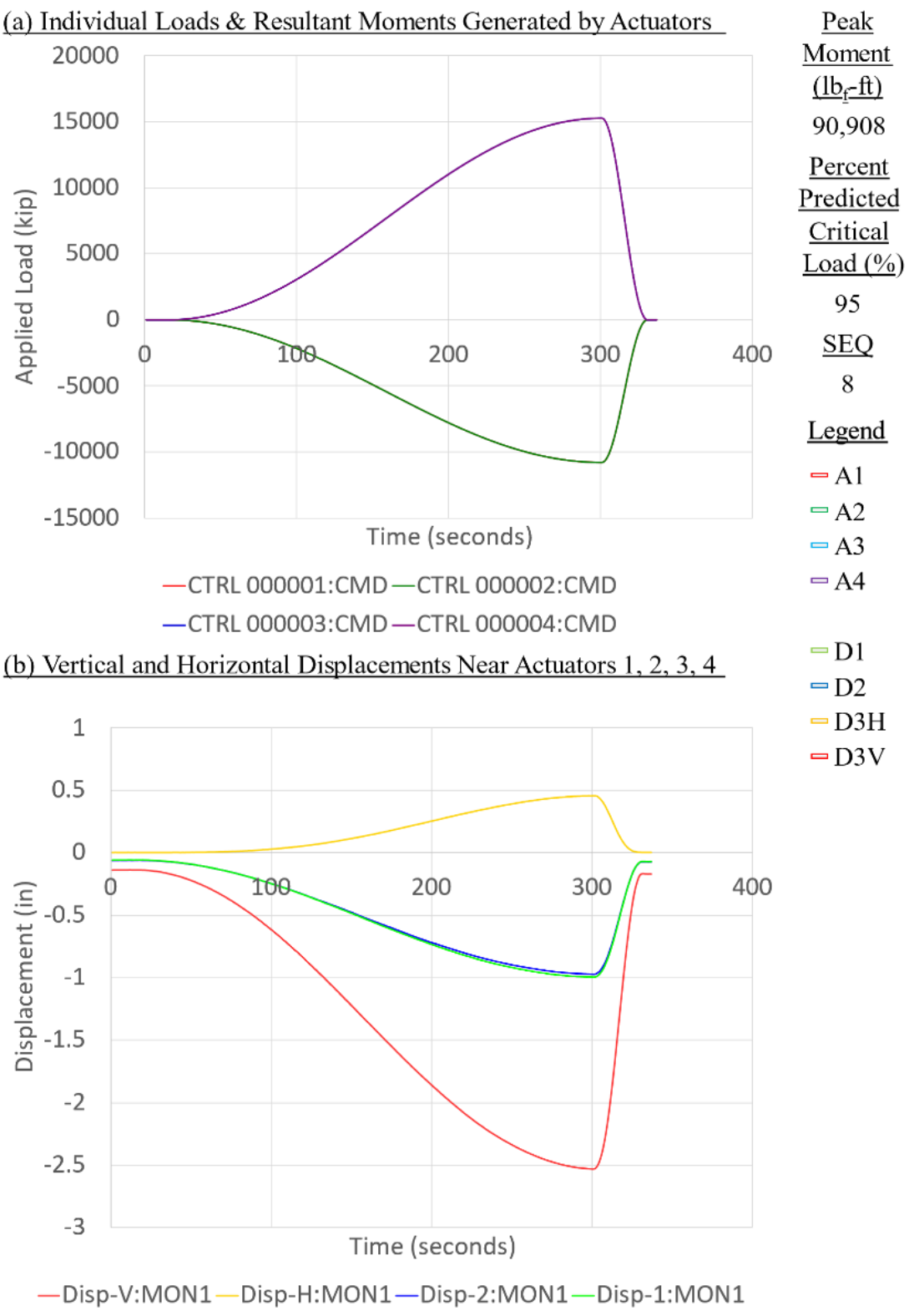

Figure C-29. Panel 7 load increment 8 (95% load level), load and displacement

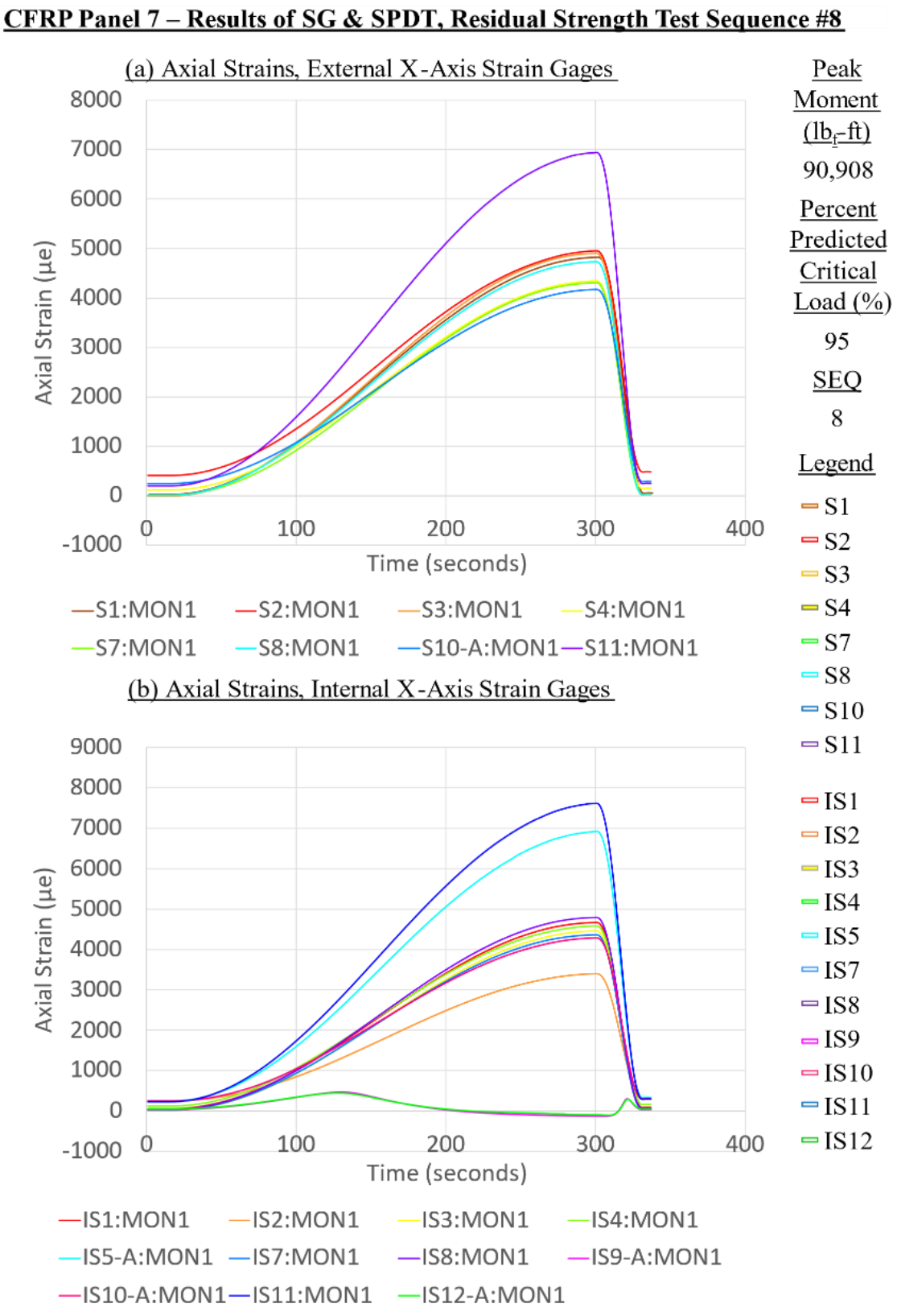

Figure C-30. Panel 7 load increment 8 (95% load level), axial strain

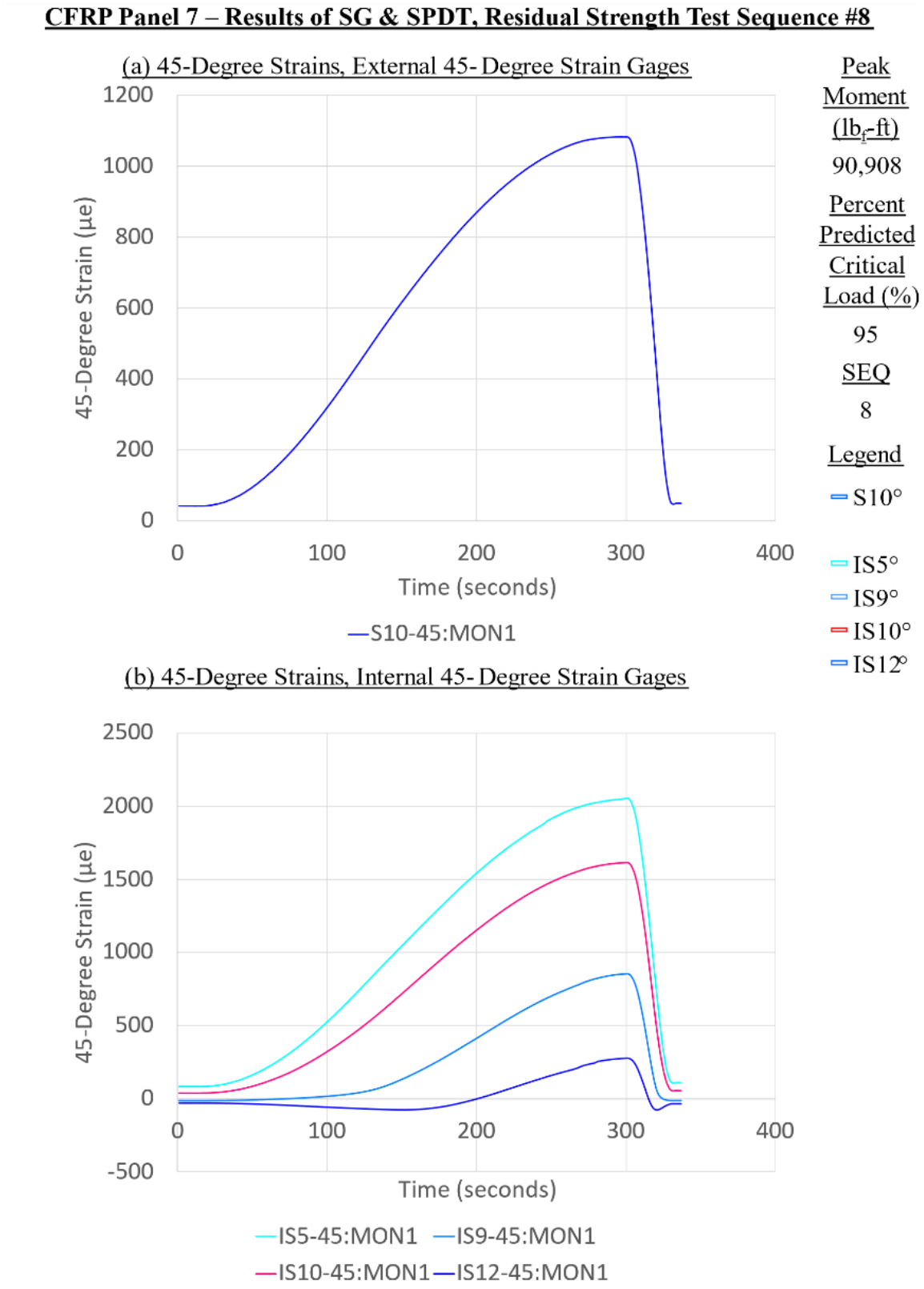

Figure C-31. Panel 7 load increment 8 (95% load level), 45-degree strain

Figure C-32. Panel 7 load increment 8 (95% load level), transverse strain

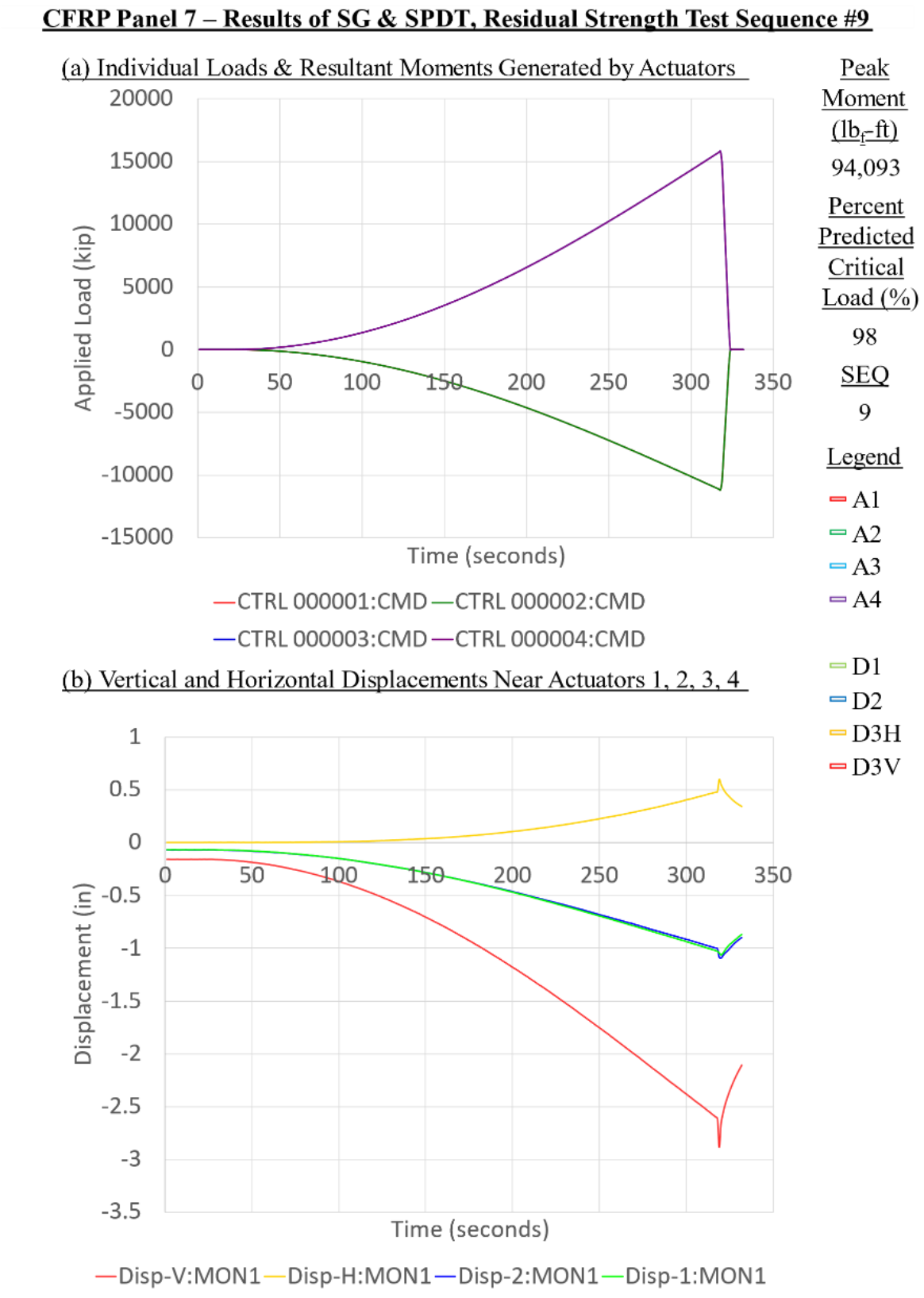

Figure C-33. Panel 7 load increment 9 (98% load level), load and displacement

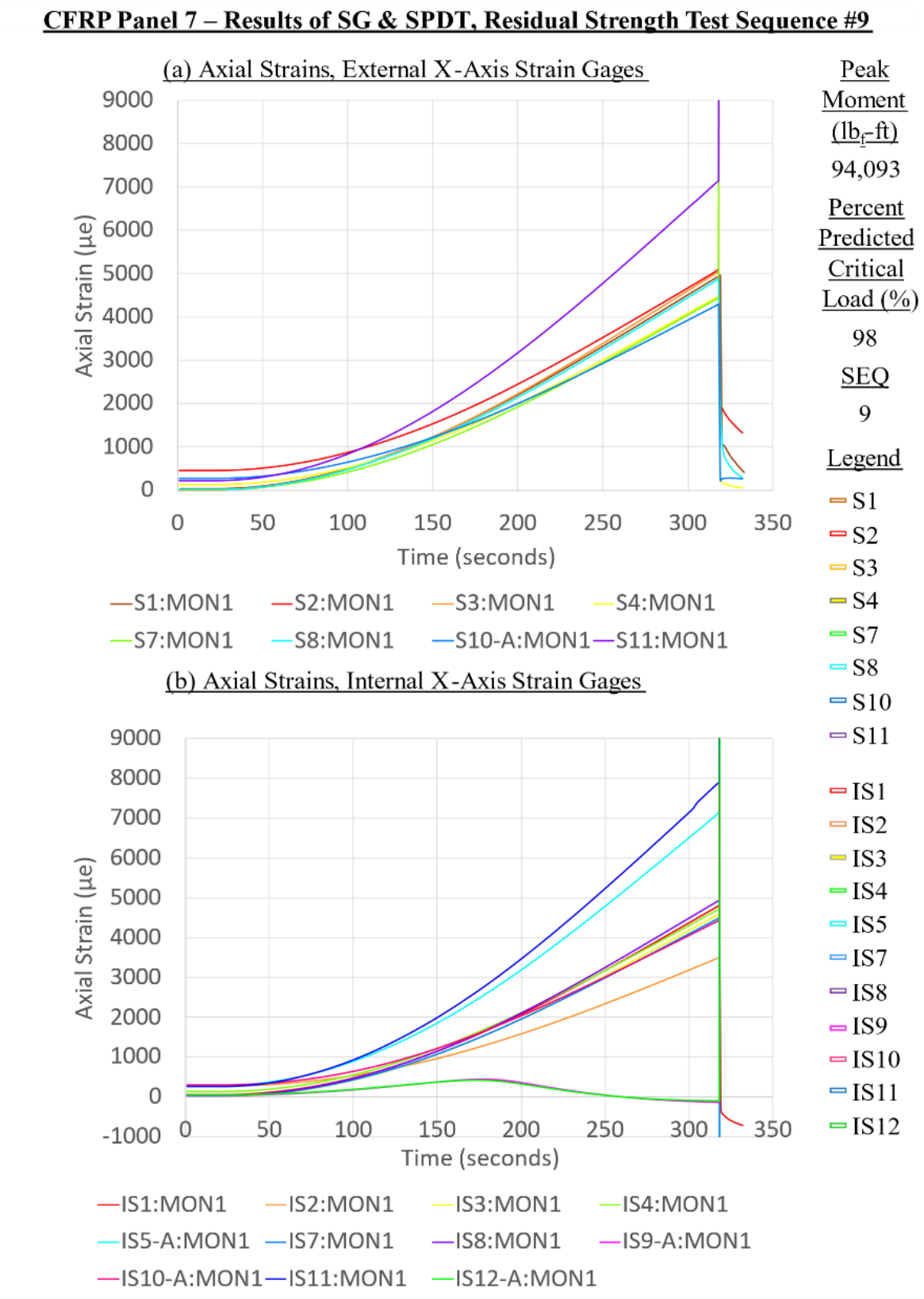

Figure C-34. Panel 7 load increment 9 (98% load level), axial strain

CFRP Panel 7 – Results of SG & SPDT, Residual Strength Test Sequence #9

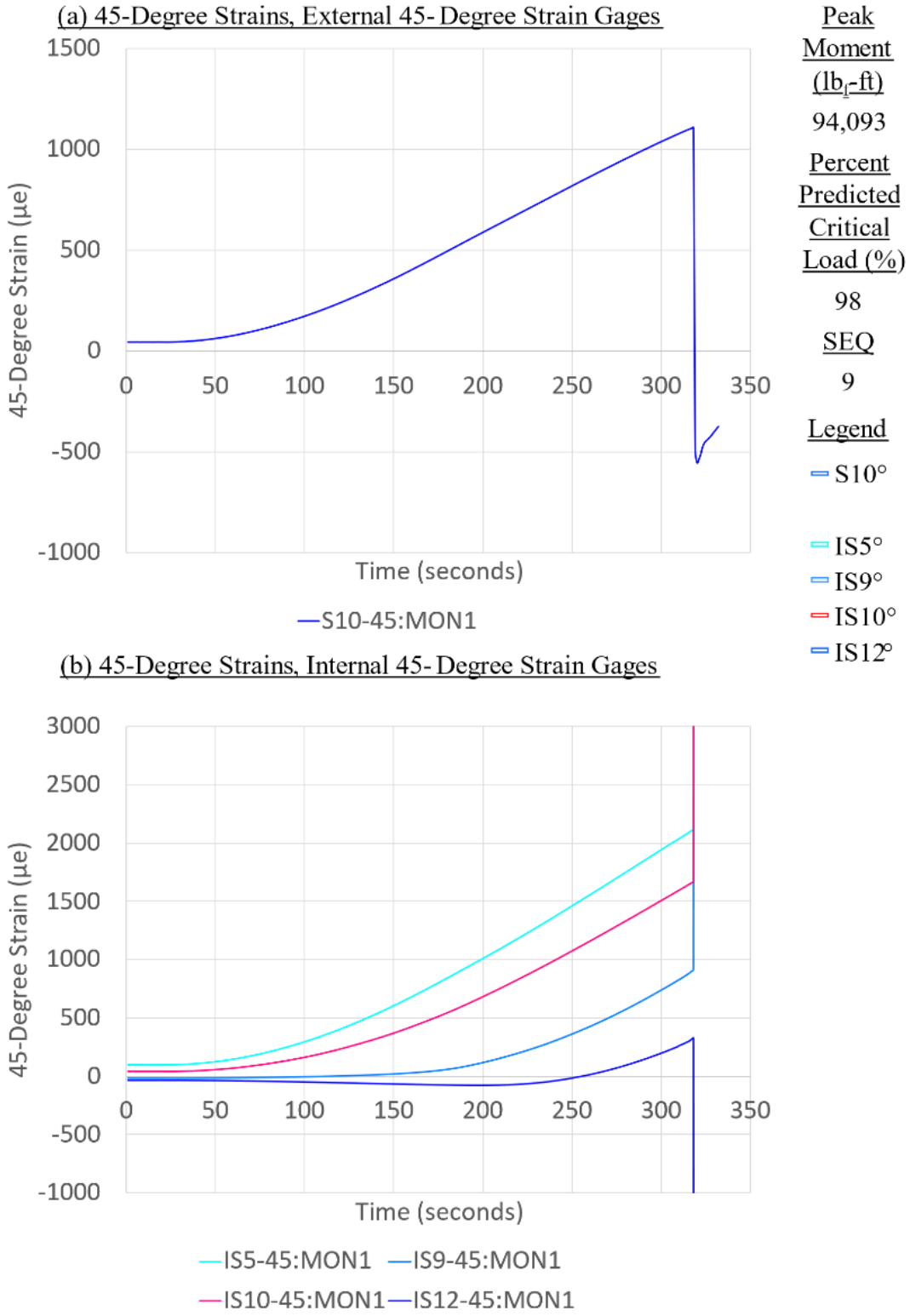

Figure C-35. Panel 7 load increment 9 (98% load level), 45-degree strain

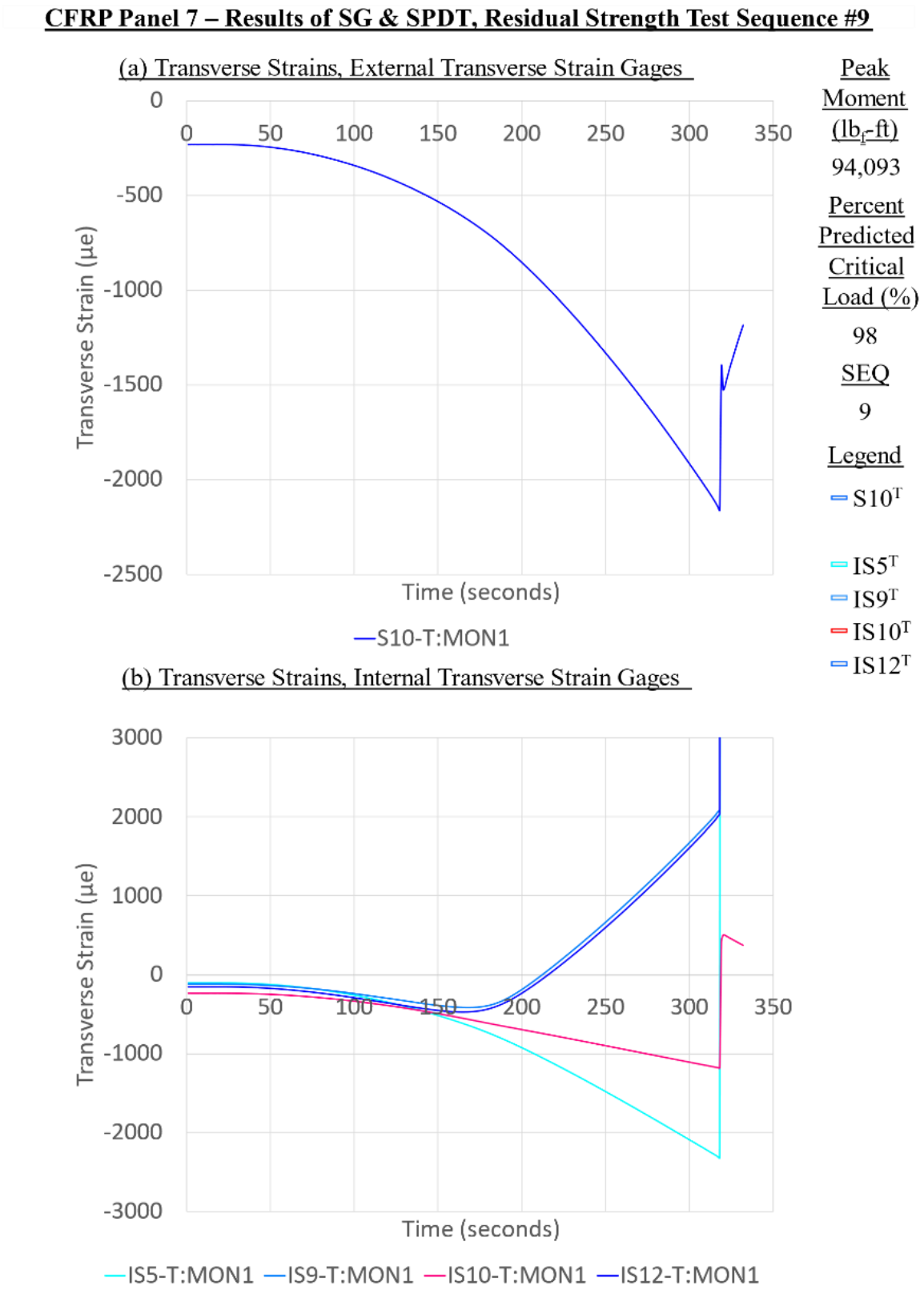

Figure C-36. Panel 7 load increment 9 (98% load level), transverse strain

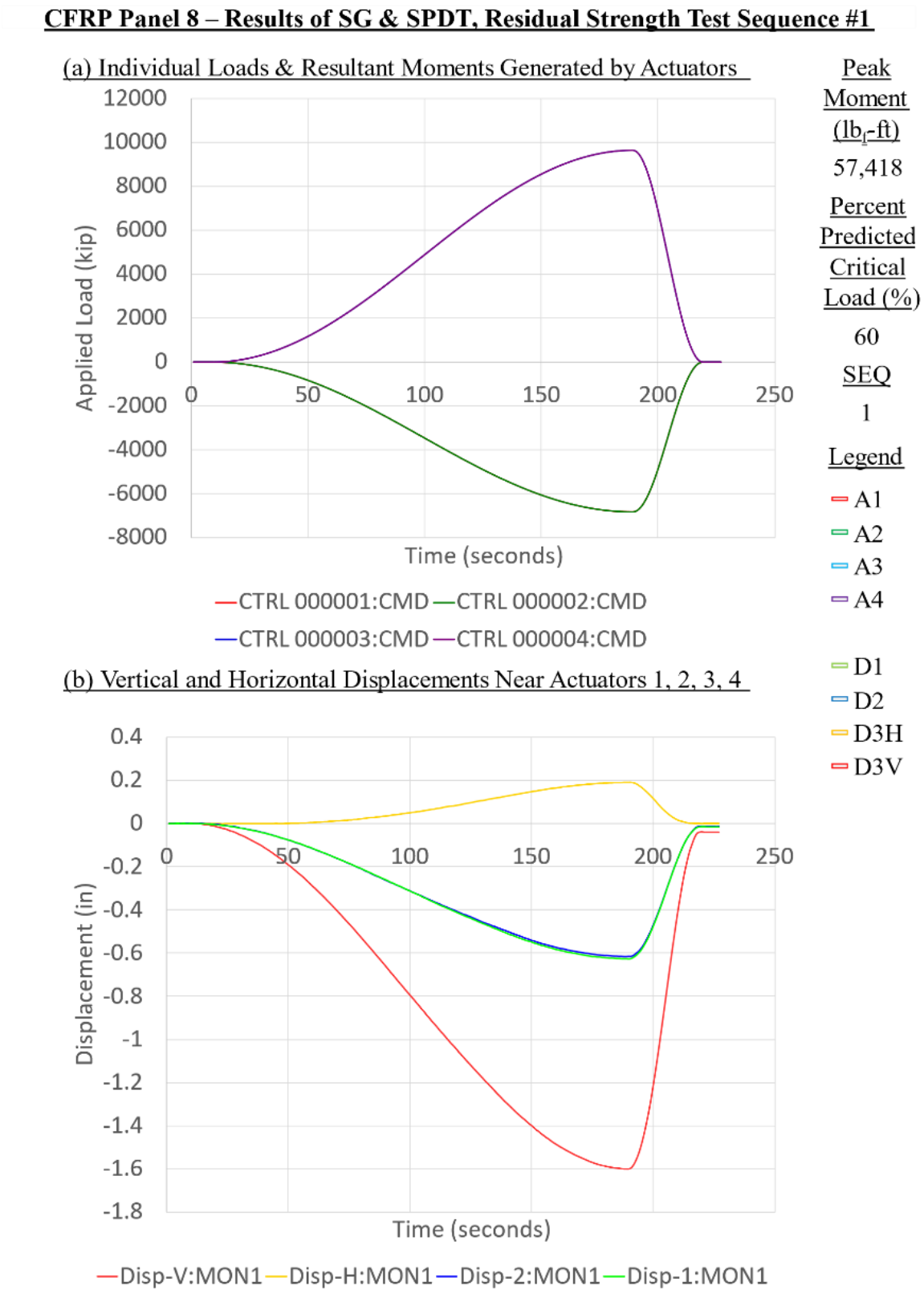

Figure C-37. Panel 8 load increment 1 (60% load level), load and displacement

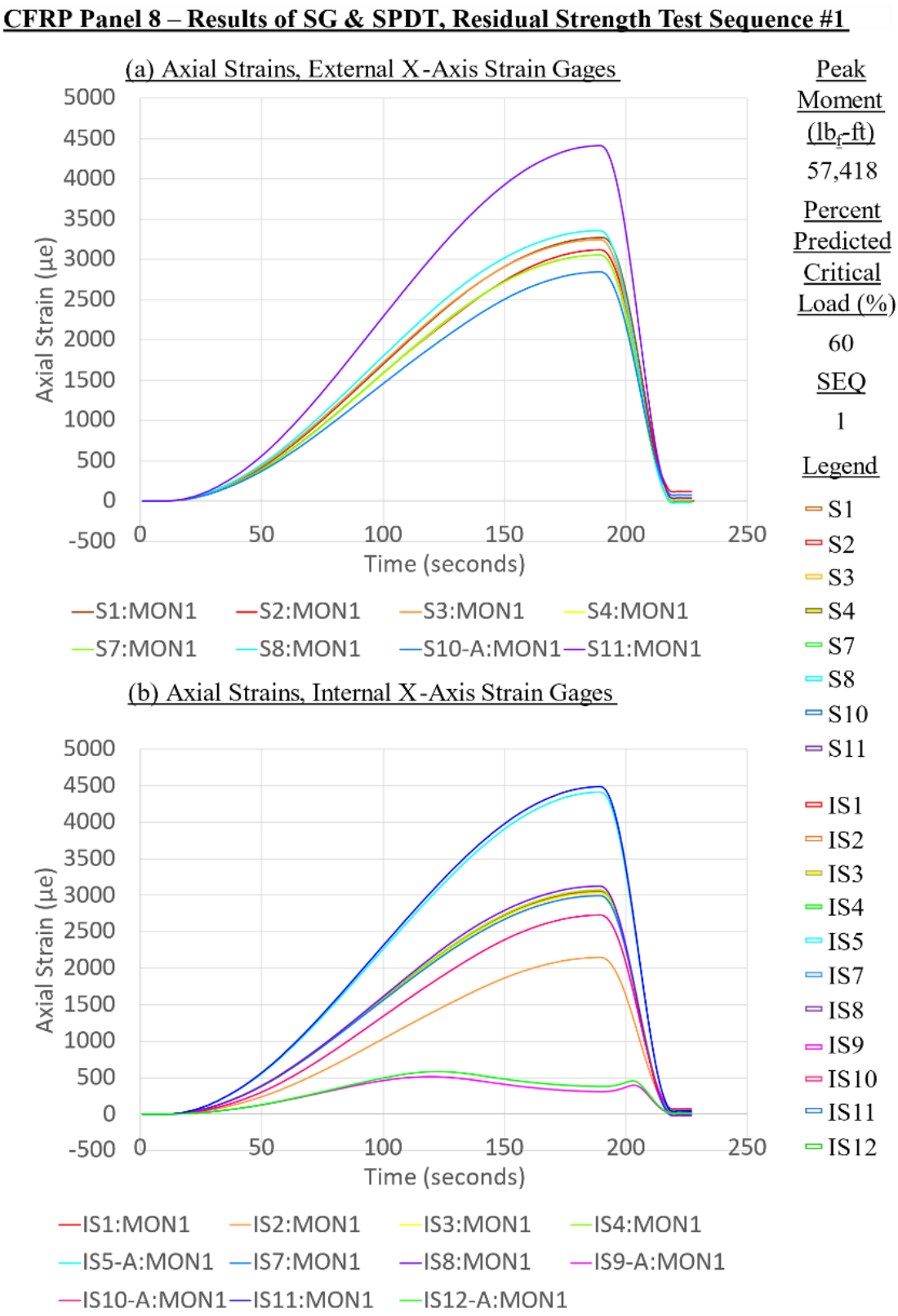

Figure C-38. Panel 8 load increment 1 (60% load level), axial strain

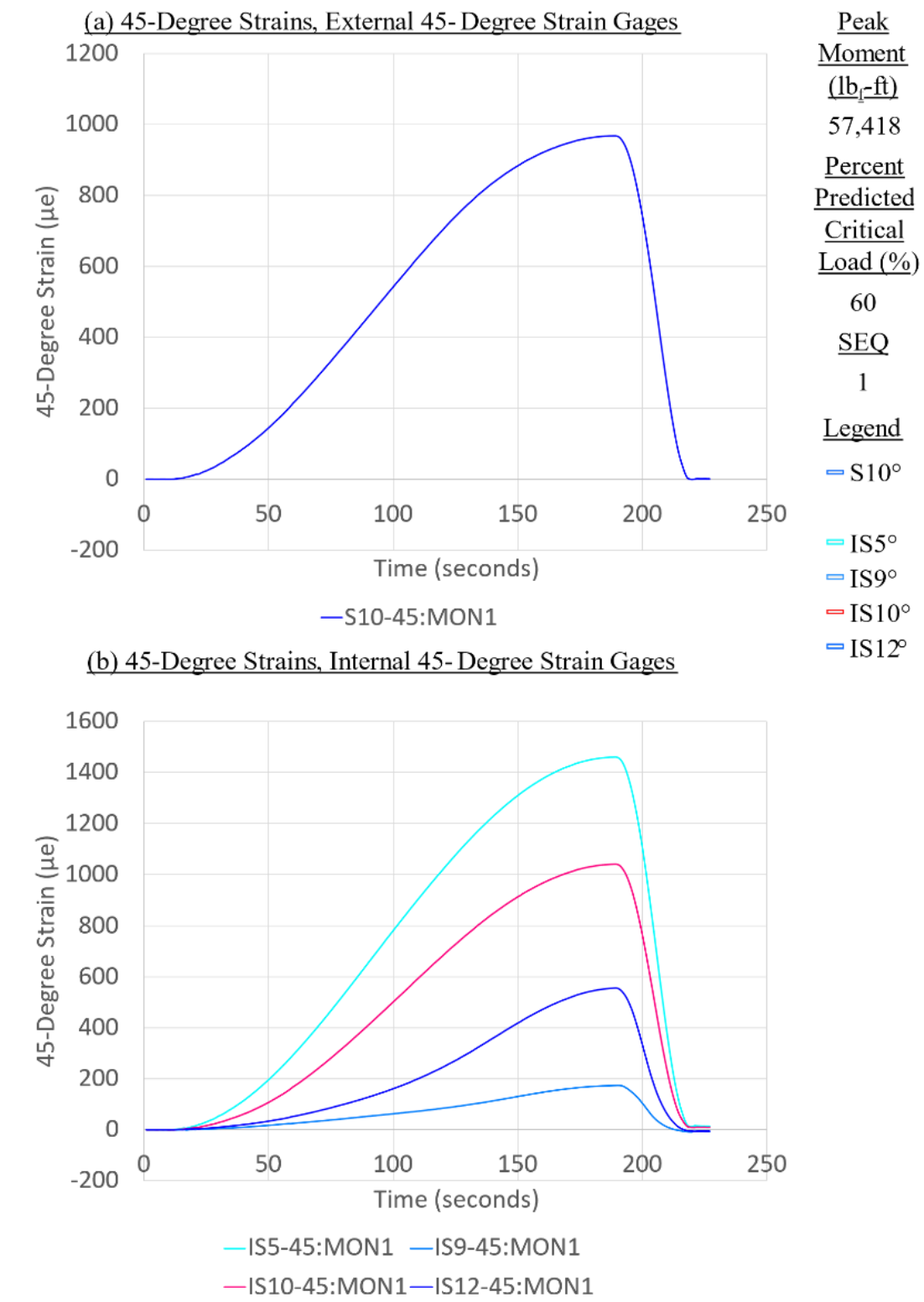

Figure C-39. Panel 8 load increment 1 (60% load level), 45-degree strain

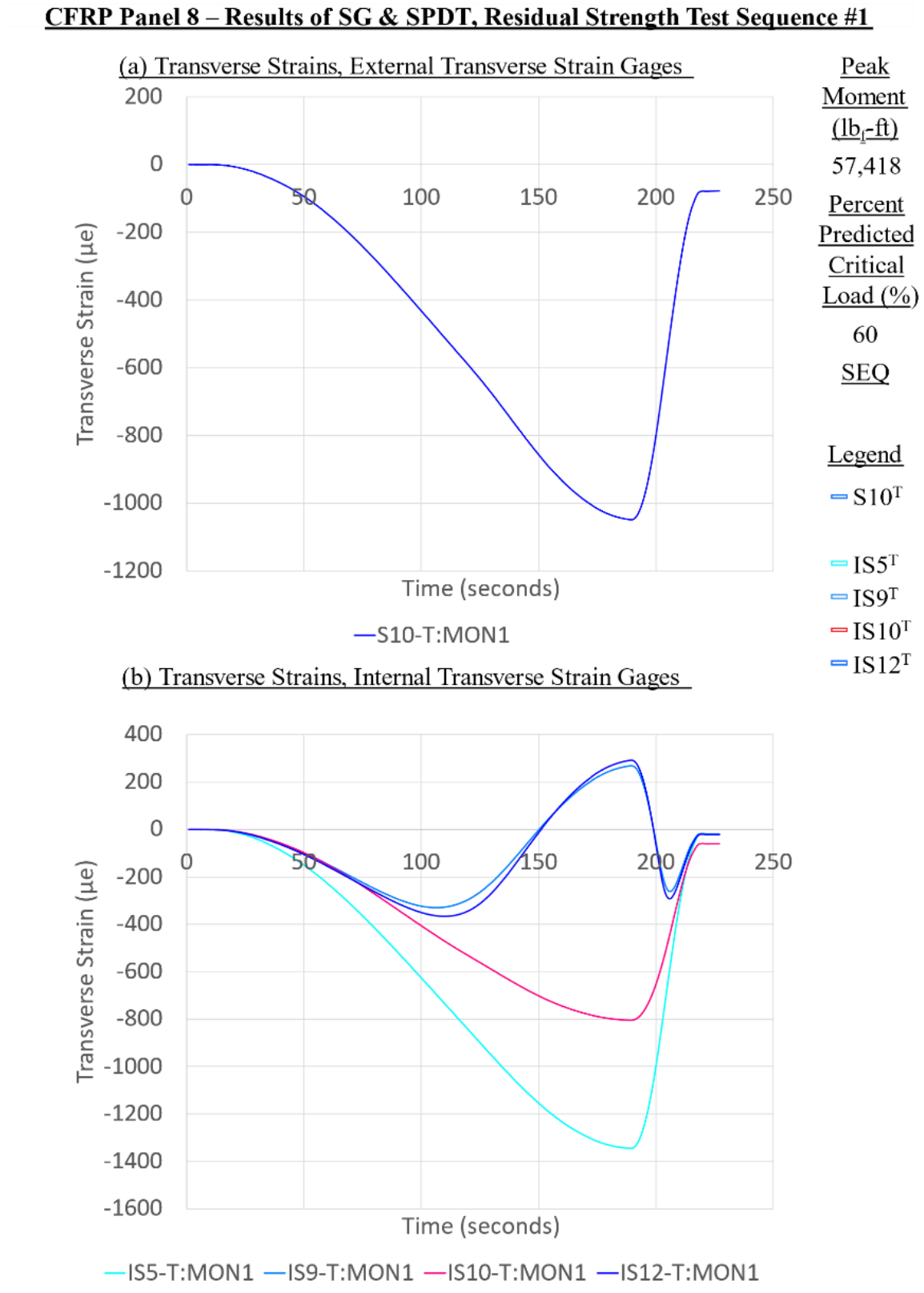

Figure C-40. Panel 8 load increment 1 (60% load level), transverse strain

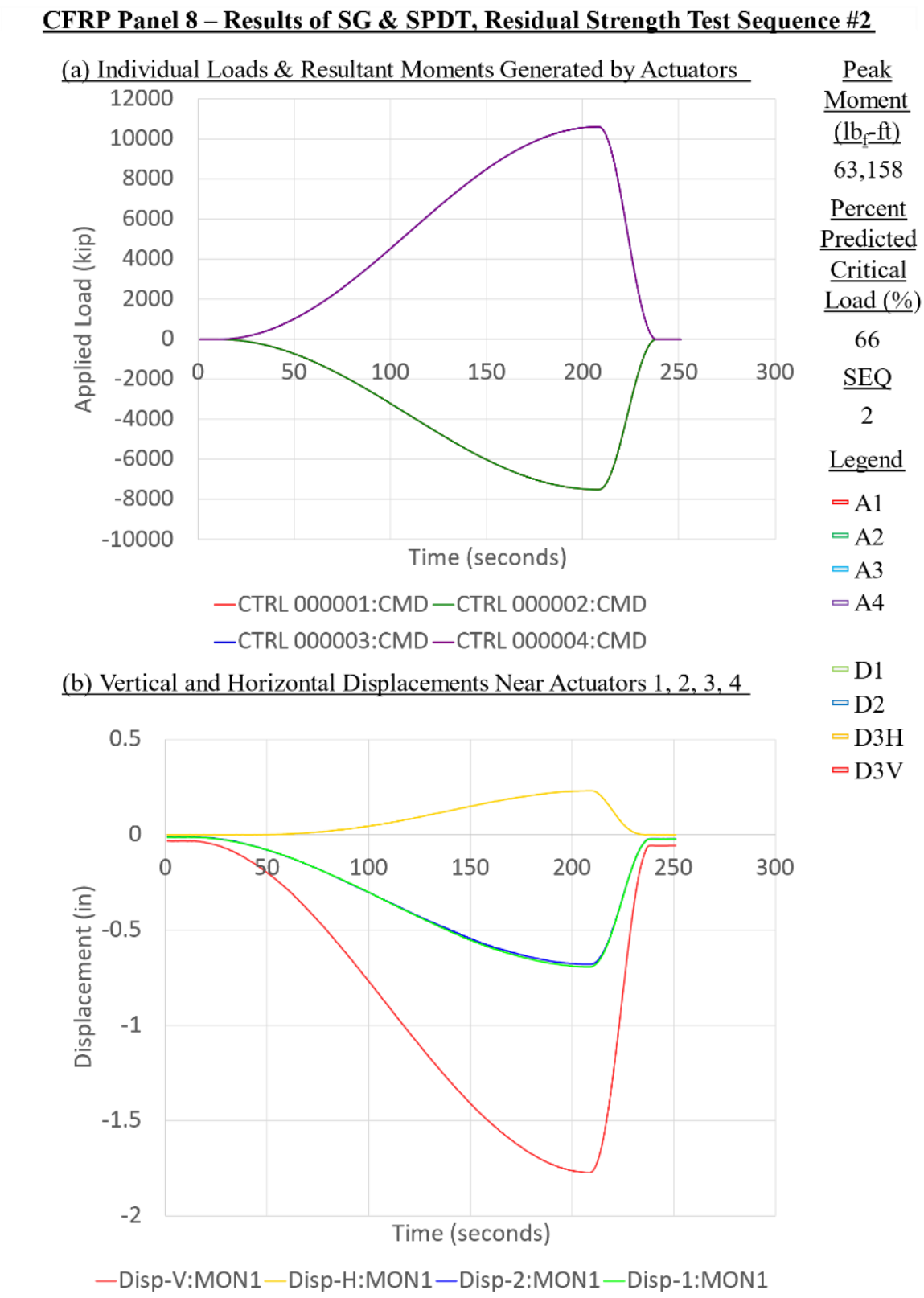

Figure C-41. Panel 8 load increment 2 (66% load level), load and displacement

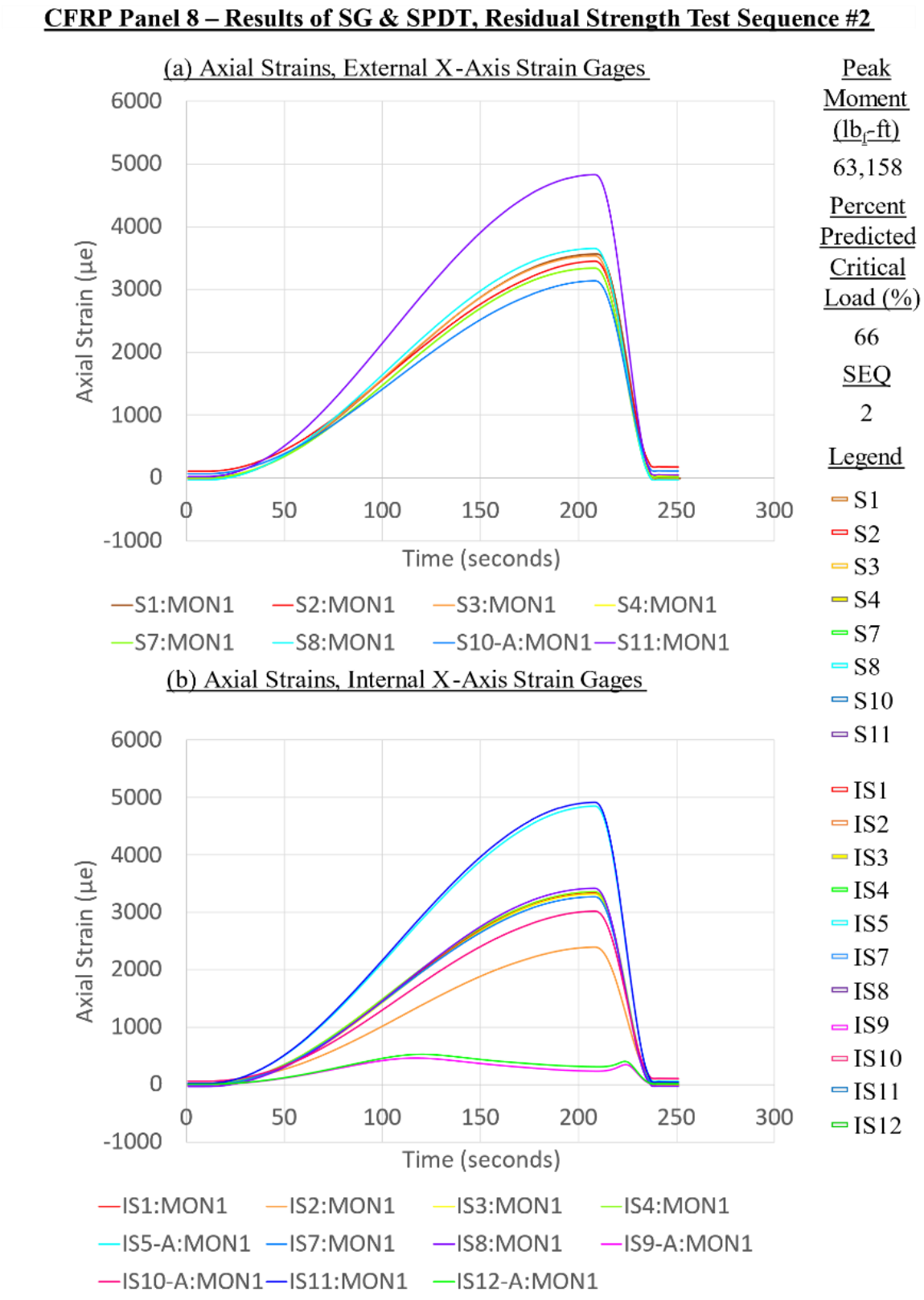

Figure C-42. Panel 8 load increment 2 (66% load level), axial strain

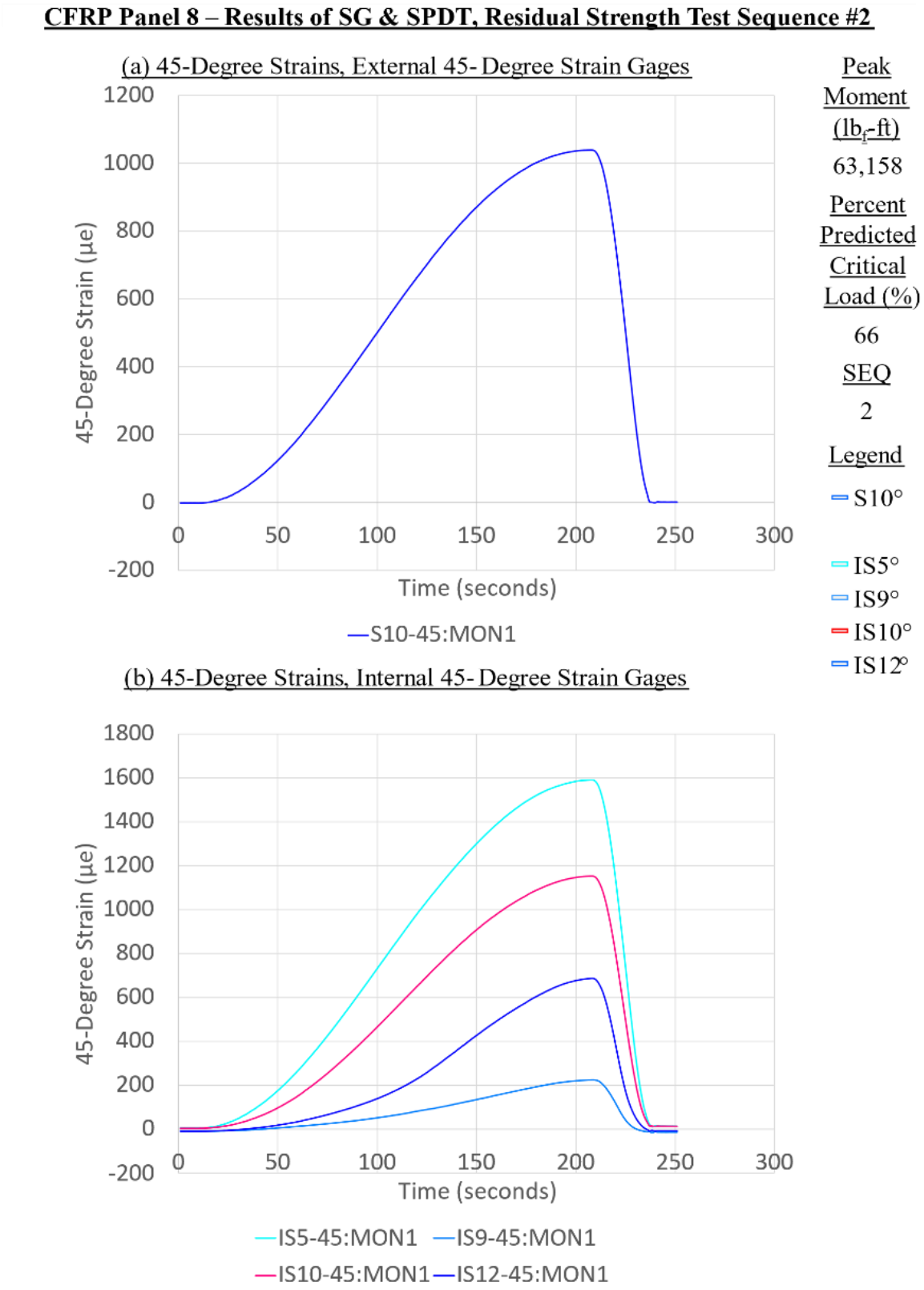

Figure C-43. Panel 8 load increment 2 (66% load level), 45-degree strain

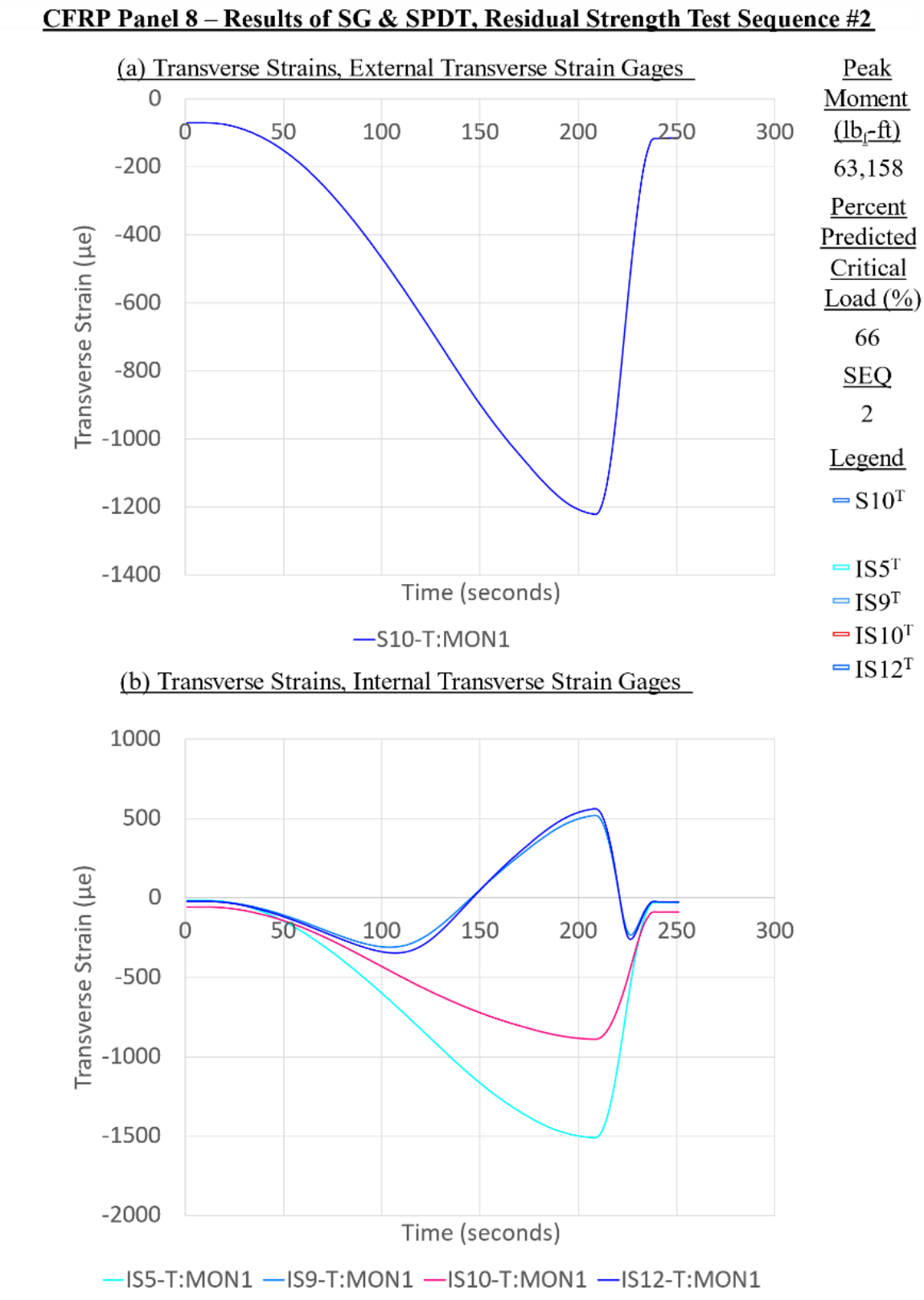

Figure C-44. Panel 8 load increment 2 (66% load level), transverse strain

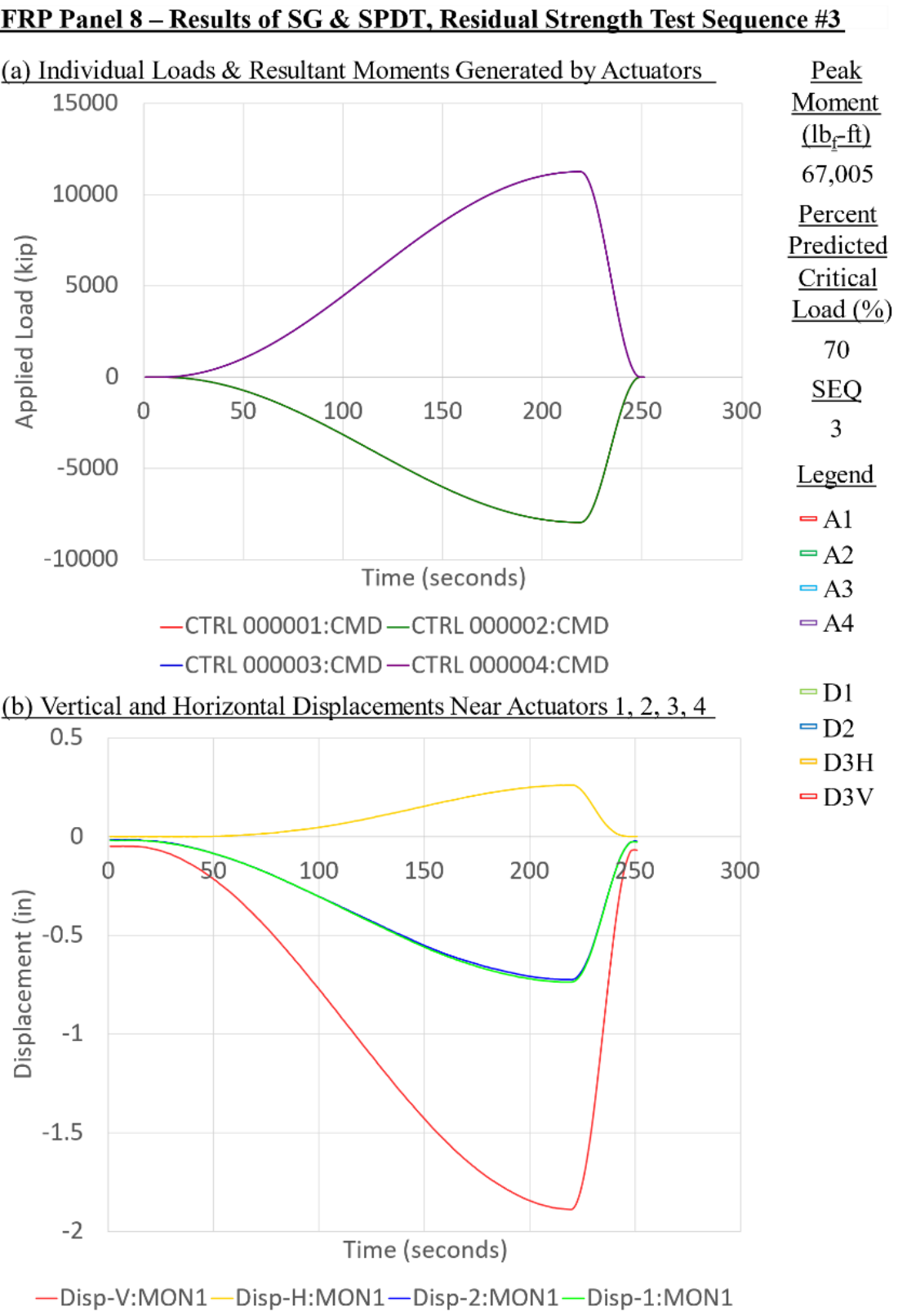

Figure C-45. Panel 8 load increment 3 (70% load level), load and displacement

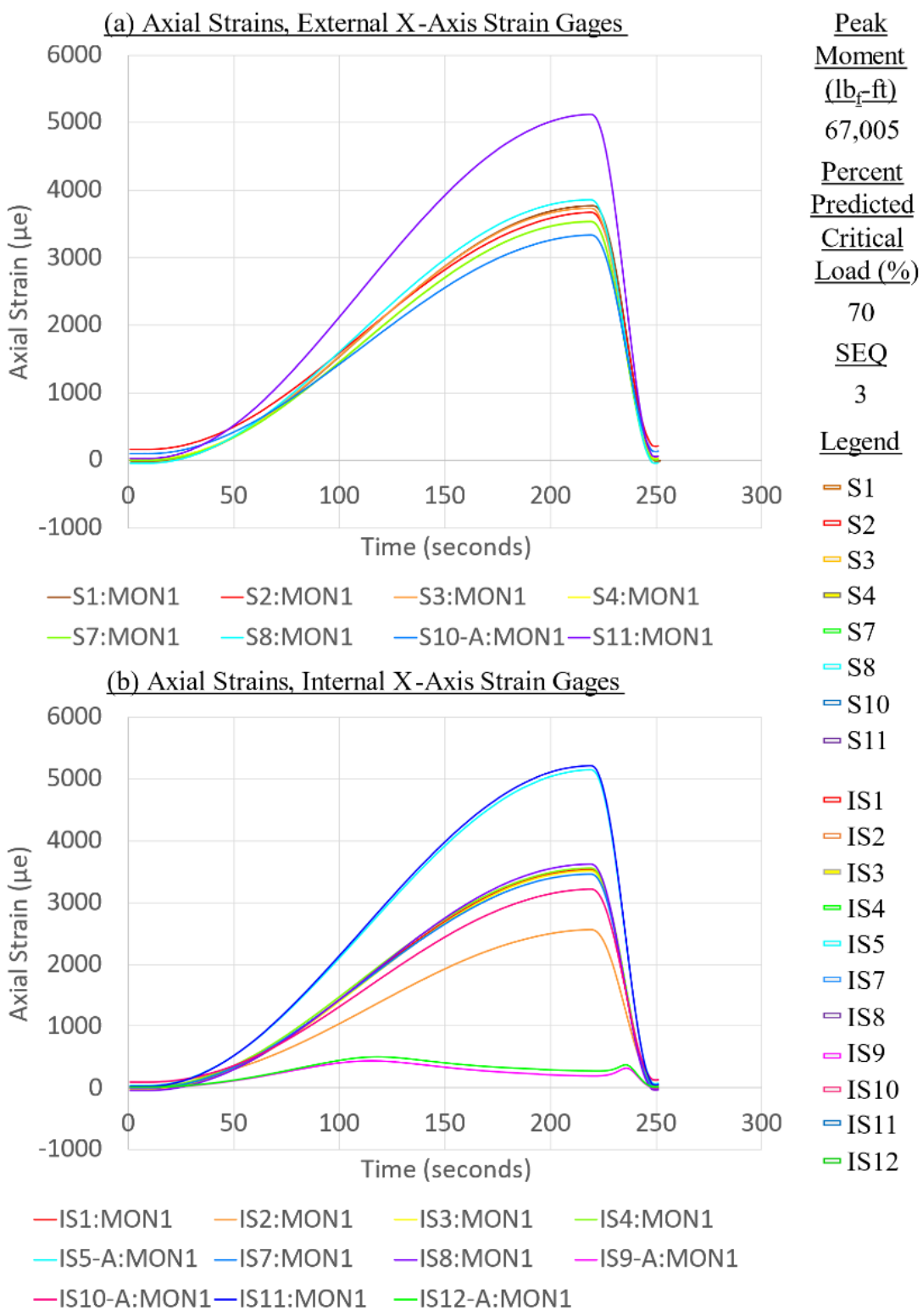

Figure C-46. Panel 8 load increment 3 (70% load level), axial strain

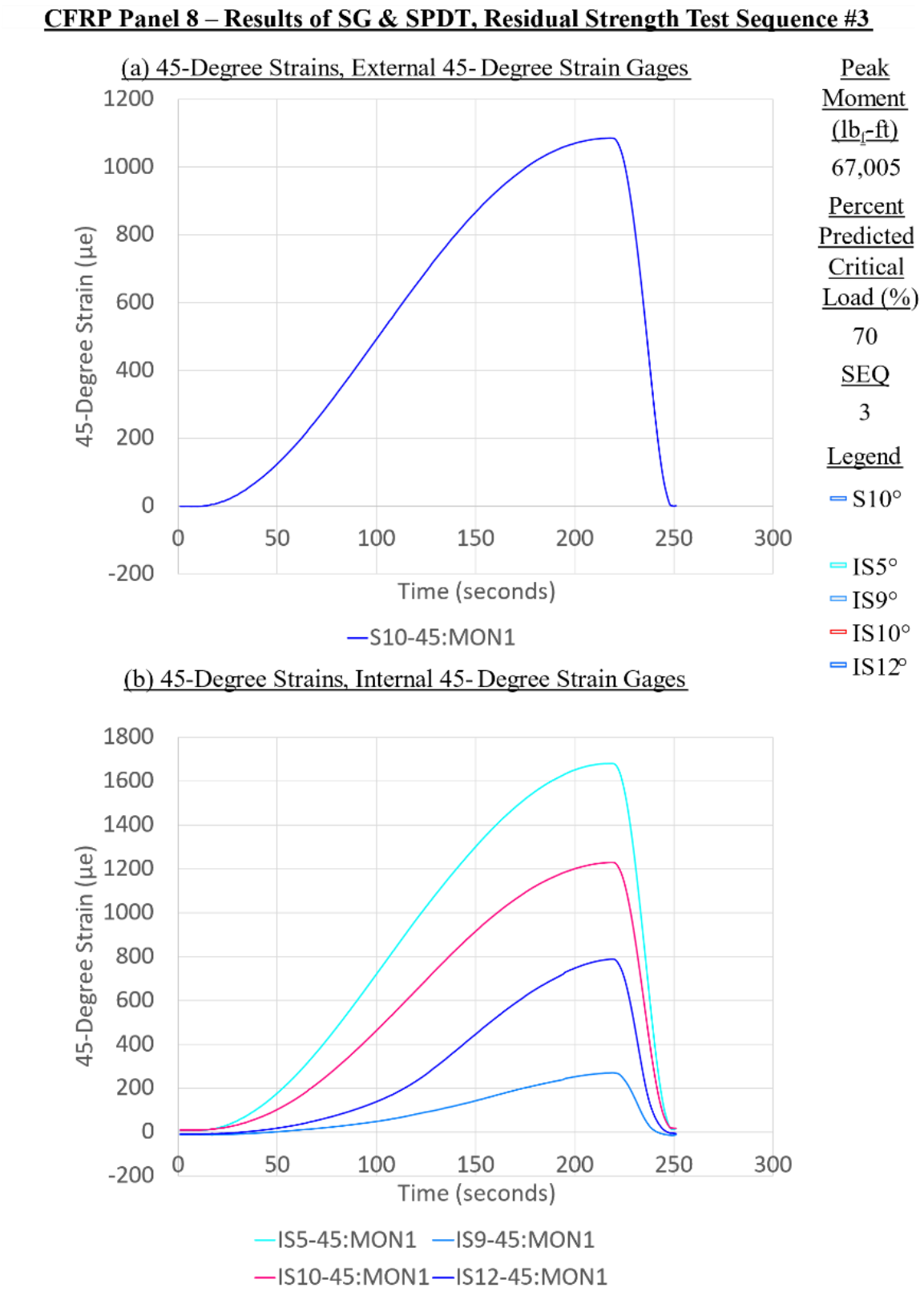

Figure C-47. Panel 8 load increment 3 (70% load level), 45-degree strain

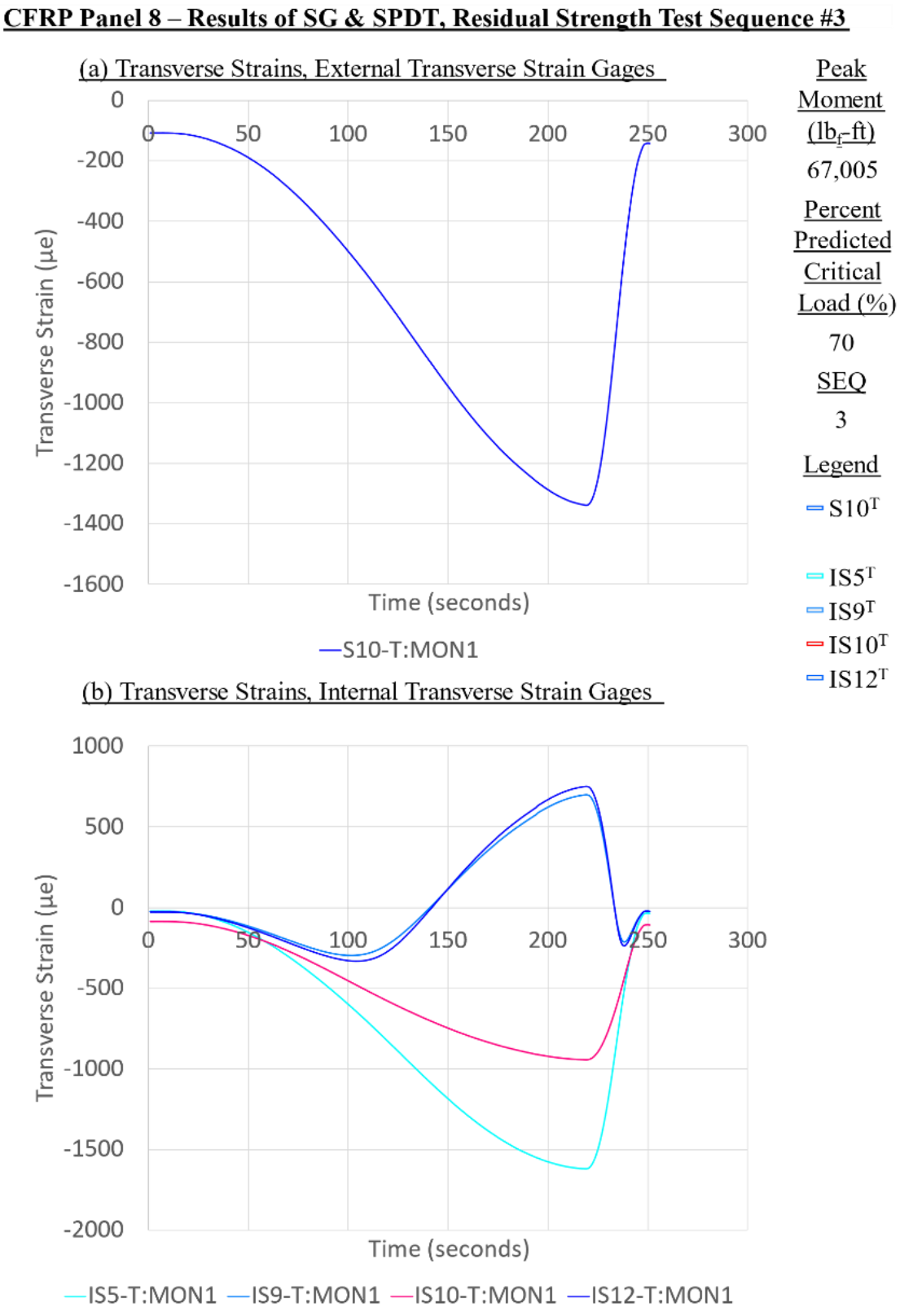

Figure C-48. Panel 8 load increment 3 (70% load level), transverse strain

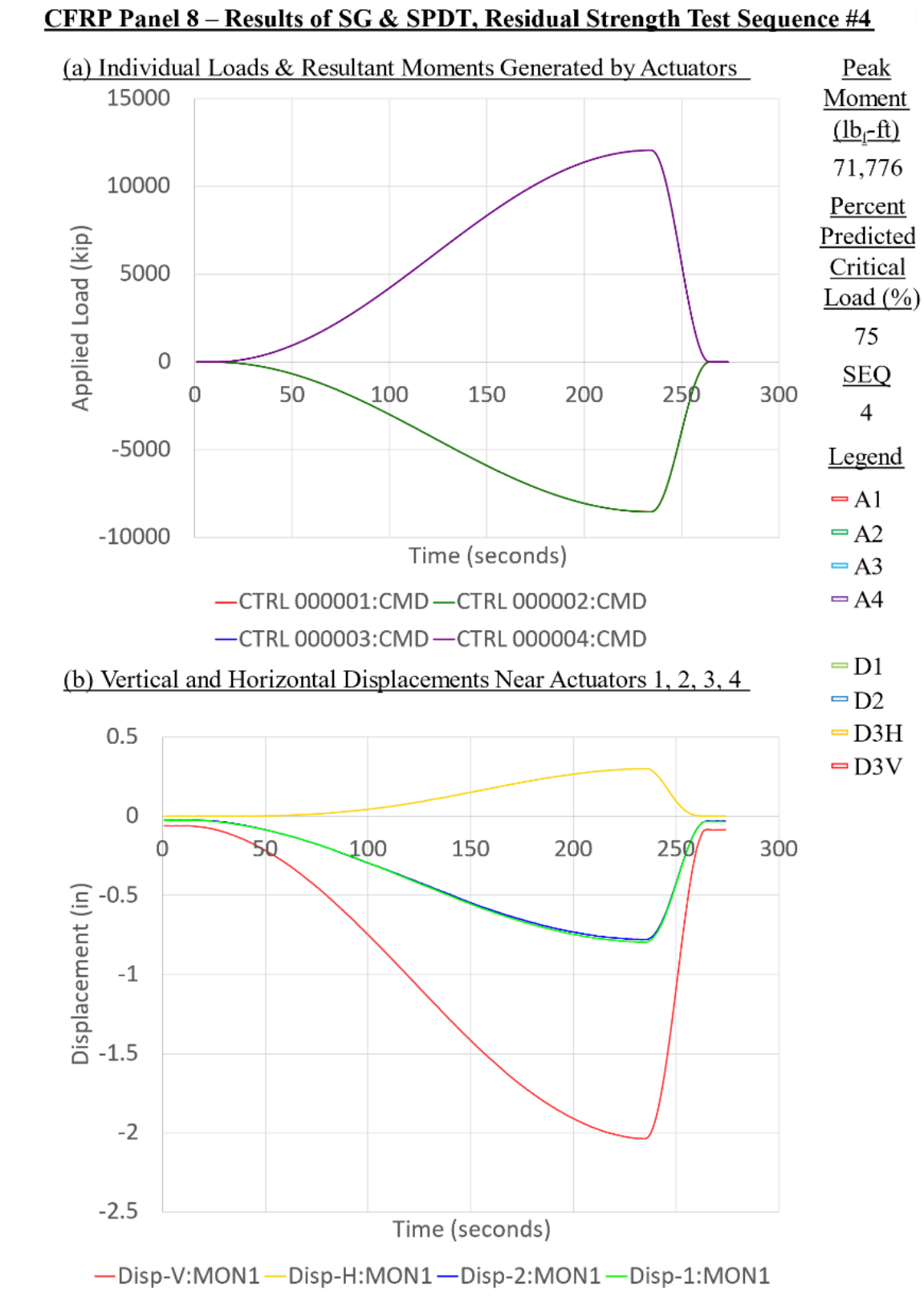

Figure C-49. Panel 8 load increment 4 (75% load level), load and displacement

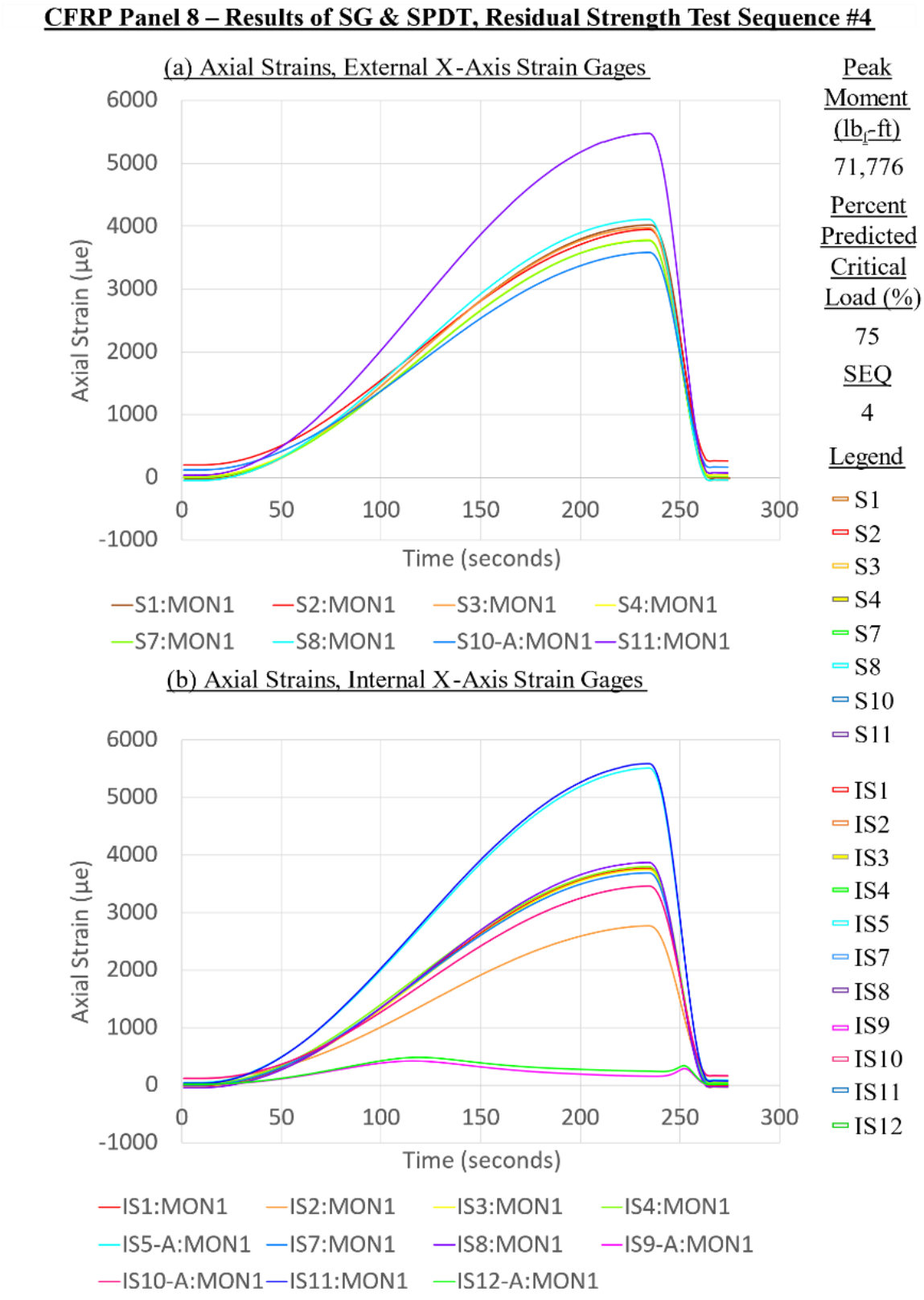

Figure C-50. Panel 8 load increment 4 (75% load level), axial strain

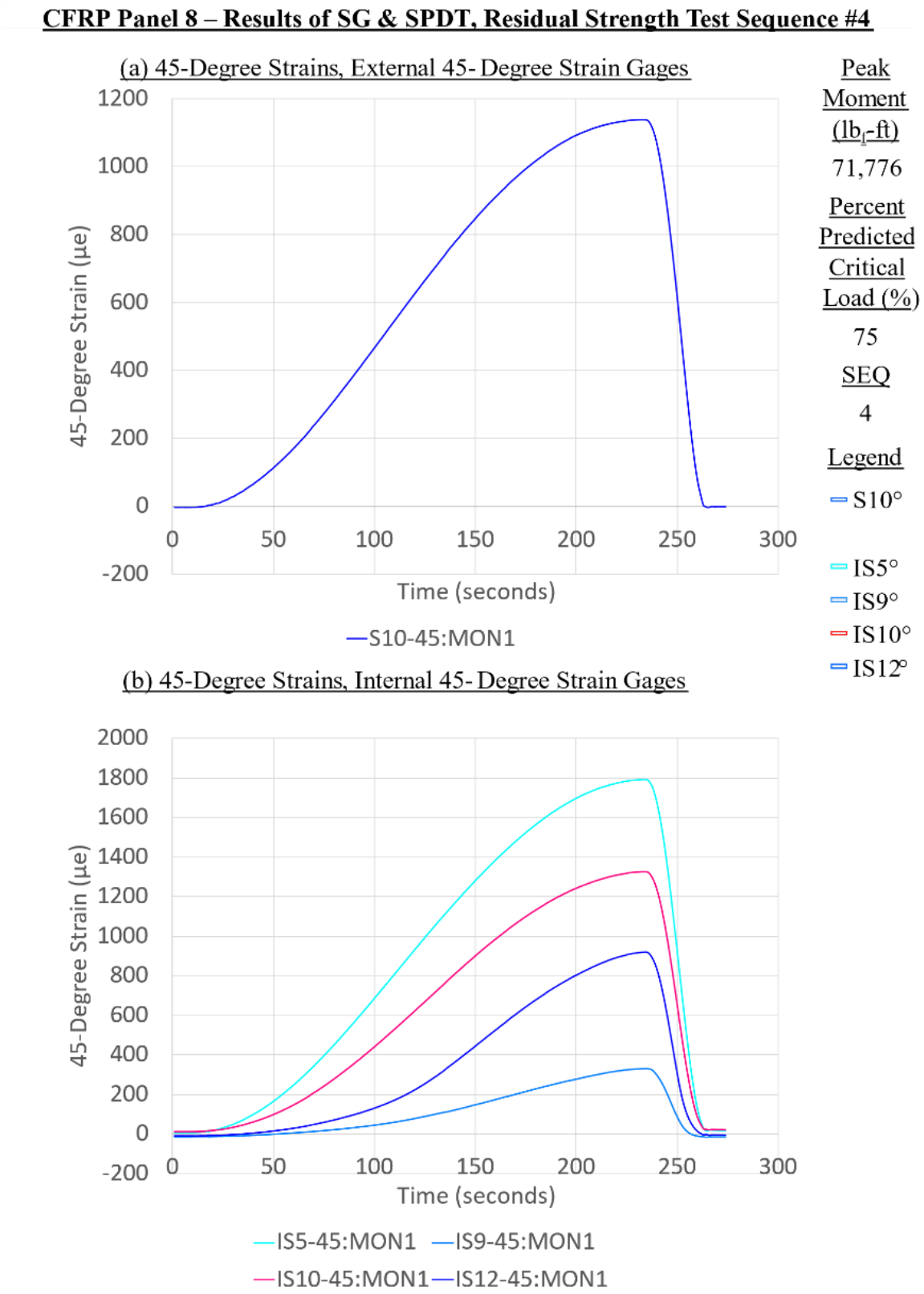

Figure C-51. Panel 8 load increment 4 (75% load level), 45-degree strain

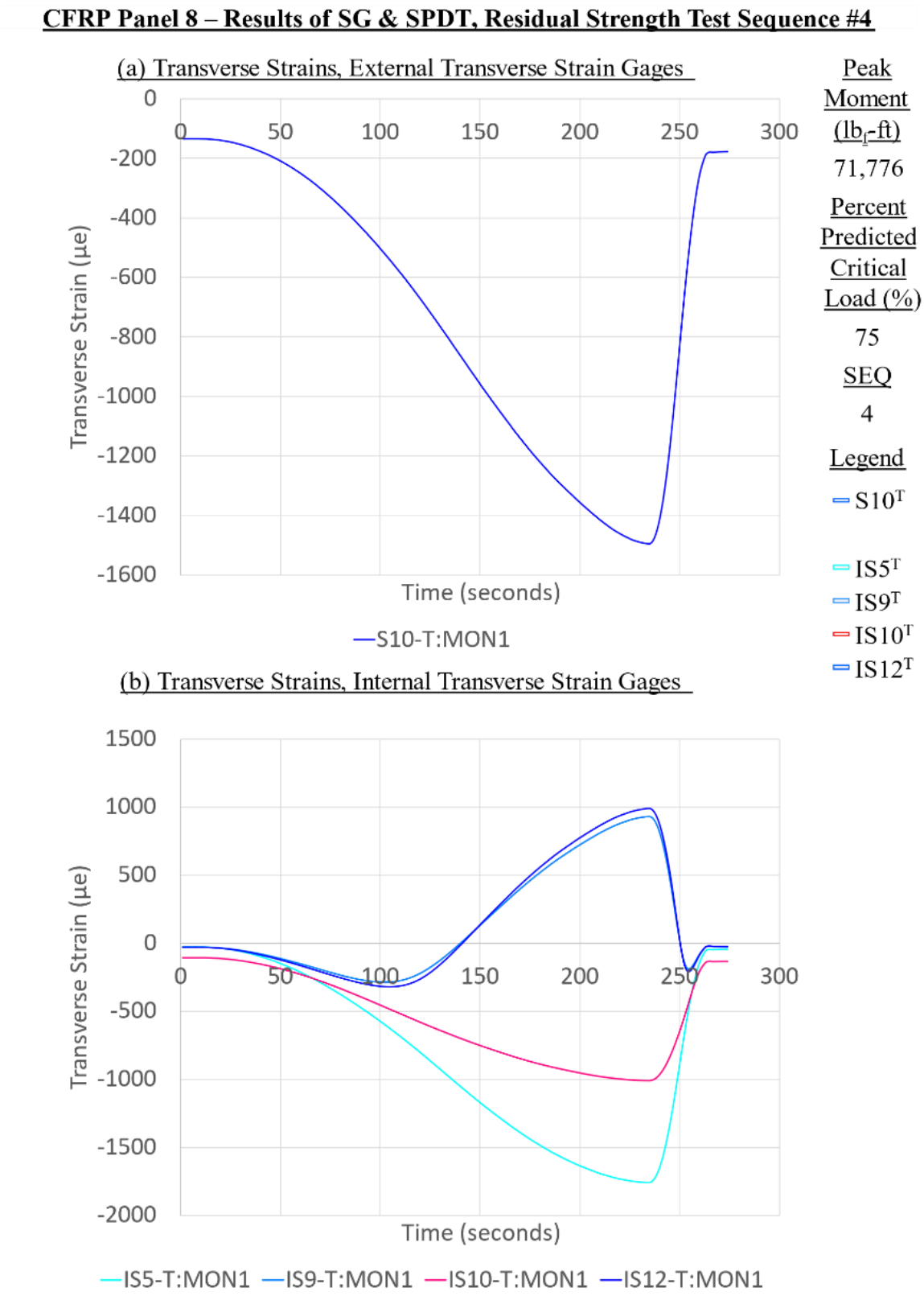

Figure C-52. Panel 8 load increment 4 (75% load level), transverse strain

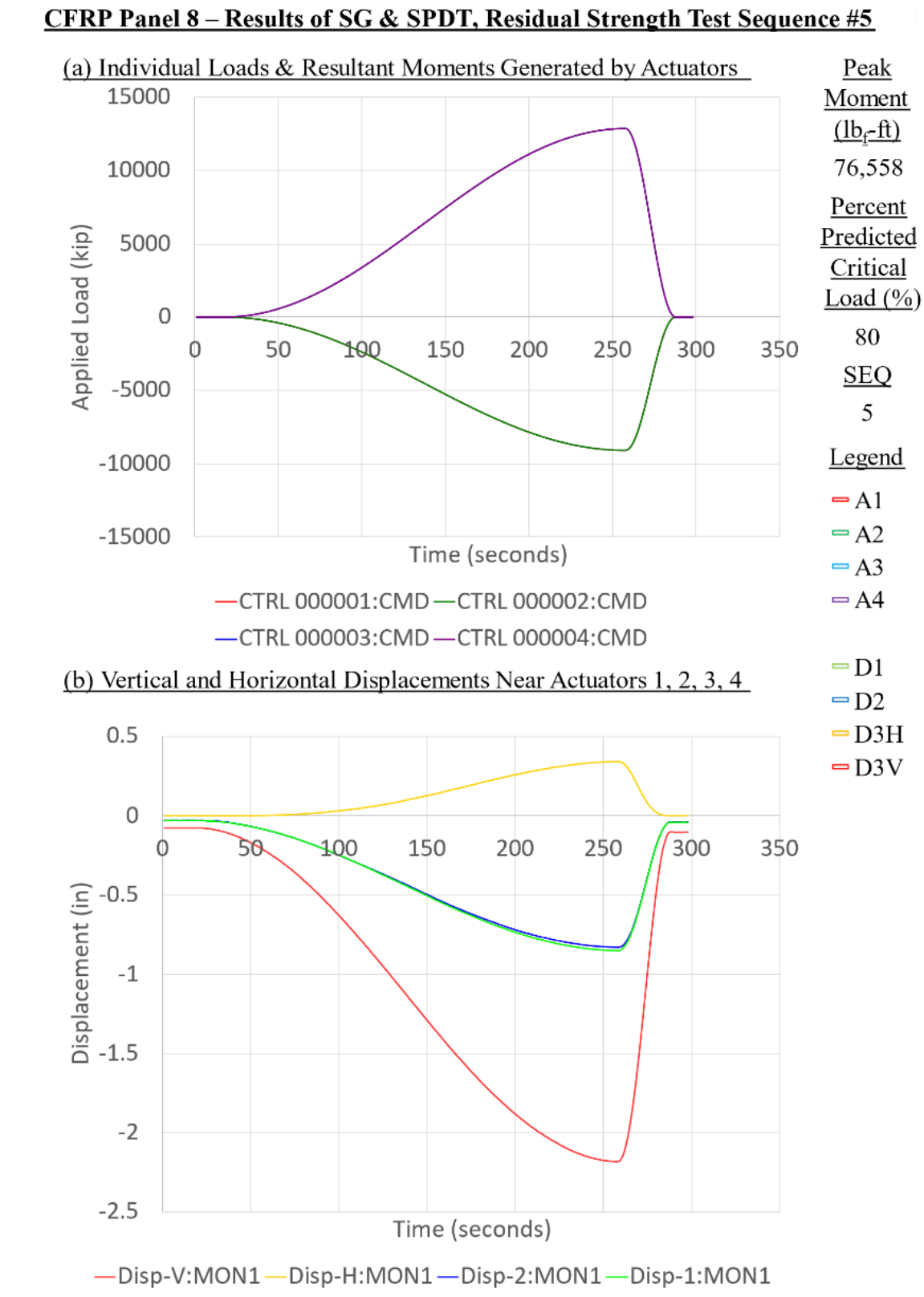

Figure C-53. Panel 8 load increment 5 (80% load level), load and displacement

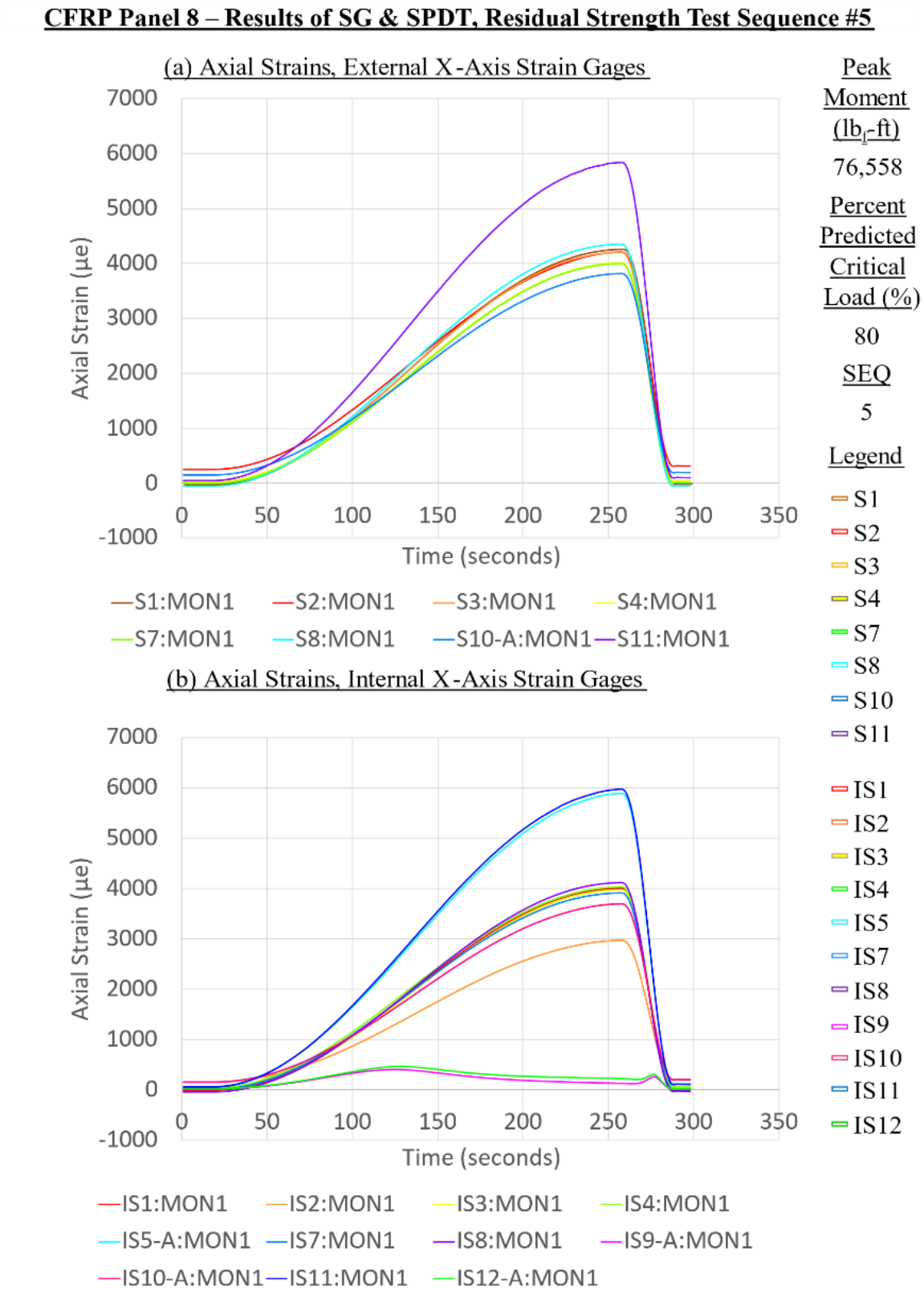

Figure C-54. Panel 8 load increment 5 (80% load level), axial strain

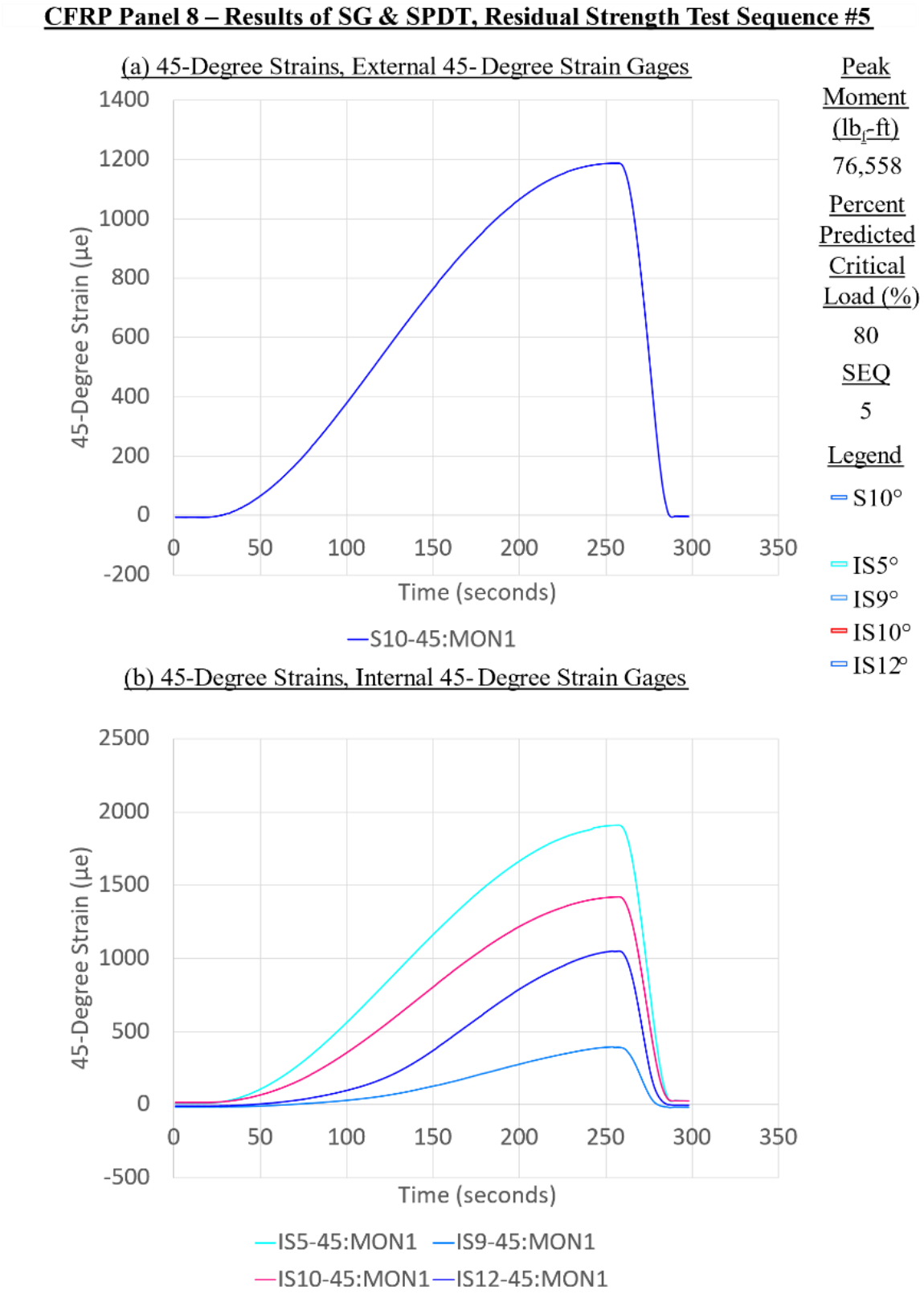

Figure C-55. Panel 8 load increment 5 (80% load level), 45-degree strain

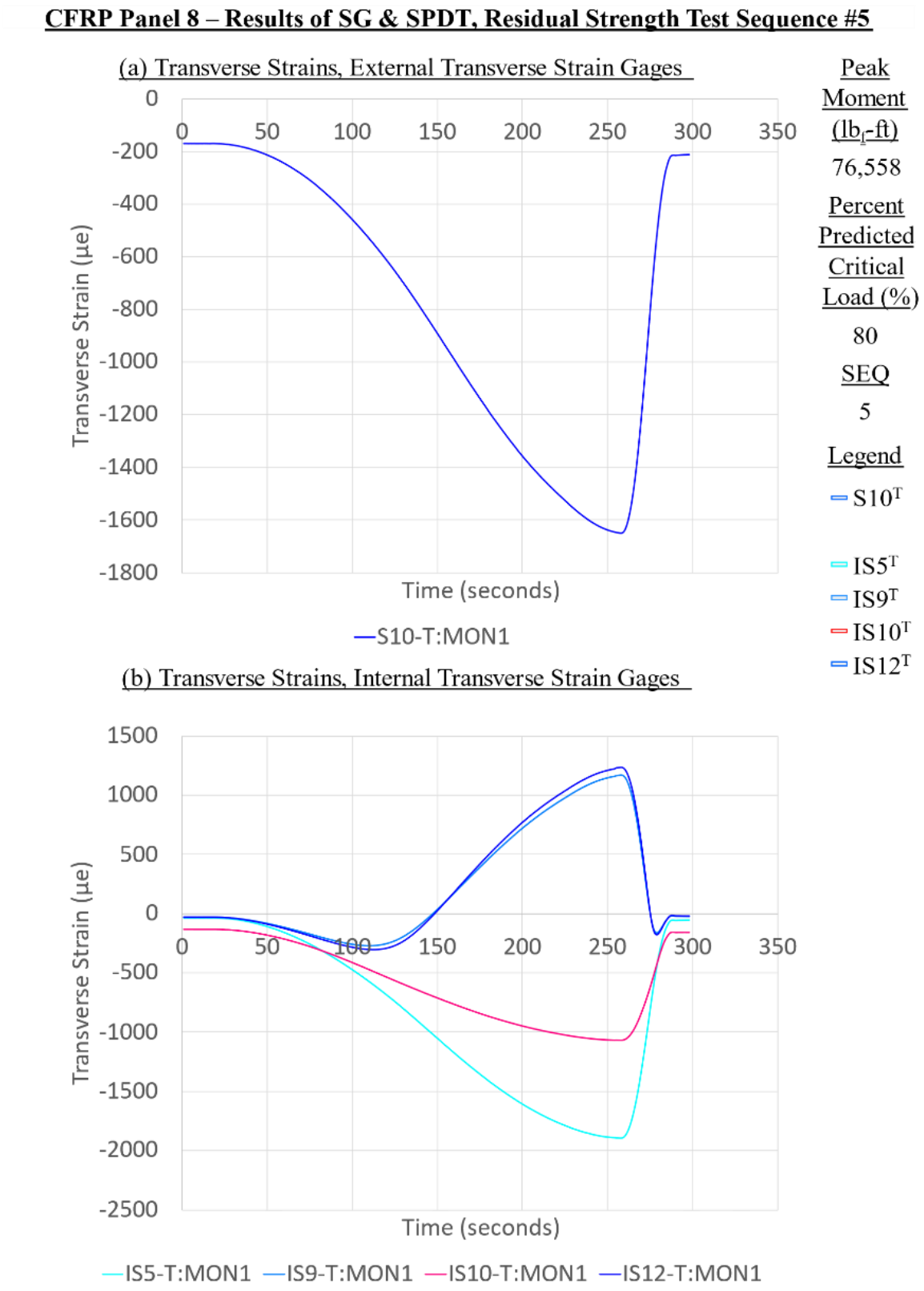

Figure C-56. Panel 8 load increment 5 (80% load level), transverse strain

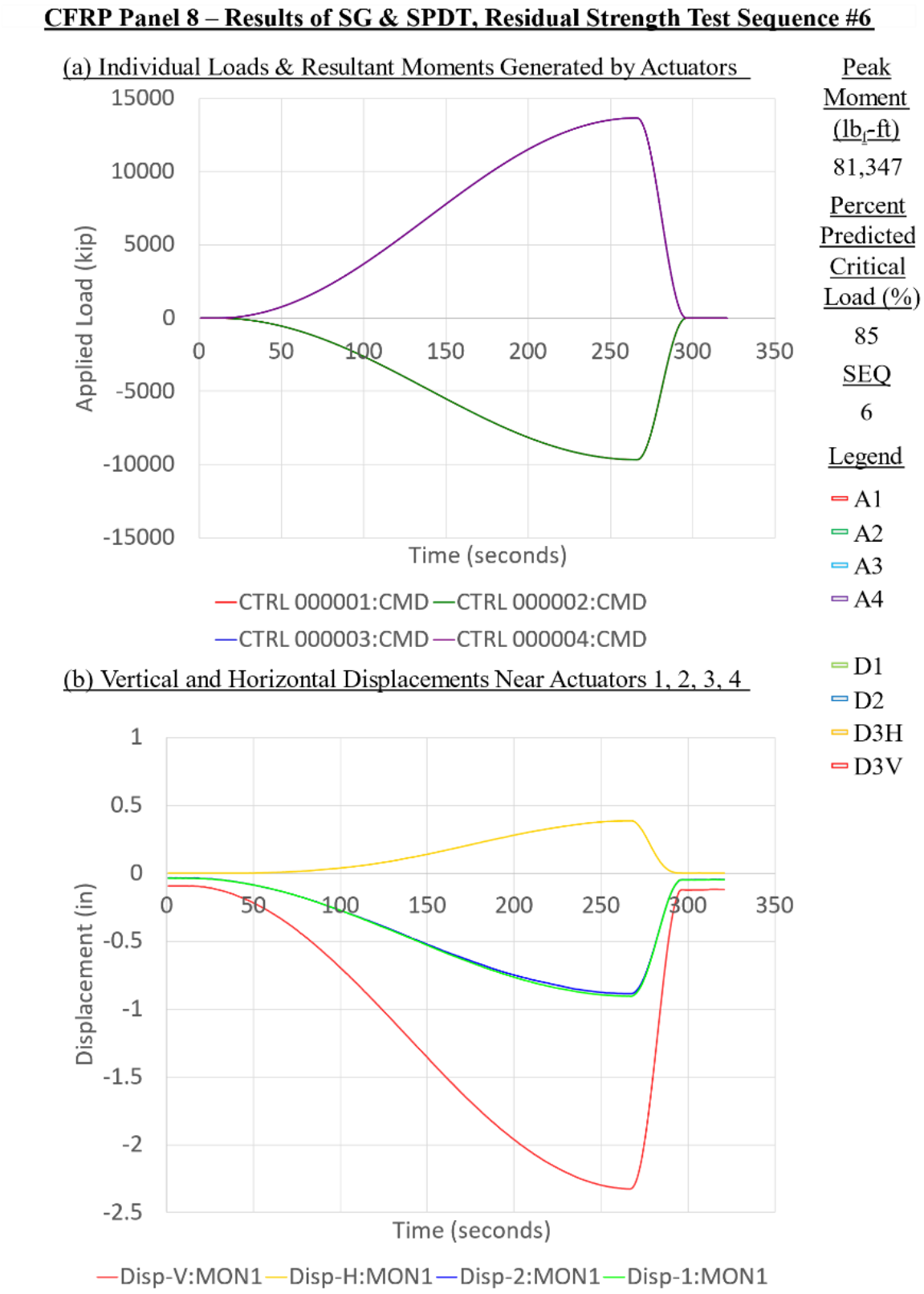

Figure C-57. Panel 8 load increment 6 (85% load level), load and displacement

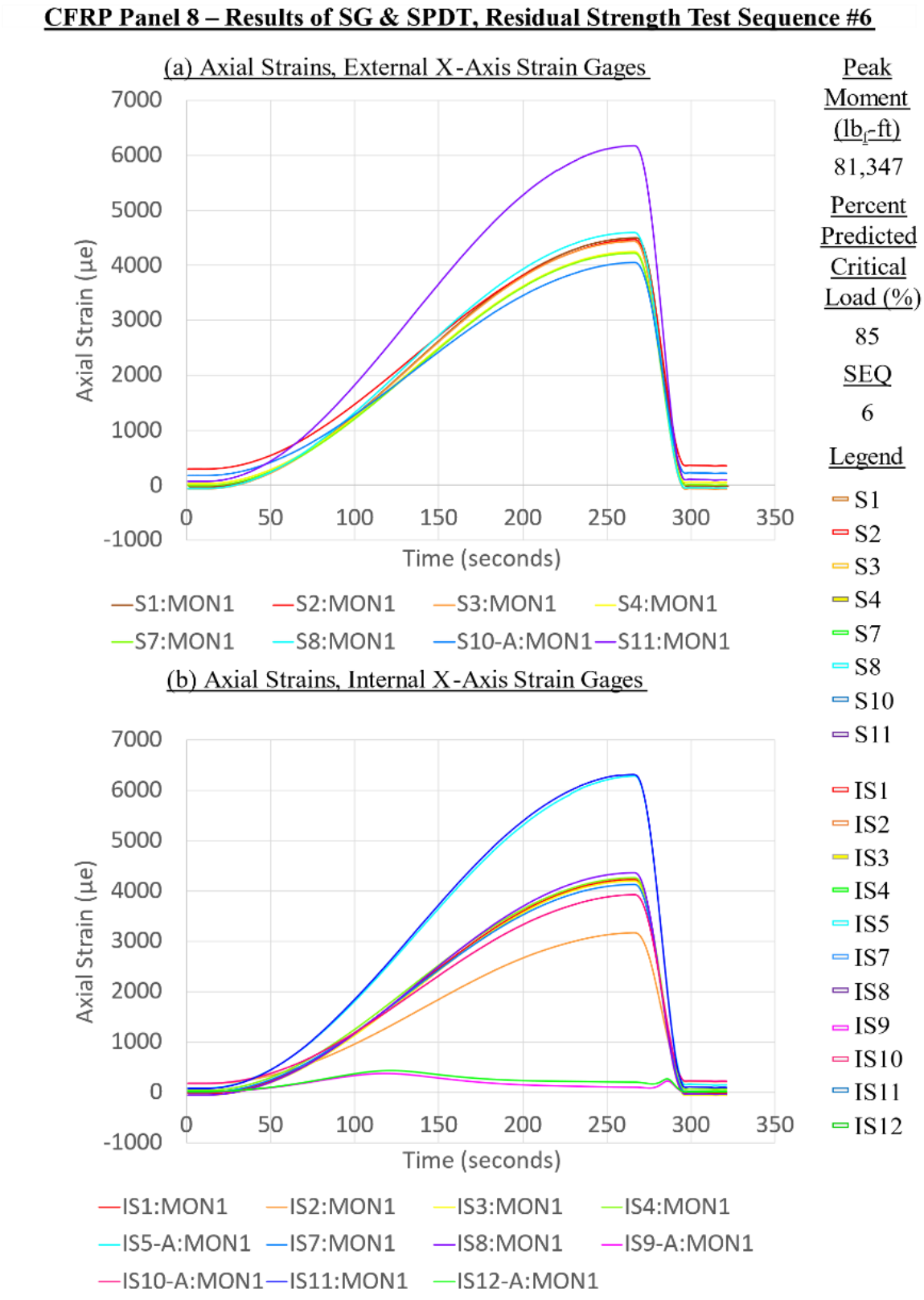

Figure C-58. Panel 8 load increment 6 (85% load level), axial strain

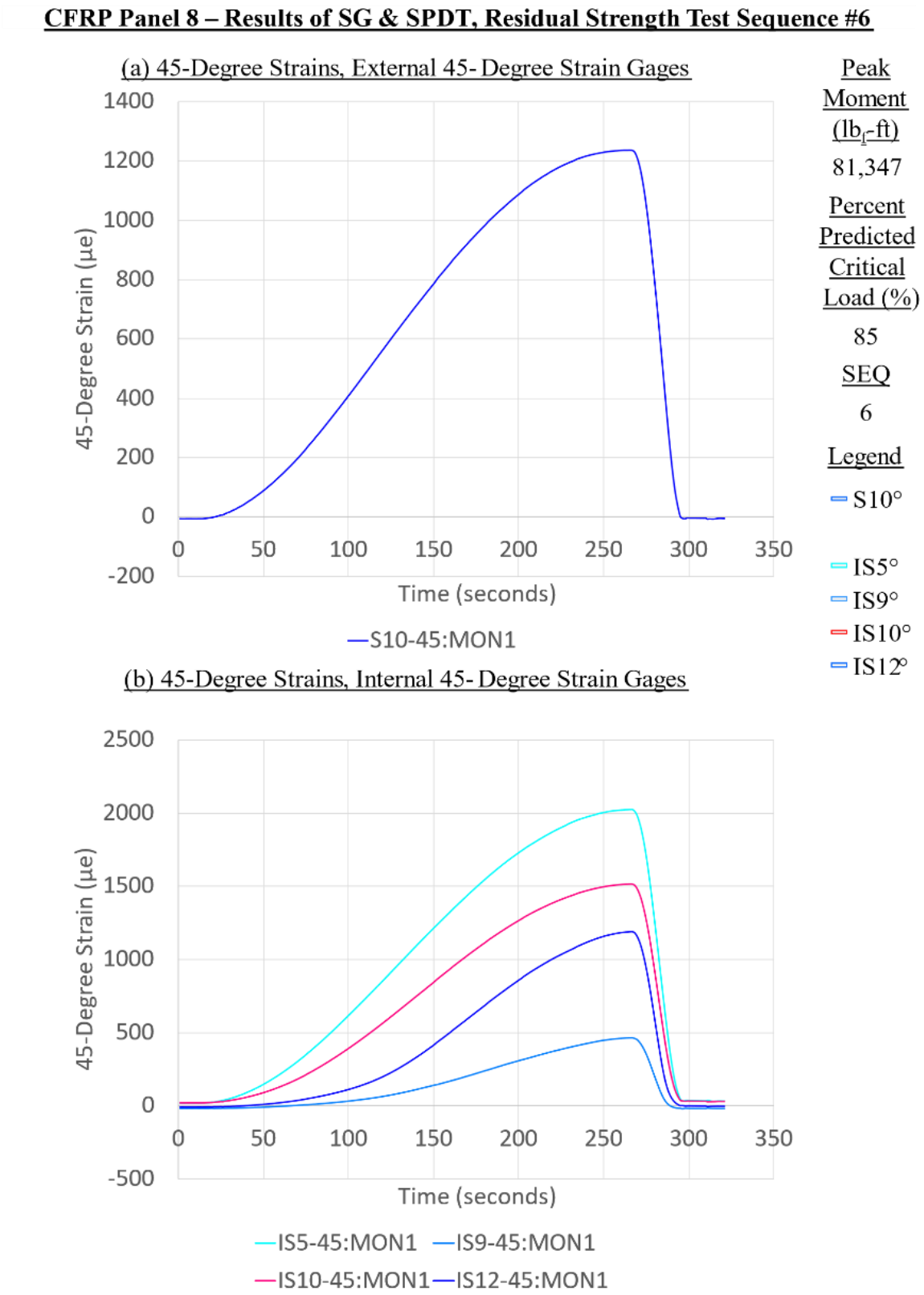

Figure C-59. Panel 8 load increment 6 (85% load level), 45-degree strain

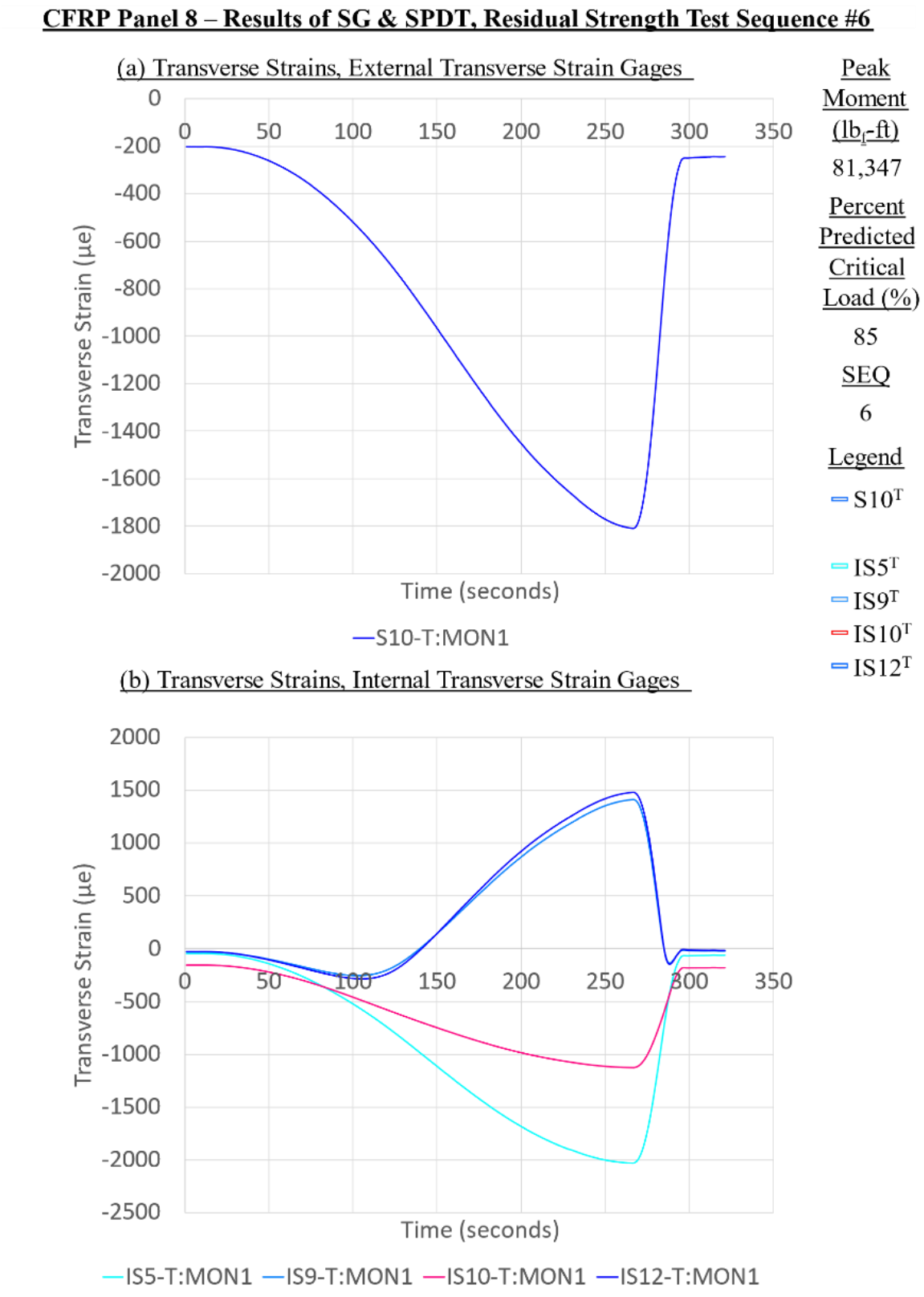

Figure C-60. Panel 8 load increment 6 (85% load level), transverse strain

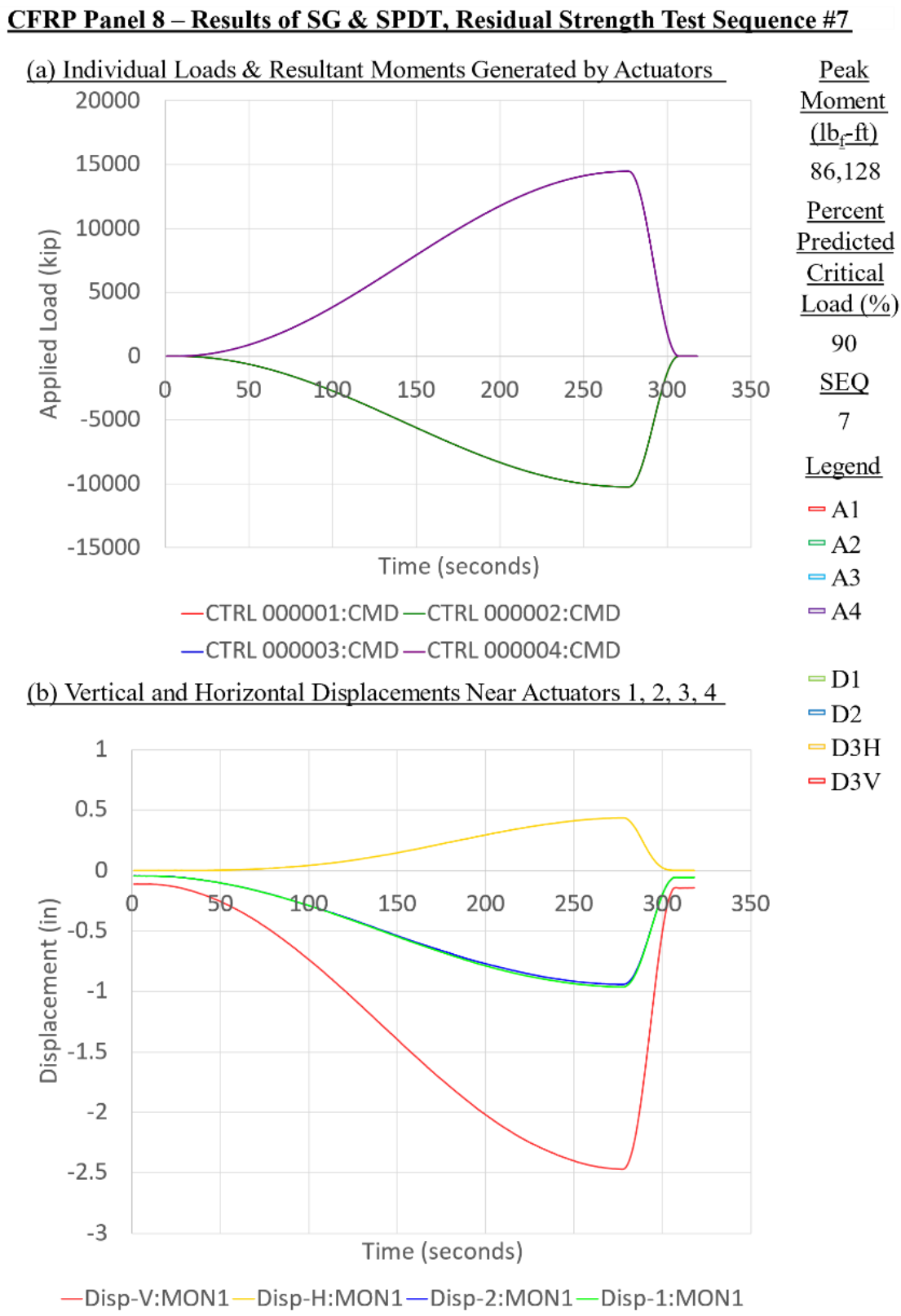

Figure C-61. Panel 8 load increment 7 (90% load level), load and displacement

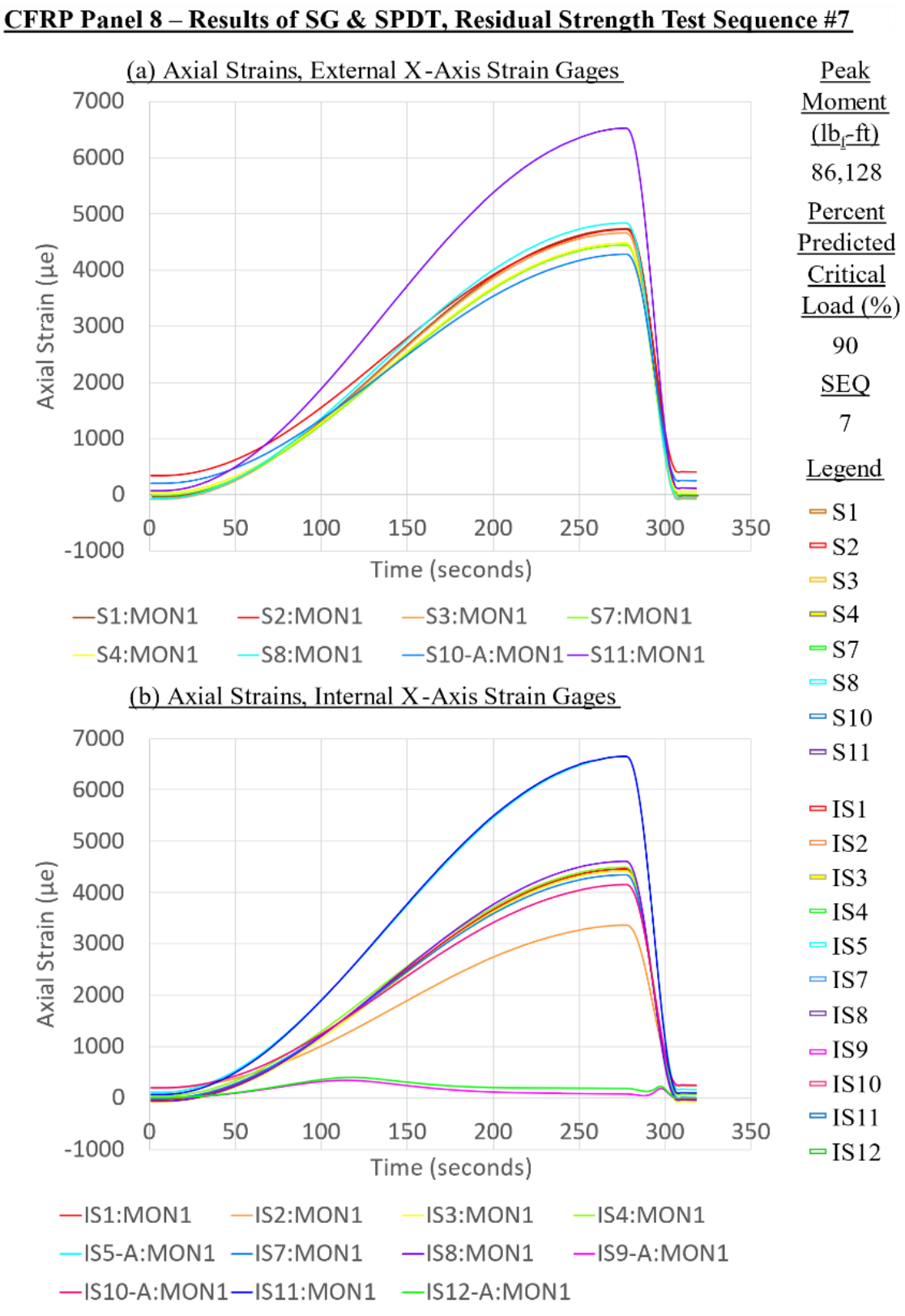

Figure C-62. Panel 8 load increment 7 (90% load level), axial strain

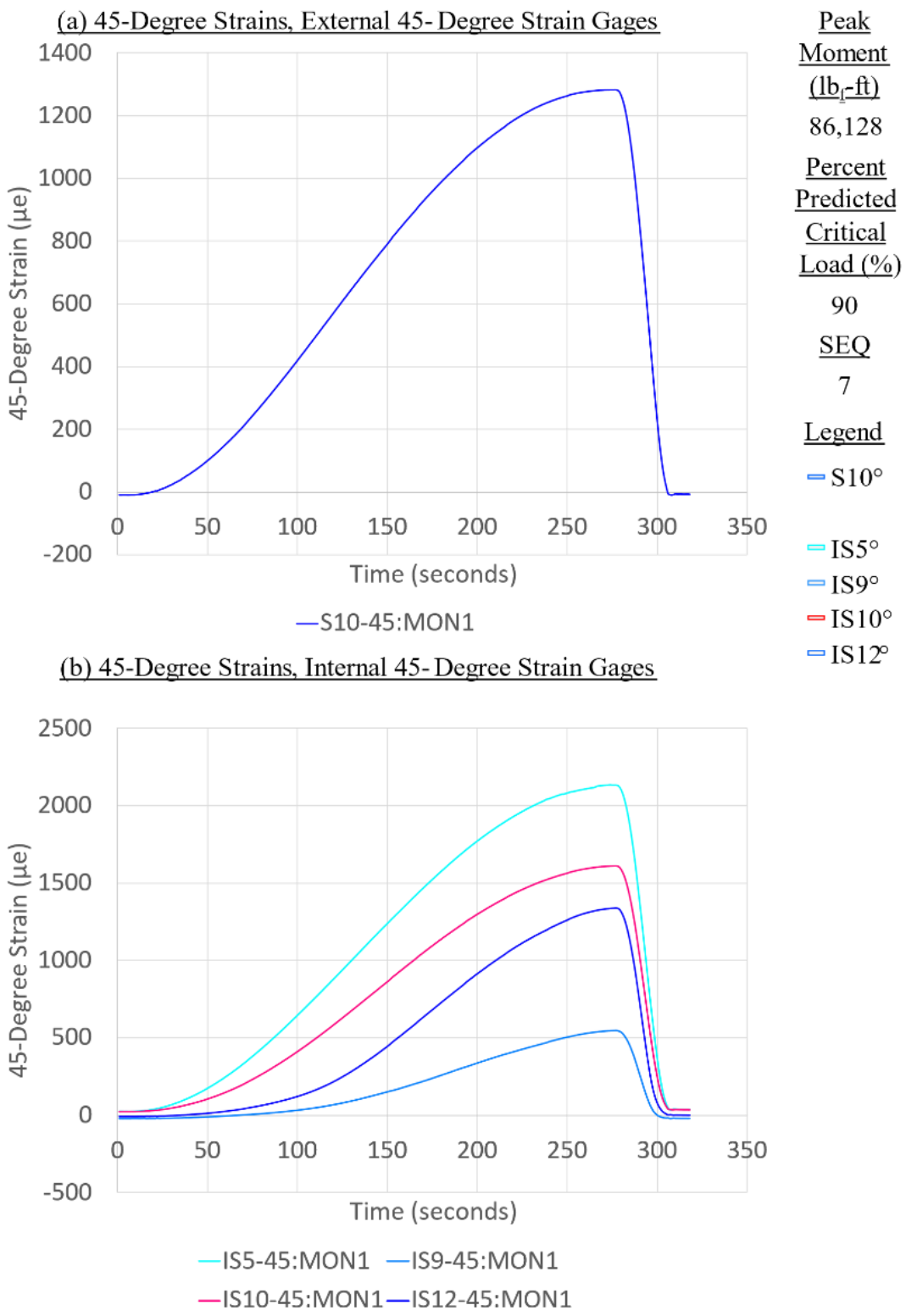

Figure C-63. Panel 8 load increment 7 (90% load level), 45-degree strain

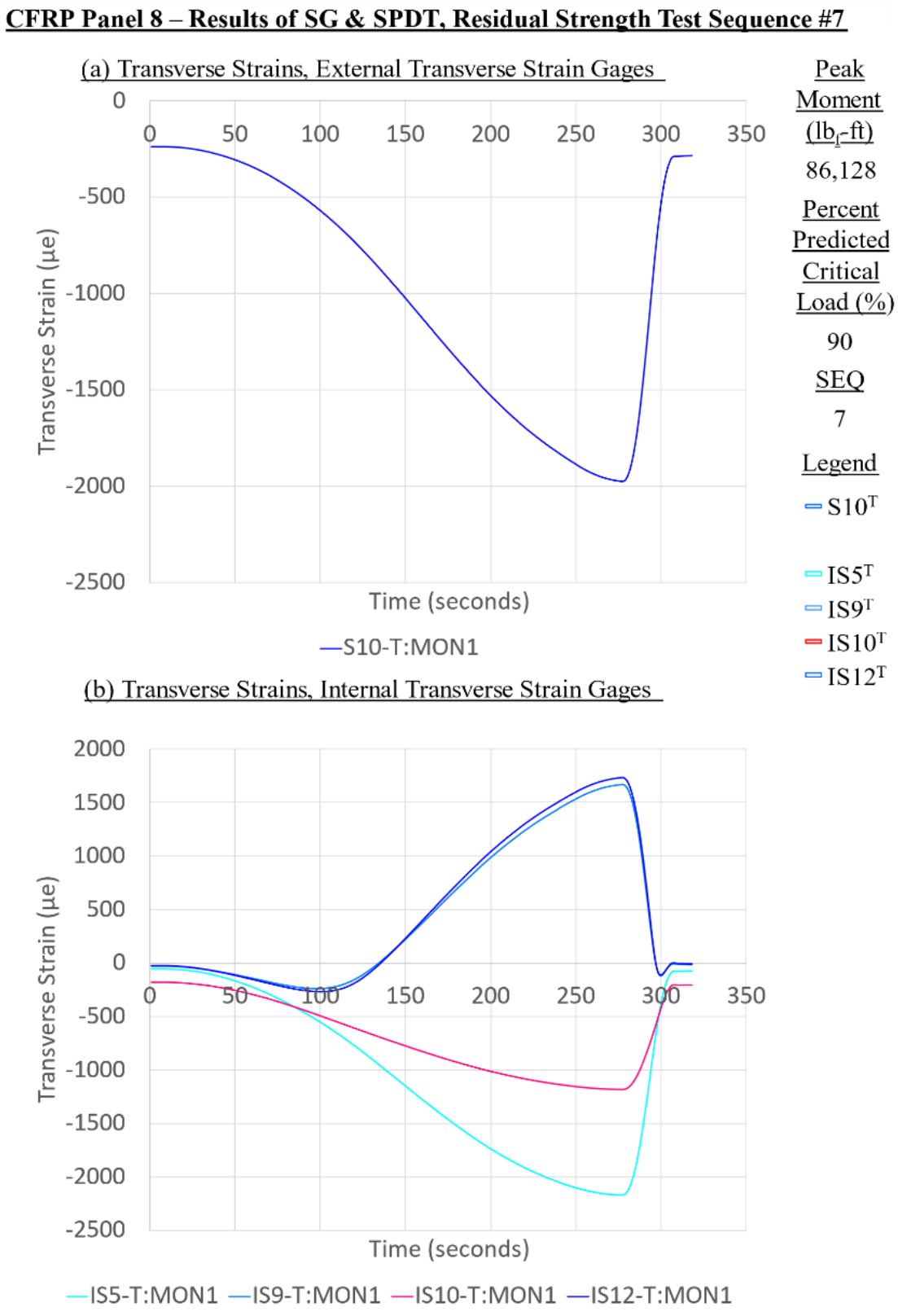

Figure C-64. Panel 8 load increment 7 (90% load level), transverse strain

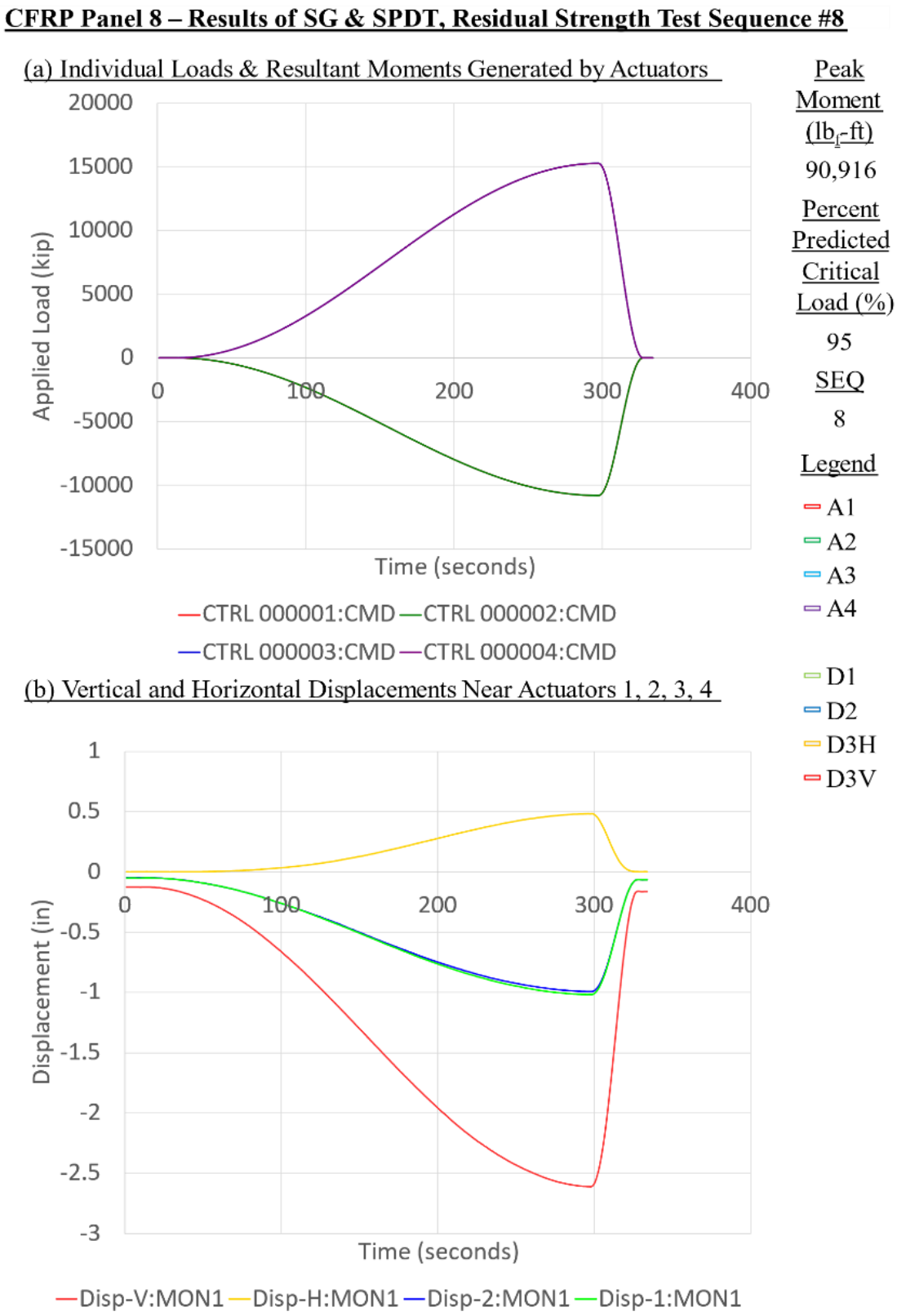

Figure C-65. Panel 8 load increment 8 (95% load level), load and displacement

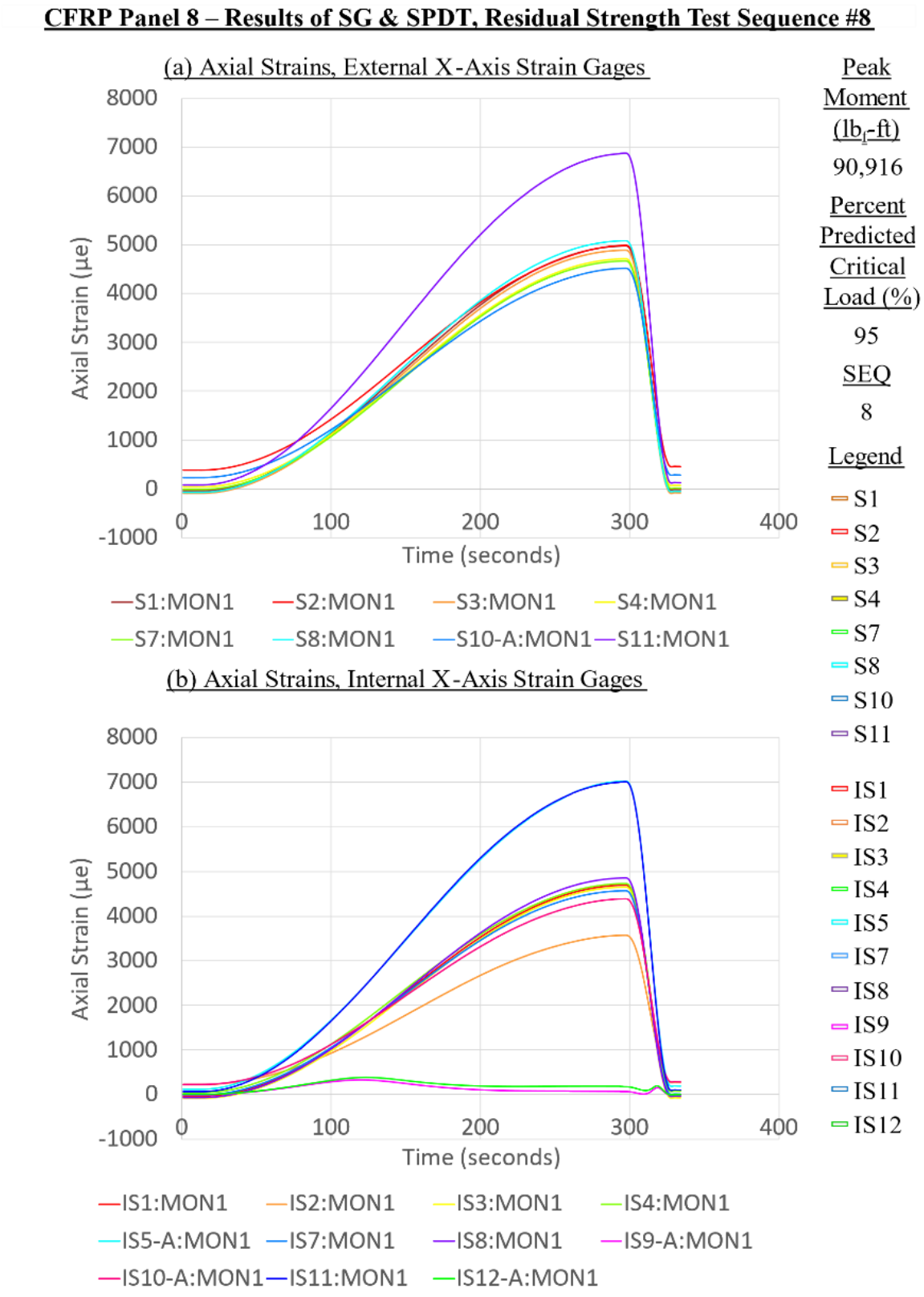

Figure C-66. Panel 8 load increment 8 (95% load level), axial strain

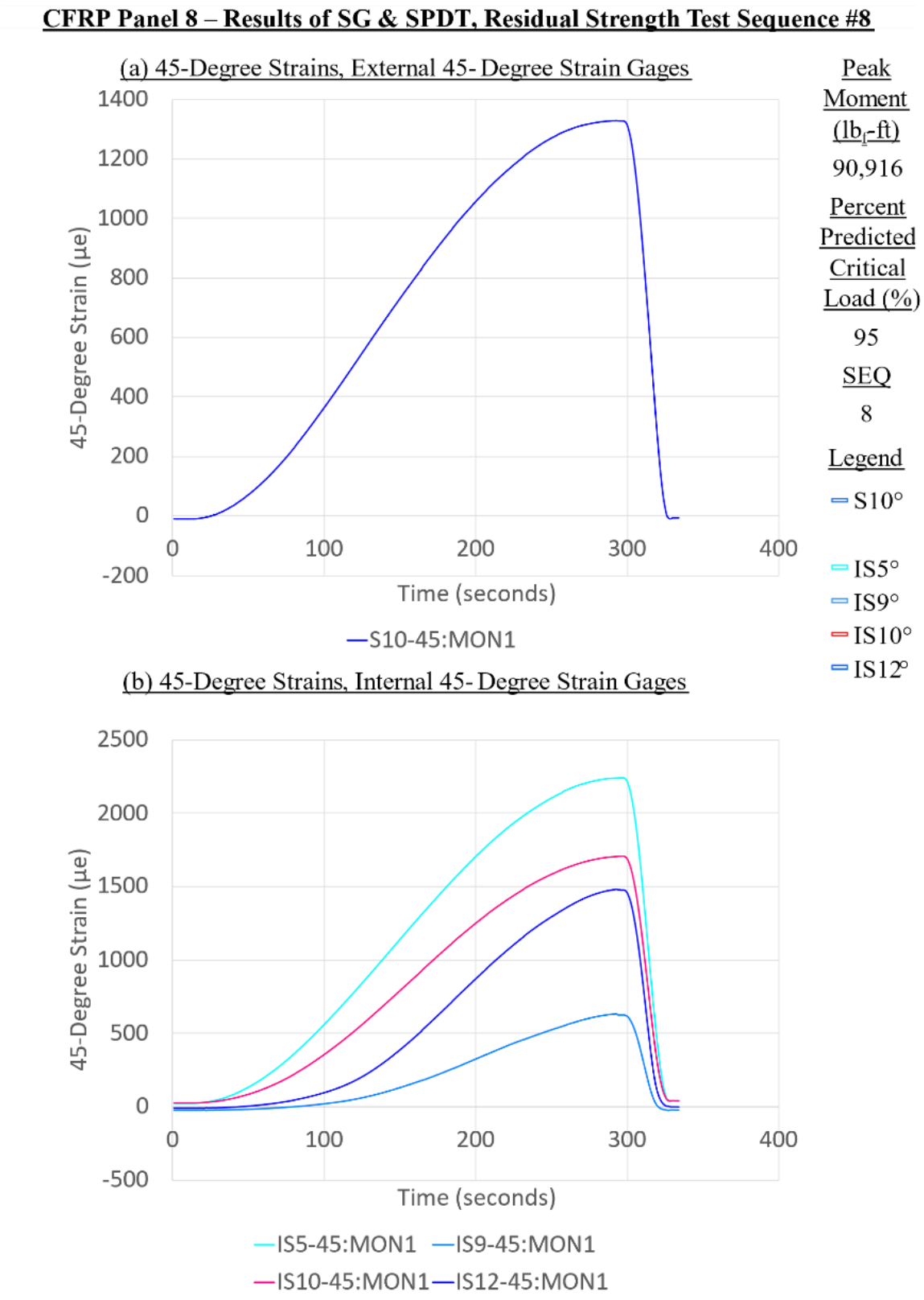

Figure C-67. Panel 8 load increment 8 (95% load level), 45-degree strain

Figure C-68. Panel 8 load increment 8 (95% load level), transverse strain

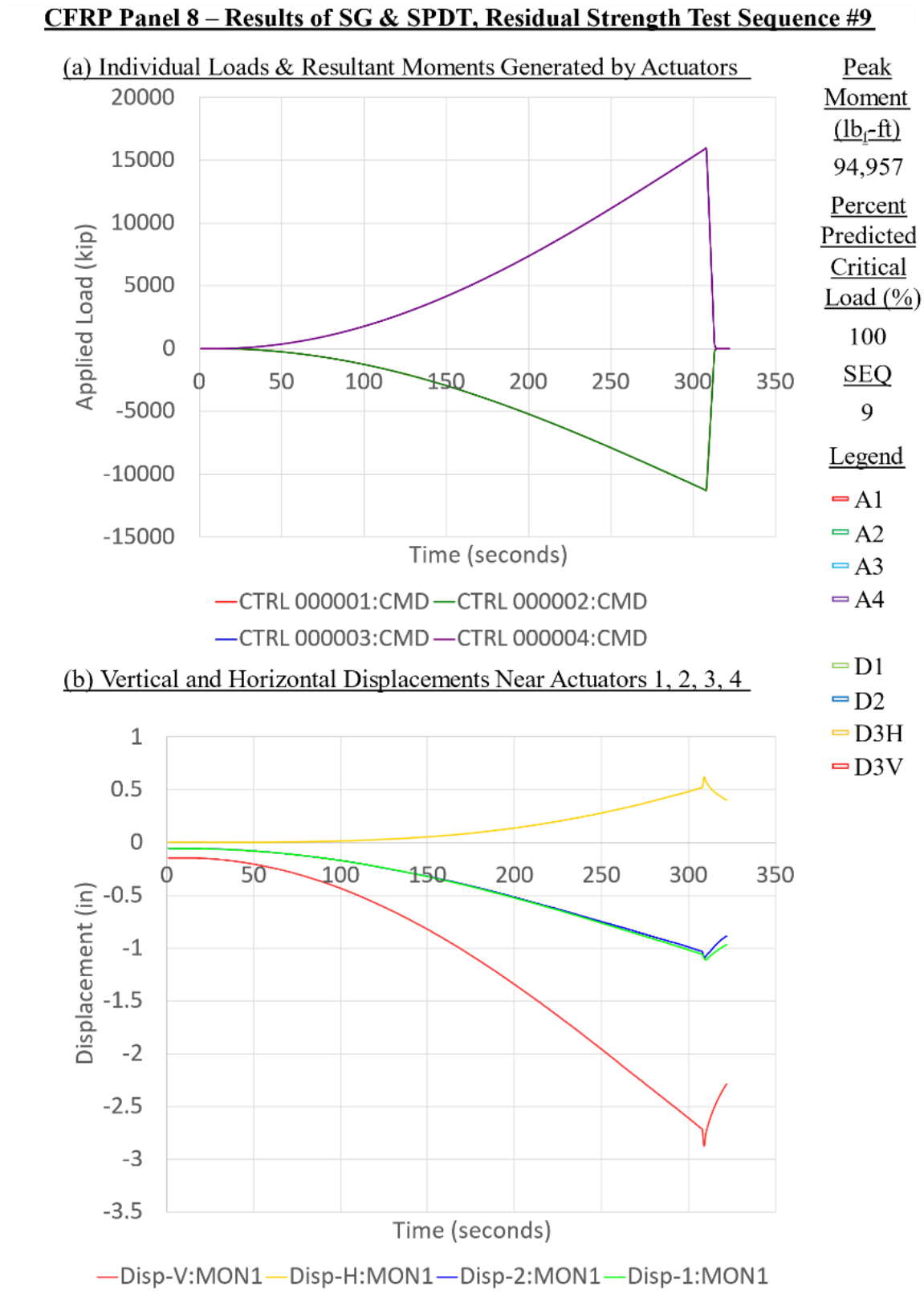

Figure C-69. Panel 8 load increment 9 (100% load level), load and displacement

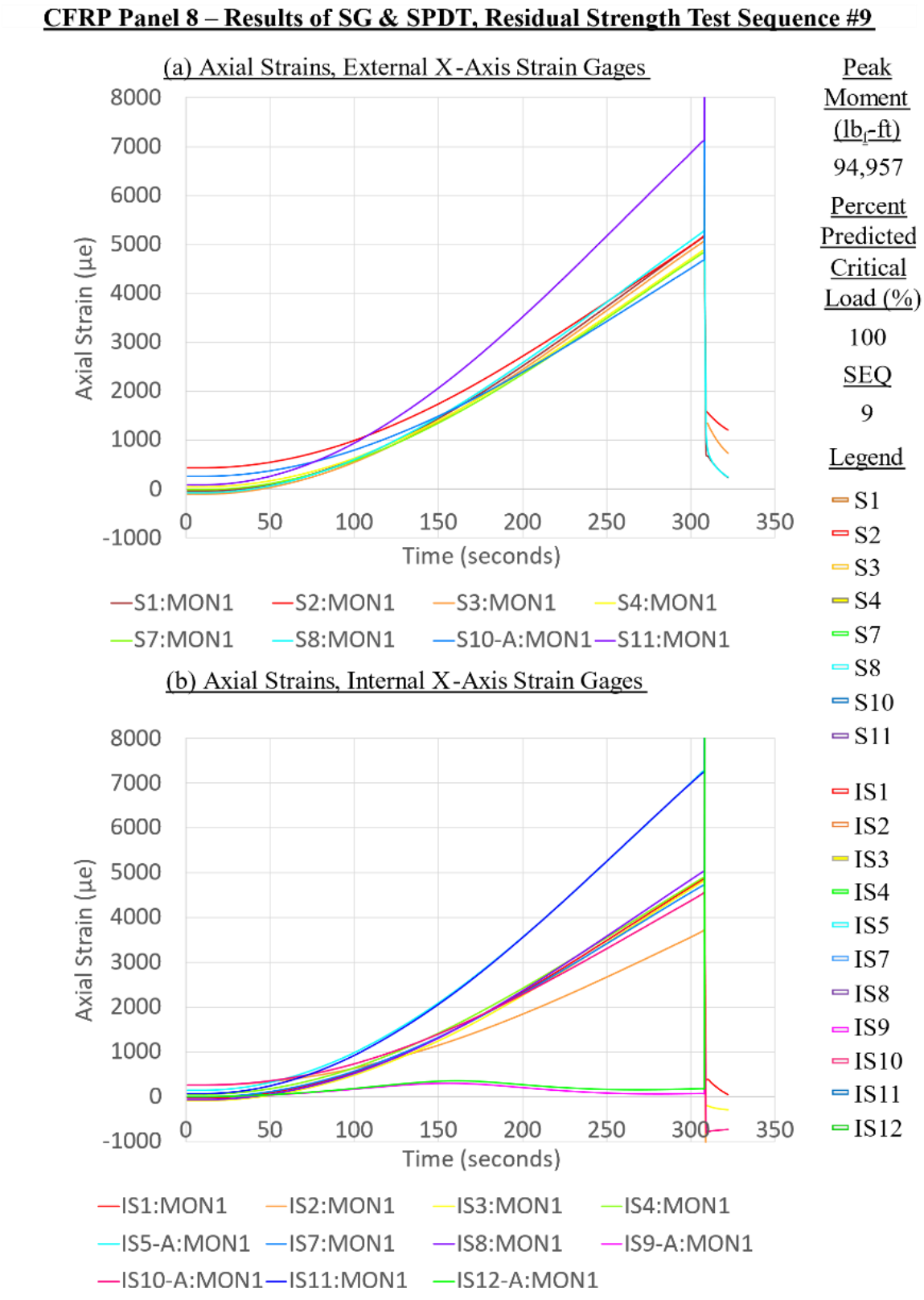

Figure C-70. Panel 8 load increment 9 (100% load level), axial strain

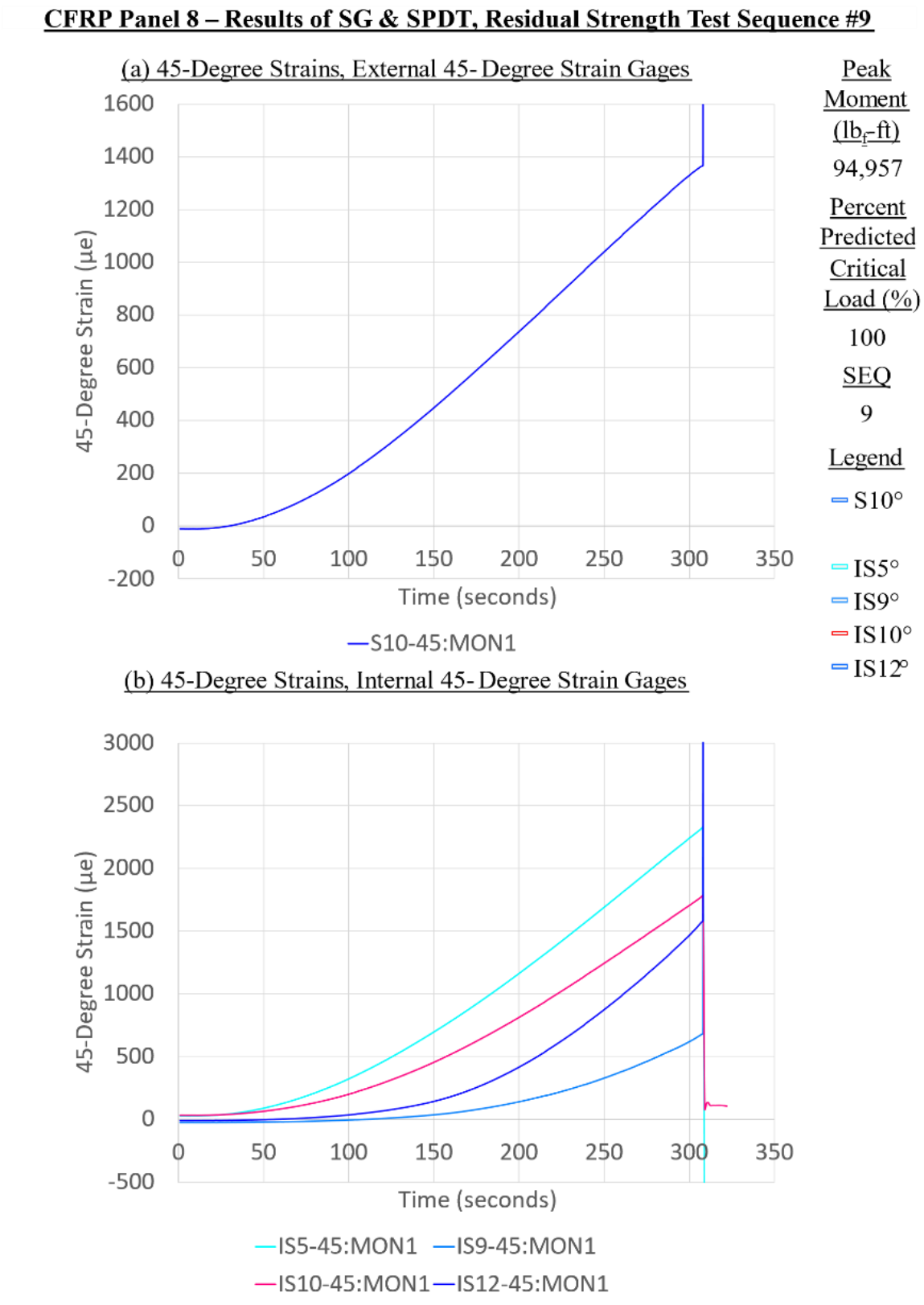

Figure C-71. Panel 8 load increment 9 (100% load level), 45-degree strain

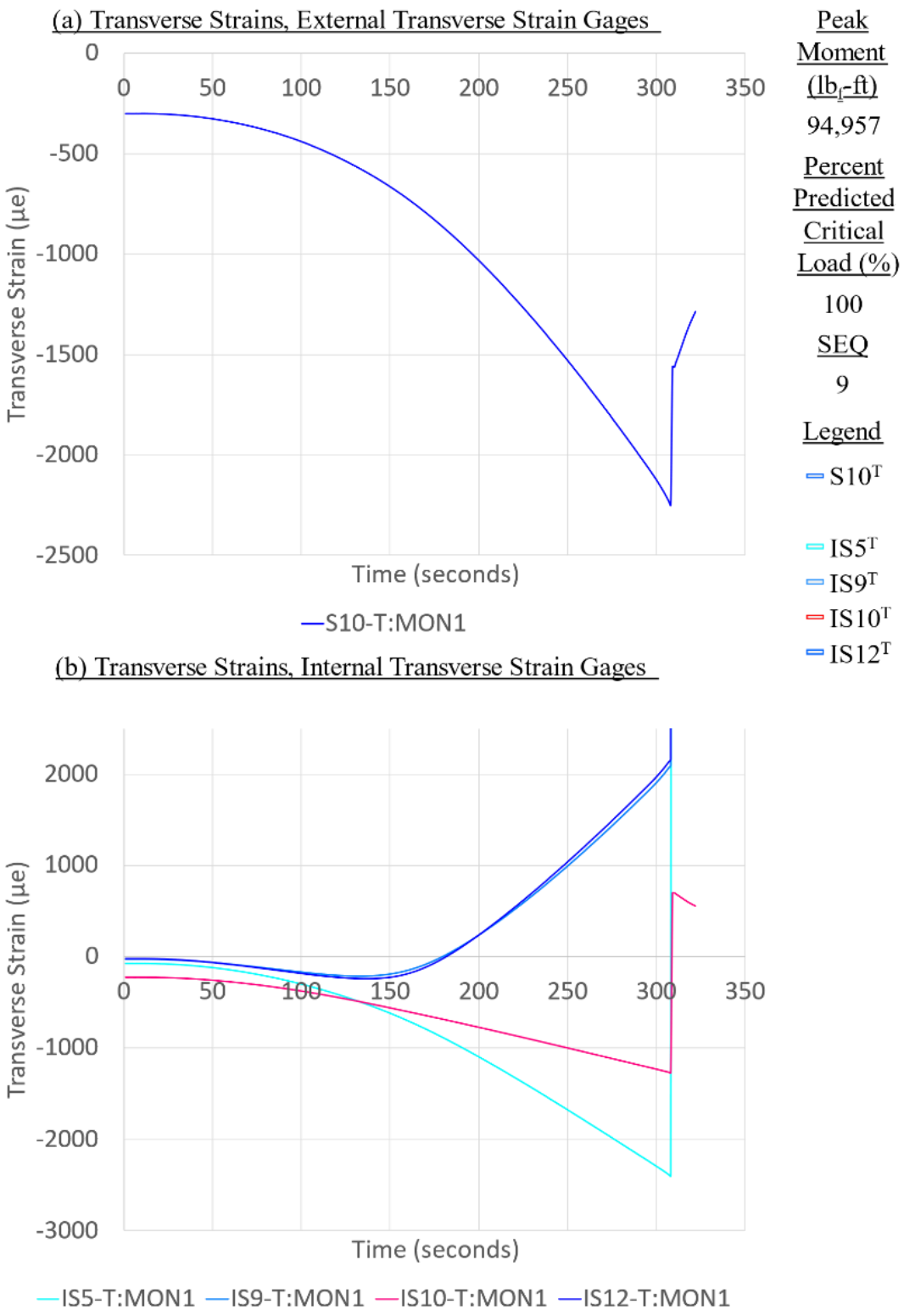

Figure C-72. Panel 8 load increment 9 (100% load level), transverse strain

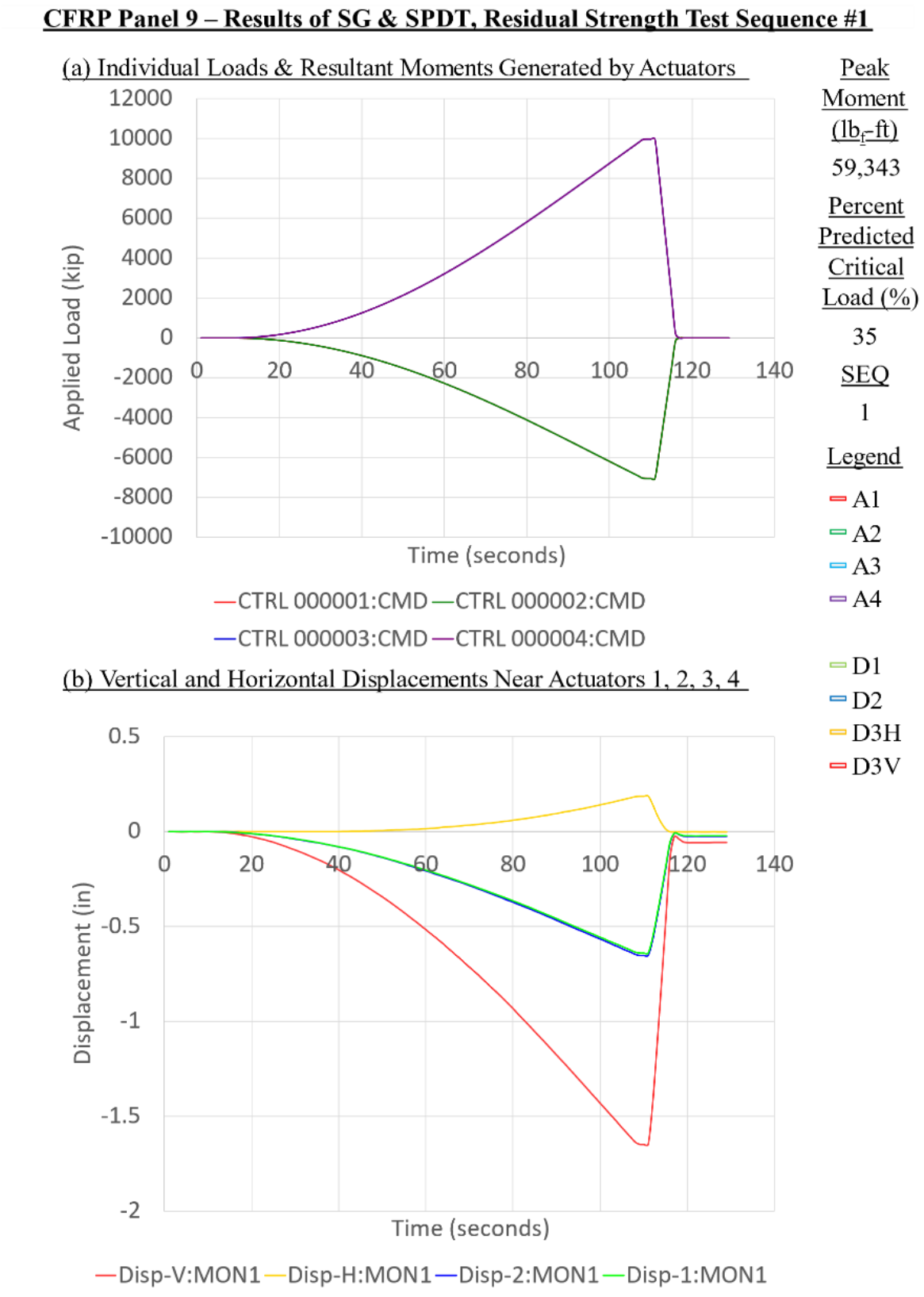

Figure C-73. Panel 9 load increment 1 (35% load level), load and displacement

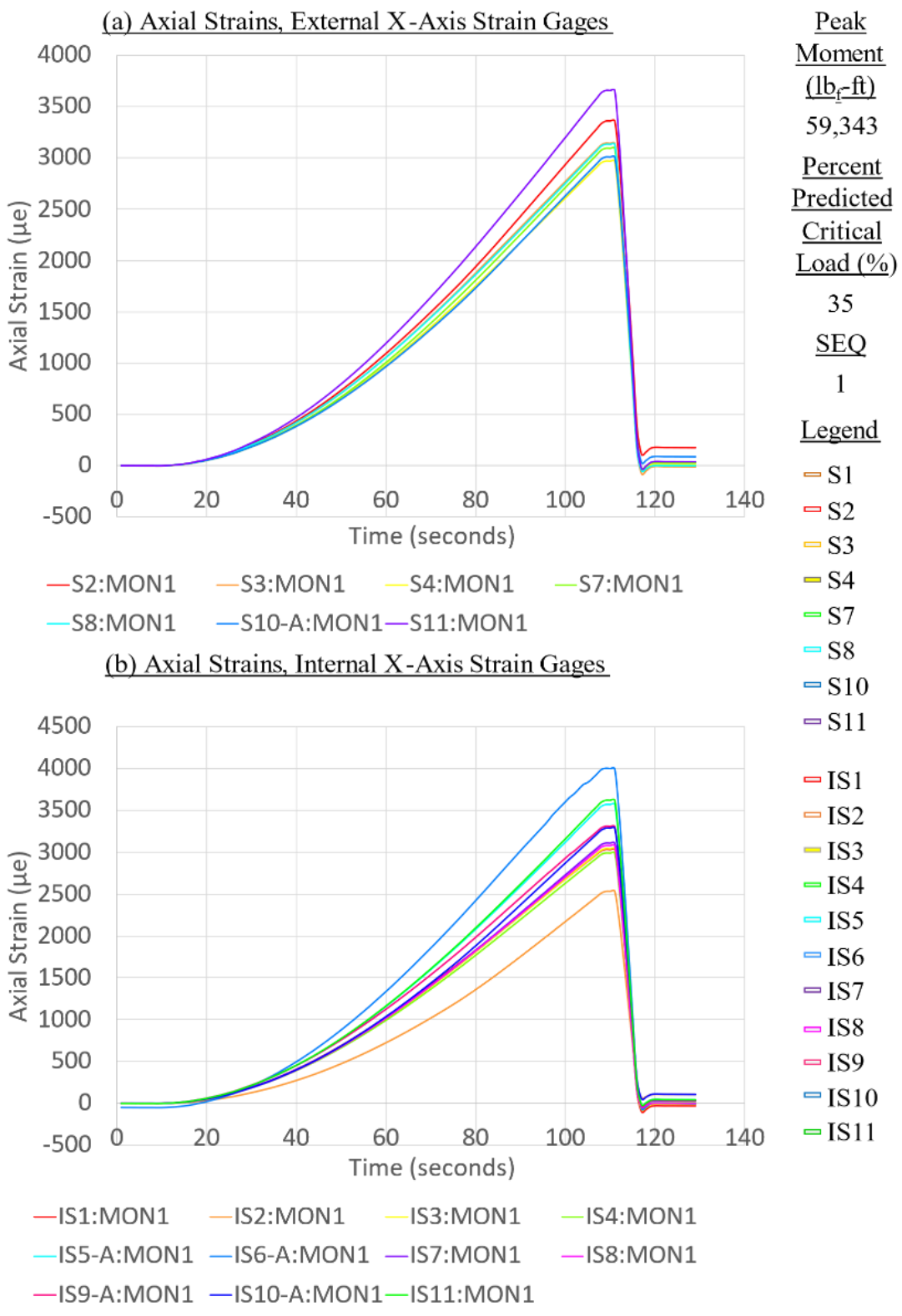

Figure C-74. Panel 9 load increment 1 (35% load level), axial strain

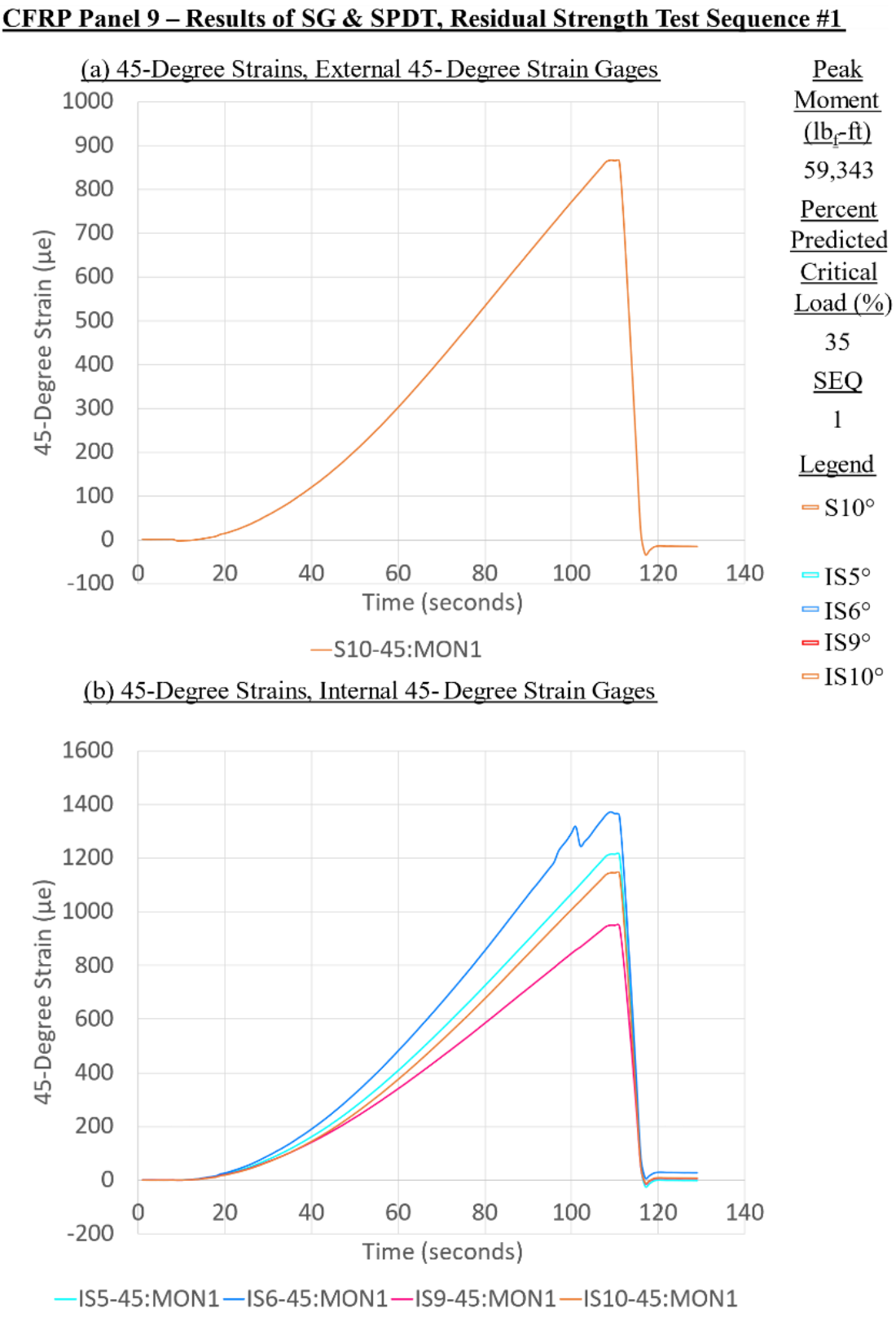

Figure C-75. Panel 9 load increment 1 (35% load level), 45-degree strain

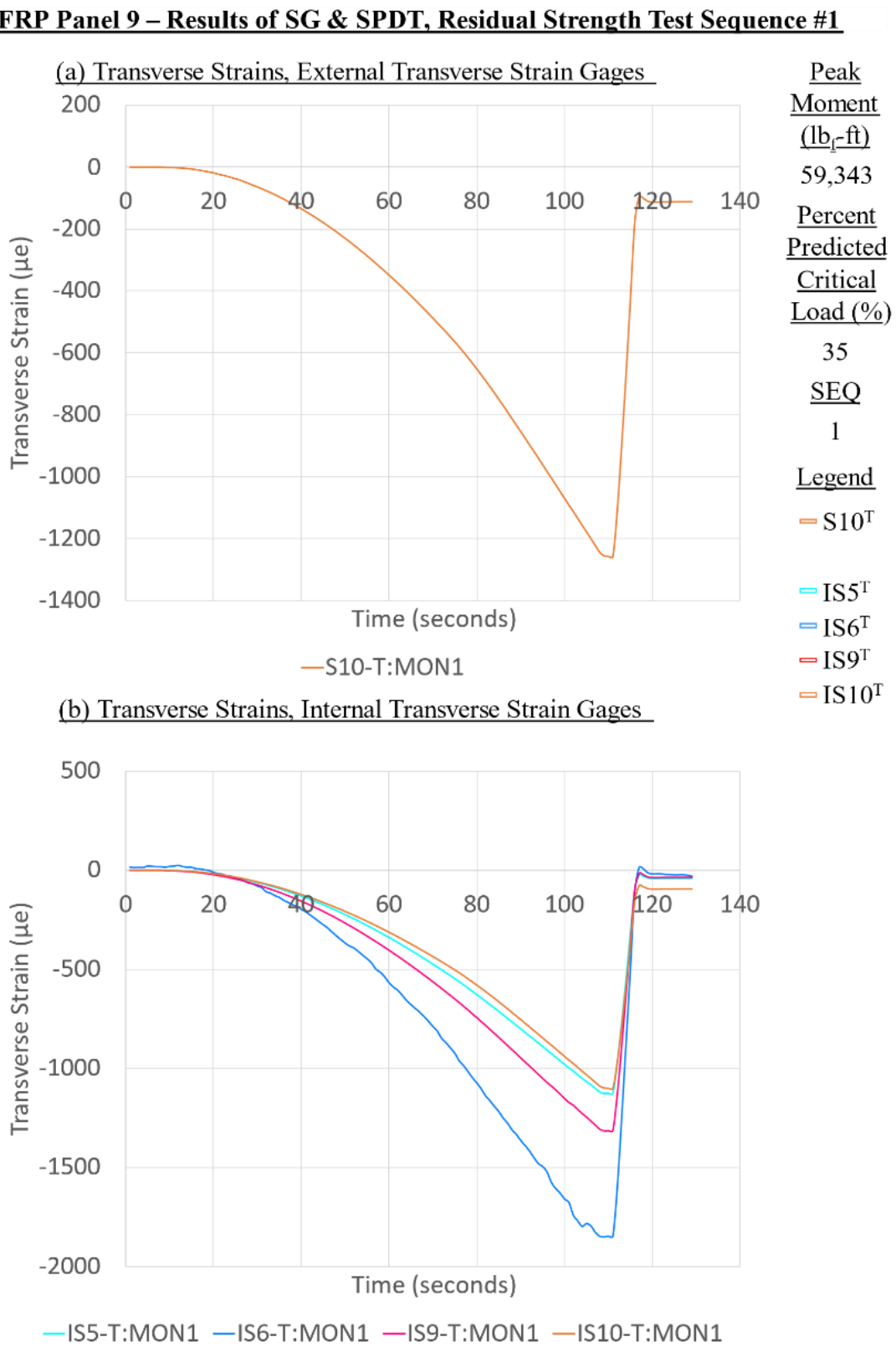

Figure C-76. Panel 9 load increment 1 (35% load level), transverse strain

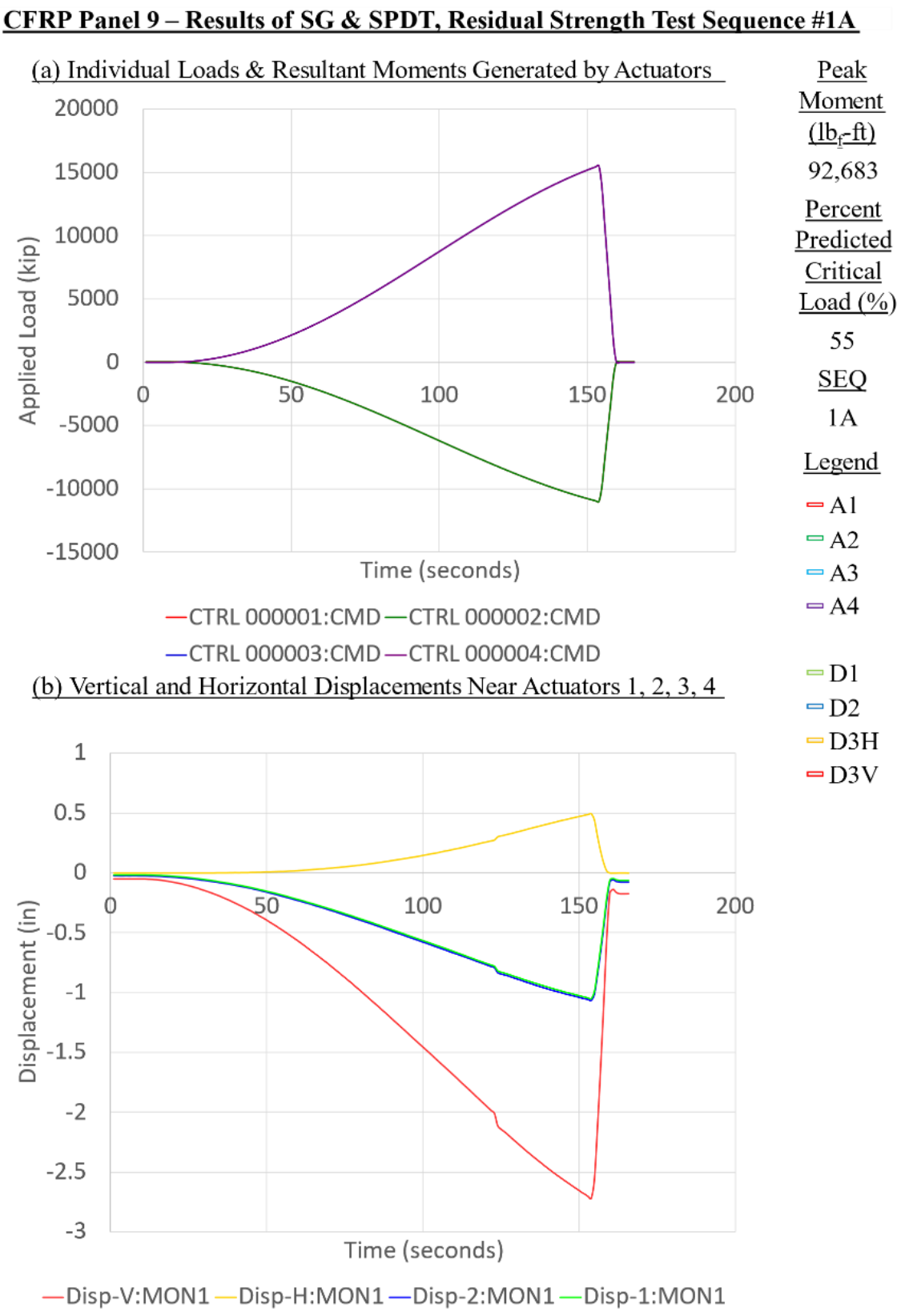

Figure C-77. Panel 9 load increment 1a (55% load level), load and displacement

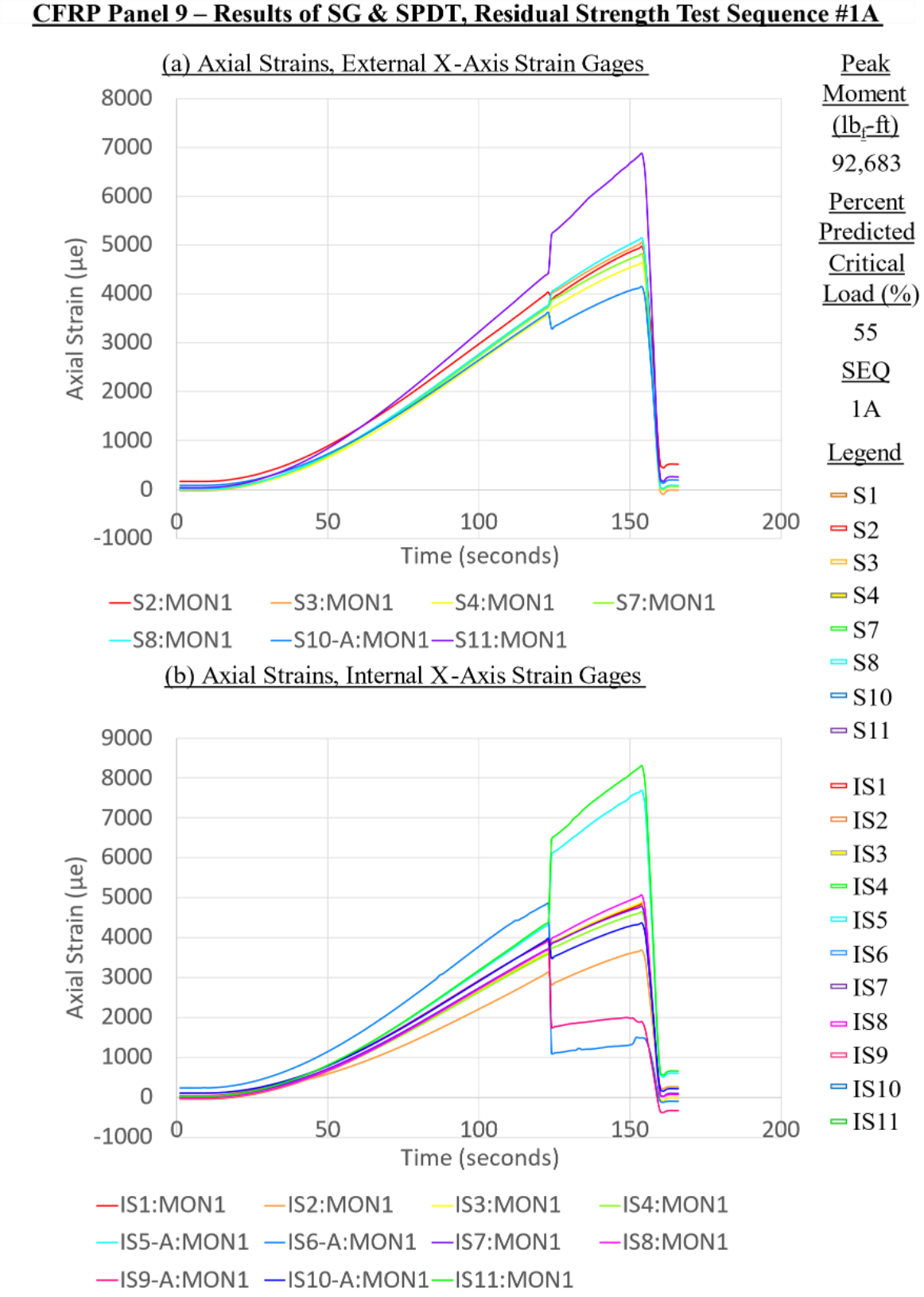

Figure C-78. Panel 9 load increment 1a (55% load level), axial strain

CFRP Panel 9 – Results of SG & SPDT, Residual Strength Test Sequence #1A

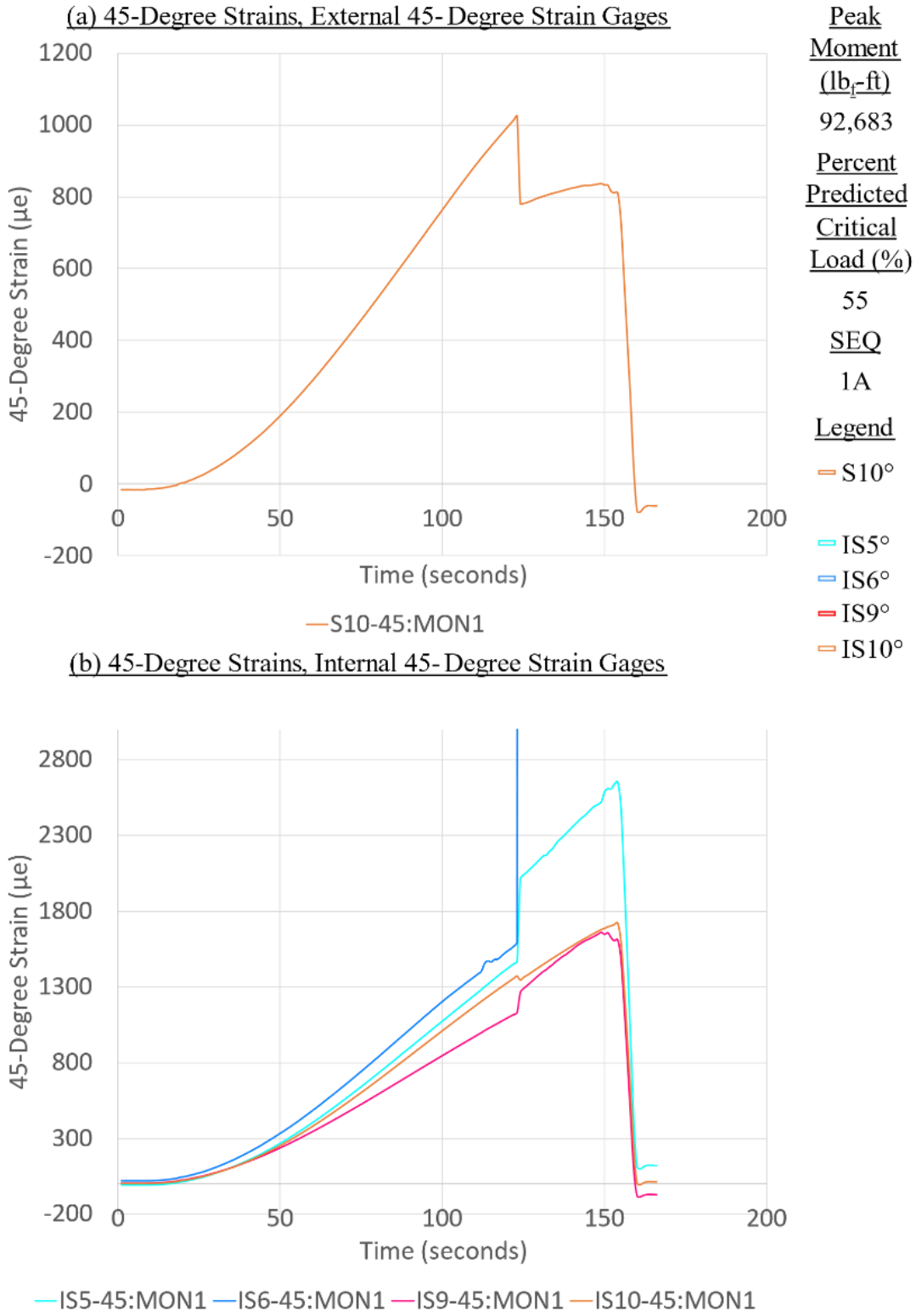

Figure C-79. Panel 9 load increment 1a (55% load level), 45-degree strain

CFRP Panel 9 – Results of SG & SPDT, Residual Strength Test Sequence #1A

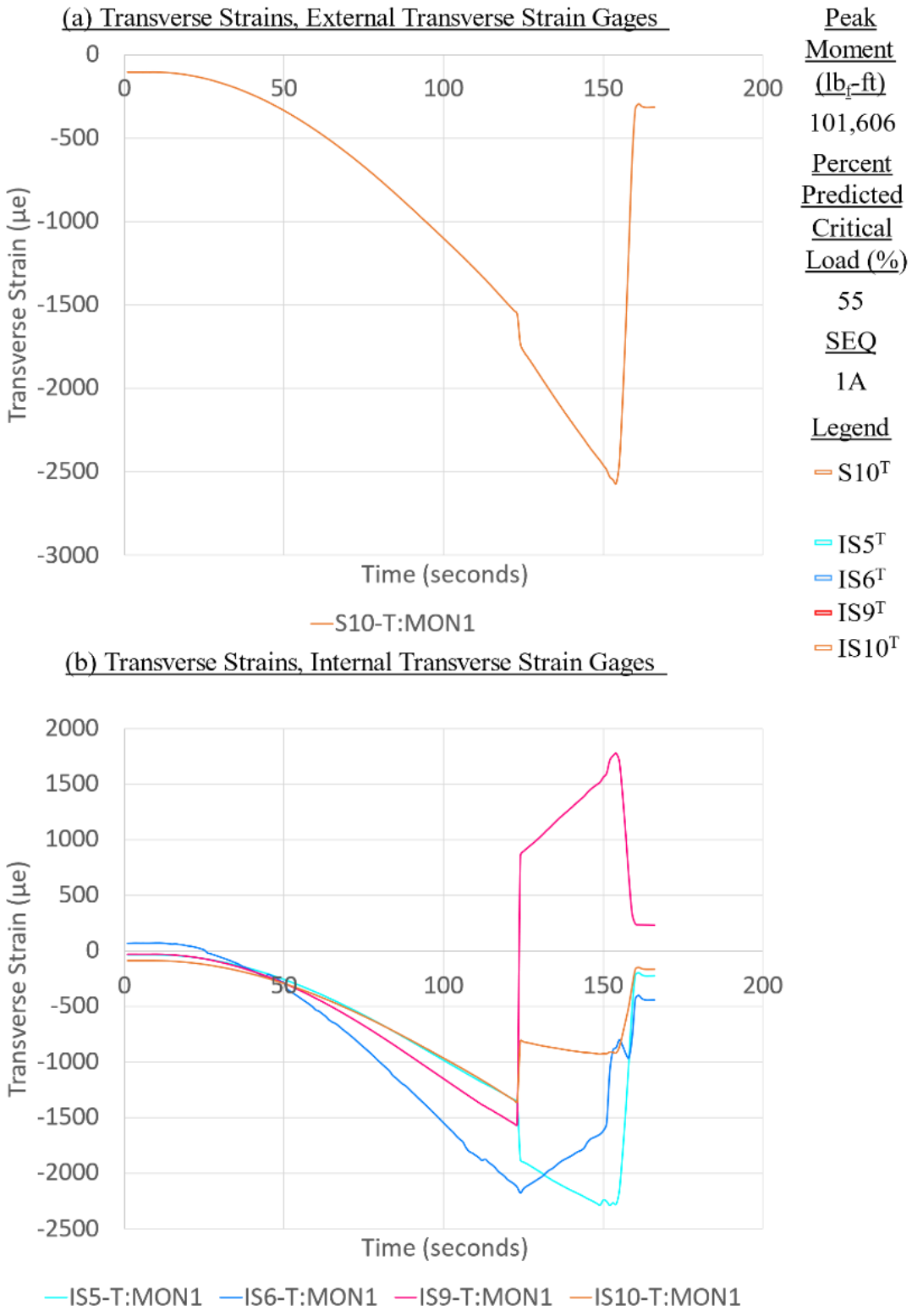

Figure C-80. Panel 9 load increment 1a (55% load level), transverse strain

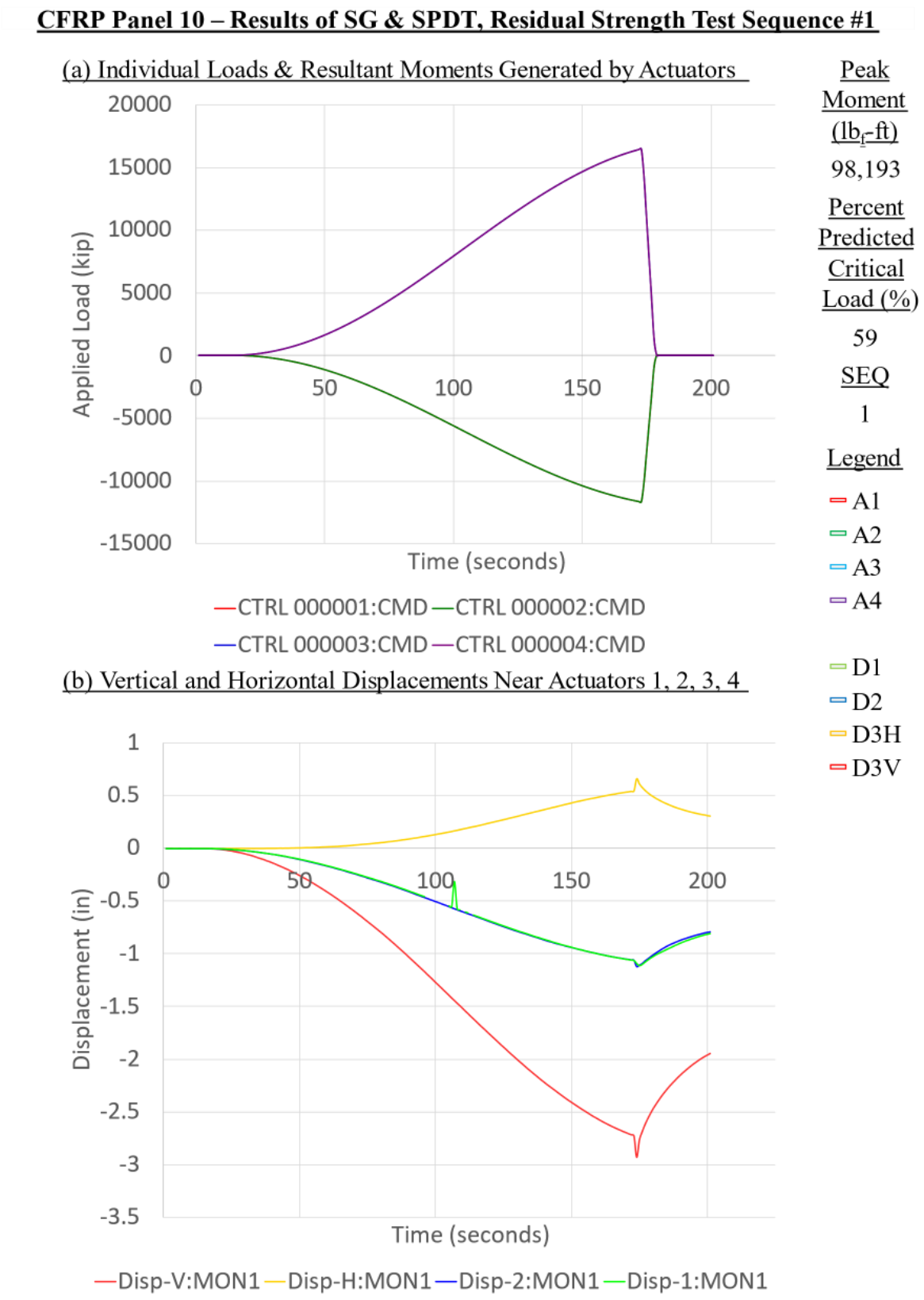

Figure C-81. Panel 10 load increment 1 (59% load level), load and displacement

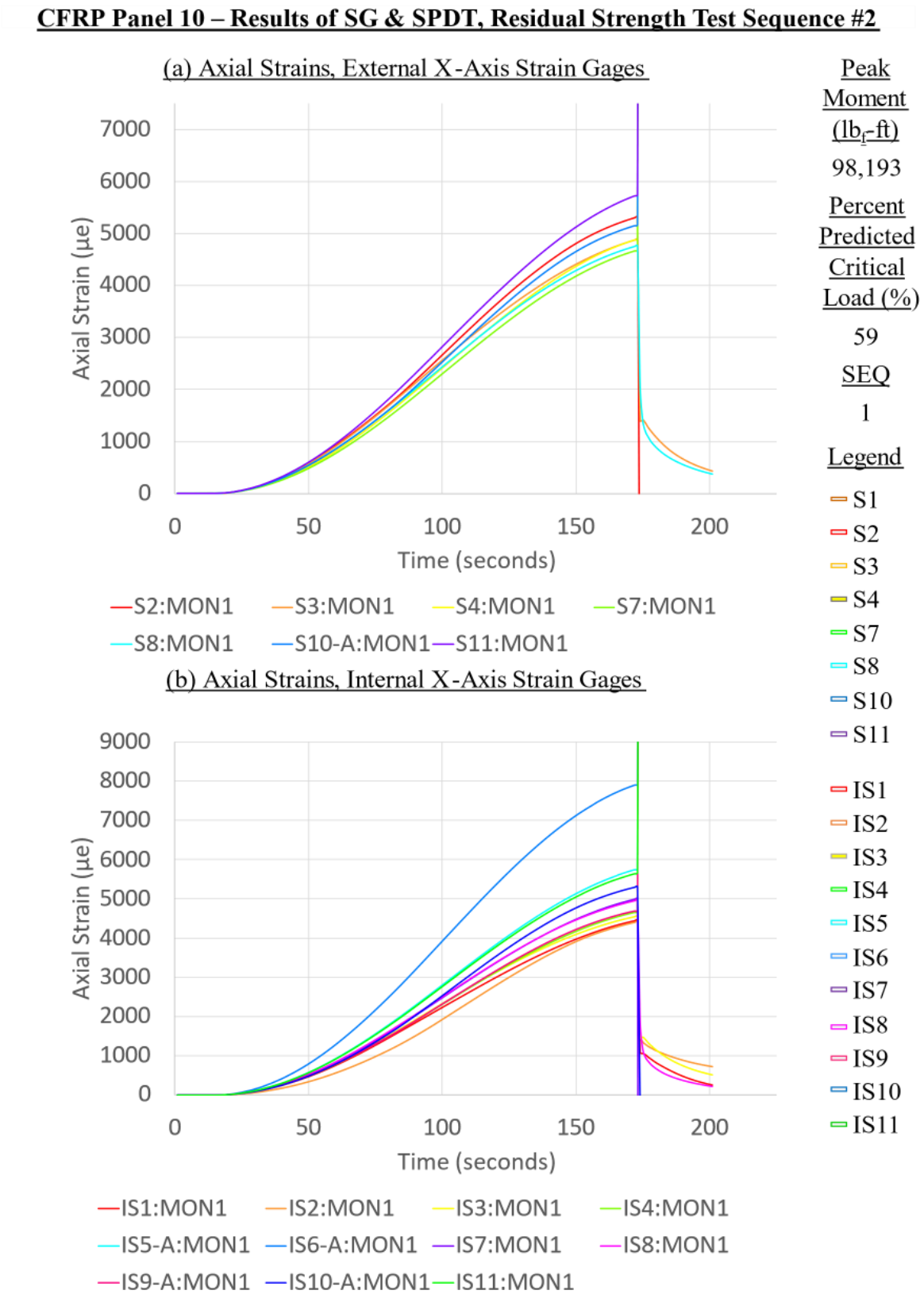

Figure C-82. Panel 10 load increment 1 (59% load level), axial strain

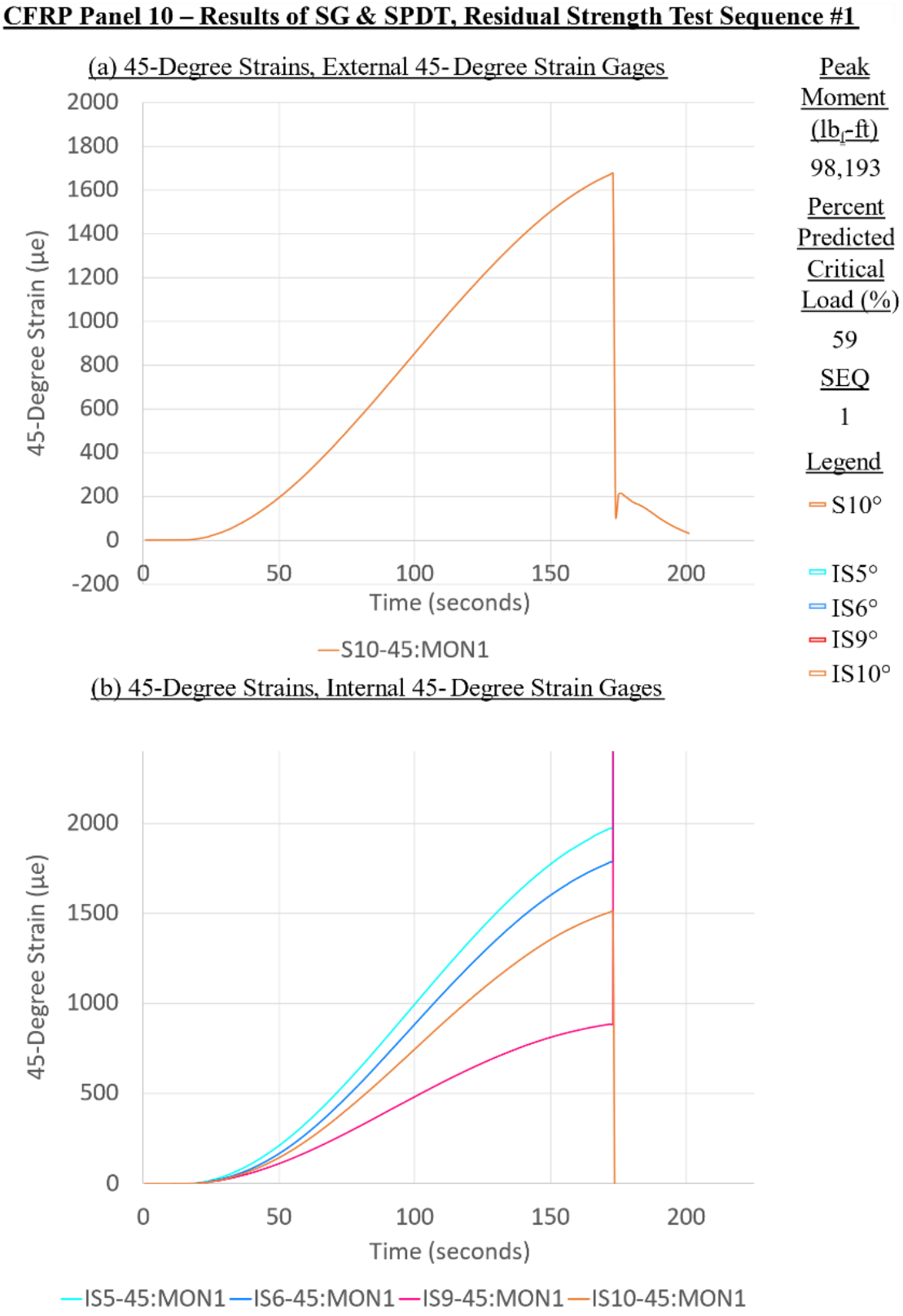

Figure C-83. Panel 10 load increment 1 (59% load level), 45-degree strain

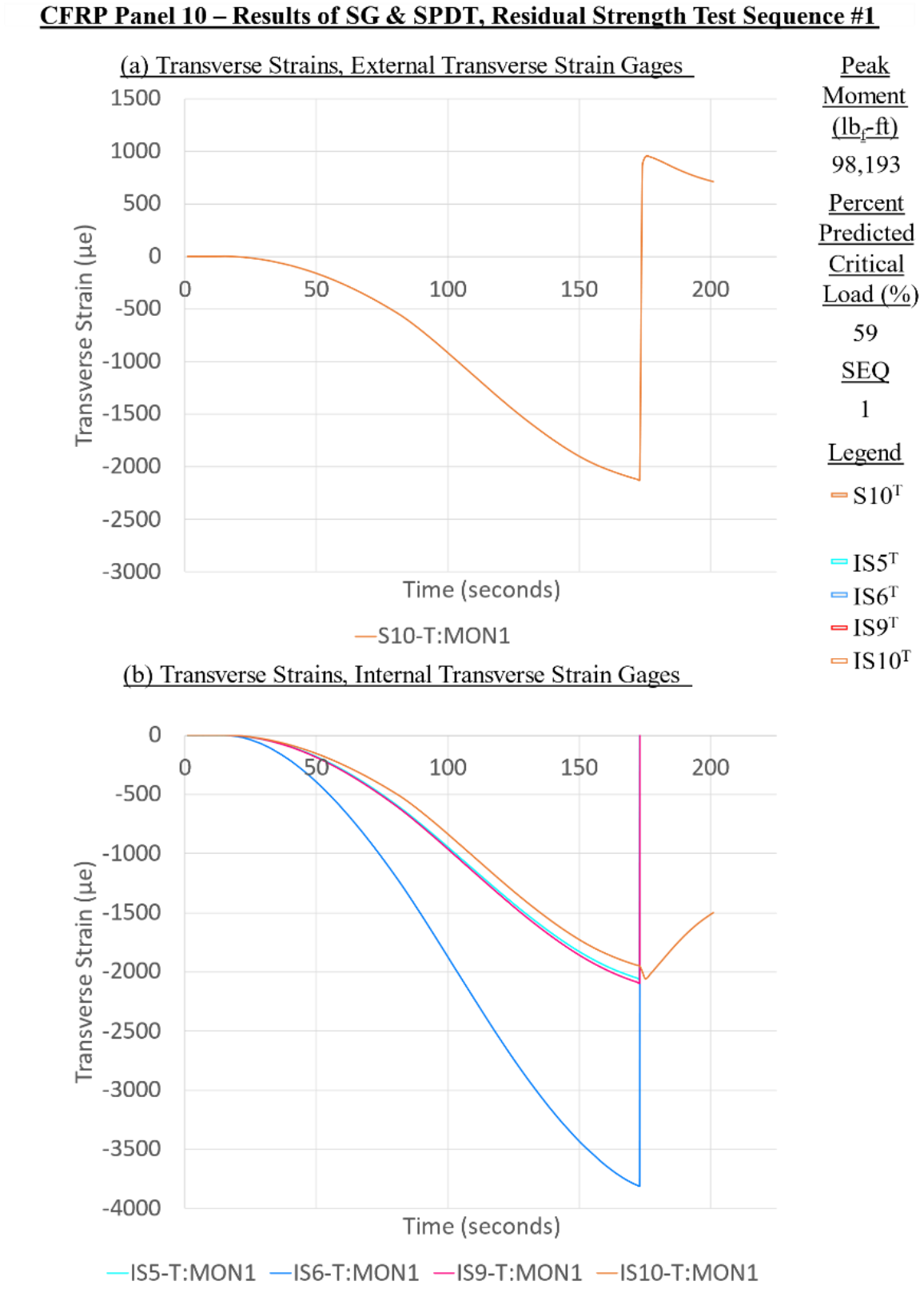

Figure C-84. Panel 10 load increment 1 (59% load level), transverse strain

CFRP Panel 11 – Results of SG & SPDT, Residual Strength Test Sequence #1

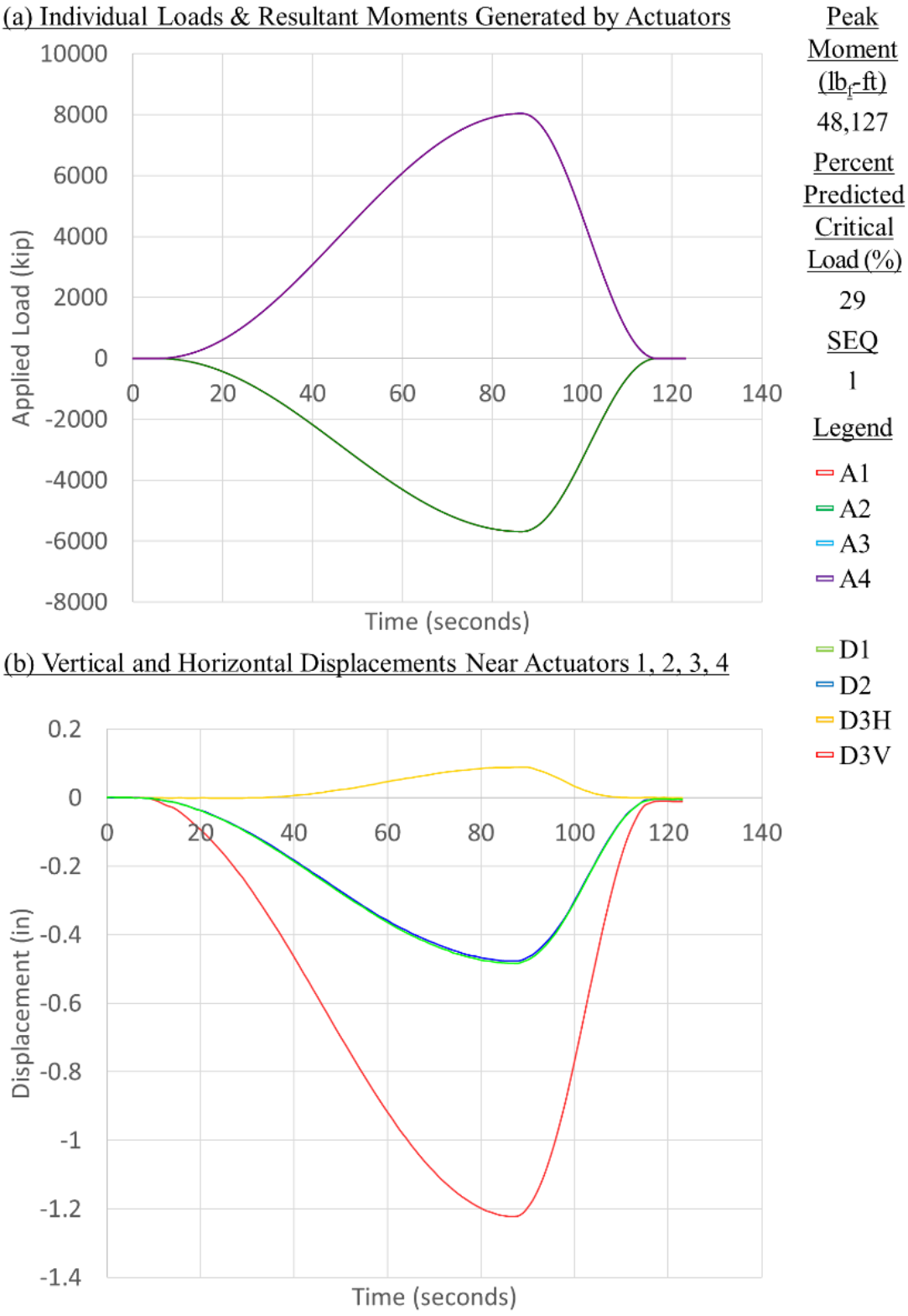

Figure C- 85. Panel 11 load increment 1 (29% load level), load and displacement

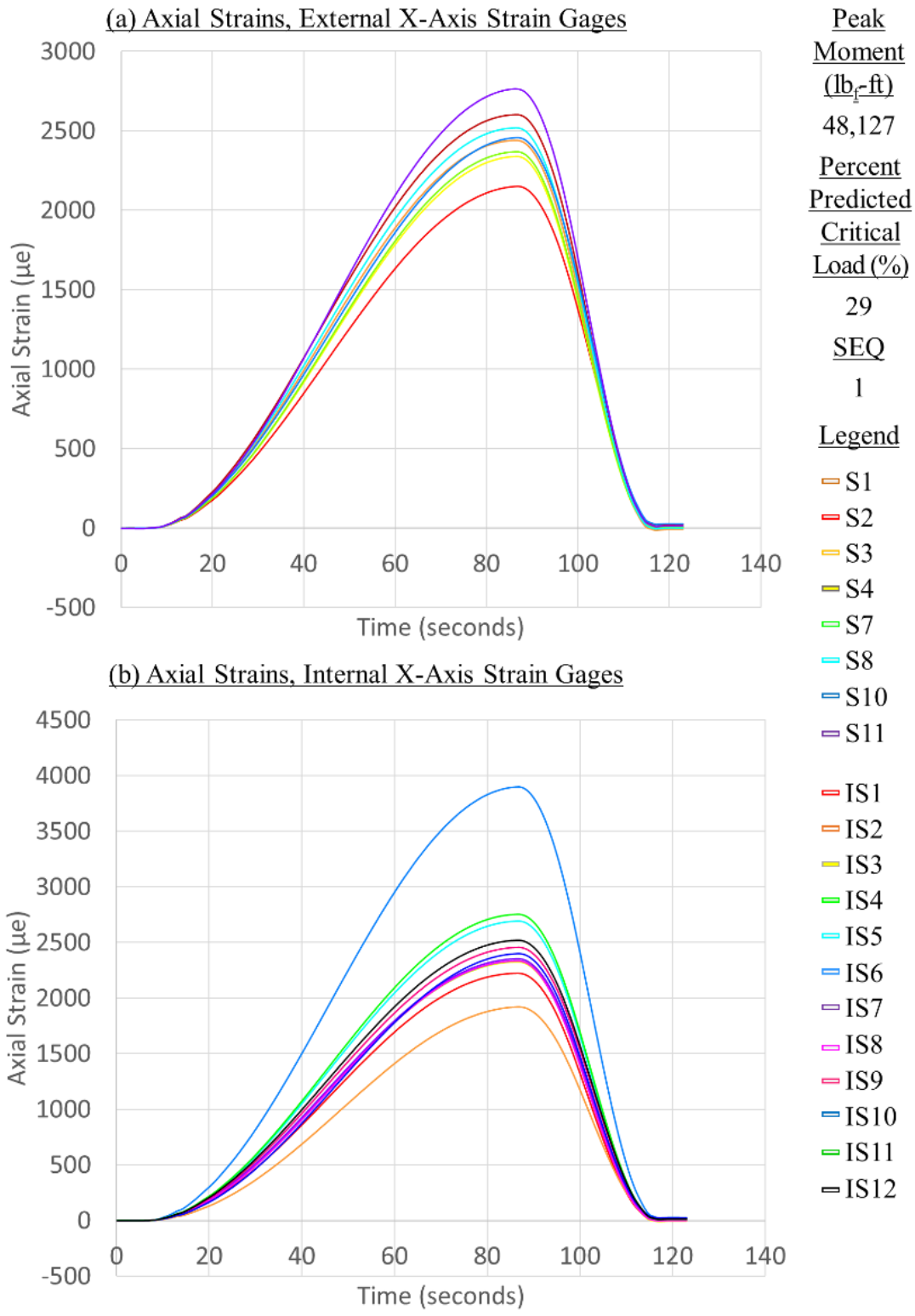

Figure C-86. Panel 11 load increment 1 (29% load level), axial strain

CFRP Panel 11 – Results of SG & SPDT, Residual Strength Test Sequence #1

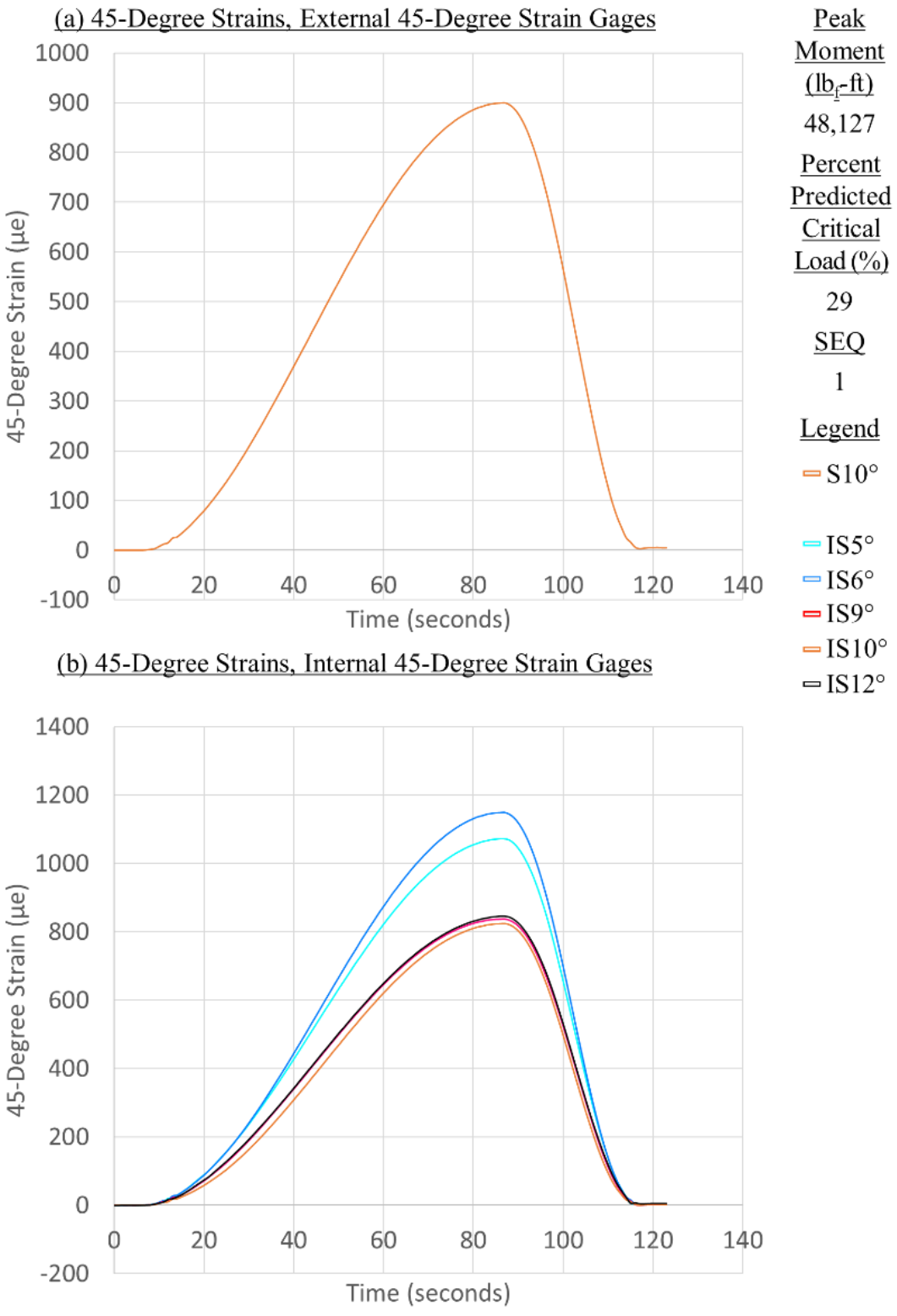

Figure C-87. Panel 11 load increment 1 (29% load level), 45-degree strain

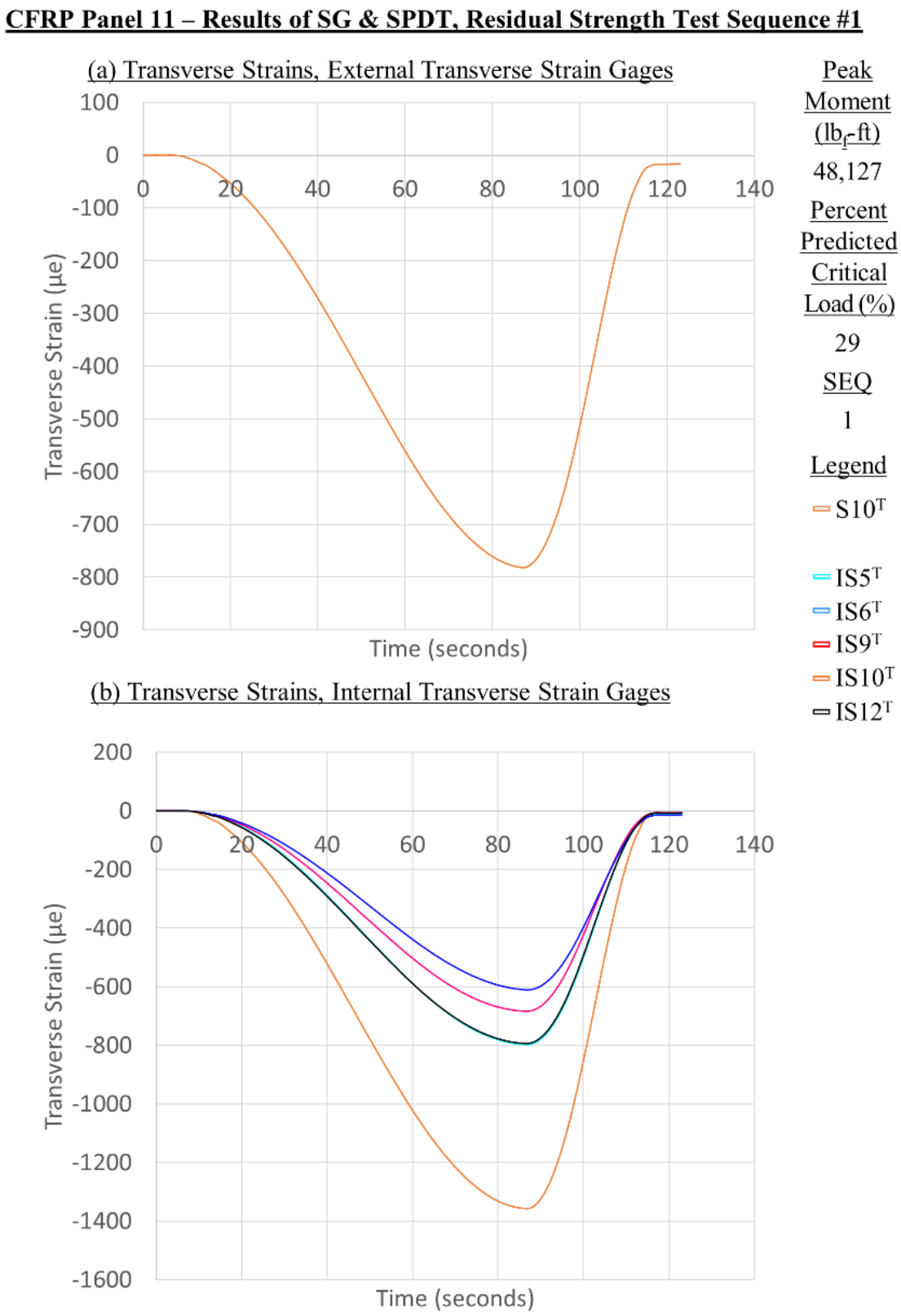

Figure C-88. Panel 11 load increment 1 (29% load level), transverse strain

CFRP Panel 11 – Results of SG & SPDT, Residual Strength Test Sequence #2

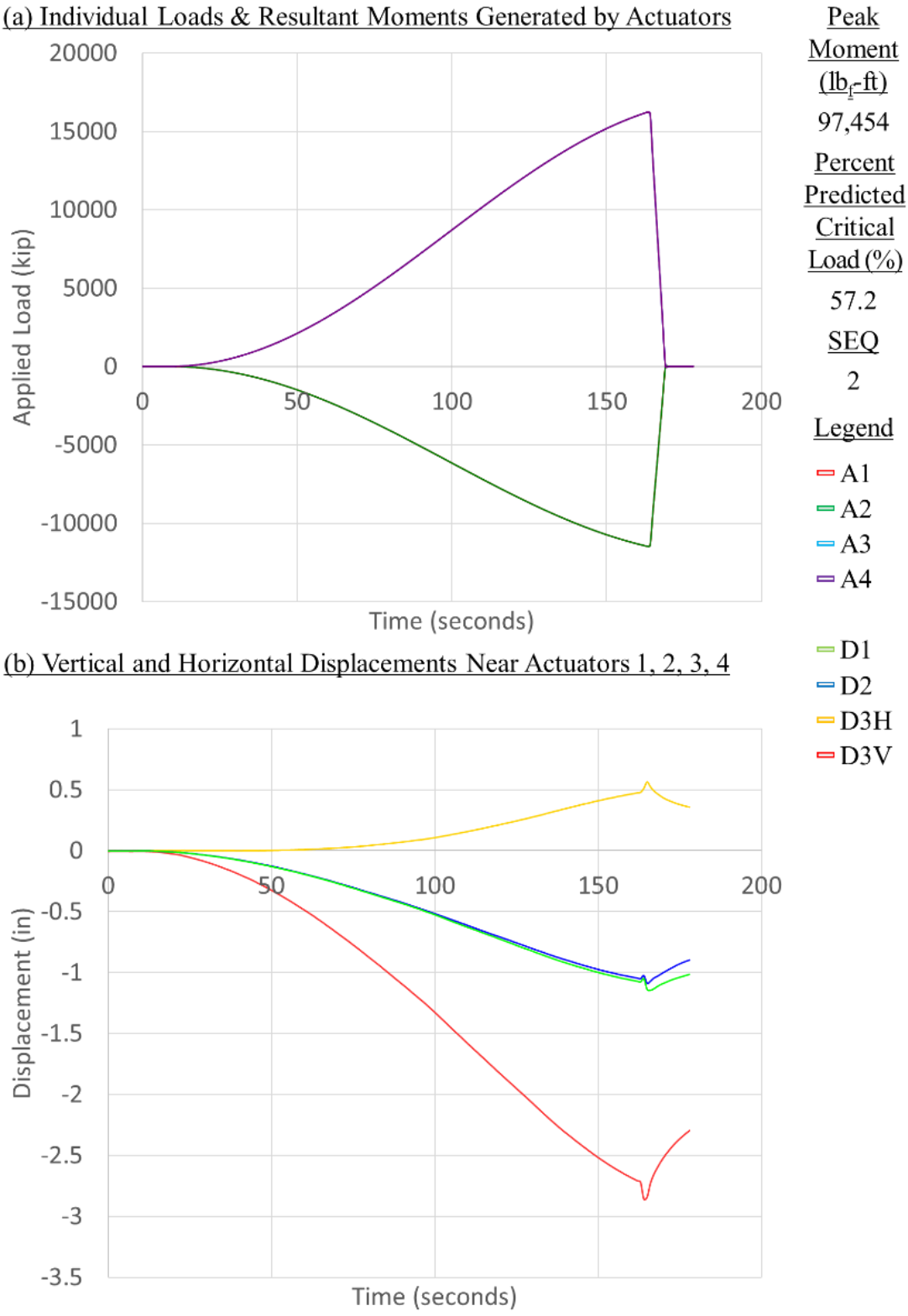

Figure C- 89. Panel 11 load increment 2 (57% load level), load and displacement

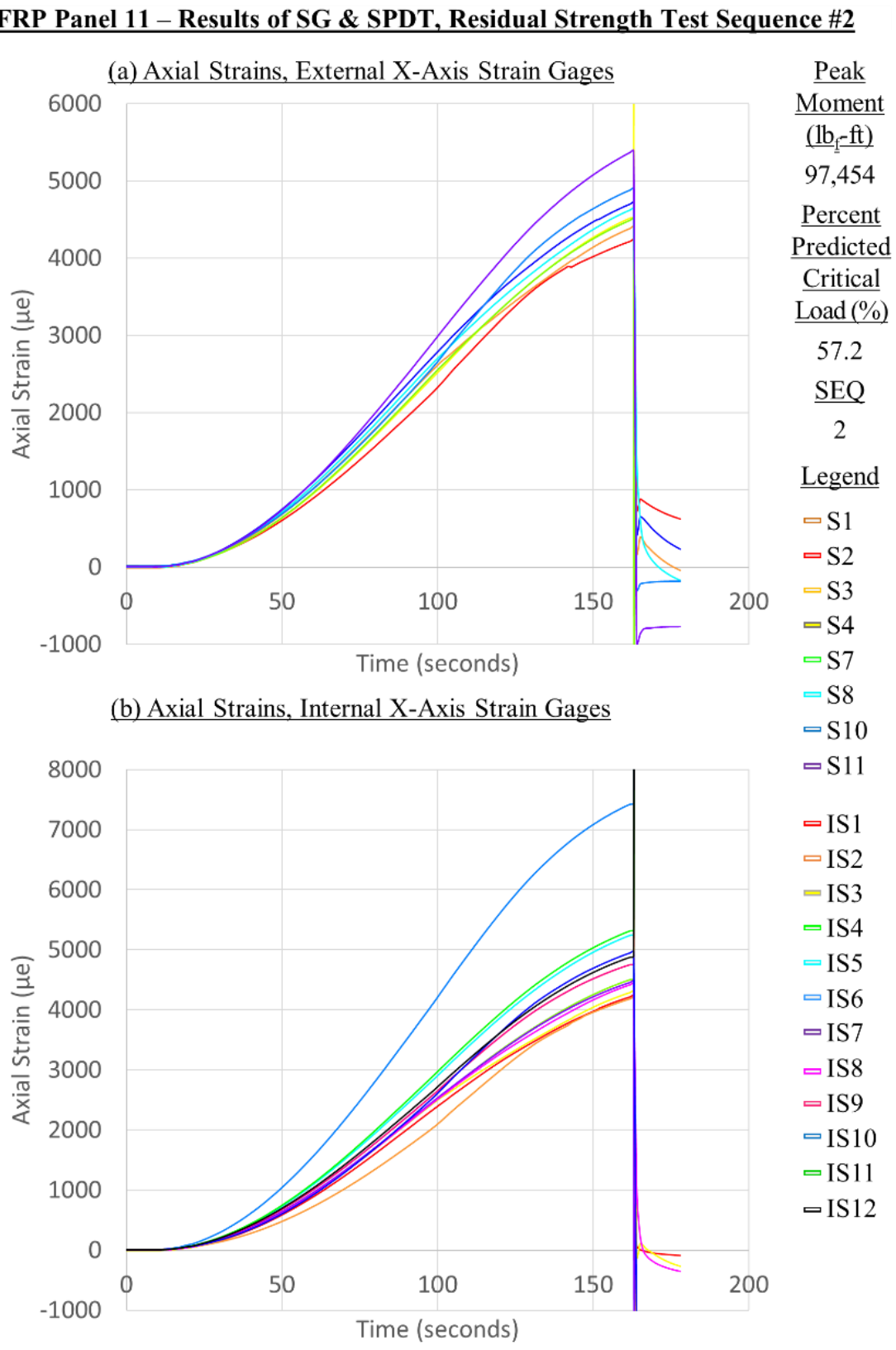

Figure C-90. Panel 11 load increment 2 (57% load level), axial strain

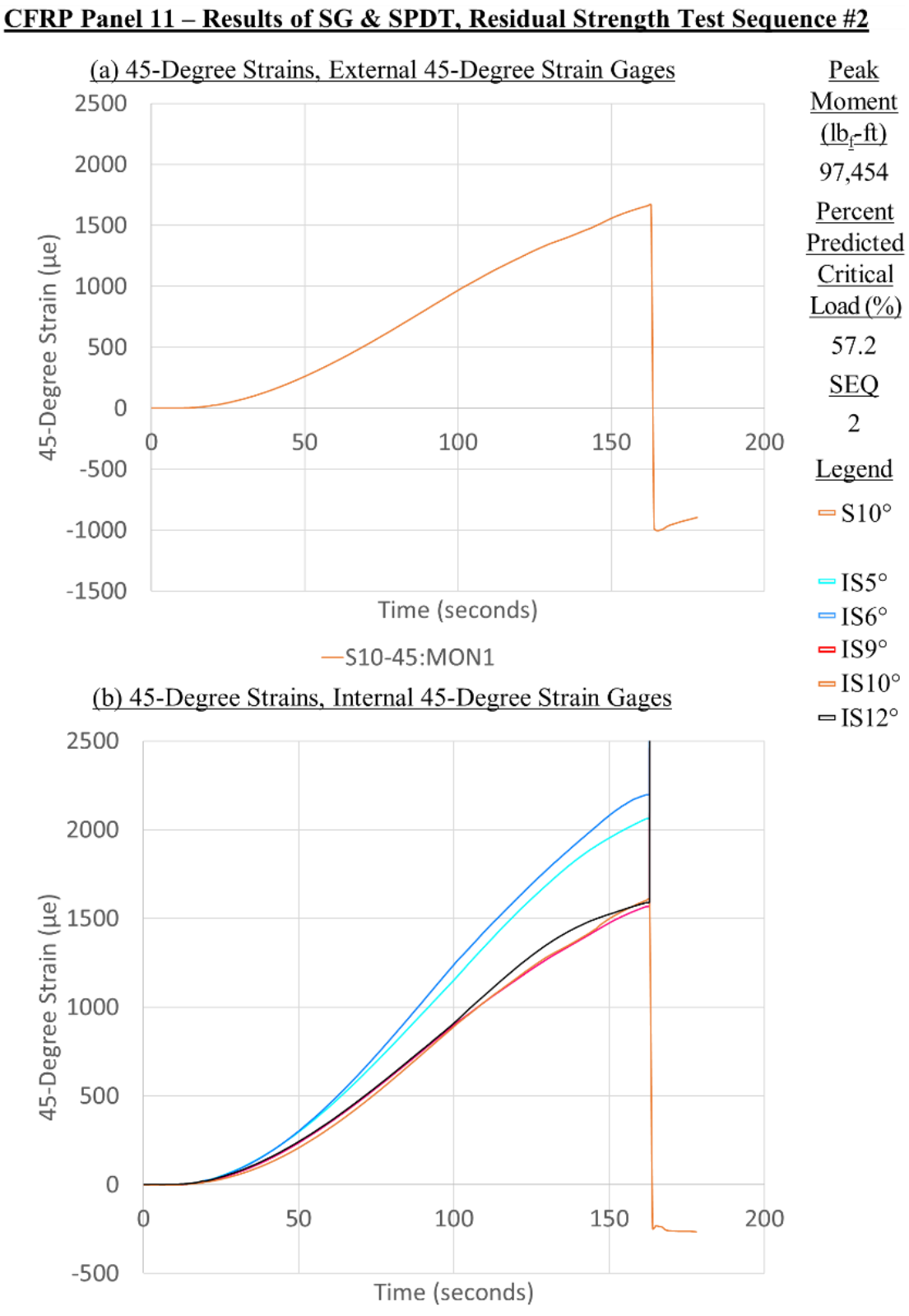

Figure C-91. Panel 11 load increment 2 (57% load level), 45-degree strain

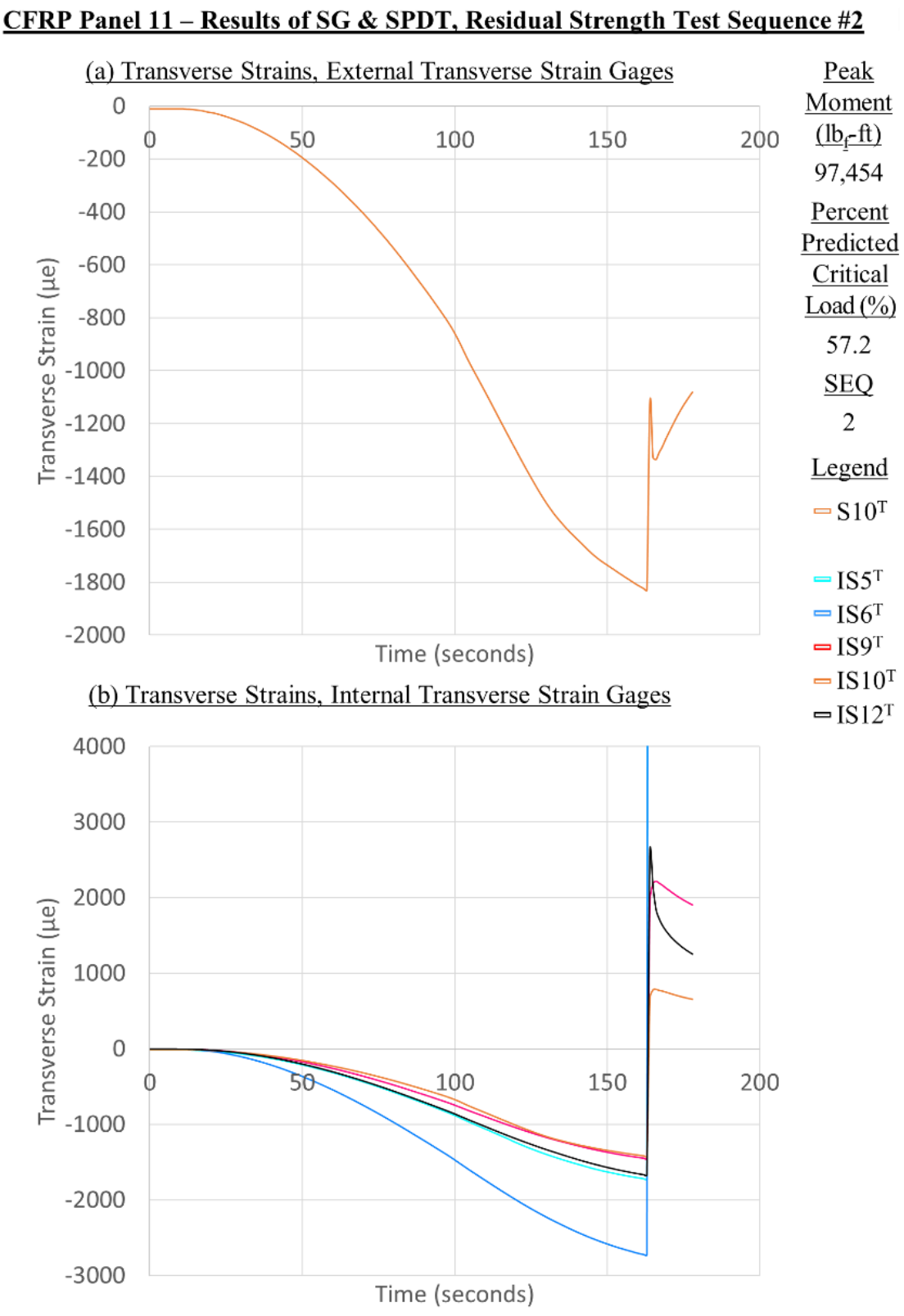

Figure C-92. Panel 11 load increment 2 (57% load level), transverse strain

D Digital Image Correlation Results

3D DIC is a non-contact, material-independent NDI method capable of utilizing sequential digital images of a specimen subjected to mechanical loading to measure in-plane deformation and strain, and in and out-of-plane displacements. Throughout the duration of the tests described herein, 5M ARAMIS 3D DIC systems were used to monitor strains exhibited in the central test sections of the panels during quasi-static strain surveys. Each 5M ARAMIS 2D DIC system consisted of a sensor unit, a sensor controller, a high-performance PC system, and ARAMIS 3D DIC analysis software. The sensor unit, which featured two 5-megapixel cameras with 12-mm (wide field of view) and 50-mm (narrow field of view) focal length lenses, a laser pointer, and two adjustable LED spotlights mounted on a circular support bar. Figures D-1, D-2, and D-5 – D-8 present von Mises strain of Panels 7-11 during respective loadings noted in the figures, from the NFOV DIC system. Figures D-3 and D-4 present axial strain during fatigue loading of Panel 8 from NFOV and WFOV DIC systems, respectively.

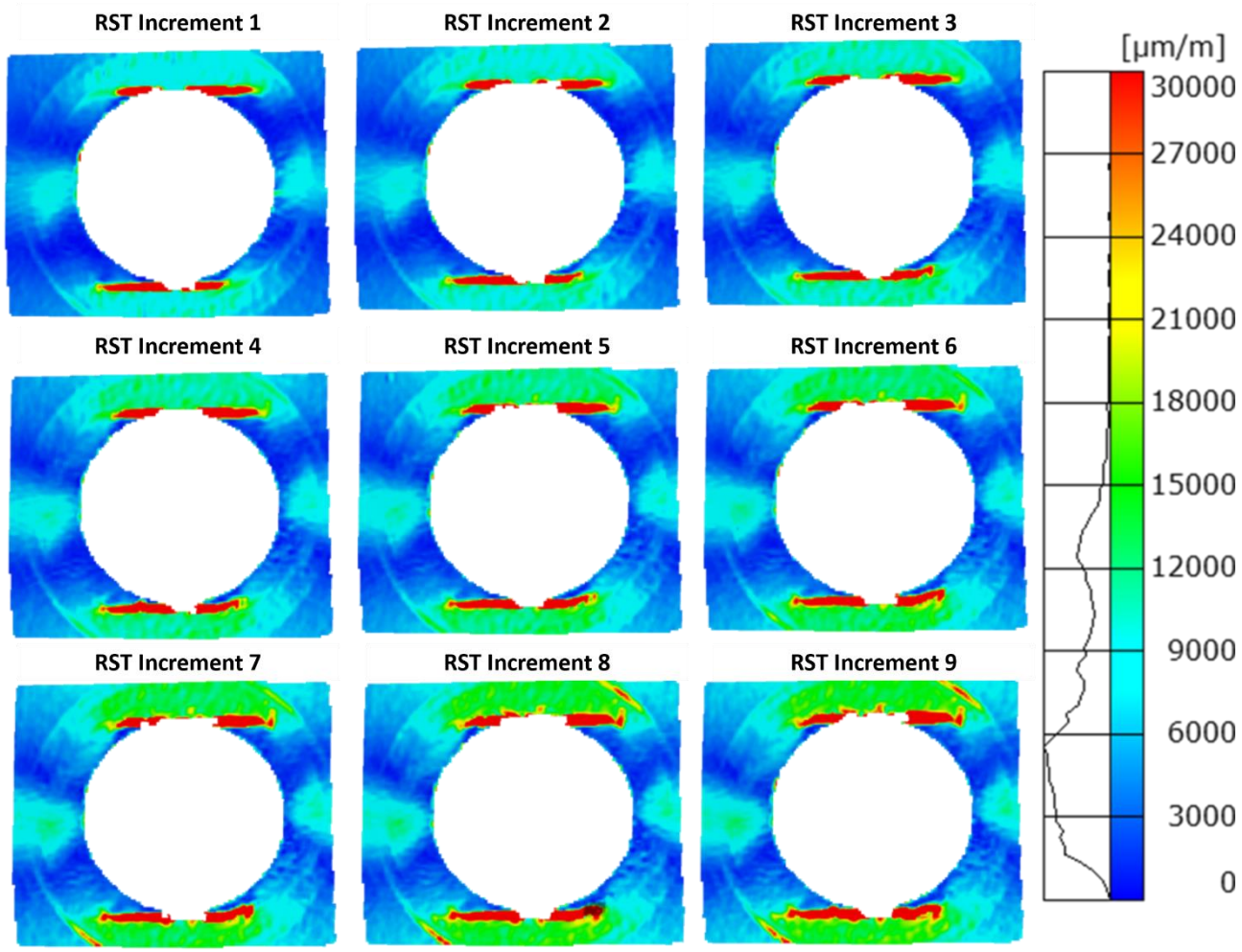

Figure D-1. Panel 7 DIC results (von-Mises) during residual strength test

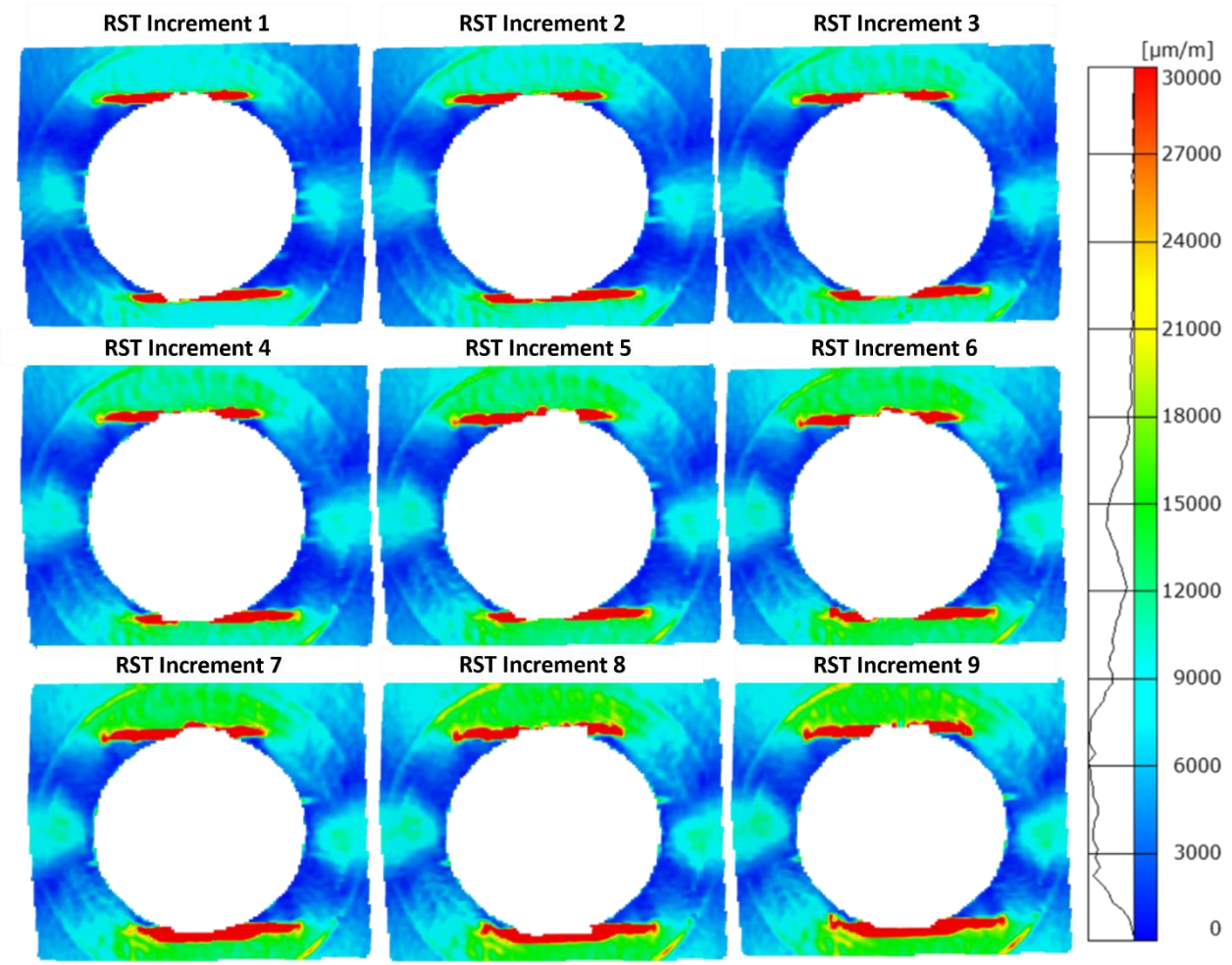

Figure D-2. Panel 8 DIC results (von-Mises) during residual strength test

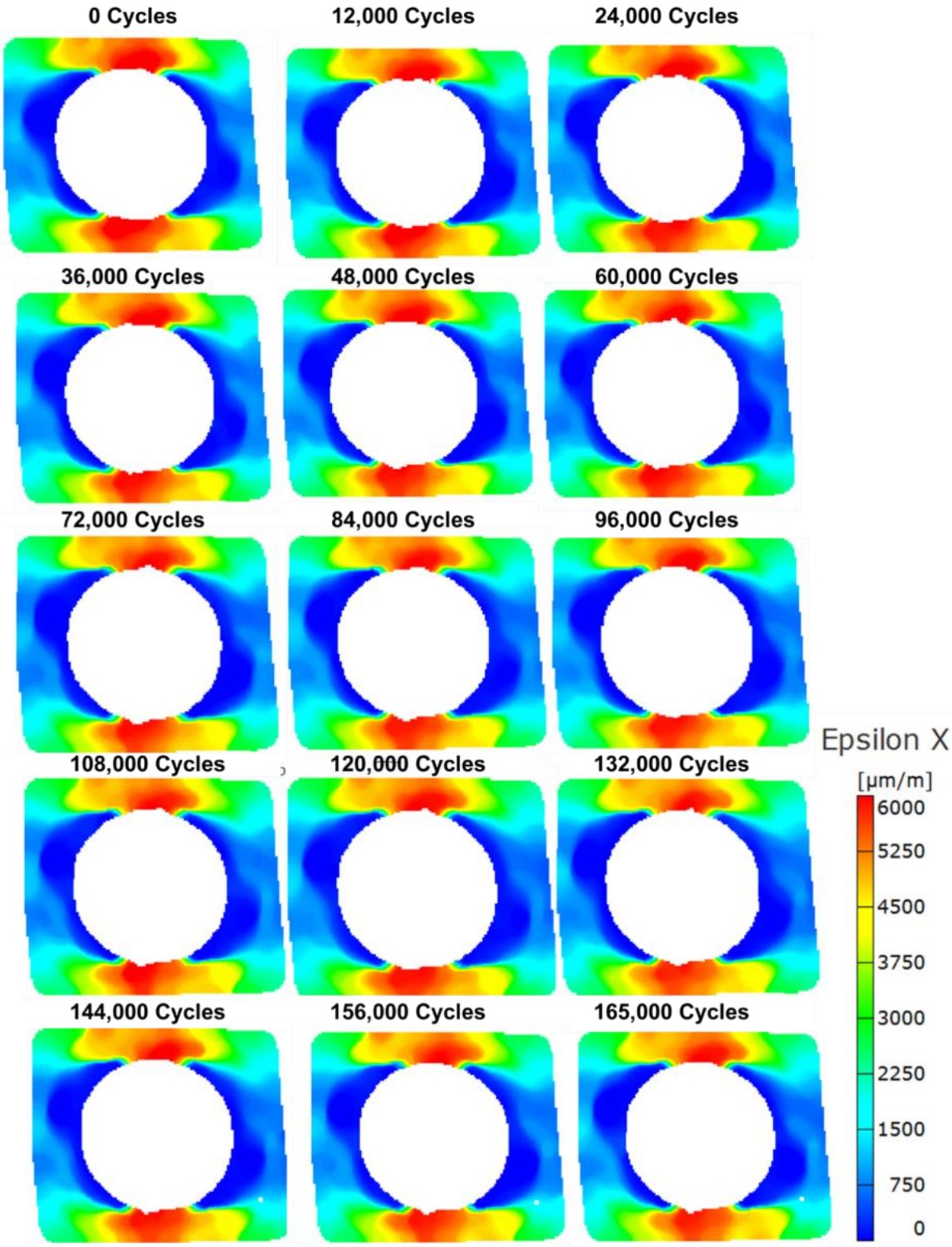

Figure D-3. Panel 8 DIC NFOV results (axial strains) during fatigue at SL strain level

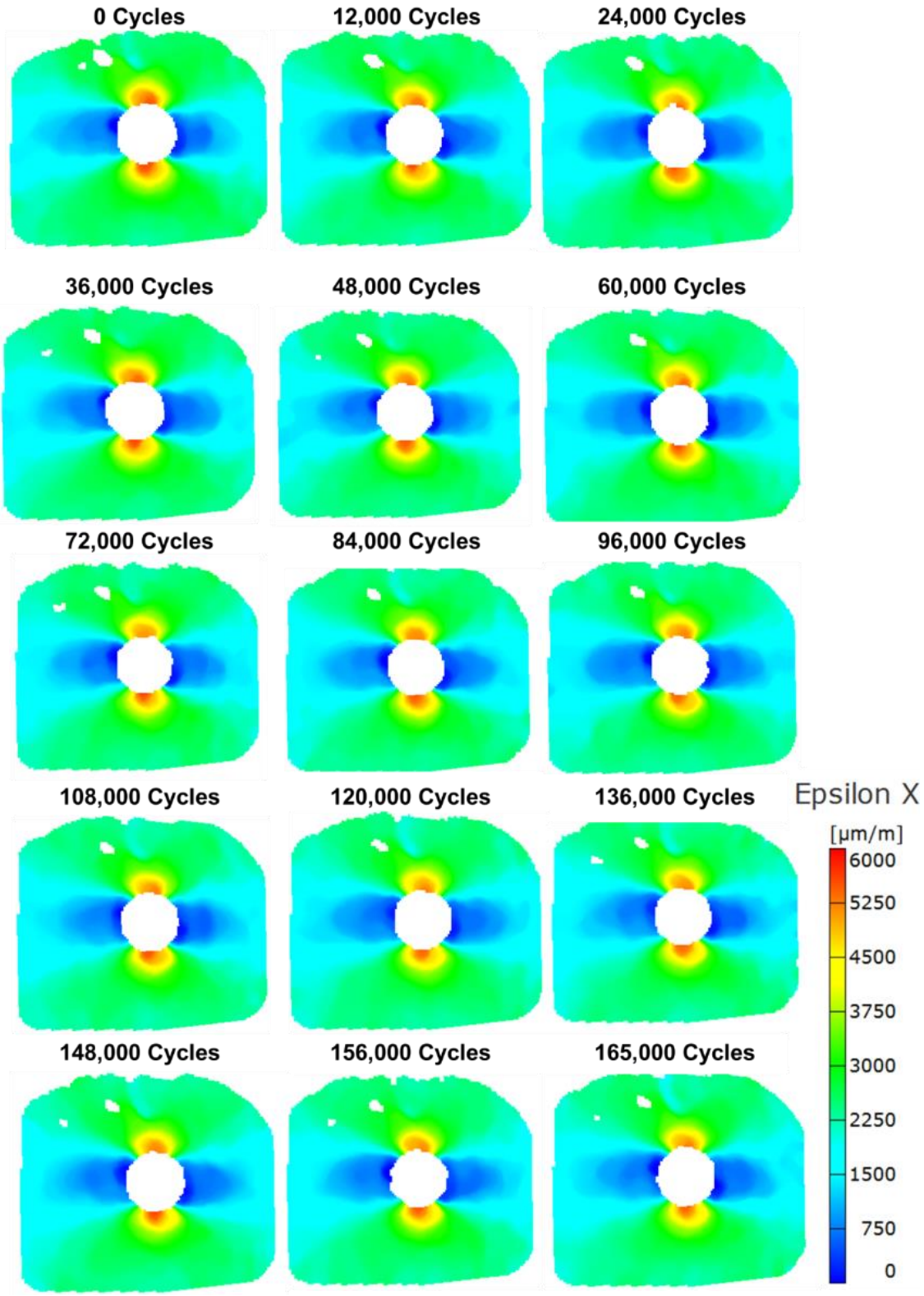

Figure D-4. Panel 8 DIC WFOV results (axial strains) during fatigue at SL strain level

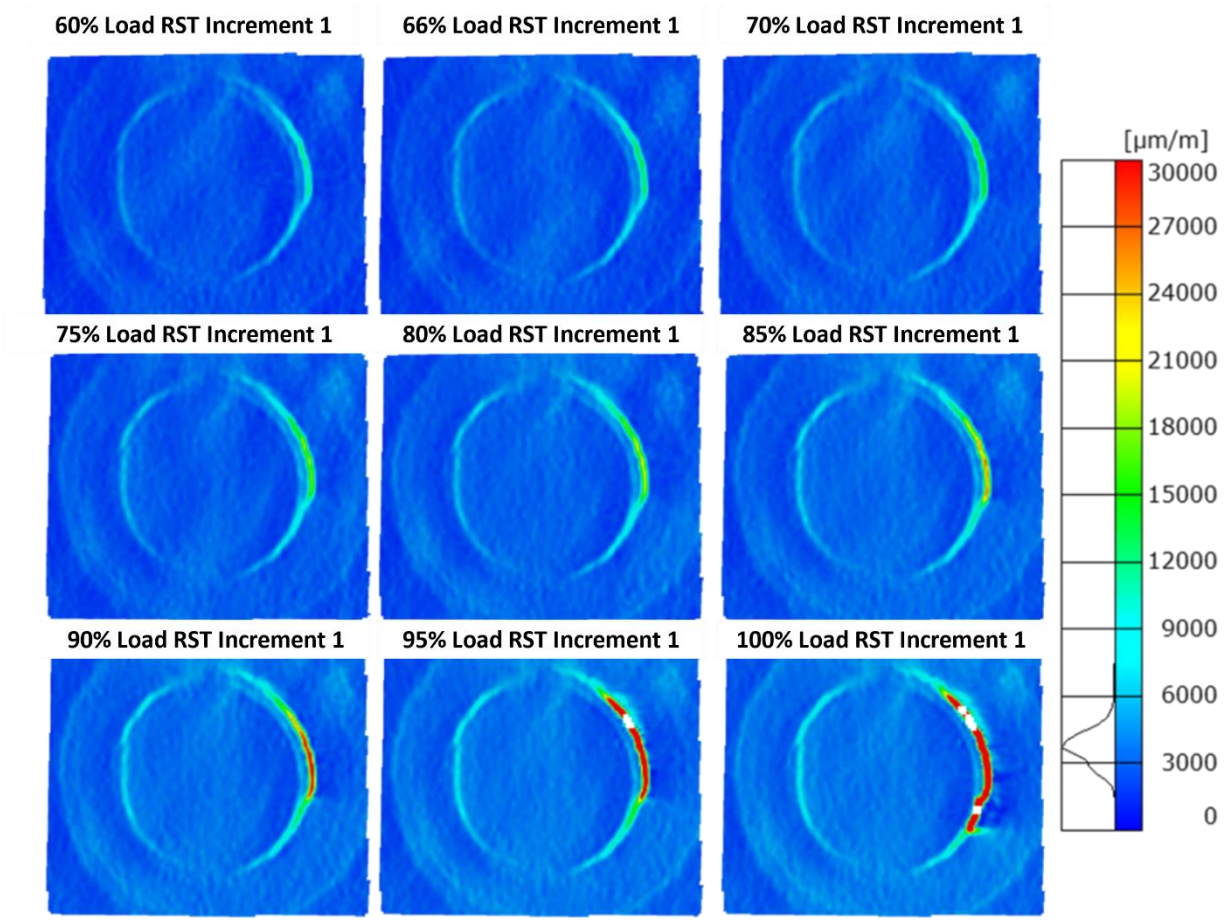

Figure D-5. Panel 9 DIC results (von-Mises) during residual strength test, percent load of load increment 1

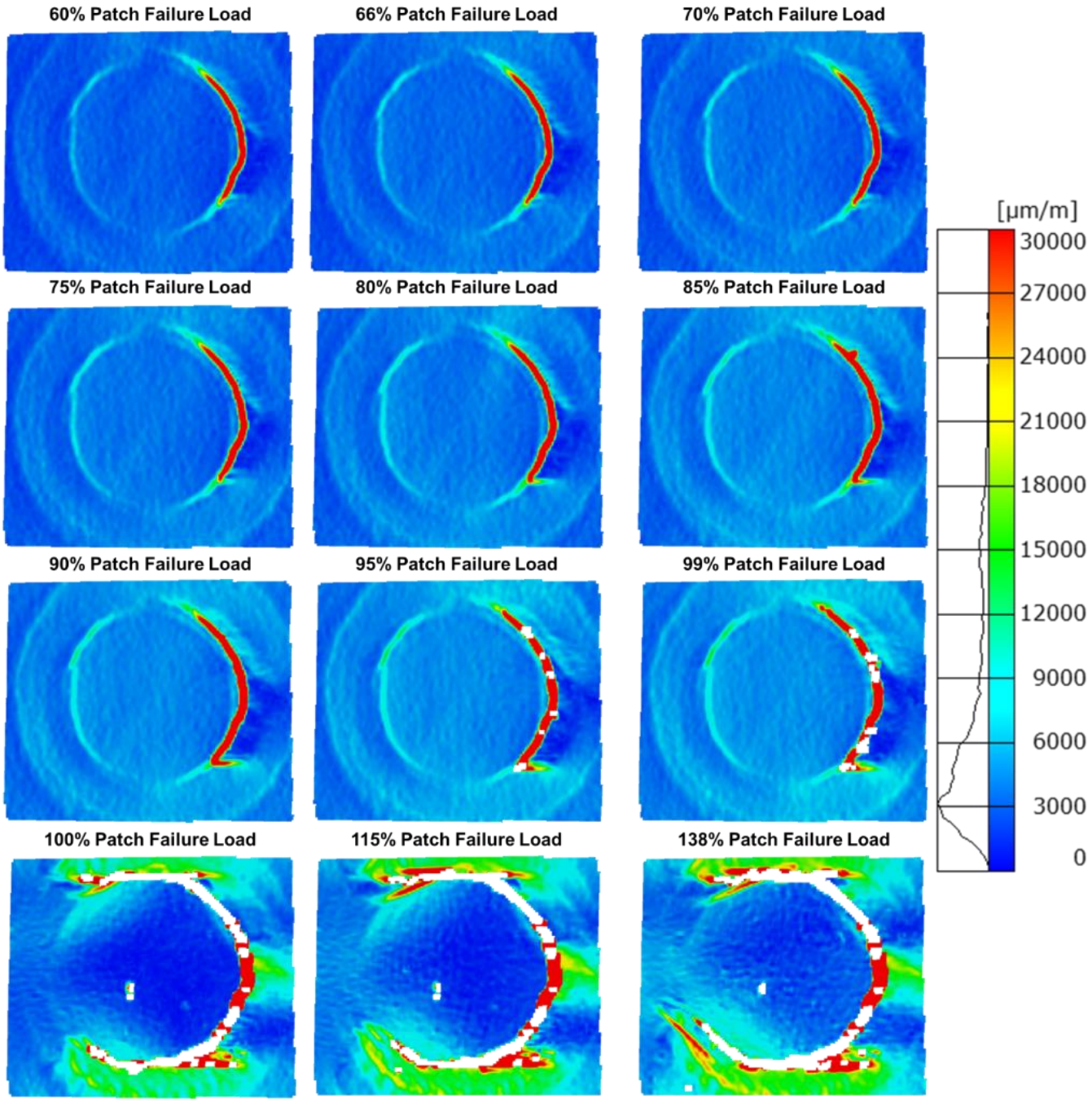

Figure D-6. Panel 9 DIC results (von-Mises) during residual strength test, percent of patch failure load during load increment 1a

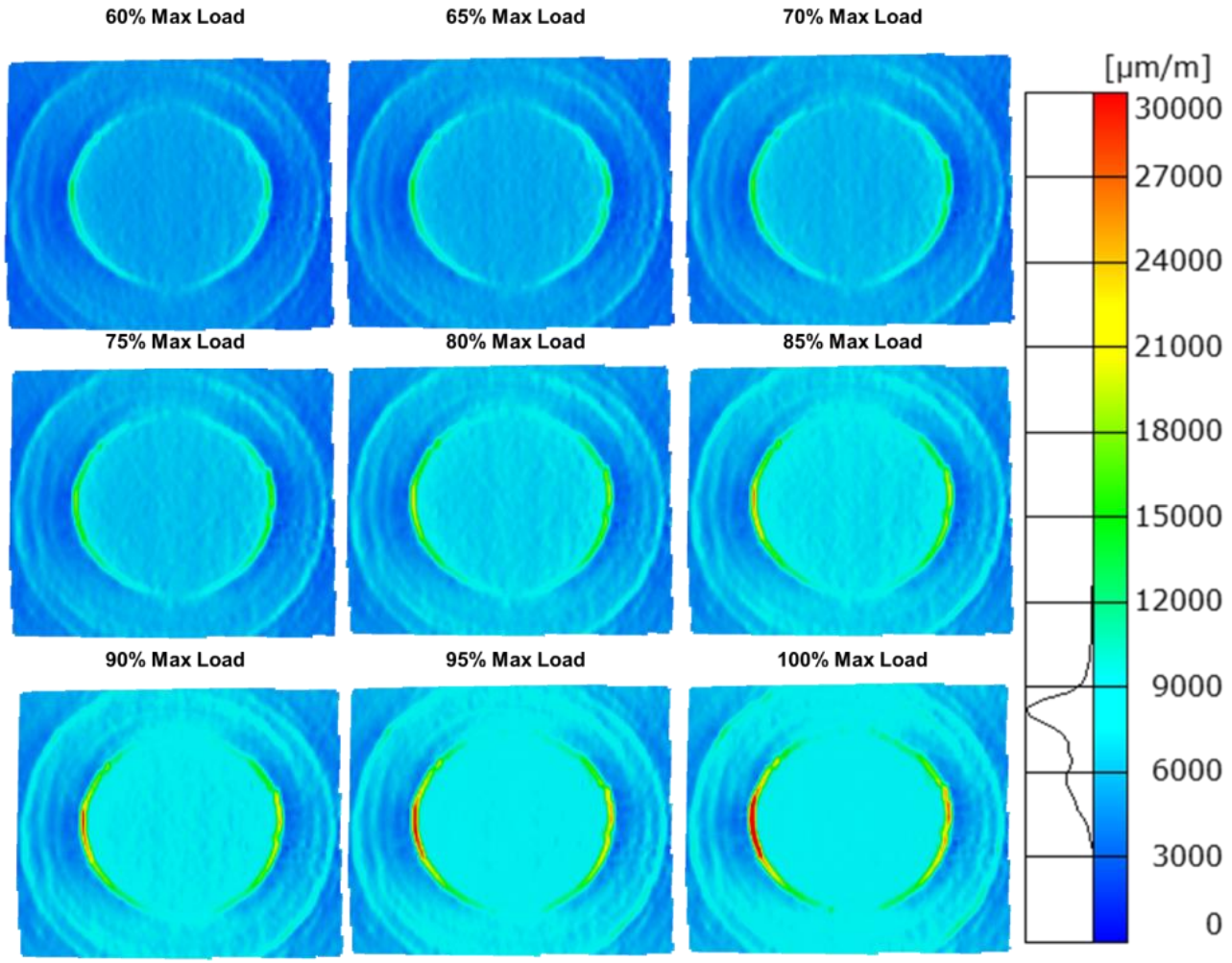

Figure D-7. Panel 10 DIC results (von-Mises) during residual strength test

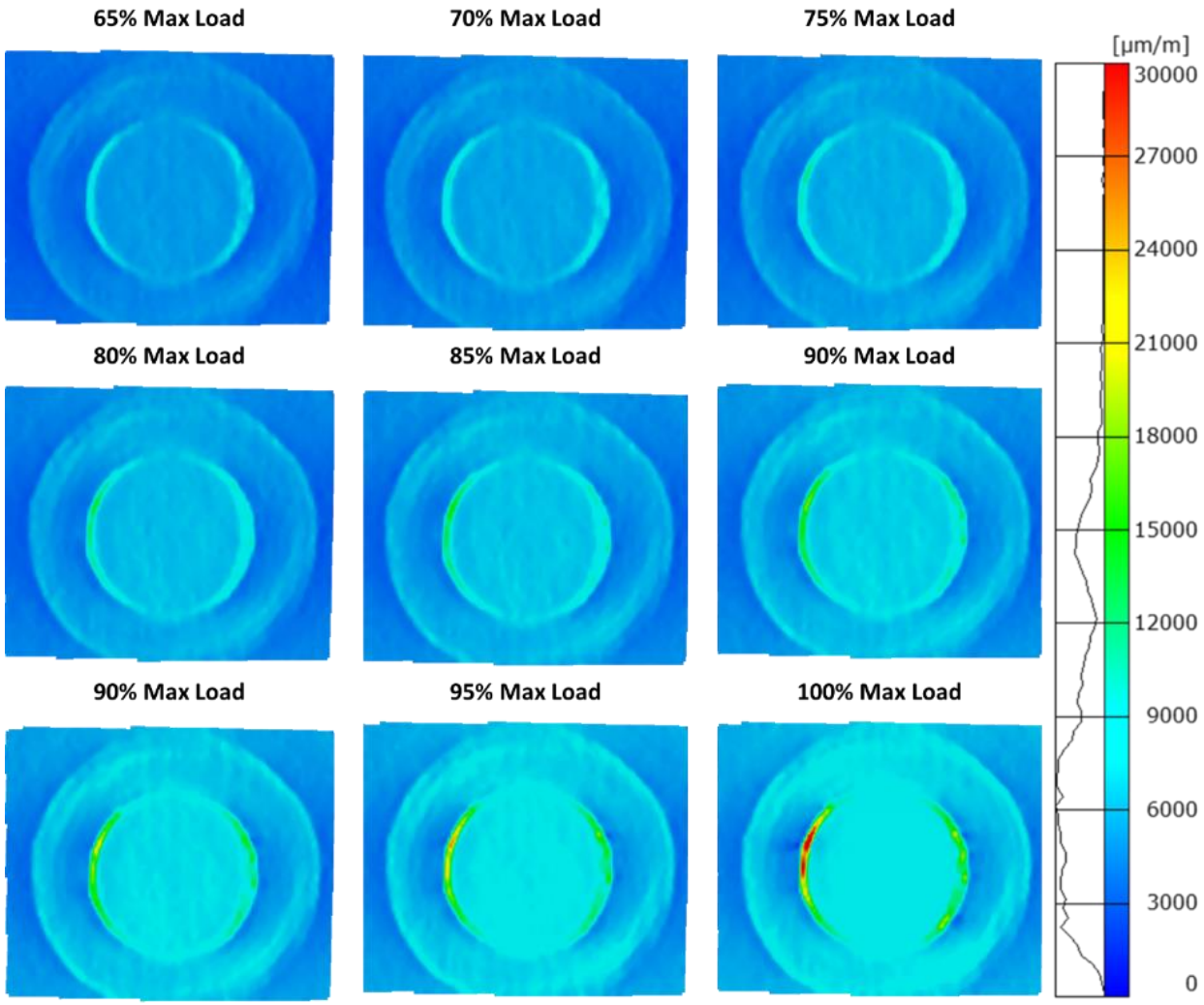

Figure D-8. Panel 11 DIC results (von-Mises) during residual strength test

E Visual Results

Provided in this appendix are post-failure visual results after residual strength loading of the double-sided scarf panels.

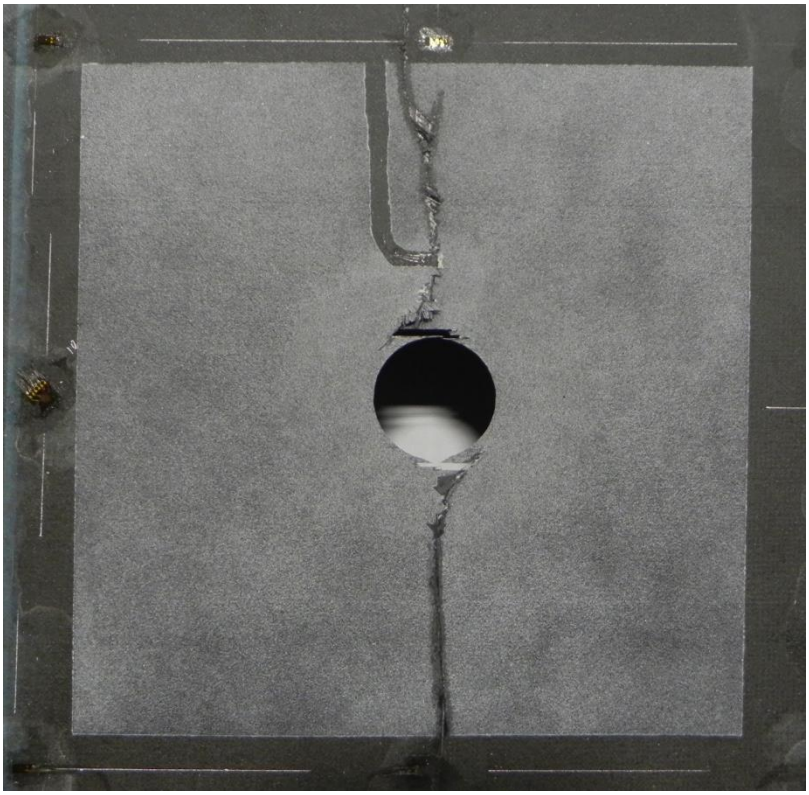

Figure E-2. Panel 7 net section failure, external surface

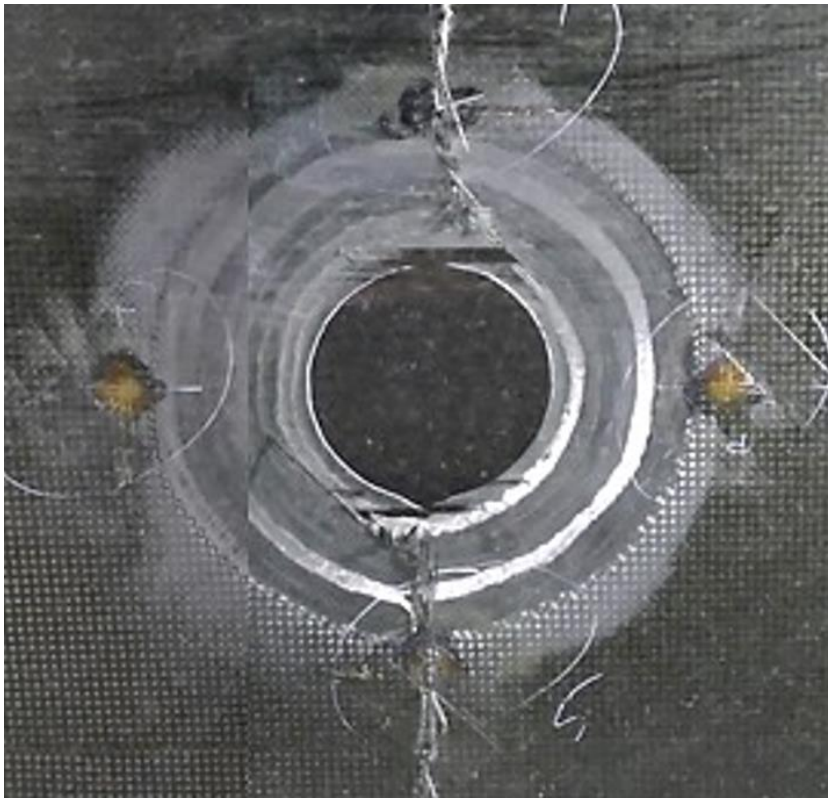

Figure E-1. Panel 7 scarf failure, internal surface

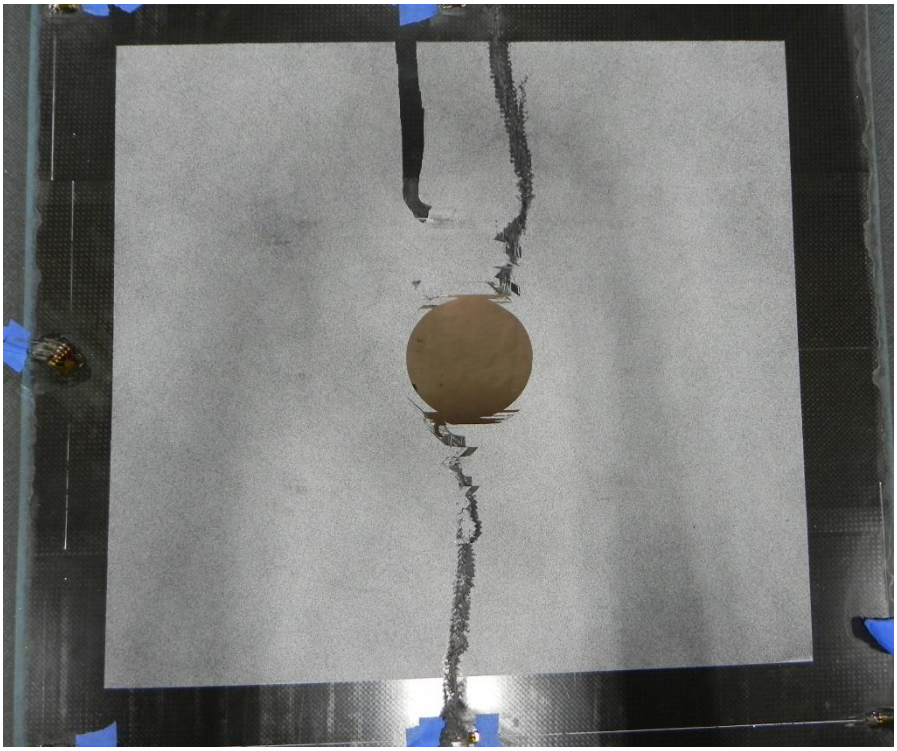

Figure E-3. Panel 8 net section failure, external surface

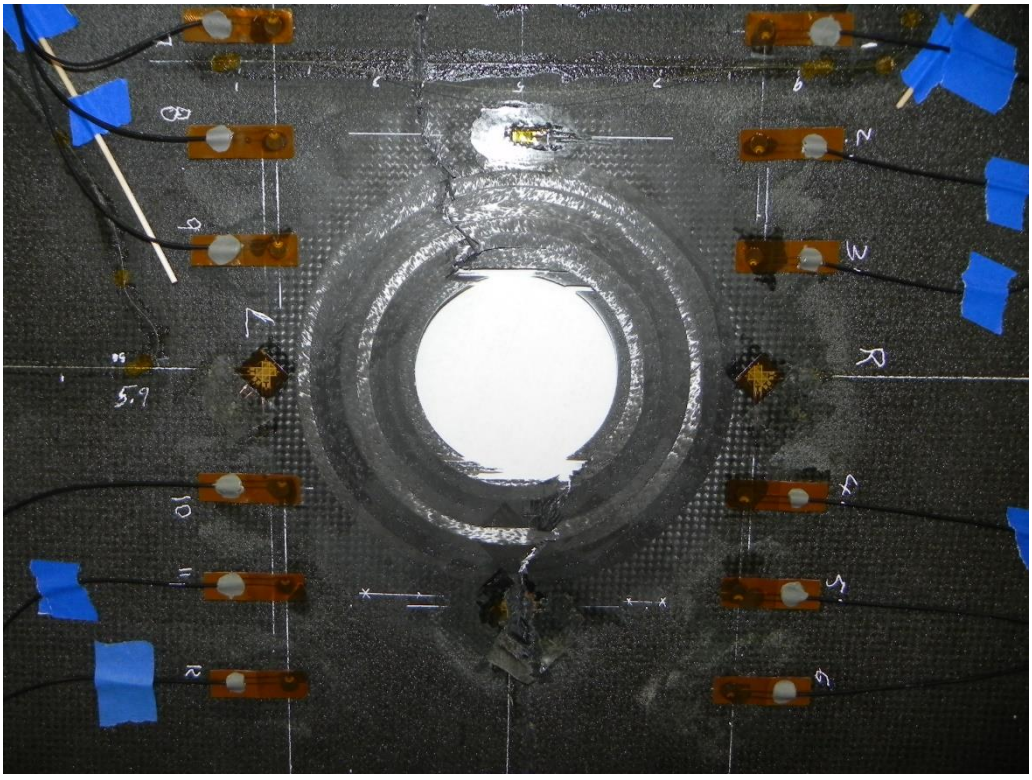

Figure E-4. Panel 8 scarf failure, internal surface

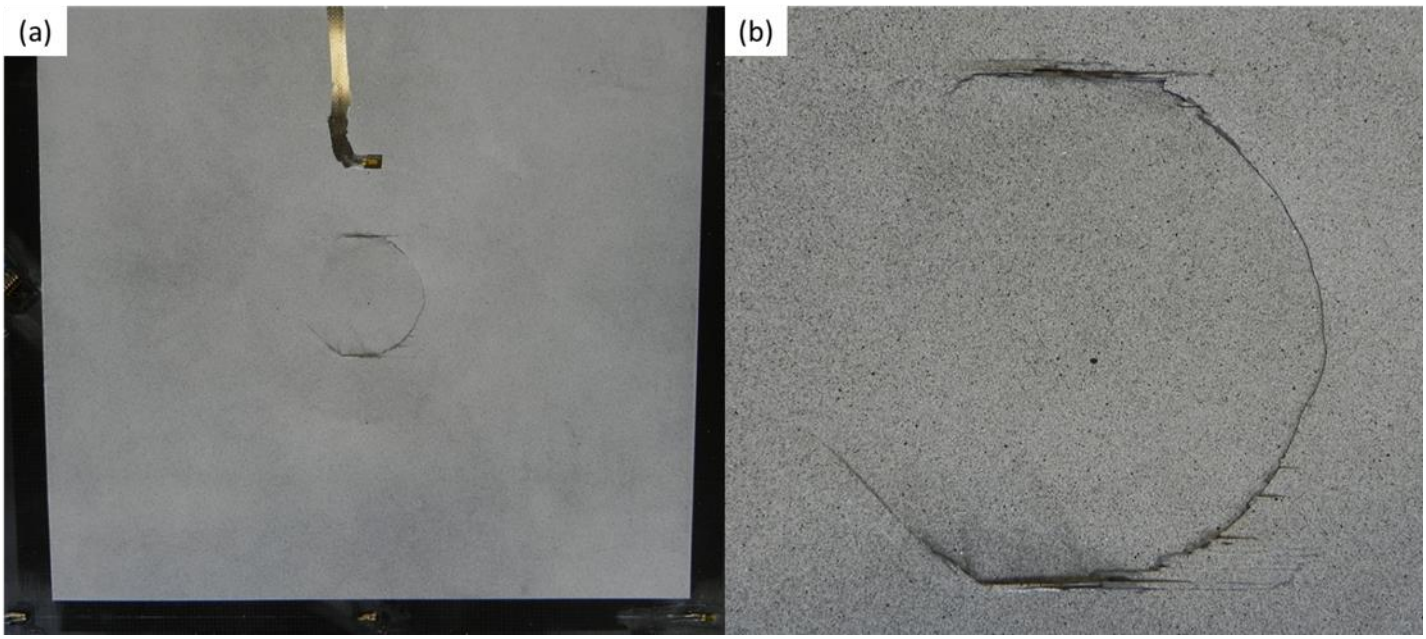

Figure E-6. Panel 9 (a) patch failure, external, (b) focused patch failure

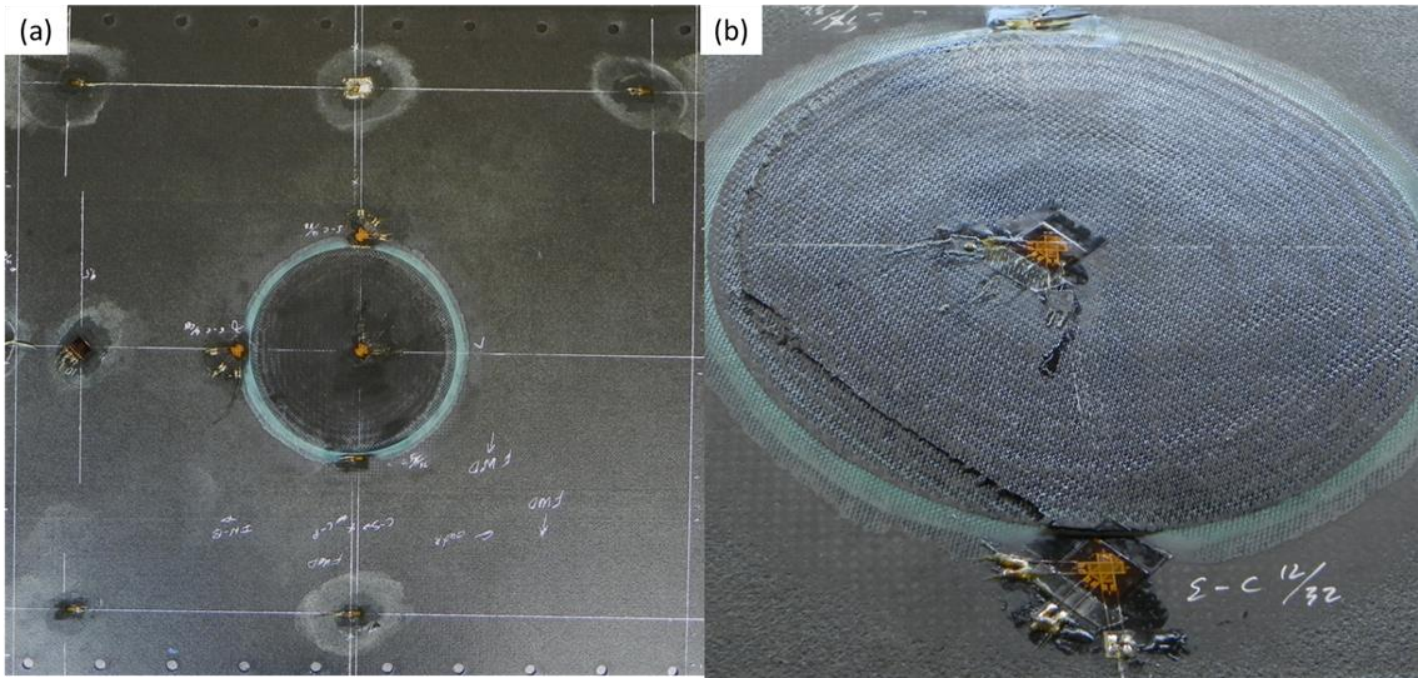

Figure E-5. Panel 9 (a) patch failure, internal surface, (b) focused patch failure

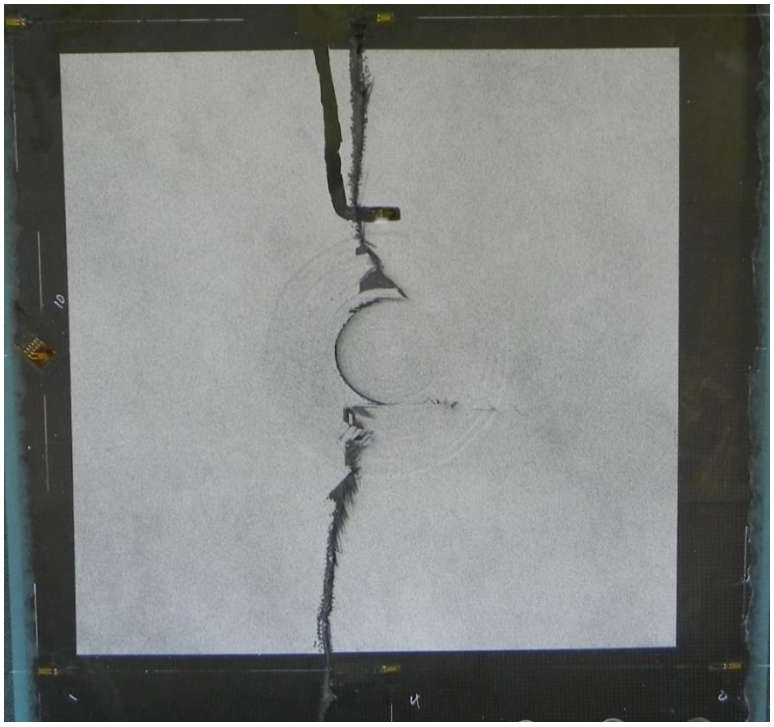

Figure E-7. Panel 10 patch and net section failure, external surface

Figure E-8. Panel 10 patch and net section failure, internal surface

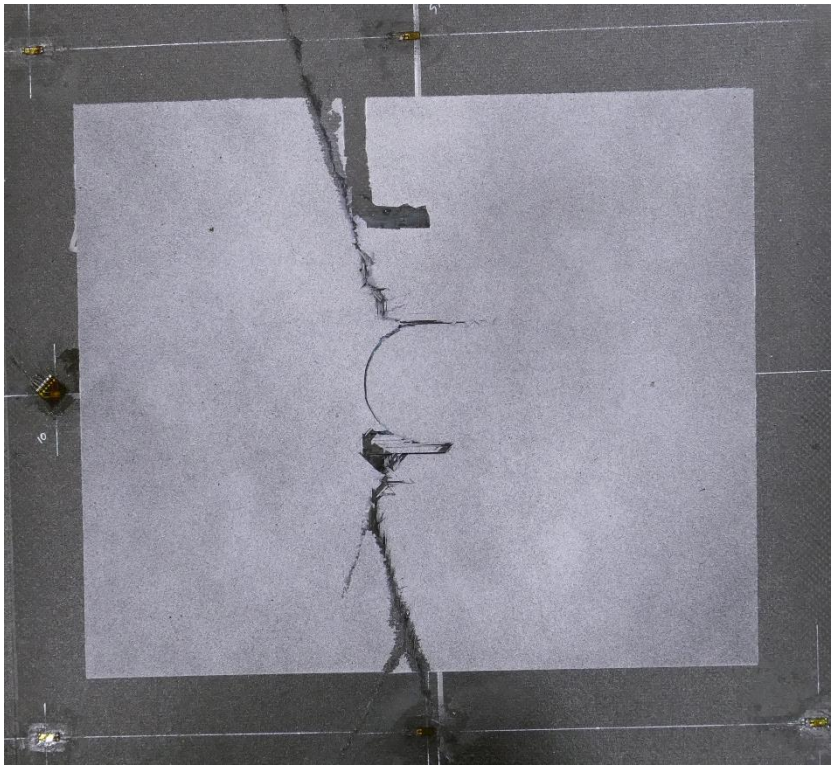

Figure E-9. Panel 11 patch and net section failure, external surface

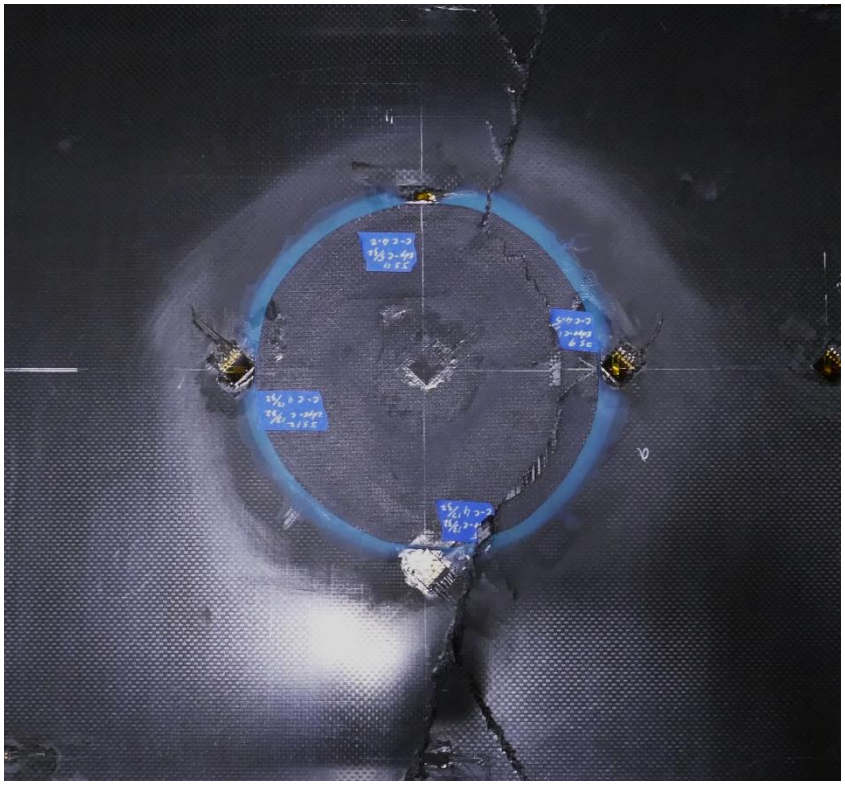

Figure E-10. Panel 11 patch and net section failure, internal surface

F Flash Thermography Results

Provided in this appendix are flash thermography results captured throughout residual strength loading of Panels 7, 8, and fatigue loading of Panel 8. Note, Panels 9-11 are omitted from this appendix, no thermography results were recorded before catastrophic final failure.

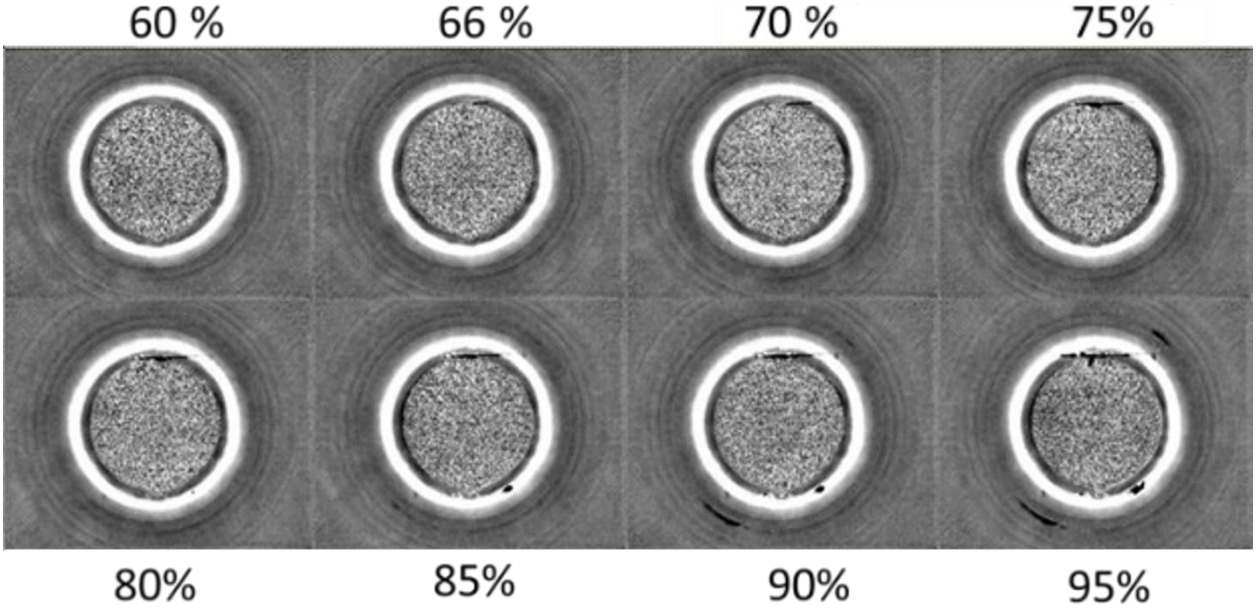

Figure F-2. Flash thermography timeline of Panel 7 RST, as percent of final load

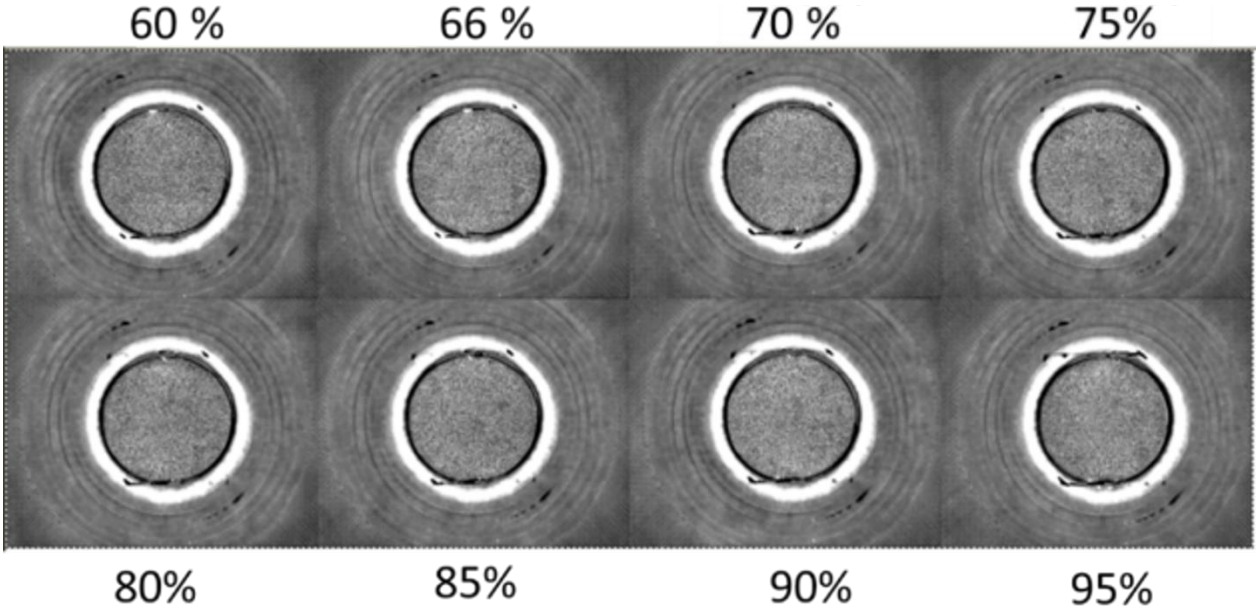

Figure F-1. Flash thermography timeline of Panel 8 RST as percent of final load

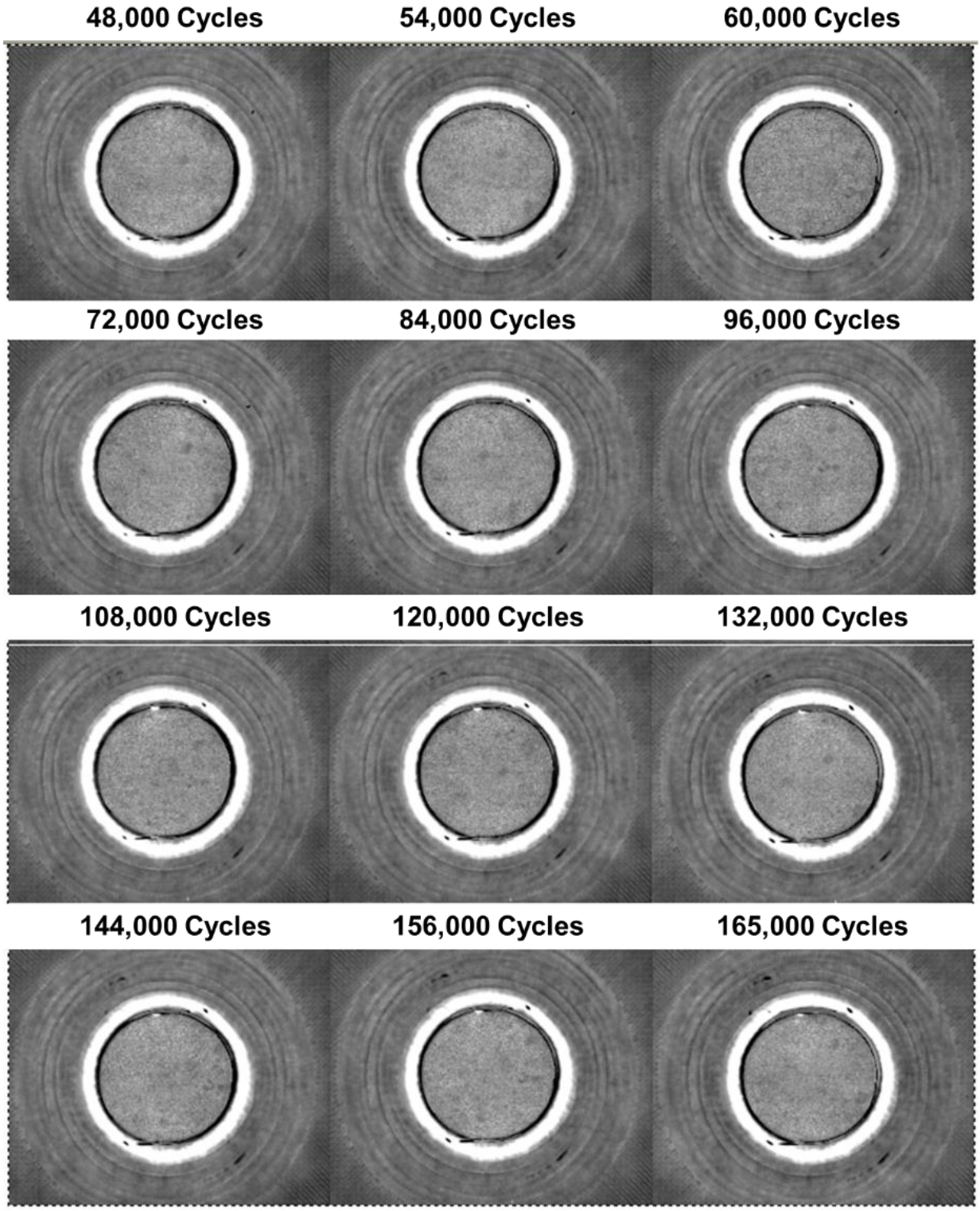

Figure F-3. Flash thermography of Panel 8 fatigue, TSR 2 skip

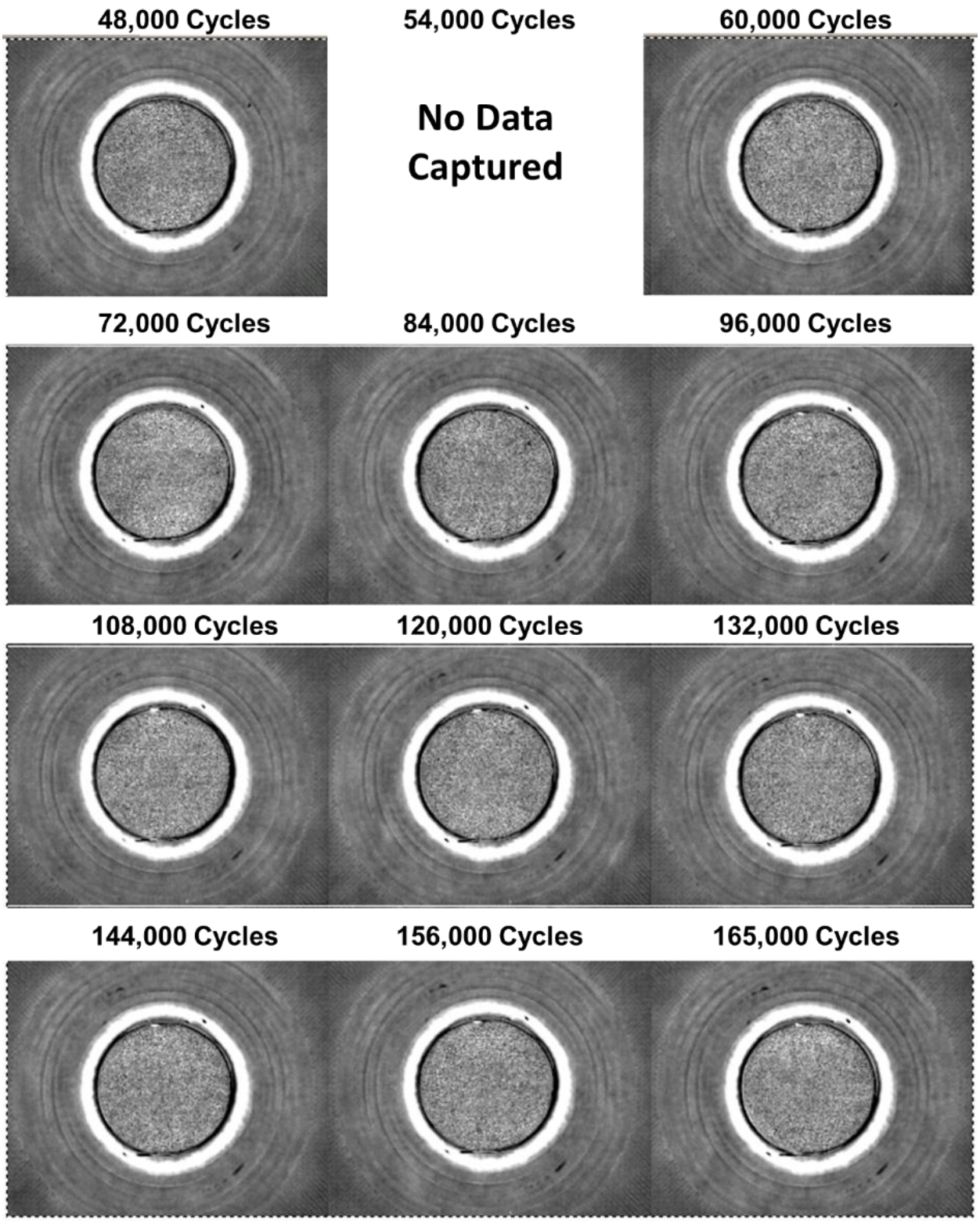

Figure F-4. Flash thermography of Panel 8 fatigue, TSR 5 skip

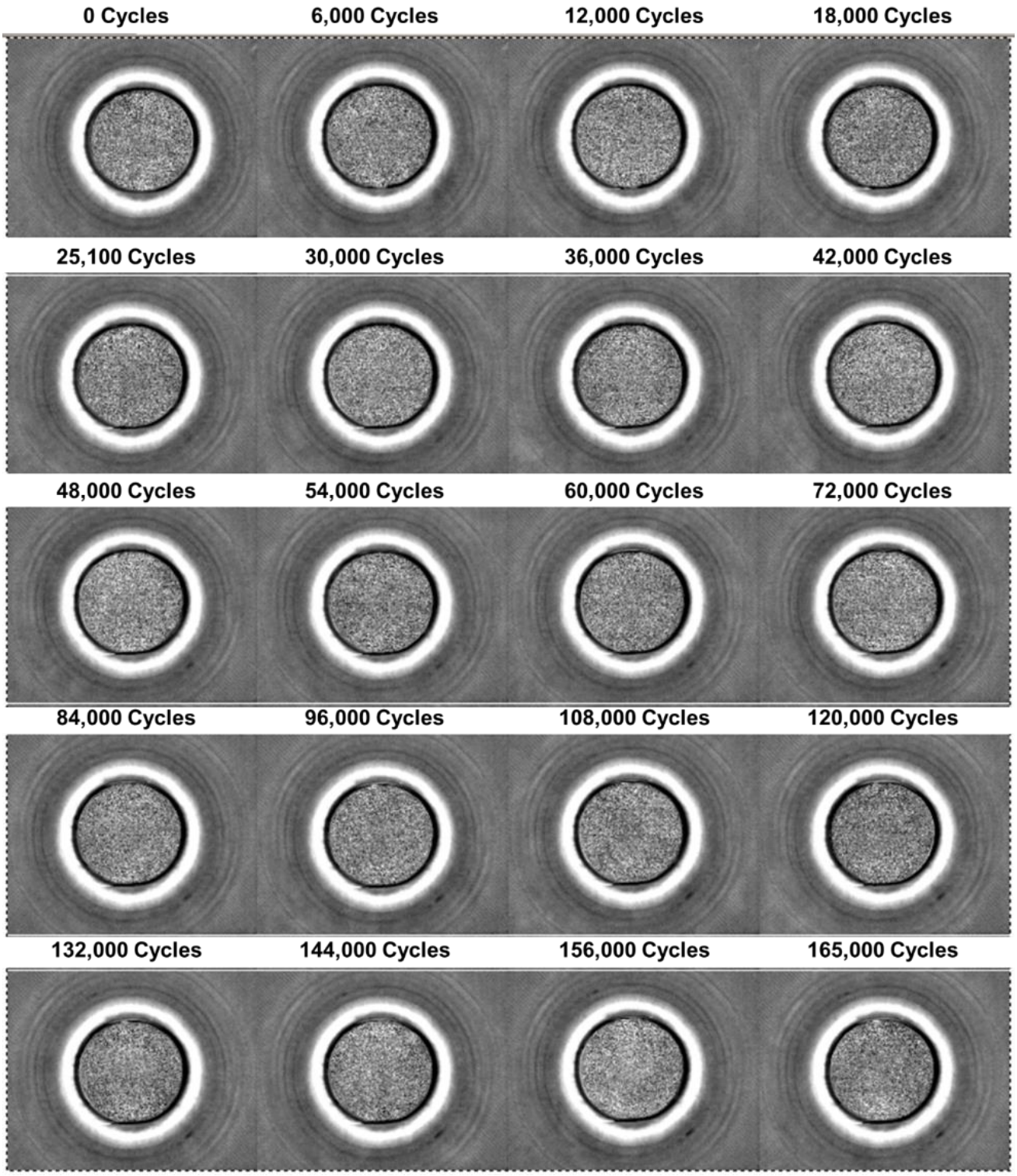

Figure F-5. Flash thermography of Panel 8 fatigue, TSR 10 skip